Optimal Control Strategy Selection for Intelligent Pressure Independent Control Valves

By

MILES RYAN

B.S., Montana State University, 2009

A thesis submitted to the

Faculty of the Graduate School of the

University of Colorado in partial fulfillment

of the requirement for the degree of

Master of Science in

Architectural Engineering

2014

This thesis entitled:

Optimal Control Strategy Selection for Intelligent Pressure Independent Control Valves

written by Miles H. Ryan

has been approved for the Department of Civil,

Environmental and Architectural Engineering

_____

Prof. Gregor Henze, PhD., P.E.

_____

Prof. Michael Brandemuehl, PhD., P.E.

_____

Prof. Moncef Krarti, PhD., P.E.

Date_____

The final copy of this thesis has been examined by the signatories, and we find that both the content and the form meet acceptable presentation standards of scholarly work in the above mentioned discipline.

Ryan, Miles Hawke (M.S., Architectural Engineering)

Optimal Control Strategy Selection for Intelligent Pressure Independent Control Valves

Thesis directed by Professor Gregor P. Henze

A scenario which has plagued chilled water distribution systems for decades occurs when the temperature difference between chilled water supply and return is diminished well below design levels. This is termed Low Delta T Syndrome and has negative effects on the energy consumption of the chilled water system. Numerous causes of Low Delta T exist, many of them laying at the cooling coils. As higher loads are put on the cooling coil, more chilled water is sent through it. A point of saturation is reached when significant increases in chilled water flow will result in negligible increases in provided cooling power.

Recognition of when such saturation is occurring, as well as the ability to implement advanced control logics to bring down the water flow in such situations, is needed to effectively combat Low Delta T. An intelligent, pressure independent control valve capable of measuring water flow rate and temperatures attempts this. It currently has three established methods of predicting when saturation is occurring; comparison of flow to a pre-established high flow limit, comparison of Delta T to a pre-established low limit, and comparison of the flow over Delta T ratio to a pre-established high limit.

A methodology was developed to produce realistic cooling coil performance data through energy simulation. This data was analyzed to further optimize the potential for the valve to combat Low Delta T and subsequently save energy. A new approach for predicting saturation was developed, through use of non-linear regression on the coil data. The resulting curve fit was first used to effectively predict whether a coil was operating in a Constant Air Volume (CAV) or Variable Air Volume (VAV) system. 132 test coils over four climates and a variety of system characteristics showed a 79.7% correct identification rate.

Simulations were performed to test the various control logics against a newly derived logic derived from this non-linear regression. On the performance metrics of Pumping Power to Cooling Power Ratio as well as Pumping Power to Thermal Discomfort Ratio, the new advanced control logic showed promise as being the optimal control strategy, particularly in CAV coils.

Acknowledgments

I want to thank my wife Kristen, who has supported me for many years in pursuing my goals and dreams. Thank you to my parents for all the many opportunities you have provided me and love you have shown me. A special thank you to my advisor Dr. Gregor Henze and Belimo's Forest Reider, Stefan Mischler, and Dr. Marc Thuillard for your continuous assistance, guidance and support throughout this whole process.

Table of Contents

Acronyms and Abbreviations

AFLV	Automatic Flow Limiting Valve		LMHD	Log Mean Enthalpy Difference
AHU	Air Handling Unit		LMTD	Log Mean Temperature Difference
°C	Celsius		m	Meter
CAV	Constant Air Volume		m^2	Square meters
CHW	Chilled Water		mA	Mass flow rate of air
CHWR	Chilled Water Return		min	Minute
CHWRT	Chilled Water Return Temperature		MIT	Massachusetts Institute of Technology
CHWS	Chilled Water Supply		mW	Mass flow rate of water
CHWST	Chilled Water Supply Temperature		m^*	Capacitance Ratio for Dehumidifying Coils
C_{max}	Maximum Capacitance Rate		NCAR	National Center for Atmospheric Research
C_{min}	Minimum Capacitance Rate		$NMBE$	Normalized Mean Biased Error
c_{pw}	Specific heat of water		NTU	Number of Transfer Units
c_s	Effective Specific Heat		NTU^*	Number of Transfer Units for Dehumidifying Coils
CV	Coefficient of Variation		PI	Proportional Integral
C^*	Capacitance Ratio		PID	Proportional Integral Derivative
DAT	Discharge Air Temperature		PP	Pumping Power
Delta T	Water-side temperature difference		Q	Cooling Power (Capacity)
DOF	Degrees of Freedom		$Q_{max,s}$	Maximum Sensible Cooling Power
ϵ	Effectiveness		Q_s	Sensible Cooling Power
EP	EnergyPlus		R&D	Research and Development
$FPMC$	Fraction of Predicted Maximum Capacity		RAT	Room Air Temperature
ft	Feet		sec	Second
ft^2	Square feet		SHR	Sensible Heat Ratio
GUI	Graphical User Interface		SSE	Sum Squared Error
h	Enthalpy		T_{ai}	Inlet Air Temperature
h_{ai}	Inlet Air Enthalpy		T_{ao}	Outlet Air Temperature
h_{dewpt}	Enthalpy of Saturated Air at Inlet Air's Dew Point		T_{dewpt}	Dew Point Temperature of Inlet Air
hr	Hour		T_n	Integral Action Time

HVAC	Heating Ventilation and Air Conditioning		T_p	Oscillation Period
$h_{w,sat,i}$	Enthalpy of Saturated Air at Inlet Water Temperature		T_v	Derivative Action Time
IDF	Input Data File		T_{wi}	Inlet Water Temperature
ISE	Integral Squared Error		T_{wo}	Outlet Water Temperature
J	Joules		T_{wr}	Mass flow rate weighted, return water temperature
K	Kelvin		μ	Mean cooling capacity
k_1	Maximum capacity		UA	Overall Heat Transfer Conductance
k_2	Exponential curvature		UA_{wet}	Overall Mass Transfer Conductance-Area Product
K_d	Derivative action coefficient		VAV	Variable Air Volume
kg	Kilogram		VFD	Variable Frequency Drive
kPa	KiloPascal		$w(t)$	DAT setpoint as function of time
K_i	Integral action coefficient		W_{ai}	Inlet Air Humidity Ratio
K_p	Proportional action coefficient		x	Observed capacity
K_{pcrit}	Critical *Kp*		X_p	Proportional Band
L	Liters		y	Predicted capacity
L	Width of cooling coil		$y(t)$	Measured DAT temperature as function of time

List of Tables

List of Figures

1. Introduction

Energy conservation has become a popular point of discussion in recent years. Rising energy prices coupled with the onset of climate change, has resulted in the implementation of stricter energy codes and added pressure on engineers to rethink the way society utilizes its energy. Buildings account for 41% of the United States' energy use (Mitchell and Braun, 2012). 16% of that is utilized by the systems in which we use to cool those buildings (Mitchell and Braun, 2012). Those systems include the chillers, pumps, cooling coils and associated control valves as well as the fans used to push the cool air onto occupants and process loads.

Chiller, pump and fan efficiencies have all improved over the years. One area of untapped potential for reducing energy consumption in chilled water (CHW) systems is the mitigation of what is known as Low Delta T Syndrome. This is the presence of a lower than design temperature difference between the chilled water supply (CHWS) and the chilled water return (CHWR). Numerous inefficiencies in a cooling system result when Low Delta T persists. Chiller efficiency is degraded due to lower evaporator temperatures. Depending on the system configuration and controls strategy, additional chillers may be prematurely brought online or the CHWR mixed with the CHWS. In the case of mixing CHWR with CHWS, higher than designed chilled water supply temperatures (CHWST) result which diminishes the potential cooling power of a cooling coil. This compromises the thermal comfort of building occupants. Perhaps the largest impact of Low Delta T Syndrome is the increase in pumping power. To illustrate this, Equation 1 below is presented as it describes the heat transfer occurring at a cooling coil.

$$Q = mW\, c_{pw}(Delta\ T) \qquad \text{Eqn. 1}$$

where Q is the cooling power, mW is the mass flow rate of chilled water, c_{pw} is the specific heat of water and $Delta\ T$ is the water-side temperature difference.

The components of a cooling system are designed for a constant *Delta T*, typically between 6 and 8 K. Assuming the Delta T stays at its design value and changes in c_{pw} are negligible, a linear relationship between cooling power (Q) and water flow (mW) exists. However, as discussed above, the Delta T does not stay constant. Due to a variety of causes as will be discussed in detail in the Literature Review, the Delta T often falls well below its design value. Thus, for a system to achieve the same amount of cooling power out of 5 K Delta T system that it would get out of a 7 K Delta T system, the water flow rate would need to increase by 40%. As Delta T decreases, there is substantial rise in water flow rate which means an even more substantial rise in pumping power. The theoretical relationship between pumping power (PP) and flow rate (mW) comes from the pump affinity laws.

$$PP \propto mW^3 \qquad \text{Eqn. 2}$$

As can be seen in Equation 2, if the flow rate is increase by 40%, the pumping power is increased 174.4%. PP is not only the power consumed, it is the power the building owner pays for. The actual exponent in Equation 2 is more on the order of 2.2 when accounting for typical pump efficiency curves, but the potential for energy and utility bill savings remains substantial. In scenarios where a building user purchases chilled water from a local utility, the owner will still be penalized as utilities often charge higher rates per ton-hour when the building's return water temperature is too low (Moe 2005). The same holds true for many district heating plants, where a maximum return water temperature is required.

The resultant Delta T across a cooling coil is dependent on numerous factors, namely the inlet water temperature (T_{wi}) and flow rate (mW), the inlet air temperature (T_{ai}), air flow rate (mA) and humidity ratio (W_{ai}), as well as the geometric parameters of the coil itself. The actual relationship between cooling power and water flow rate is not linear at all, but closer to the

exponential relationship shown in Equation 3 (Reider, 2012; Thuillard *et al.,* 2014; Bellucci, 2012; Buchanan, 2012).

$$Q = k_1(1 - e^{-k_2 mW}) \qquad \text{Eqn. 3}$$

where k_1 is the maximum cooling capacity attainable and k_2 is the exponential curvature. Such a relationship is most clearly shown when mA, T_{ai}, W_{ai} and T_{wi} are held constant as is graphically depicted in Figure 1.

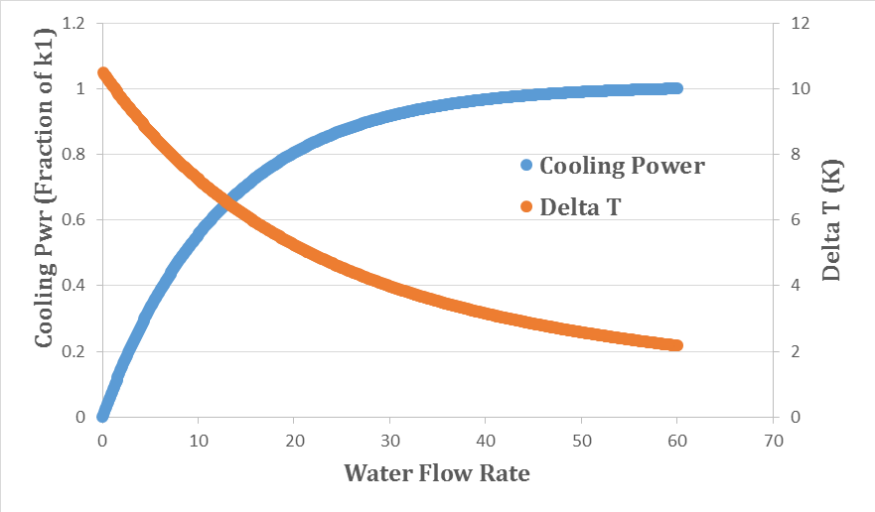

Figure 1: Exponential Behavior of Cooling Coils.

As the slope of the line becomes more and more horizontal, the water-side Delta T across the coil is diminishing. There comes a point where the amount of additional cooling power the system provides with an increase in mW is negligible compared to the amount of additional pumping power required. When this occurs, it is said that the coil has been pushed into the saturation region. Identification of when such saturation is occurring is made difficult when fluctuations are occurring in the inlet water temperature, inlet air temperature, inlet air humidity ratio and in the case of VAV systems, the mass flow rate of air. Figure 2 shows actual coil data taken

from a coil located on the campus of Massachusetts Institute of Technology (MIT) where fluctuations to such inlet parameters are present.

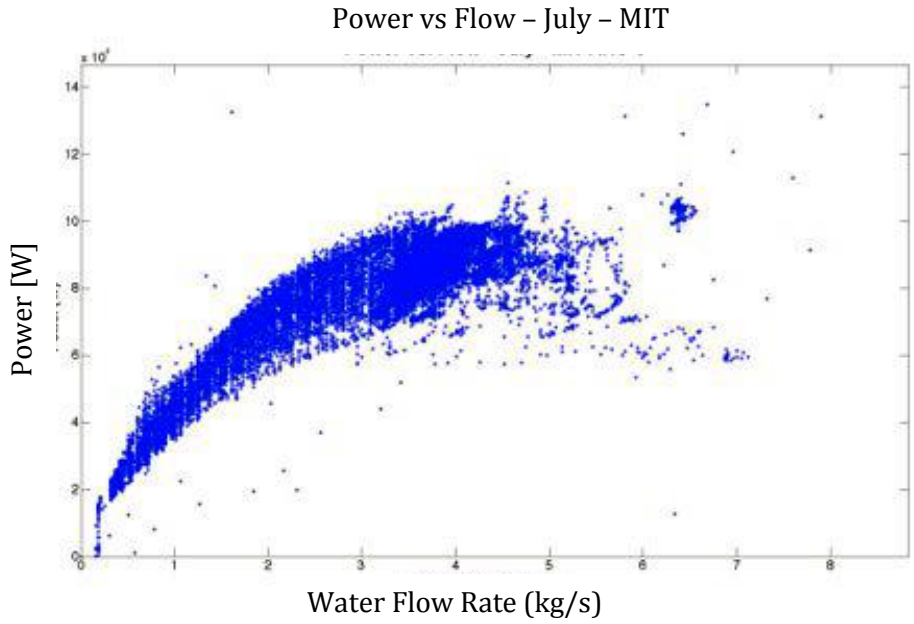

Figure 2: Actual cooling coil data (Bellucci, 2012).

Large strides toward creating more energy efficient cooling systems will come from identifying when such saturation is occurring and performing mitigation measures to reduce the water flow rate during those instances. Conventional chilled water control valves do not have the capabilities to identify saturation nor do they follow a control sequence which allows for such restriction.

The Energy Valve™ by Belimo does maintain those capabilities however. The Energy Valve™ is an intelligent, pressure independent, two-way, equal percentage control valve. It consists of a controller and actuator, feedback wiring to allow for an analog control signal to track on a discharge air temperature (DAT) setpoint, inlet and outlet water temperature sensors, and a magnetic flow meter. Additionally, it contains several microprocessors for use in the analysis of data for saturation detection, maintenance investigation and implementation of advanced control strategies. It also has a built in web server which allows for remote upload of new control

strategies for already installed valves. The Energy Valve™ is currently on the market and its success has been documented as will be discussed in the Literature Review. This body of research is dedicated to further improving future generations of the valve's performance and potential for energy savings. With the valve relatively new to the marketplace, coupled with the difficulty in attaining logged data from building operators who maintain such valves, there is a lack of sufficient data available to aid in the development of more refined control strategies that identify and mitigate saturation. Hence, the first goal of this body of research is to develop a methodology to produce realistic, surrogate coil data for a variety of climates through energy simulations alone.

Currently, three advanced control strategies exist for the Energy Valve™: Flow Limiting, Delta T Limiting and Flow/Delta T Limiting. As will be described in more detail in the Literature Review, the performance of the coil to both save on pumping energy and not prematurely restrict cooling capacity to system depends heavily on what input parameter fluctuations (T_{wi}, T_{ai}, W_{ai} , or *mA*) are dominating the coil's performance (Thuillard *et al.*, 2014). It can be expected that the optimal selection of these three advanced control strategies will depend on whether the coil serves a CAV system, or a VAV system. Thus, the second goal of this research is investigating if the Energy Valve™ can determine by itself which type of system it serves. This determination would need to come from evaluation of water-side data alone, as that is the only data logged by and available to the Energy Valve™. Such an ability to determine the type of system will avoid installation input error which could result in an inappropriate selection of the optimal advanced control strategy.

Additional insight from Thuillard *et al.* (2014) is that various combinations of input parameter fluctuations will occur from climate to climate. The third goal of this research is then to investigate if an optimal control strategy for each combination of climate, application (CAV or VAV) and facility priority (thermal comfort, energy savings etc.) can be identified. Such testing will be performed with existing advanced control strategies identified above, as well as a new strategy developed during this research.

2. Literature Review

This Literature Review is split into three parts. First, a review of Low Delta T Syndrome is conducted to investigate its causes, effects and mitigation procedures. Next, focus will be put on how some of the causes that inherently stem from the cooling coils can be addressed with the advent of the intelligent control valve, named the Energy Valve™. Lastly, a brief description of the coil model used for generation of surrogate data in this research is given.

2.1. Low Delta T Syndrome

The scenario of Low Delta T Syndrome is well documented (Taylor, 2002; Fiorino, 1996 and 1999). Possibly the most thorough explanation of the impacts, causes and mitigation techniques for Low Delta T Syndrome is described in Taylor (2002). The paper identifies the two most common chiller staging strategies for primary/secondary systems and how each strategy is susceptible to increased net energy usage when the chilled water system is experiencing Low Delta T.

2.1.1. Chiller Staging Logics

A flow based approach for a chiller staging logic operates in a manner to keep the primary flow always larger than secondary flow, thus the flow direction in the common pipe (labeled “crossover decoupler") in Figure 3 below should always be downward. When flow is sensed to be in the opposite direction, this indicates to the chiller that increased secondary loop flow is due to increased cooling requirements on the secondary loop’s loads. A second chiller and associated primary pump will be staged on. When Low Delta T is present in the system, it is apparent from Equation 1 that higher flows will be present in the secondary loop, which in turn will set in motion the staging of additional chillers and primary pumps when the initial operating chiller has not reached its maximum capacity. The resulting use of multiple chillers at part load not only increases

primary pumping energy consumption, but the operating efficiencies of the chillers will be much lower than if the chillers were fully loaded.

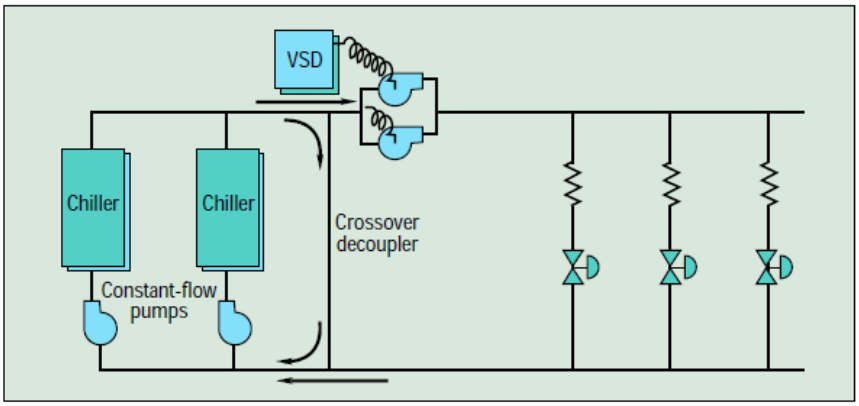

Figure 3: Typical primary/seconding piping configuration for a chilled water system (Kirsner, 1996).

A load based staging logic senses the chilled water return temperature (CHWRT) coming back to the chiller from the secondary loop. When the CHWRT exceeds a prescribed limit, a second chiller with corresponding primary pump will stage on to ensure adequate CHWST is available for the secondary loop. When secondary loop loads are increased, the secondary pumps will push more flow to meet those loads. If a Low Delta T scenario is occurring, supplemental chillers will not stage on as the CHWRT will not exceed its prescribed threshold (i.e. CHWST setpoint plus design water-side Delta T). This would then allow for flow in the direction from the CHWR to the secondary pumps through the common pipe leg. The mixing of the two streams would increase the secondary loops CHWST. A warmer CHWST decreases the coil's performance which results in even lower water-side Delta T across the heat exchanger. Decreased Delta T means increased flow, and subsequently the entire chain of events spirals out of control. The net impacts of Low Delta T Syndrome on this staging configuration is not only increased secondary pumping power, but the inability of the system to recognize a high load scenario and subsequently those loads will not be met and occupant thermal comfort will be compromised.

2.1.2. Causes of Low Delta T

Taylor (2002) further classifies the various causes of Low Delta T Syndrome as those which can be avoided, those which can be reduced but at the sacrifice of energy consumption and those which cannot be avoided, but may be mitigated. The causes which can be avoided are mostly attributed to ignorance on the part of the engineer, contractor and facility managers. One cause is that often unattainable supply air temperature setpoints are programmed into the control sequence as a quick fix to thermal discomfort complaints from building occupants. However, the decreased cooling performance is most likely attributed to air side limitations such as undersized ductwork and fans. When the water-side Delta T reaches a point in which coil capacity is so reduced that supply air temperature setpoints are unable to be met, the fan speed in a VAV system will ramp up, further increasing the building's energy costs (Moe 2005).

Excessive use of three way valves in variable flow hydronic loops allows for short cycling of chilled water, which will in turn decrease the CHWRT (Taylor, 2002). These valves are often installed without the required balancing valve on the bypass line, thus a lower pressure drop in this bypass line will further increase the amount of CHWS being directly transported to the CHWR pipe. This increased flow would drive up pumping requirements as well.

Cooling coils themselves have been found to be installed backwards exhibiting a parallel flow arrangement in place of the more effective counter flow arrangement (Taylor, 2002). This decreases the coil's performance and the attainable water-side Delta T.

Improper coil and accompanying control valve selection often contributes to Low Delta T as well (Taylor, 2002). The specification of a lower design water-side Delta T across the coil when compared to the primary plant's design Delta T is often due to a lack of communication between various entities working on the chilled water distribution system. The installation of oversized

chilled water control valves takes away from the system's ability to control to a prescribed supply air temperature setpoint.

Simple oversights in the sequence of controls can have devastating effects on water-side Delta T as well. The absence of a "proof of life" signal from the air side supply fan to the chilled water control valve will entice the valve to operate fully open to meet a supply air temperature setpoint when the fan is not in use (Taylor, 2002). That setpoint will not be attained without any air flow however, and essentially a short circuit occurs across the coil with a negligible Delta T resulting. This type of short cycling has higher pressure losses than those accompanied with short cycling through a three way valve, further adding to the net energy consumption. Improper control strategies on a tertiary pumping sequence and the lack of control valves on process loads also can lower a CHW system's Delta T, but will not be discussed in detail in this Literature Review.

Though not a major contributor to Low Delta T, implementation of water-side laminar flow in coils in an effort in minimize water-side pressure drops can drastically reduce the coil's effectiveness due to increased convective resistance on the inside of the coil's tubes (Taylor, 2002).

The implementation of a CHWST reset schedule to maximize the efficiency of the chiller plant's performance at times will promote an increase in net energy consumption. This is due to the decreased effectiveness of cooling coils at higher inlet water temperatures and the resulting increase in pumping power requirements to make up for the subsequently lower water-side Delta T. Taylor states an increase of 6°F (3.33 K) in CHWST will increase flow by 76% and decrease Delta T by 56%. Zhang (2012) also proved through extensive simulation that such a reset schedule with higher T_{wi} during low load periods drastically decreases water-side Delta T, at times by 3 K. Both lowering the design water flow rate or implementing a CHWST reset schedule may in some instances provide energy savings, but results are system specific and would need to be analyzed through energy simulation on a case by case basis.

The last two identified causes of Low Delta T according to Taylor (2002) are ones that cannot be avoided, but mitigated. Coil fouling on the either water or air side in addition to decreased air flow due to the dirtying of the air filter reduces the performance of a cooling coil. Proactive maintenance programs can mitigate such effects. Additionally, the use of Dedicated Outdoor Air Systems (DOAS) and air side economizers create a challenge for a coil to maintain a high water-side Delta T. Both provide opportunity for ample energy savings during times of favorable outdoor air conditions, but the thermal potential for the coil to raise the water temperature to the design limit is diminished with such lower inlet air temperatures. For example, if small amounts of cooling is needed to bring entering air at 58°F down slightly to the supply air setpoint and the design CHWRT is 60°F, the second law of thermal dynamics will prevent this water from achieving such a temperature. Zhang (2012) demonstrates through coil simulation that the use of an economizer will result in lower water-side Delta T on the order of 1 K during low load scenarios.

2.1.3. Addressing Low Delta-T

Taylor (2002) argues that even with attention being paid to all the previously outlined causes of Low Delta T, it will still exist. His proposals for accommodating such a system to mitigate its net impacts include the use of variable speed chillers, primary only pumping systems, the addition of a check valve in the common leg of the primary/secondary piping loops, unequally sized chillers to allow for higher chiller efficiencies in a host of operating scenarios and lastly, having a lower design Delta T on the primary equipment compared to the secondary equipment which would allow for proper chiller staging even in the occurrence of Low Delta T. Further investigation into variable speed chillers and primary only pumping is conducted below.

The traditional primary/secondary configurations with constant speed primary pumps that exacerbates Low Delta T Syndrome at part load conditions comes from central heating plants

requiring higher return temperatures to avoid condensation (Henze & Floss, 2011) and to maintain primary equipment minimum flow requirements (Kirsner, 1996). With the advent of condensing boilers for heating applications and variable speed chillers for cooling applications, the necessity of this system configuration is now questioned as it degrades the performance and increases overall energy consumption.

Kirsner (1996) discusses in further detail the limitations of classical primary/secondary pumping configurations seen in the industry to deal with Low Delta T. Traditionally, constant flow in the primary loop was required for the chillers. This is primarily due to the inherent slow response time of chillers' pneumatic controls to load fluctuations. If the load seen by the constant volume chiller is instantaneously decreased by 50%, flow in the common leg from the CHWS to the CHWR would occur to make up for the reduction of secondary flow returning to the chiller. This excess flow through the common leg in the piping configuration would drop the CHWRT (halving the Delta T initially seen) through the blending of the CHWR and the short-circuited CHWS. With pneumatic controls, it would take some time before the chiller to dial back its outputted capacity and the CHWST leaving the chiller would drop a bit. Decreased efficiencies of the chiller with the now colder evaporator temperature would prevent the CHWST from dropping an equal amount to the drop in CHWRT, however. The same chiller in a variable primary flow configuration would see the reduction in load through the reduction in flow to the chiller. In this scenario, the CHWRT would remain the same and degrading efficiencies of the chiller due to a lower evaporator temperature would not be realized. If the chiller is operating at full capacity, in the moments after an instantaneous load reduction, the CHWST leaving the chiller would drop significantly (twice the original Delta T across the chiller could theoretically be realized). The resultant CHWST coming from a load reduction in a variable flow scenario would be lower than in a constant flow scenario. As the CHWST approaches freezing, the chiller may be tripped off to prevent the freezing in the

evaporator. This tripping off may be performed prematurely with older pneumatic controls, thus the scenario was traditionally avoided by the use of constant flow chillers.

The advent of direct digital controls (DDC) has provided more responsive capacity controls for chillers. Kirsner (1996) details the additional advancements that DDC provide in the control logic for the low evaporator temperature shutoff. For example, Trane Inc. uses a microprocessor which determines the risk of freezing through an algorithm that looks at how long and to what extent the discharge water temperature leaving the chiller falls below freezing. With these new control capabilities, Kirsner advocates for the introduction of a variable frequency drive (VFD) to the primary pumping loop. In many scenarios this could lead to the elimination of secondary pumps. Such a configuration would prevent excess short cycling of CHWS to the CHWR and with only one set of pumps, the efficiency of the pumps could be higher and the amount of overall chilled water flow reduced. An additional benefit is the pumps could be oversized to allow for more flow to be pushed through a single chiller when Low Delta T is encountered, as opposed to the premature staging of an additional chiller and corresponding primary pump which occurs in the classical constant volume primary loop configuration. This would eliminate added energy consumption that comes with the staging on of additional chillers and primary pumps when the current chiller is not entirely loaded.

The use of variable speed chillers can also aid in energy saving during periods of Low Delta T. Variable speed chillers typically do not have their chiller efficiencies drop off until below 20-25% of full capacity, compared to efficiency degradation in fixed speed chillers starting around 40-50% of full capacity (Taylor Engineering, 2009). Correct staging of chillers to achieve energy performance is not as high of a concern in such variable speed chiller plants, as three chillers loaded at 30% capacity often use less energy than one chiller at 90% capacity (Taylor Engineering, 2009). Moreover, premature staging of additional chillers is not of concern in this scenario as it is often more efficient to stage the chiller earlier than to play catchup (Taylor Engineering, 2009).

2.1.4. Focus on the Cooling Coil's Contribution to Low Delta T

As previously described, there are numerous causes of Low Delta T Syndrome throughout hydronic systems. Focusing solely on some of the causes for Low Delta T that occur at the terminal units themselves, Henze and Floss (2011) attempted to quantify and rank the effects of four such causes: hydraulic network imbalances, control valve oversizing, incorrect inherent valve characteristics and control loop parameters. Their established metric for such rankings was in the form of an average, mass flow rate weighted, water return temperature (T_{wr}) as seen in Equation 4 below.

$$T_{wr} = \int_0^t T_{wo}(t) mW(t) dt \; / \; \int_0^t mW(t) dt \qquad \text{Eqn. 4}$$

where T_{wo} is the exiting water temperature and mW the water flow rate at given time.

Their investigation was done by the formulation of a two-circuit hydronic system model which included six fan coil units in a heating application. The model coupled pressure-flow relationships with provided thermal loads. The fan coil units were controlled with proportional integral (PI) controllers. Hysteresis effects and control valve slew rate limitations were also incorporated. The system was simulated for a heating application, but the results shed insight into cooling applications. As noted by the authors, "the causes for high return water temperatures in central heating systems are the same as low return water temperatures in chilled water systems" (Henze & Floss, 2011). Simulations found all investigated situations resulted in degrading water-side Delta T. The order of severity being: the inherent characteristic and size of the control valve, the quality of hydraulic network balancing, and control loop parameters. The collective results of these four shortcomings of a hydronic system was a Delta T reduction of 6°C, which has been found to increase primary pumping energy consumption by 4-12% (Wirths, 2008).

Fiorino (1999) details 25 best practices for achieving higher Delta T in hydronic cooling systems. He identifies Low Delta T as any water-side temperature difference below 5.6°C. The paper focuses on the terminal loads (cooling coils) as the major culprits for Low Delta T Syndrome. Using a case study from the NASA Johnson Space Center, the paper states that doubling the chilled water flow rate from that of design would only produce an additional 15% in cooling power, while decreasing the water-side Delta T by 40%. The scenario of excessive water flow being available to a coil during times when the supply air temperature setpoint is not being achieved is all too common and is a major contributor to Low Delta T Syndrome. His recommendations to achieving higher water-side Delta T across cooling coils range from coil selection (i.e. choosing a higher design Delta T than the primary plant), to controls selection (i.e. actuator shutoff ratings should include a 50% safety factor to prevent leak-by), to piping configurations (e.g. allowing process loads requiring lower CHWS temperatures to be located after comfort cooling coils). One deviation in the recommendations here from Taylor (2002), is that Fiorino (1999) advocates for a CHWST reset schedule as it will allow for higher CHWRT and preclude laminar flow regions from developing in the cooling coils during low load periods. The latter of which would decreases the coil's heat transfer coefficients. Taylor (2002) would argue this would increase pumping power due to the higher flow rates during times of higher CHWST. It is obvious a tradeoff between the benefits and drawbacks of such a strategy would be system specific as well as depend on the parameters of the reset schedule itself. The net energy consumption would need to be modeled on a case by case basis to correctly identify the most optimal balance.

Wang *et al.* (2013) utilized a cooling coil model that had been calibrated to a real world coil for use in Low Delta T fault detection. Their method compared simulated water-side Delta T's to actual measured data based on of binned outdoor air conditions (dry bulb and wet bulb temperatures). Such comparisons could identify when the real world coil was operating worse than predicted.

The Wang study also investigated the effect of laminar flow on coil degradation. Though increased water-side film resistances are seen by the system when a laminar flow scenario is realized, the added time period for the water to stay within the coil increases the heat taken in by the water, effectively offsetting any major downfalls of an increased film resistance.

The Wang study performed parametric runs of the model with varying DAT setpoints and compared such results to the measured data. Lower DAT temperatures resulted in lower Delta T, which confirms Taylor's explanation that too low of discharge air temperature setpoints can degrade a coil's performance and Low Delta T can prevail.

Further analysis of the effect of economizers on cooling coil performance was conducted (Wang *et al.*, 2013). Lower mixed air temperatures reduce the driving potential of the cooling coil and can subsequently reduce water-side Delta T. However, it is in this author's opinion that for the majority of the time, overall energy savings will occur due to the decreased cooling load on the system, despite the fact the coil may not be operating ideally.

2.2. Pressure Independent Control Valves

2.2.1. Introducing the Energy Valve™

The focus of this research is on mitigating the causes of Low Delta T Syndrome that occur at the terminal units, in our case the cooling coils. The Energy Valve™ is an intelligent, pressure independent, two-way, equal percentage control valve specifically designed to combat Low Delta T.

2.2.2. Balancing Discussion

Another potential benefit of the Energy Valve™ is the drastic reduction in time for the balancing of the complex hydronic systems it is installed on. Typical manual balancing operations for complex hydronic systems are highly labor intensive, and often require several iterations of

adjustments to each coil's throttling valve before design specifications are met. Improper balancing can lead to unwanted fluctuations in water flow rates when disturbances elsewhere in the system create pressure fluctuations in the CHWS piping. Such an example would be that the shutting off of other coils due to reduction in loads would initially drive up the supply side water pressure and increase flow to the coils remaining open. These fluctuations reduce the controllability and performance of the system and are only detected in deviations from the DAT setpoint, and also contribute to Low Delta T Syndrome as is shown in the Floss and Henze (2011) study.

Taylor & Stein (2002) evaluated seven of the most common design techniques used for balancing large commercial buildings. Though six of the seven techniques analyzed in the article resulted in the elimination of the post-construction balancing process, only one of those six options was shown to truly eliminate flow variability due to pressure fluctuations in dynamic hydronic systems, such as a CHW distribution system. That option included the use of automatic flow limiting valves (AFLV) in lieu of the typical, manually adjusted throttling valves. This option not only eliminated the need for a post-construction balancing effort, it also allowed for coils to be added or subtracted from the system without negatively affecting the performance of exiting coils. This option of using AFLVs was not recommended however, due to the increased costs. These valves would be installed in addition to the control valve, two isolation valves and a required strainer.

The Energy Valve™ maintains the capabilities of the AFLV without the need for an additional control valve. Pressure independent control valves allow the water flow rate to be the manipulated variable when attempting to track the DAT setpoint (control variable). This would curb any unintended increase in flow due to pressure fluctuations which would result in a decrease in water-side Delta-T.

2.2.3. Non-intelligent Pressure Independent Control Valve Case Studies

The advent of high performance, pressure independent control valves allows for the possibility of buildings attached to a district cooling system to forego the use of a building pump (Moe 2005). Additionally, removing the decoupling bridge that would accompany such a building secondary pump, would prevent blending of CHWR with CHWS, which decreases coil performances as well as water-side Delta T. Higher inlet water temperatures, better flow control, reduced pumping and fan power can all be benefits when this strategy is employed. Moe (2005) evaluated the benefits of removing such building pumps and retrofitting with pressure independent (non-Energy Valve™) control valves on a building designed for a 2,460 kW cooling load, 37,760 L/s air flow rate, 1.5 kPa air side pressure drop and 71 L/s design water flow rate. The savings were climate dependent, but were estimated between $40,000 and $160,000 annually (Moe 2005).

Installation of 62 such pressure independent control valves (non-Energy Valves) at Building 42 at Eglin Air Force Base, FL in conjunction with VFDs being installed on the secondary pumping arrangement accounted for an estimated 30% reduction in building energy consumption (HPAC, 2007). That is substantial savings with valves designed to curb the effects of hydronic system pressure fluctuations. The added capabilities of the Energy Valve™ have potential for even better benefits when used in building retrofits, as detailed below.

2.2.4. Energy Valve™ Case Studies

Several cases studies highlighting the performance of the Energy Valve™ in mitigating Low Delta T Syndrome exist. Henze *et al.* (2013) retrofitted five Air Handling Units (AHU) at Massachusetts Institute of Technology's (MIT) Hayden Library. The building-wide average water-side Delta T for a prescribed period in 2011 was found to be 3.42 K. The same time frame in 2012, after installation of the Energy Valves, recorded an average water-side Delta T of 6.74 K. The

curtailment strategy used by all five Energy Valves was Delta-T Limiting, which restricted water flow when water-side Delta T fell below 6.67 K.

The MIT Energy Valve™ retrofit further demonstrated that coils can be found to operate better than design with proper control of its chilled water flow. Several of the coils were designed for water-side Delta-T's much smaller than realized after the retrofit (Henze *et al.*, 2013; Belimo, 2011). If such retrofits were performed campus wide, the Manager of Sustainable Engineering and Utility Planning at MIT, Peter Cooper, estimates an annual savings of $1.5M (Belimo, 2011). He further notes the potential for savings is even higher due to the new found ability to squeeze more cooling capacity from the existing chilled water plant. Future expansion of the district cooling system may now not need additional chillers.

The University of Miami's Leonard M. Miller School of Medicine is served by a 47,000 ft^2, 12,000 ton central chilled water plant that was experiencing far less than design water-side Delta T. The 300,000 ft^2 Clinical Research Building served by this plant was only eight years old, but experiencing an average water-side Delta T of just 7°F. Installation of the Energy Valve™ on its 175 ton chilled water coil brought the water-side Delta T from 3.5°F to 6.5°F within its first hour of operation, and brought the eventual running average water-side Delta T to over 10°F (Belimo). Such initial success prompted the university to install eleven more Energy Valves in its 450,000 ft^2 Rosenstiel Medical Science Building. Average building water-side Delta T was found to rise from 7-8°F to 10.5-11°F. Estimated utility cost savings for that building of $60,000 annually have the potential for a four year simple payback.

2.2.5. Energy Valve™ Research at University of Colorado Boulder

Substantial research on the Energy Valve™ has been performed at the University of Colorado Boulder in conjunction with Belimo Inc. Buchanan (2012) attempted to quantify the cost savings in pumping power due to the added benefits of pressure independence and the Delta T

Limiting curtailment strategy of the Energy Valve™ through energy simulation alone. EnergyPlus was utilized for a 14 hour simulation with weather inputs approaching that of cooling design day conditions. Various combinations of chiller performance and ambient conditions were found to have between 2.6% and 3.6% in secondary pump cost savings when implementing the Energy Valve™. Buchanan notes that real world results are expected to be higher as the hydronic network modeled in EnergyPlus was inherently more balanced than that typically seen in the field. Additionally, the coil used in the simulation was quite oversized and the coil was not thoroughly pushed into its saturation region as can be seen in the capacity (Q) versus water flow (mW) plot of the simulated day in question.

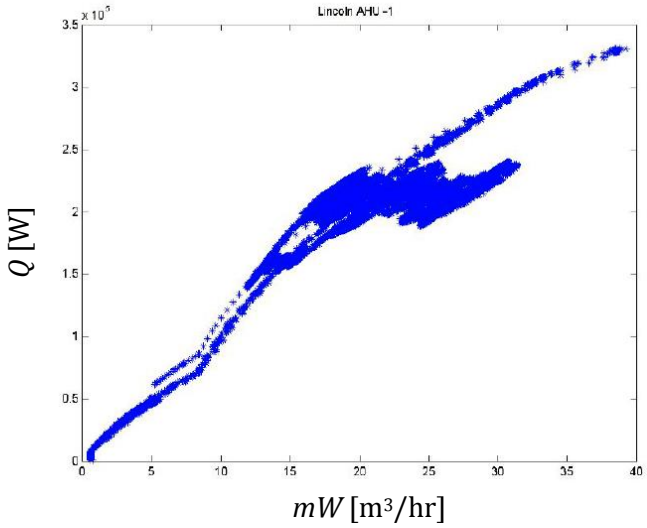

Figure 4: Model coil performance in EnergyPlus (Buchanan, 2012).

The coil was obviously quite oversized for the system it was serving as its performance curve remained quite linear. This is due to numerous, default oversizing factors EnergyPlus has in its cooling coil model methodology. Part of this particular body of research reexamines this behavior and attempts to more appropriately induce saturation in modeled cooling coils. The methodology of producing surrogate data through energy simulation software for further analysis

and development of the Energy Valve's control logics laid out by Buchanan set the foundation for which this research was built upon.

Bellucci (2012) took measured Energy Valve™ data and derived a calibrated model from that data. He was then able to perform parametric investigations to identify the effects that changing input parameters have on a coil's performance. The cooling coil model was developed in Matlab-Simulink and calibrated to the measured data from Energy Valves located at both MIT and the University of Colorado at Boulder. Those models were then used to perform isolated parametric runs to investigate the effects on inlet water temperature (T_{wi}), inlet air temperature (T_{ai}), inlet air humidity (W_{ai}) and air mass flow rate (mA) on the coil characteristics. Saturation curtailment strategies of Delta T Limiting and Flow Limiting were also investigated. A tool for facility managers was developed in Excel to aid in the characterizing of coil data attained by the Energy Valve™ and provide curtailment setpoints. One setpoint was provided that would optimize energy performance and an additional, more conservative setpoint was provided that would make occupant thermal comfort the priority. A procedure was further detailed on how to perform real time coil characterization based off Energy Valve™ recorded data. An estimated coil capacity would then be derived and the implementation of a curtailment strategy performed.

There lays a potential for the Energy Valve™ to restrict flow prematurely and thus hold back considerable cooling capacity from the system. The Energy Valve's ability to perform curtailment strategies only when periods of saturation occur will depend on the accuracy of a prediction as to when true saturation is occurring. As found in the available field data and detailed in the Bellucci (2012) report, fluctuations in input parameters effect the shape of the coil curve and thus the k_1 and k_2 coefficients in Equation 3 that define it. In an effort to accurately predict the coil's performance, and whether or not it is operating in saturation and curtailment should be implemented, Reider (2012) developed a methodology to predict the k_2 coefficient of the curve in which the coil was operating in without the need for storing large amounts of time series data. A basis spline approach

was used to develop a knot vector with assigned knot values for the observed data, which in turn was used to perform least squares regression through logarithmic transformation to produce the predicted *k* coefficients. This method requires minimal computational power and will serve well in limiting the amount of hardware the Energy Valve™ would need to perform such analysis.

This approach allowed for *k* coefficients prediction to occur to within 2.5% of values derived from several months of data. Errors in maximum predicted capacity (k_1) were found to be within 12 and 16% for real world data and surrogate data from energy simulations, respectively.

Thuillard *et al.* (2014) extrapolated on the work of Bellucci (2012) by investigating the performance of three advanced control strategies. The application of Flow, Delta T and Flow/Delta T Limiting strategies were investigated through use of a coil in Matlab capable of computing coil capacities for completely wet, completely dry and partially wet/partially dry coil scenarios (Brandemuehl *et al.*, 1993). Isolated parametric runs were performed to see how each of these strategies compared in a host of varying input parameters, namely T_{ai}, T_{wi}, mA, and W_{ai}. The optimal strategy was defined as the one which "most closely maintains the normalized capacity limit while exceeding the minimum acceptable coil performance" (Thuillard *et al.,* 2014). It was discovered that for fluctuating inlet water and air temperatures, the Flow Limiting strategy prevailed as the superior case. For fluctuating mA and W_{ai}, Delta T Limiting was superior. In all scenarios, the Flow/Delta T limiting strategy came in second on the superiority scale and would be the suggested strategy for applications which experience deviations in all of the investigated input parameters.

2.3. Coil Models

Coil modeling for use in investigating coil performance as well as quantifying the causes and effects of Low Delta T Syndrome has been performed extensively, some of which research is described previously in this section (Henze & Floss, 2011; Bellucci, 2012; Moe, 2005, Wang *et al.*, 2012; Zhang *et al.*, 2012). The bulk of the research conducted in this report included the

production of cooling coil data through energy model simulations as well, and then the subsequent analysis of that data. A brief explanation of the cooling coil model used for the production of climate specific surrogate data in this report is described here for reference.

The potential for both sensible and latent heat transfer in cooling coils and the complex geometries these coils maintain can make estimation of cooling power difficult. Elmahdy and Mitalas (1977) developed a steady state model for dehumidification coils that has been a foundation for numerous succeeding models. Their model incorporated their proposed methodology of classifying a cooling coil as completely wet, completely dry or as partially wet/partially dry based of known inlet water and air states, as well as coil geometry. Once the classification was made, in the case of a partially wet/partially dry coil, an iterative process was performed to determine the fraction of wet versus dry coil surface areas. Their resultant model was tested against experimental results from four and eight-row cooling coils. Model estimation of total cooling capacity fell within 4% of experimental results. A slightly modified version of their model that allows for convergence in a larger set of geometric inputs has been incorporated into EnergyPlus as the model Coil:Cooling:Water:DetailedGeometry (Dept. of Energy, 2012). This was the model used for the data generation and resultant data analysis in this report.

3. Methodology

3.1. Program Selection

3.1.1. EnergyPlus

The US Department of Energy's EnergyPlus (EP) software is free for download and is a widely used energy simulation engine by professionals for building performance (EnergyPlus). It is highly robust and trusted with a wide selection of options to accurately simulate building energy use. This simulation engine was used to produce the realistic, surrogate coil data to allow for analysis and refinement of the Energy Valve's advanced control strategies. The program has the ability to perform simultaneous energy simulations on all aspects of the building at user selected timesteps and provide realistic mixed air conditions that would be expected to be entering a cooling coil. EnergyPlus can model a cooling coil's performance at a localized level, thus maintaining the ability to output not only inlet and outlet air conditions, but also inlet and outlet water conditions, instantaneous cooling power provided as well as identify when the coil fails to meet the prescribed DAT setpoint. This ability provided an abundance of synced data which allowed for analysis of coil performance in a variety of climates, building configurations and coil geometries.

The Department of Energy provides a host of template building models available for download for training purposes (Commercial Prototype Building Models). These buildings are highly detailed and provide a good starting point to generating the sought after surrogate data. The hospital template building model was initially selected for use in developing the coil data as it had four separate, multi-zoned heating ventilation and air conditioning (HVAC) systems, two of which are served by CAV supply fans, and two of which are served by VAV supply fans. The building models can be automatically downloaded to meet building envelope specifications appropriate for

the selected climate they will be simulated in. This allowed for quick generation of buildings typical to the climates this research will focus on.

3.1.2. Matlab

Matlab was used in conjunction with the EnergyPlus software to develop the surrogate coil datasets. In many ways it was used as a Graphical User Interface (GUI) to adjust simulation parameters and compile the EnergyPlus outputs in more organized formats. Two capabilities in particular that were of use. The first was Matlab's ability to produce gscatter plots. Gscatter plots allow for the plotting of two variables where a third variable can be identified by the color of the datapoint markers. This allows for the production of Q vs mW plots, where different bins of a third parameter (such as T_{wi}, T_{ai}, etc.) could be represented by different colors for the plot's datapoint markers. This allowed for easy to read graphical representations of how the cooling coils performed over a host of fluctuating input parameters. The second was its ability to convert the limited psychrometric outputs from EnergyPlus into all appropriate measurements of water/air mixtures.

Towards the end of the research, Matlab was again used to perform testing of the various control strategies. Mixed air inputs and inlet water temperatures pulled from earlier EnergyPlus simulations were run through a coil modeled in Matlab. Simulink, a block diagram environment within Matlab, was used to model various control logics and run such simulations (MATLAB).

3.1.3. RStudio

Analysis of the EnergyPlus produced data was conducted through use of RStudio, a GUI for the R language. This statistical analysis tool allowed for ease in code generation/manipulation, quick sorting and evaluation of the large datasets as well as high quality plots to aid in the understanding of the various coils' performance.

3.2. Climate Specific Data Generation

3.2.1. Cooling Coil Theory

A review of the applicable theory in regards to cooling coil performance is appropriate as it will shed insight into what trends one would expect from energy simulations, as well as clarify the difficulties that persist when trying to predict coil performance with water-side data alone, as the Energy Valve™ attempts to do.

A common approach used to demonstrate the effects of the various input parameters have on a heat exchanger comes from the effectiveness-NTU model (Braun and Mitchell, 2012). The model is used to estimate coil performance in regards to sensible heat transfer based off the thermodynamic limits for the heat exchanger in question. To understand these relationships, several parameters need to be defined. The thermal capacitance rate is the product of the specific heat and mass flow rate of a given fluid. In a cooling coil, there are two such fluids, the air and the chilled water. C_{min} is defined as the minimum of these two capacitance rates, while C_{max} is defined as the maximum of the two.

$$C_{min} = \min[mAc_{pa},\ mWc_{pw}] \quad \text{Eqn. 5}$$

$$C_{max} = \max[mAc_{pa},\ mWc_{pw}] \quad \text{Eqn. 6}$$

The ratio of these two parameters will be of interest later in the explanation of this methodology, and is defined as the capacitance rate ratio C^*.

$$C^* = C_{min}/C_{max} \quad \text{Eqn. 7}$$

The maximum possible sensible heat transfer ($Q_{max,s}$) that could occur across a heat exchanger for a given set in inlet parameters would occur if the fluid corresponding to C_{min} was

brought from its inlet temperature to that of the inlet temperature of the other fluid. Such a relationship is shown in Equation 8.

$$Q_{max,s} = C_{min}(T_{h,i} - T_{c,i}) \quad \text{Eqn. 8}$$

Such levels of heat transfer never fully realized in heat exchangers. A measure of effectiveness (ε) would then indicate how closely the heat exchanger is to obtaining $Q_{max,s}$.

$$\varepsilon = Q_s/Q_{max,s} \quad \text{Eqn. 9}$$

It is then apparent that the actual heat transfer can be predicted if the inlet temperatures and mass flow rates of the two fluids, as well as a predicted effectiveness, are known. Substantial research in this area has found that effectiveness is a function of the capacitance ratio (C^*), the number of transfer units (NTU) and the flow arrangement. NTU is defined as

$$NTU = UA/C_{min} \quad \text{Eqn. 10}$$

where UA is the overall heat transfer conductance that is a function of the coil's geometry. Typically, cooling coils that are four or more rows deep are classified as counter-flow heat exchangers. The effectiveness for such a configuration has been found to be as follows

$$If\ C^* \neq 1 \qquad \varepsilon = \frac{1-e^{-NTU(1-C^*)}}{1-C^*e^{-NTU(1-C^*)}} \quad \text{Eqn. 11}$$

$$If\ C^* = 1 \qquad \varepsilon = \frac{NTU}{1-NTU} \quad \text{Eqn. 12}$$

As C^* is not often exactly unity, combining Equations 8, 9 and 11 yields the following

$$Q_s = \frac{1-e^{-NTU(1-C^*)}}{1-C^*e^{-NTU(1-C^*)}} C_{min}(T_{ai} - T_{wi}) \quad \text{Eqn. 13}$$

Equation 13 shows that the actual sensible heat transfer is a function mW, mA, T_{wi}, T_{ai}, and UA. However, cooling coils often provide more than just sensible cooling power. The heat extracted during the dehumidification that can occur when the surface temperature of the cooling coil is

below that of the inlet air's dew point is defined as latent cooling. This is the measure of heat extracted from air through the condensing of water vapor in the air stream onto the coil. A modification of the effectiveness-NTU model detailed above is used to account for the additional heat transfer. The total cooling power (Q) is defined similarly to Equation 9, where there is a measure of an effectiveness multiplied by the maximum obtainable amount of cooling.

$$Q = \varepsilon \dot{m} A (h_{ai} - h_{w,sat,i}) \quad \text{Eqn. 14}$$

where h_{ai} is the inlet air enthalpy and $h_{w,sat,i}$ is the enthalpy which corresponds to completely saturated air at the inlet water temperature. This should make sense since the lowest temperature obtainable for the air would be the inlet water temperature. In a latent cooling scenario, T_{wi} would be below that of the dew point for the inlet air, thus the exiting air would in fact be saturated. The measure of effectiveness in the wet coil model in a counter-flow configuration is defined by Equations 11 and 12 above, but with the replacement of C^* and NTU with m^* and NTU^*, respectively. m^* is defined as

$$m^* = \dot{m} A c_s / (\dot{m} W c_{pw}) \quad \text{Eqn. 15}$$

where c_s, termed the effective specific heat, is the change in enthalpy with respect to temperature along the saturation line. It is defined as follows

$$c_s = \frac{h_{dewpt} - h_{w,sat,i}}{T_{dewpt} - T_{wi}} \quad \text{Eqn. 16}$$

where h_{dewpt} is the enthalpy of saturated air at the inlet air's dew point (T_{dewpt}). The NTU^* term involves a slight modifications to Equation 10.

$$NTU^* = UA_{wet} / \dot{m} A \quad \text{Eqn. 17}$$

where UA_{wet} is the overall mass transfer conductance-area product and is analogous to the UA found in the sensible heat transfer methodology (Braun and Mitchell, 2012). Combining of Equations 11

and 14, it can be seen the total cooling power in a coil experiencing dehumidification is a function of mW, mA, $h_{w,sat,i}$ and h_{ai}. As h_{ai} is a function of T_{ai} and W_{ai}, and $h_{w,sat,I}$ is a function of T_{wi}, it can be seen then that all the variables previously discussed in the Introduction do play a role in coil performance.

$$Q = \frac{1-e^{-NTU^*(1-m^*)}}{1-m^* e^{-NTU^*(1-m^*)}} \, mA(h_{ai} - h_{w,sat,i}) \qquad \text{Eqn. 18}$$

To demonstrate the effects that the variables mA, T_{wi}, W_{ai} and T_{ai} have on Q, parametric runs were performed for each through use of an effectiveness-NTU cooling coil model in MATLAB's Simulink. Q vs mW plots for each parametric run were produced. While one variable was adjusted through a reasonable range of values, all others were held constant. Figure 5 below shows the effects of variable mA on coil performance. It should be noted in the following figures, the bump in the Q vs mW curves for values of mW around 4.5 kg/s is due to the transition of the chilled water out of the laminar flow region.

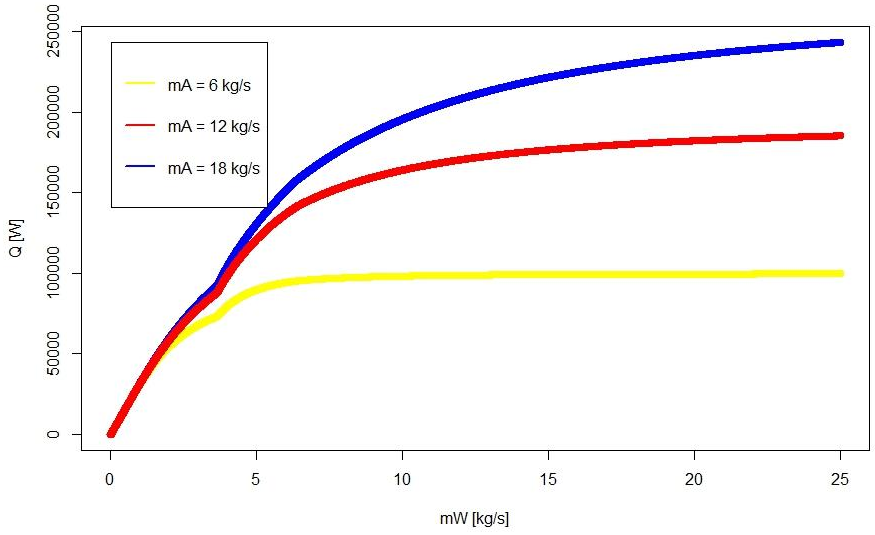

Figure 5: Q's dependency on mA.

It is apparent that increases in mA results in higher Q for a given value of mW. Additionally, the exponential curvature of the coil is seen to change as well. Figure 6 shows the effects of the variable T_{wi} on Q.

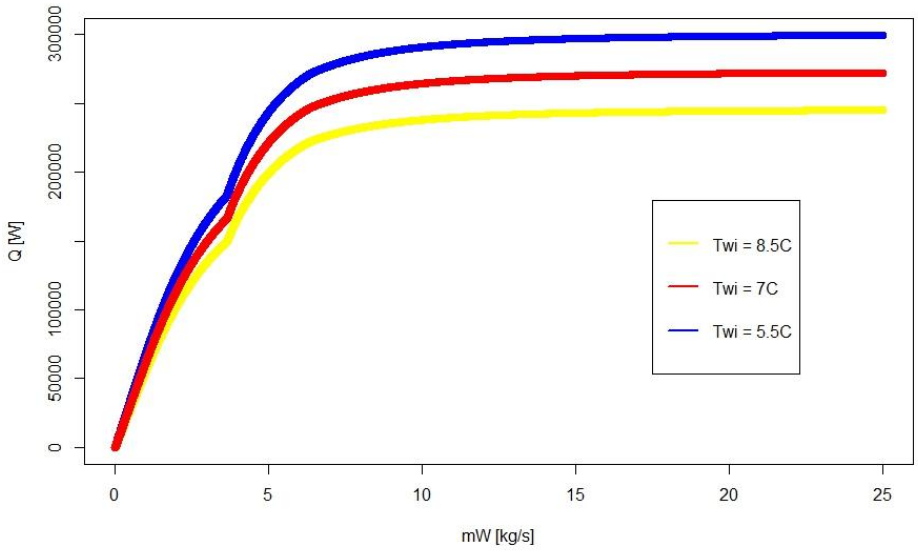

Figure 6: Q's dependency on T_{wi}.

Decreases in T_{wi} results in increased Q for a given mW. Changes to the exponential curvature seem negligible, however it should be noted that all such simulations depicted here are performing sensible only cooling. A dehumidifying coil may not necessarily exhibit such behavior. Figure 7 below shows the effects of T_{ai} on Q.

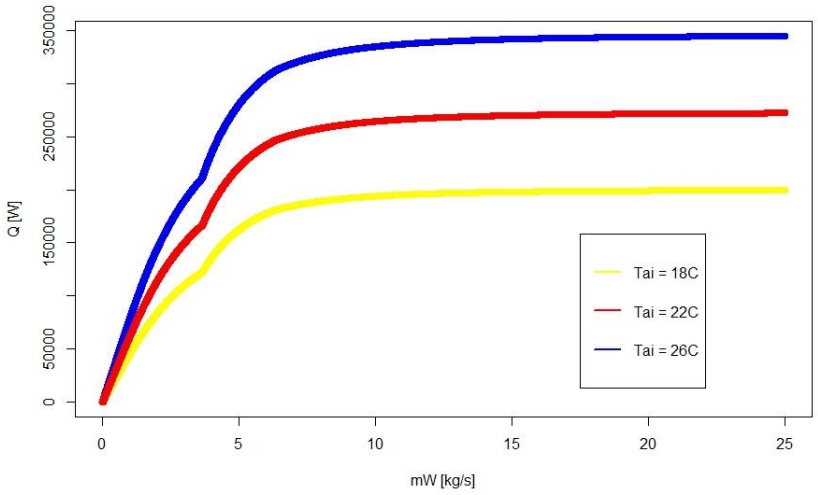

Figure 7: Q's dependency on T_{ai}.

It can be seen that increases in T_{ai} results in increasing Q for a given mW. Again, changes to the exponential curvature seem negligible. Figure 8 below shows the effect of W_{ai} on Q.

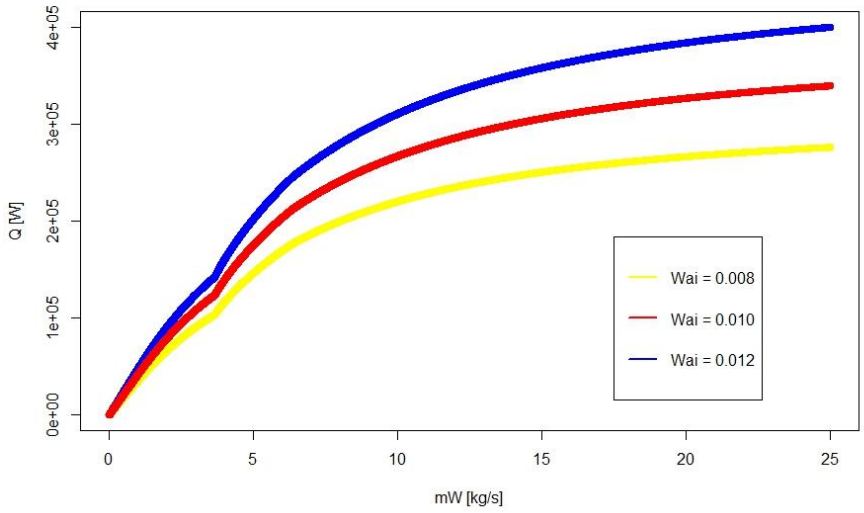

Figure 8: Q's dependency on W_{ai}.

It can be seen that increases in W_{ai} increases Q for a given mW. Negligible variation in exponential curvature realized. From all the plots above, it is apparent that in additional to the water-side variables mW and T_{wi}, airside variables also affect coil performance. This speaks to the inherent difficulty the Energy Valve™ has in attempting to predict coil behavior with water-side measurements alone.

3.2.2. Coil Model Selection and Manipulation

The EnergyPlus template "hospital" was downloaded from the Department of Energy (Commercial Prototype Building Models). The buildings can be automatically generated to meet a typical building envelope for the locations chosen. Initially, four climates were looked at: Los Angeles, CA (ASHRAE climate zone 3B), Boulder, CO (ASHRAE climate zone 5B), Atlanta, GA (ASHRAE climate zone 3A) and Miami, FL (ASHRAE climate zone 1A). Corresponding weather inputs for those select locations in the form of an EnergyPlus Weather file (.epw) were downloaded from the same location (Commercial Prototype Building Models).

The hospital template model is five stories high with a basement. It is 22,422 m^2 with an aspect ratio of 1.31. The construction consists of a mass wall, a built-up flat roof with insulation above the deck and a 14.6% collective window-to-wall ratio. Its envelope's thermal properties meet the ASHRAE 90.1-2004 minimums for its respective climate. The building consisted of two CAV and two VAV, multi-zoned HVAC systems. The cooling coils which serve these systems can be modeled in one of three ways: The Coil:Cooling:Water model with DetailedAnalysis is an unspecified geometry model which initially autosizes a coil's UA value based on of inputted design inlet and outlet air states, air flow rate, inlet water temperature, and water flow rate. This steady state coil model then performs simulations at every timestep through partially wet/partially dry analysis as first described by Elmahdy and Mitalas (1977). The second method of modeling the coil performance is to take the same Coil:Cooling:Water model and produce an autosized UA parameter,

but each timestep simulation will be performed by computing the completely dry coil capacity as well as the completely wet coil capacity (Dept. of Energy, 2012). The higher of the two calculated capacities at each timestep is then taken as it has be found that such a simplification will provide accurate capacity estimates to within 5% of those found by the more robust Elmahdy and Mitalas method (Mitchell & Braun, 2013). This SimpleAnalysis requires substantially less computation power and computing time. The third option for coil modeling is in the form a specified geometry coil which only has the option of DetailedAnalysis in the capacity calculation. The resultant UA used in the DetailedAnalysis is calculated by use of the inputted geometric parameters. This model is referenced as Coil:Cooling:Water:DetailedGeometry in EnergyPlus (Dept. of Energy, 2012).

Simulation of the template models without any further manipulation would produce unrealistic cooling coil behavior regardless of the coil modeling method implemented. After preliminary simulation, cooling power (Q) versus water mass flow rate (mW) plots of the four default building coils were nearly perfectly linear, perfectly vertical with all Q measurements taken at the same mW, or a combination of these two phenomena. The linearity came from drastic amounts of oversizing factors used throughout the building's Input Data File (IDF). The vertical behavior in the plots were a result of premature restriction on the maximum chilled water flow rate, as specified in the Controller:WaterCoil.

Manipulation of the unspecified geometry model Coil:Cooling:Water would not simultaneously allow for under sizing of the coil and for higher than design water flow rates. This was due to the coil's UA value being a direct function of the inputted design water mass flow rate and the inability to specify a maximum water mass flow rate in the Controller:WaterCoil to any value above that design value.

Appropriate manipulation of the specified geometry model Coil:Cooling:Water:Detailed-Geometry was performed to allow for a geometrically smaller cooling coil, while also allowing for

higher than design water mass flow rates. To get appropriately sized coils to begin with, all parameters within the model capable of being autosized were selected to be as such. All the parameters that were required to be specified were left at the defaulted values with two exceptions. First, the EnergyPlus default fin thickness of 0.0015 m is an order of magnitude larger than values typically found in industry. Comparing that value to fin spacing, it can be seen that the air is restricted to a flow area of 10% of the coil's cross-sectional area. This value seems to be an obvious typo and was replaced with 0.00015 m. The second parameter adjusted was the number of coil rows. It was changed from six to eight for reasons that will be described below.

Defaulted oversizing factors within the building model needed to be addressed prior to autosizing the coil through simulation. First, in the Controller:WaterCoil model, the control variable for all chilled water coils was changed from "Temperature and Humidity Ratio" to just "Temperature". Second, in the Sizing:Parameters simulation parameter, the Cooling Sizing Factor was brought down from 1.2 to 1.0. Third, in the System:Sizing simulation parameter, the Precool Design Temperature and Central Cooling Design Supply Air Temperature for all systems were changed from the defaulted 7.2°C to 11.1°C. The Central Cooling Design Supply Air Humidity Ratio was increased from 0.007 to 0.008 and the Sizing Option for all systems was changed to "Coincident". This last adjustment accounts for diversity amongst the zones on the same system and subsequently sizes the coil for the maximum instantaneous cooling load on the system as a whole, not a sum of each zone's maximum cooling load.

For simplicity in future parametric investigations, adjustment to the how the chilled water control valve tracked its control variable's setpoint needed to be performed. By default, the chilled water control valve for each system was tracking a supply air temperature of 11.1°C. Each air handling unit (AHU) was of a pull-through configuration however, thus the discharge air temperature was the temperature leaving the coil and entering the fan, where it was slightly heated by the fan (on the order of 0.5-2 K) to the final supply air temperature of 11.1°C. This is not an

unrealistic configuration and control strategy, however to maintain the ability to do future parametric simulations on the effect of changing the DAT setpoint (as discussed in Taylor (2002) in Literature Review), some adjustments were made. In the SetpointManager:MixedAir simulation parameter, the *Fan Inlet Node Name, Fan Outlet Node Name* and *Setpoint Node or Nodelist Name* were changed to the same node. For instance, in the CAV 1 system the node needed to be used here was CAV_1_CoolC-CAV_1_HeatCNode. This essentially forces the Controller:WaterCoil into tracking the DAT actually coming off the coil, not the supply air temperature leaving the fan.

As pointed out in Bellucci (2012), real world chilled water coils are subjected to varying inlet water temperatures throughout the day, at times on the order of 4 K fluctuations. The default schedule for chilled water supply temperature for the downloaded building model had a constant 6.7°C supply water temperature. To subject the cooling coil to more realistic input parameters, this schedule was manipulated. Fluctuations in inlet water temperature can follow one of two scenarios (interview w/ Dr. Michael Brandemuehl, 2 Jun 2014). The temperature can drop during the hottest part of the day if the chilled water plant was utilizing a reset schedule on the CHWST setpoint. The other option would be the CHWST actually being the highest during the hottest part of the day. This would be representative of the chilled water plant being either too small to meet the building load, or the chilled water plant is operating on a "load based" chiller staging sequence. Such a staging sequence is described by Taylor (2002) and is discussed in the Literature Review. It is a strategy in which the chiller plant is unaware of its failure to meet the load due to a lower CHWRT present in a system suffering from Low Delta T. This second scenario is the one selected to initially be modeled. Such a degrading chilled water supply temperature schedule was implemented in the Schedule:Compact simulation parameter. The temperature fluctuated from a low of 5°C during nighttime hours to 9°C to the hottest times of the day.

Step by step instructions of all described manipulations to the initial template building model can be found in Appendix A.1.

3.2.3. Generation of Coil Geometries

Once all manipulations were complete, an energy simulation was performed to allow for EnergyPlus to output all "autosized" parameters for the geometry of the cooling coil model, Coil:Cooling:Water:DetailedGeometry. The autosized parameters for each coil were recorded and input back into the IDF file. Typical outcomes of these autosized cases were that the coils were still slightly oversized for the system they were serving. Thus, four copies of the IDF files were produced for each building location. The original IDF had coils with eight-row configurations. The first copy maintained the coils' same cross-sectional geometry, but reduced the configuration to seven-rows and proportionally reduced all other applicable parameters as well (i.e. fin surface area, total tube inside surface are, total tube outside surface area, etc.). The same reduction methodology was performed for each copy until the coil was four rows deep. As a result, for each of the four HVAC systems, there will be five coils of differing sizes that can be simulated. The coil parameters used for Atlanta CAV 1 simulations can be seen in Table 1 below. The decision for the range of four to eight-rows for the coils came from configurations which are typically seen in industry (interview with Dr. Michael Brandemuehl, 2 Jun 2014). Detailed, step by step instructions for generating these geometric parameters can be seen in Appendix B. The results of such geometric parameter development can be seen in Appendix C.

Table 1: Developed coil geometries for Atlanta Hospital, CAV 1 system.

	8 Row	7 Row	6 Row	5 Row	4 Row
ATLANTA - CAV 1					
Load [W]	374157				
Max Water Flow Rate [m3/s]	1.34E-02	1.34E-02	1.34E-02	1.34E-02	1.34E-02
# of Tubes per Row	184	184	184	184	184
Fin Diameter [m]	5.93761	5.9376	5.9376	5.9376	5.9376
Minimum Airflow Area [m2]	7.79865	7.7987	7.7987	7.7987	7.7987
Fin Surface Area [m2]	1391.351	1217.432	1043.513	869.5943	695.6755
Total Tube Inside Surface Area [m2]	93.58976	81.89104	70.19232	58.4936	46.79488
Tube Outside Surface Area [m2]	95.95968	83.96472	71.96976	59.9748	47.97984
Coil Depth [m]	0.208	0.182	0.156	0.13	0.104
# of Rows	8	7	6	5	4

Simulations were performed for all coils in each location. This provided an initial 80 coil datasets to begin analysis with. Simulations were performed from April 1st to September 31st on five minute timesteps. Matlab was used to call such simulations and organize the generated output data. The applicable Matlab scripts and directions for their use in the data generation process can be seen in Appendix D. Matlab not only organized the data for future extraction into RStudio, it also was used to produce bin plots for a variety of input parameters. Those parameters include inlet water temperature, inlet air temperature, inlet air humidity ratio, inlet air relative humidity, air mass flow rate, time of day, inlet air enthalpy and water-side Delta T.

3.3. VAV vs CAV Investigation

3.3.1. Exponential Curve Variation

Based on the paper by Thuillard *et al.* (2014) it is obvious the optimal advanced control logic to be used by the Energy Valve™ will be dependent on inlet water and air conditions. Their research found that specific combinations of inlet parameters produce distinct saturation behavior on the Q vs mW plots, following the exponential form of Equation 3. When adjusting only inlet

water temperature (T_{wi}) or inlet air temperature (T_{ai}) individually, changes in maximum capacity k_1 were found, while the exponential curvature k_2 remained constant. Additionally, changes in air mass flow rate (mA) change both the maximum capacity output k_1 as well as the exponential curvature k_2. Thus, it is entirely feasible that differing control logics may be required to optimize the Energy Valve's cooling coil performance depending on whether the coil is being used in a constant air volume (CAV) or a variable air volume (VAV) application. See Figures 9 and 10 below as they are excerpts from this paper. The figures show the normalized curves of various simulations. The normalized curve is produced when dividing the capacity values by k_1. This allows for easy comparison of the exponential curvature (k_2) of the different simulations.

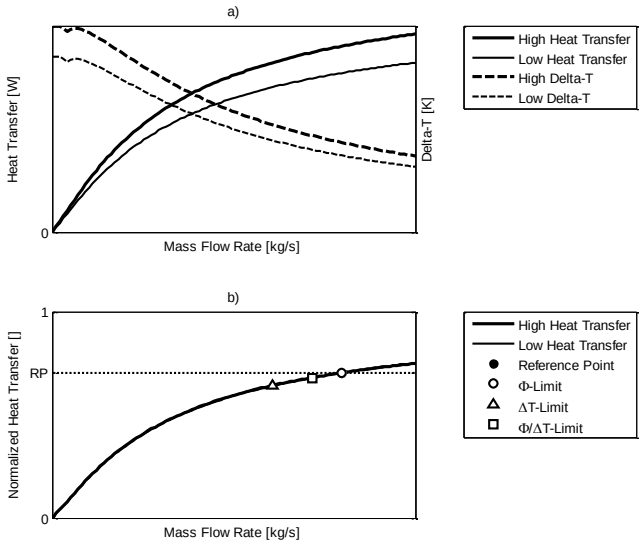

Figure 9: (a) Q vs mW plots for varying T_{wi} inputs. (b) Normalized Q vs mW show negligible change in exponential curvature (k_2) (Thuillard *et al.,* 2014).

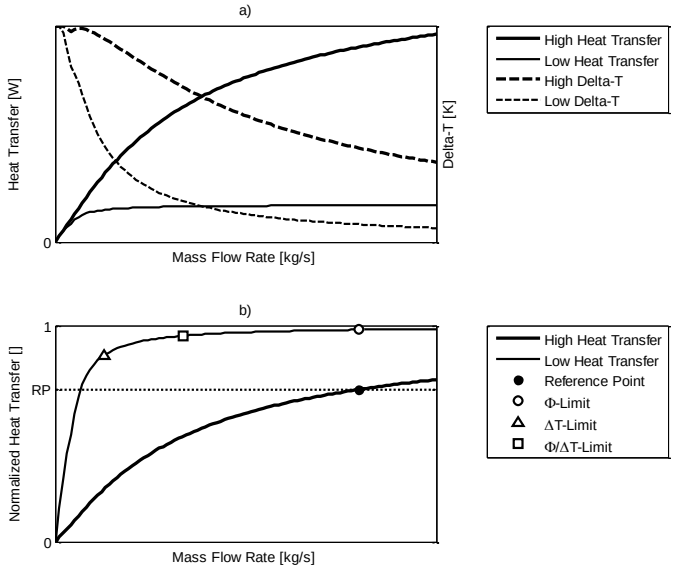

Figure 10: (a) Q vs mW plot for varying mA inputs. (b) Normalized Q vs mW plot shows appreciable change in exponential curvature (k_2) (Thuillard *et al.,* 2014).

A goal of Belimo with the Energy Valve™ is to provide a product that not only provides excellent performance, but one that minimizes the potential for error in installation that may preclude the device from reaching it maximum potential. With the large datasets that will be developed for four distinctly different climates, analysis will be performed to see if from the measured water-side data alone (T_{wi}, T_{wo} and mW), can the valve explicitly determine whether the coil is operating in a CAV or VAV application? If such a distinction can be made, and it is determined that the different applications require differing control logics, it would be beneficial for the Energy Valve™ to perform that analysis internally. This would avoid any potential for erroneous inputs during the installation phase in regards to whether to coil operates in CAV or VAV. It should be noted that though such a distinction would aid in the reduction of input errors, the true benefits may lie in the journey of this investigation. The ample knowledge gained of what airside

information can be gleaned from water-side data alone may pay dividends in the development of more robust control strategies.

The investigation into whether such a distinction can be made will begin with a focus on the exponential behavior of the Q vs mW plots. Non-linear regression will be performed in RStudio on the datasets. A script has been developed that allows for the data to be binned into equal water mass flow rate intervals. Various quantiles (i.e. the 5%, 25%, 50%, 75% and 95%) of Q for each mW bin can be determined. Plotting of the quantiles of interest against the center of each water mass flow rate bin will allow for non-linear curve fits to the data following an exponential of the form seen in Equation 3.

As stated earlier, it has been found that fluctuations in the T_{wi} and T_{ai} input parameters had no change in the exponential curvature (k_2) of the Q vs mW plot (Thuillard *et al.,* 2014). Fluctuations in the input parameters mA did change the values of k_2 however. Working off the results of Thuillard *et al*., the only remaining input parameter that may affect the exponential curvature would be the inlet air humidity ratio (W_{ai}). The article did not explicitly identify the effects of such fluctuations, only noting

> "The scaling of normalized curves with respect to humidity depends largely on whether the exchanger heat transfer is sensible only (the air passing through the heat exchanger never cools to the dew point temperature), or if there is latent energy transfer in the form of dehumidification. When mass transfer occurs (dehumidification), as is typically observed in cooling application, the results are fairly similar to changing air mass flow rate." (Thuillard *et al.,* 2014)

From this alone it is not easy to distinguish the magnitude of any such variation in k_2 as a result of changes in W_{ai}. Additionally, the net effects of simultaneous changes in all four inlet parameters (mA, W_{ai}, T_{ai}, and T_{wi}) and the relative amounts of influence each of those parameters have on the net result are not known.

Working off the initial assumption that changes in W_{ai} have negligible effect on k_2, it can be hypothesized that CAV coils would maintain nearly constant k_2 values across the various quantiles

in the data distribution. VAV coils are subjected to changes in air mass flow rates (mA) which would change the exponential curvature between different quantiles of the data distribution. An R script has been written to apply curve fits to the 5% and 95% quantiles. That script can be seen in Appendix E.2. For each dataset, the coefficients k_1 and k_2 for both quantiles will be documented to allow for the testing of this initial hypothesis.

3.3.2. Four-Parameter Curve Fit

A supplementary approach to estimating the k_1 and k_2 values for the lower and upper regions of the Q versus mW plots may need to be developed if the quantile bin approach as described above is not as robust and reliable to fully test the hypothesis. Figure 11 below shows a typical T_{wi} bin plot from one of the coils simulated in EnergyPlus.

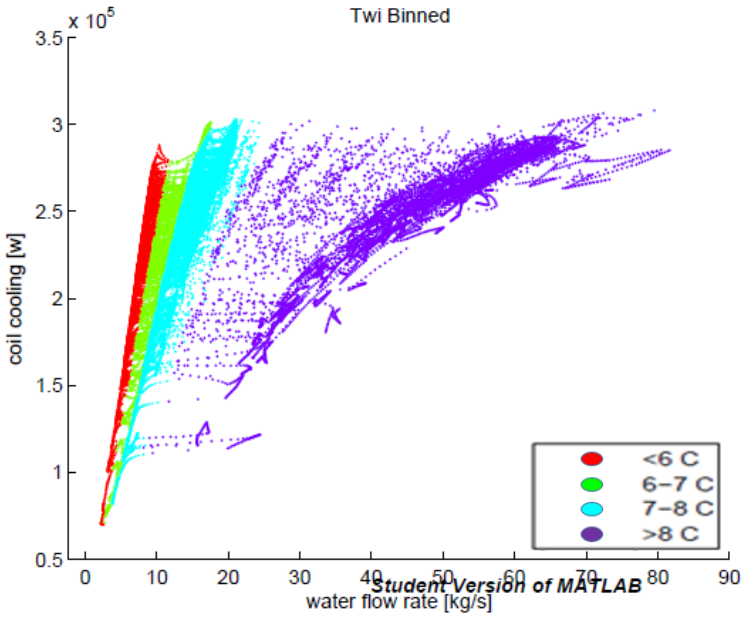

Figure 11: Q vs mW plot with binned corresponding T_{wi} inputs.

It is can be observed that the coefficient k_1 in the exponential form seen in Equation 3 seems to be highly dependent on inlet water temperature (T_{wi}). As T_{wi} increases, the maximum capacity k_1 decreases. Deviation in k_2 across the T_{wi} bins is hard to distinguish at this point. A suggestion from

Stephan Siam, a statistician at National Center for Atmospheric Research (NCAR), was a simple adjustment to Equation 3 making both k_1 and k_2 linear functions of T_{wi}. Hence,

$$k_1 = b_o + b_1 T_{wi} \quad \text{Eqn. 19}$$

$$k_2 = b_2 + b_3 T_{wi} \quad \text{Eqn. 20}$$

$$Q = (b_o + b_1 T_{wi})(1 - e^{-(b_2 + b_3 T_{wi})mW}) \quad \text{Eqn. 21}$$

Equation 21 is from here on called the Four-Parameter Curve Fit. RStudio can apply non-linear regression following this relationship with the datasets available. The application of this Four-Parameter Curve Fit may lead to a more effective control logic, as the Energy Valve™ may now have a much better estimate as to how far the coil is from or into the saturation region for a given inlet water temperature. Utilization of the Four-Parameter Curve Fit as an advanced control logic will be discussed later in this text.

3.3.3. Evaluation of Theory for Linear Dependence of k_2 and k_1 on T_{wi}

Reexamination of the theory to validate the suggestion of a linear dependence of k_2 and k_1 on T_{wi} is performed in this section. For a given set of inlet parameters, cooling capacity for both a completely dry and a completely wet coil follow Equations 13 and 18 as shown again below.

$$Q_s = \frac{1-e^{-NTU(1-C^*)}}{1-C^* e^{-NTU(1-C^*)}} C_{min}(T_{ai} - T_{wi}) \quad \text{Eqn. 13}$$

$$Q = \frac{1-e^{-NTU^*(1-m^*)}}{1-m^* e^{-NTU^*(1-m^*)}} mA(h_{ai} - h_{w,sat,i}) \quad \text{Eqn. 18}$$

For a given set of parameters T_{wi}, T_{ai}, W_{ai} and mA, the value of k_1 can be found by taking the limits of either Equations 13 or 18 as mW goes to infinity, depending on whether the coil is dehumidifying or not. As k_1 occurs when the mW is quite large, for the case of the sensible only coil, C_{min} is equal to mAc_{pa} and the limit is shown as

$$k_1 = \lim_{mW\to\infty}\left[\frac{1-e^{-UA/mAc_{pa}\left(1-mAc_{pa/(mWc_{pw})}\right)}}{1-(mAc_{pa/(mWc_{pw})})e^{-UA/mAc_{pa}\left(1-mAc_{pa/(mWc_{pw})}\right)}} mAc_{pa}(T_{ai}-T_{wi})\right] \quad \text{Eqn. 22}$$

Thus, through evaluation of the effectiveness-NTU model, k_1 indeed shows a linear dependence on T_{wi}.

$$k_1 = (1-e^{-UA/mAc_{pa}})mAc_{pa}(T_{ai}-T_{wi}) \quad \text{Eqn. 23}$$

The coefficients b_o and b_1 from Equation 19 would defined as follows

$$b_o = (1-e^{-\frac{UA}{mAc_{pa}}})mAc_{pa}T_{ai} \quad \text{Eqn. 24}$$

$$b_1 = -(1-e^{-\frac{UA}{mAc_{pa}}})mAc_{pa} \quad \text{Eqn. 25}$$

The same approach when applied to the wet coil model follows

$$k_1 = \lim_{mW\to\infty}\left[\frac{1-e^{-\left(\frac{UA_{wet}}{mA}\right)\left(1-\frac{mAc_s}{mWc_{pw}}\right)}}{1-\frac{mAc_s}{mWc_{pw}}e^{-\left(\frac{UA_{wet}}{mA}\right)\left(1-\frac{mAc_s}{mWc_{pw}}\right)}} mA\left(h_{ai}-h_{w,sat,i}\right)\right] \quad \text{Eqn. 26}$$

$$k_1 = (1-e^{-\frac{UA_{wet}}{mA}})mA(h_{ai}-h_{w,sat,i}) \quad \text{Eqn. 27}$$

The value of $h_{w,sat,i}$ is actually a higher order polynomial function of T_{wi}, but for the relatively small range of T_{wi} that cooling coils experience, evaluation of a psychrometric chart will show a near linear dependence of $h_{w,sat,i}$ on T_{wi}. For brevity, $h_{w,sat,i}$ is written as

$$h_{w,sat,i} = r_o + r_1 Twi \quad \text{Eqn. 28}$$

where r_o and r_1 are merely coefficients. Substituting Equation 28 into Equation 27 would show a linear dependence of k_1 on T_{wi} for wet coils as well with k_1's coefficients from Equation 19 being defined as follows

$$b_o = \left(1-e^{-UA_{wet}/mA}\right)mA(h_{ai}-r_o) \quad \text{Eqn. 29}$$

$$b_1 = -\left(1 - e^{-UA_{wet}/mA}\right)mAr_1 \qquad \text{Eqn. 30}$$

It has therefore been derived from the establish theory of cooling coil performance that a completely dry and a completely wet coil both would maintain a linear dependence of k_1 on T_{wi}. It should be noted that often times coils experience a scenario where only the later portion of the coil is wet. In such cases, an iterative process for determining the fraction of the coil which is dry is performed (Elmahdy and Mitalas, 1977). The total cooling power would be achieved by adding the sensible cooling power from the dry portion of the coil to the total cooling power from the wet portion. Thus, such a linear dependence of k_1 on T_{wi} would be expected to persist even in a partially dry/partially wet scenario.

Proving such a dependency on T_{wi} for the parameter k_2 from the established theory is slightly more complicated. First, the derivative of Equation 3 with respect to mW needs to be taken.

$$Q = k_1(1 - e^{-k_2 mW}) \qquad \text{Eqn. 3}$$

$$d\left(\frac{Q}{dmW}\right) = k_1 k_2 e^{-k_2 mW} \qquad \text{Eqn. 31}$$

Thus, if the limit of that derivative is taken as mW goes to zero, the following relationship is produced

$$\lim_{mW \to 0} d\left(\frac{Q}{dmW}\right) = k_1 k_2 \qquad \text{Eqn. 32}$$

This would indicate a constant slope, or linear behavior, is expected on the Q vs mW plot for low values of mW. That is indeed seen in both the simulated data (Figures 5 - 8) as well as actual coil data (Figure 2). Functions for k_1 have already been developed in Equations 23 and 27. The effectiveness-NTU and modified effectiveness-NTU models also provide an avenue for obtaining the left hand portion of Equation 32 to see if the suggested linear dependence of k_2 on T_{wi} is indeed validated by the theory. Since the region of minimal mW is to be investigated, the C_{min} for the dry

coil would then be mWc_{pw} which is different from the previous investigation into k_1. Thus, Equation 13 would be expanded to:

$$Q_s = \frac{1-e^{-UA/(mWc_{pw})\left(1-mWc_{pw}/(mAc_{pa})\right)}}{1-(mWc_{pw}/(mAc_{pa}))e^{-UA/(mWc_{pw})\left(1-mWc_{pw}/(mAc_{pa})\right)}} mWc_{pw}(T_{ai}-T_{wi}) \quad \text{Eqn. 33}$$

The derivative of the above equation with respect to mW is substantially long and complicated, however taking the limit of that derivative as mW approaches zero simplifies quite nicely to

$$\lim_{mW\to 0} d\left(\frac{Q_s}{dmW}\right) = c_{pw}(T_{ai}-T_{wi}) \quad \text{Eqn. 34}$$

Putting Equations 34 and 23 back in Equation 32 allows for the solving of k_2 provides the following

$$k_2 = \frac{c_{pw}}{\left[\left(1-e^{-\frac{UA}{mAc_{pa}}}\right)mAc_{pa}\right]} \quad \text{Eqn. 35}$$

The term (T_{ai} – T_{wi}) appeared both in numerator and denominator and thus canceled out. This leaves k_2 independent of T_{wi} for completely dry coils. The same approach for determining k_2 can be applied to the wet coil model. Equation 18 can be expanded to

$$Q = \frac{1-e^{-(UA_{wet}/mA)\left(1-mAc_s/(mWc_{pw})\right)}}{1-mAc_s/(mWc_{pw})\, e^{-(UA_{wet}/mA)\left(1-mAc_s/(mWc_{pw})\right)}}\, mA(h_{ai}-h_{w,sat,i}) \quad \text{Eqn. 36}$$

The derivative of Equation 36 is also substantially long and complicated, however taking the limit of that derivative as mW approaches zero simplifies to

$$\lim_{mW\to 0} d\left(\frac{Q}{dmW}\right) = c_{pw}(h_{ai}-h_{w,sat,i})/c_s \quad \text{Eqn. 37}$$

Putting Equations 37 and 27 back in Equation 32 allows for the solving of k_2.

$$k_2 = \frac{c_{pw}}{\left[\left(1-e^{-\frac{UA_{wet}}{mA}}\right)mAc_s\right]} \quad \text{Eqn. 38}$$

A proof of the derivations for k_1 and k_2 from the effectiveness-NTU model's equations was performed using the open source algebra system Maxima. That proof can be found in Appendix O. The ($hai - hw,sat,i$) term canceled out which would seem to show k_2 is independent of T_{wi} for a wet coil as well. Though c_s does have dependency on T_{wi} as seen in Equation 16, that value can be assumed a constant. Utilizing the same Simulink model used to produce Figures 5-8 in the subsection Cooling Coil Theory of this report, the value of c_s was investigated and found to fluctuate no more than 6.5% across a range of T_{wi} from 5 to 9°C while maintaining a constant W_{ai}.

Comparison of Equations 35 and 38 shows that for a completely dry or completely wet coil, there is effectively no dependence of k_2 on T_{wi}. However, those values of k_2 for the two cases would not be the same for a given set of inlet parameters. Coils often experience partially wet/partially dry scenarios. Thus, it would be assumed the resultant k_2 would lay somewhere between the two calculated values from Equation 35 and 38. The fraction of wet and dry sections of a coil does depend on the inlet water temperature, thus a dependence of k_2 on T_{wi} does exist. The same could be said for a k_2 dependence on W_{ai}. Various regression fits in RStudio on data sets produced in EnergyPlus indicated a linear dependency of k_2 on T_{wi} showed a stronger correlation than that of higher order or inverse dependencies on T_{wi}.

It is apparent from the above derivations of k_1 and k_2 from the effectiveness-NTU models that coil performance depends on more than inlet water temperatures. The degree to which the other variables fluctuate will be dependent on the climate in which the coil operates. Thus, the application of the Four-Parameter Curve Fit, which only accounts for T_{wi} in its estimations of k_1 and k_2, will be expected to have differing levels of performance across the various climates.

3.3.4. Spread of Inlet Water Temperature Bins

An additional investigation into the use of the Four-Parameter Curve Fit as tool for predicting whether a coil operates in a CAV or VAV application was performed. Of the original 80

coils produced in EnergyPlus, no single coil geometry was applied to both a CAV and a VAV application. In an effort to see if any differences in the resultant datasets could be distinguished, the system originally identified as CAV 1 in the Miami hospital model was retrofitted with a VAV system. The original CAV 1, six-row coil was again used in this system, now operating with fluctuating air flow rates. As the Energy Valve™ only measures and logs water-side data, it is appropriate to investigate the T_{wi} bin plots of this coil operating in different applications. This particular bin plot was found to be the most valuable. Figures 12 (a) and (b) show such plots.

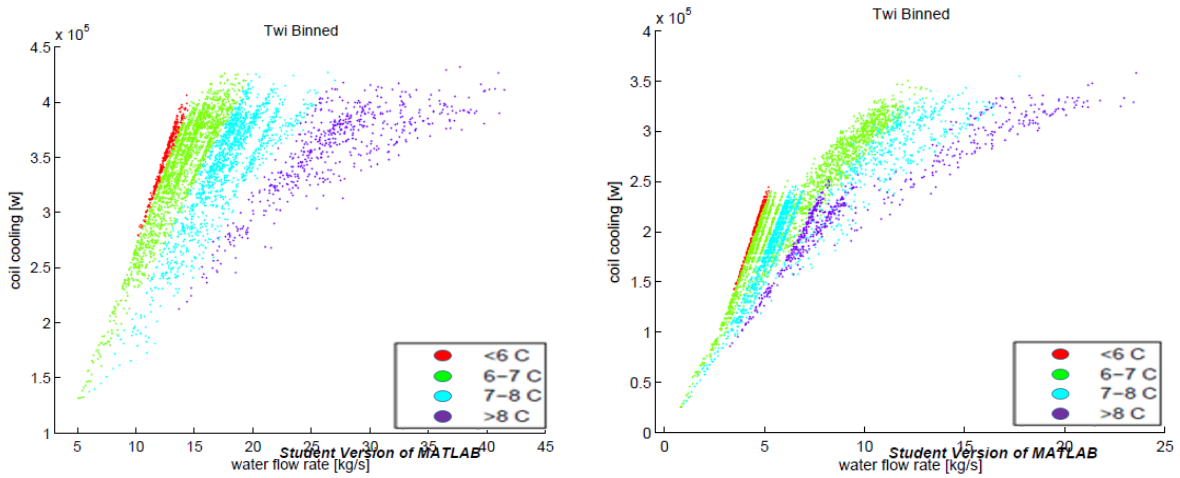

(a) (b)

Figure 12: (a) Coil data under CAV application. (b) Same coil used in VAV application.

It can be seen the T_{wi} bins are much more distant in the CAV application when compared to a VAV application. The left most region in Figure 12 (b) exhibits characteristics similar to the CAV application in Figure 12 (a). Bin plots of air flow rates indicate that this is the region in which the minimum allowable air flow are being maintained. For this particular system, the minimum air flow rate was set to 25% of the design air flow rate. Application of the Four-Parameter Curve Fit via RStudio to the two datasets would be expected to have better results for the CAV case, as the spread of the T_{wi} bins are much more defined. An appropriate measurement of the quality of such a non-linear regression fit would be the Coefficient of Variation (CV). It is defined as the average

percent deviation of a data point to its predicted value when compared to the mean of the capacities in the dataset.

$$CV = \left(\frac{100}{\mu}\right)\sqrt{SSE/(N - DOF)} \qquad \text{Eqn. 39}$$

with

$$SSE = \sum_{i=1}^{N}[(x - y)^2] \qquad \text{Eqn. 40}$$

where x is an observed capacity data point, y is the corresponding predicted capacity from the Four-Parameter Curve Fit, SSE is the sum squared error, N is the number of data points in which the non-linear regression is being performed on, μ is the mean observed capacity in the dataset, and DOF is the number of degrees of freedom which in this case is always four as there are only four coefficients (b_o, b_1, b_2 and b_3) the curve fit can adjust to best fit the data.

There are more variables at play in this measurement to correctly distinguish a CAV from a VAV application for a given dataset. Figures 13 (a) through 13 (c) below shows the T_{wi} bin plots for the Miami CAV 2 coil in its eight-row, six-row and four-row configurations. It is obvious that the T_{wi} bins become less defined as the coil becomes smaller relative to the size of the system it is serving. This in turn should lead to a less accurate curve fit and a resulting higher CV.

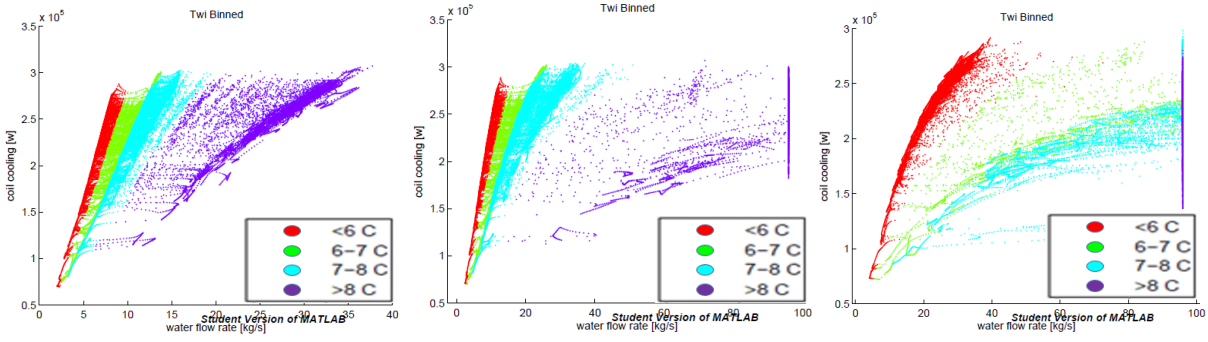

(a) (b) (c)

Figure 13: T_{wi} bin plots for Miami Hospital CAV 2 coil in (a) 8-row, (b) 6-row, and (c) 4-row configurations.

A second measurement must then be made before a measure of *CV* from the Four-Parameter Curve Fit could distinguish whether the coil serves a CAV or VAV system. That measurement is defined as the Fraction of Predicted Maximum Capacity (*FPMC*), which is essentially the ratio of the cooling requirements of the system compared to the potential output of the coil serving that system. In laymen's terms, it is a measure of how "undersized" or "oversized" the coil is for the system it serves.

$$FPMC = (maximum\ observed\ Q\ at\ a\ given\ T_{wi})/(b_o + b_1 T_{wi}) \qquad \text{Eqn. 41}$$

where T_{wi} is the chosen T_{wi} to be the "indicator temperature" and b_o and b_1 are coefficients provided by RStudio after application of the Four-Parameter Curve Fit. The maximum observed Q at the indicator temperature is found by taking the maximum recorded Q in an inlet water temperature bin of the indicator T_{wi} +/- 0.2 K. Ideally, one would look only at data points matching the indicator temperature, but few or no such points may exist due to the fluctuating T_{wi} schedule implemented on the system. Thus, a small bin both above and below the indicator temperature needs to be analyzed to ensure a dependable value of measured Q is used in determining the *FPMC*. The denominator of Equation 41 is essentially the value of k_1 for that particular T_{wi}. This is also the theoretical maximum capacity the coil can output at that T_{wi}. Consistency of the value of T_{wi} used in the numerator and denominator of Equation 41 is required. Additionally, it can be seen that using different indicator T_{wi} values would lead to a different *FPMC*. Investigation into which T_{wi} proves to be the best indicator temperature will be discussed in Results section of this report.

The following is provided to further explain the variable *FPMC*. Increasing values of *FPMC* at a particular T_{wi} would indicate the coil is reaching saturation at its chosen indicator temperature, thus the coil is becoming more "undersized" for the system it serves. Lower values of *FPMC* would

indicate the coil is not coming close to realizing its full potential of cooling capacity, and the coil could be considered "oversized" for the system it is serving.

It is therefore hypothesized that for any particular coil (CAV or VAV), a decreasing *FPMC* leads to a lower *CV* in the Four-Parameter Curve Fit. However, for a particular *FPMC*, a CAV coil will always have lower values of *CV* than that of the VAV coil. VAV coils are expected to perform worse due to the added fluctuations in *mA*. If this hypothesis holds, relationships between *CV* and *FPMC* could be established for both CAV and VAV coils in each location. Those relationships could subsequently be used in predicting if unknown coils are operating in a CAV or VAV application based on their computed values of *FPMC* and *CV*.

3.4. Limitation Strategy Testing

Determination of a coil's application, whether it be CAV or VAV, would not provide any benefit for the Energy Valve™ unless such a distinction would change how the valve operates. As pointed out in Thuillard *et al.* (2014), three advanced control strategies for the Energy Valve™ have been looked at: Flow Limiting, Delta T Limiting, and Flow/Delta T Limiting. Current commercially available Energy Valves use Delta T Limiting and Flow Limiting strategies. The Thuillard paper found the superior limiting strategy to be dependent on which input parameter was fluctuating. Combined fluctuations of all inlet parameters simultaneously was not addressed.

With realistic inlet water and air state parameters produced by the EnergyPlus simulations, this research further investigates the implementation of these strategies. It is hypothesized that the system application (CAV or VAV), climate, and facility priorities (i.e. energy savings, thermal comfort, etc.) all will have an effect on which advanced control logic is superior.

3.4.1. Establishing the Coil

To test these strategies against each other, a Simulink model was produced. The model takes input data of T_{ai}, T_{wi}, W_{ai}, and mA at five minute timesteps and sends it through the steady state cooling coil model developed by Bellucci (2012). The water flow rate mW is the manipulated variable in all instances and is allowed to be controlled by a proportional, integral, derivative (PID) controller. Such PID controllers track on either a DAT setpoint, a Flow Limiting setpoint, a Delta T Limiting setpoint, a Flow/Delta T Limiting setpoint or a saturation setpoint in the case of a new control logic that was devised through the advent of the Four-Parameter Curve Fit. All such strategies will be discussed in detail below.

The coil model incorporates inputs from the EnergyPlus generated data (W_{ai}, T_{ai}, T_{wi}, and mA), the mW controlled by the selected control strategy, the coil's geometric parameters as well as governing properties of air that are elevation dependent. The coil model outputs total cooling power (Q), sensible cooling power (Q_s), outlet water temperature (T_{wo}), discharge air temperature (T_{ao}), and the sensible heat ratio (SHR). The Simulink coil model differs slightly from the EnergyPlus model in its computational algorithms and adjustments are needed to be made to account for such discrepancies. Bellucci's Simulink coil is an NTU-effectiveness coil which operates as completely wet or completely dry. It is simplified by not accounting for partially wet/partially dry scenarios. If inlet air dew point is above T_{wi}, coil performance is calculated as completely wet. This will slightly underestimate the total cooling capacity (Mitchell and Braun, 2013). If inlet air dew point is below T_{wi}, the coil is calculated as completely dry. The EnergyPlus coil model was a Log Mean Temperature Difference/Log Mean Enthalpy Difference (LMTD/LMHD) coil (Dept of Energy, 2012). It utilizes logic from Elmahdy and Mitalas (1977) that performs an iterative process for each timestep in which the coil is determined to be in a partially wet/partially dry scenario. This theoretically makes the EnergyPlus coil simulations slightly more accurate. These differences

in solving algorithms coupled with slight differences in the outputted geometric parameters from EnergyPlus from the required inputs for the Simulink coil produced slightly different Q vs mW profiles.

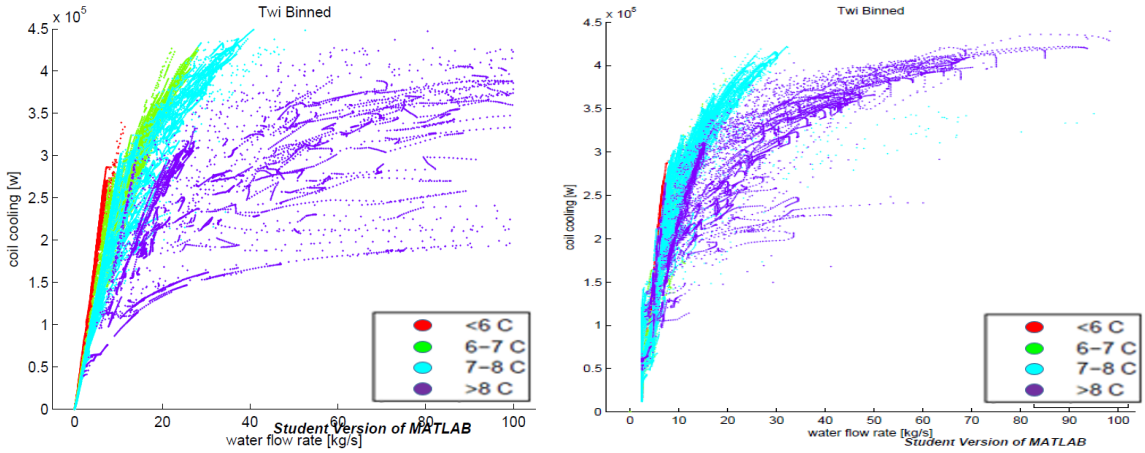

(a) (b)

Figure 14: (a) EnergyPlus coil outputs. (b) Corresponding Simulink outputs.

The left image in Figure 14 above is the T_{wi} bin plot from the EnergyPlus coil (LMTD/LMHD modeling) simulations for the Atlanta Hospital VAV 1 coil. The right image is the T_{wi} bin plot from the Simulink model (NTU-Effectiveness modeling) simulation which utilized the generated inlet air and water states that resulted from the EnergyPlus simulation. The three lower T_{wi} bins match up nearly identically. The >8°C bin (purple) varies slightly. This is due to a mismatch in simulation periods between the two plots shown. The right hand image (Figure 14 (b)) is just August data, and thus none of the sensible-only cooling instances occurred (that is the portion of the purple bin in the left hand plot that saturates out just below 200,000 W). It should be noted EnergyPlus's Chilled Water Valve controller is perfectly tuned, if flow is not restricted, the DAT setpoint error would be zero. The Simulink model had hysteresis, let-by and slew rate limitations incorporated into it. Regardless, perfect calibration is not needed to effectively test the varying strategies. Every effort was made to match the coils as best as possible though, since inlet air conditions would be effected

by instances when the DAT setpoint is not met, as this would mean the room air temperature (RAT) setpoint would not be met. To effectively test the strategies, realistic coil behavior from the Simulink model is needed, which to within reasonable accuracy was achieved here.

The Matlab scripts for establishing the geometric and thermodynamic properties for the cooling coil model, along with the scripts that establish tuning parameters for each of the control strategies can be seen in Appendix L.

The Classical PID controller which tracks a DAT setpoint is initially used to establish mW and Q data for the coil. Though this data was already generated through the EnergyPlus model, it needs to again be generated through the Simulink cooling coil model due to the slight variations between the coil models.

The Classical PID control logic model can be seen in Figures 15 (a) through 15 (c). The valve utilized in the control logic is an equal percentage valve with a valve authority of 0.5 and it accounts for 1% hysteresis, 1% valve let-by as well as actuator positioning rates of +/- 60 seconds. The PID controller is the Simulink default with reverse action implemented by the use of negative control parameters K_p, K_i and K_d.

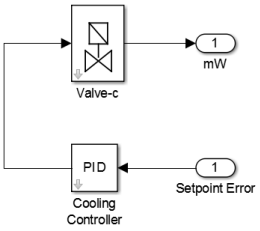

(a)

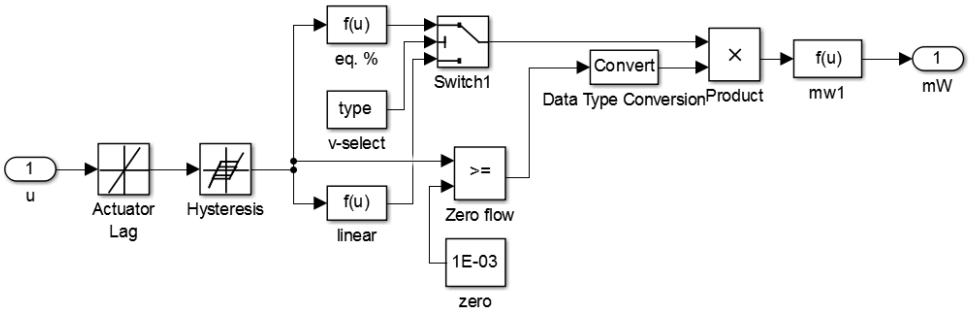

(b)

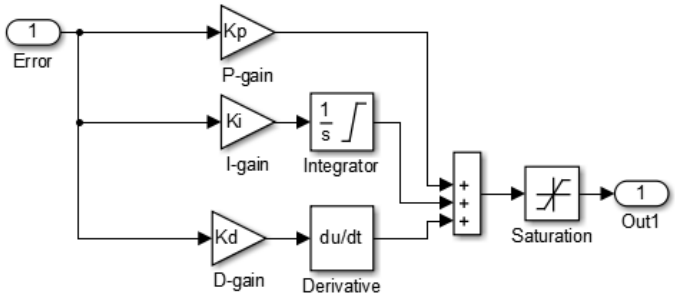

(c)

Figure 15: Simulink models of (a) Controller-valve assembly. (b) Valve model. (c) PID controller model.

Constant values of the mean input parameters of T_{wi}, T_{ai}, W_{ai} and mA were used to effectively tune the K parameters of the PID controller through use of Ziegler Nichols closed loop tuning rules. A step change in DAT setpoint from 12 to 11°C was implemented. With integral action coefficient

(K_i) and derivative action coefficient (K_d) initially set to zero, the proportional action coefficient (K_p) was increased in magnitude until periodic oscillations occurred in the T_{ao} around the DAT setpoint. The K_p which induced such behavior was labeled the critical K_p (K_{pcrit}) and the associated oscillation period (T_p) was recorded. Those values were then used to output Z-N suggested tuning parameters from Table 2 below.

Table 2: Ziegler and Nichols Closed Loop Tuning Parameters (Siemens Building Technologies).

Controller	P	PI	PD	PID
X_p	$2 \cdot X_{p\ crit.}$	$2.2 \cdot X_{p\ crit.}$	$1.5 \cdot X_{p\ crit.}$	$1.7 \cdot X_{p\ crit.}$
T_n		$0.83 \cdot T_P$		$0{,}5 \cdot T_P$
T_v			$0.1 \cdot T_P$	$0.12 \cdot T_P$
K_R	$0.5 \cdot K_{P\ crit.}$	$0.45 \cdot K_{P\ crit.}$		$0.6 \cdot K_{P\ crit.}$

It should be noted that inputs in the Simulink's PID controller call for values of K_p, K_i and K_d, not the proportional band (X_p), integral action time (T_n) and derivative action time (T_v). Thus the following equations were used in developing those parameters.

$$K_p = 1/X_p \qquad \text{Eqn. 42}$$

$$K_i = K_p/T_n \qquad \text{Eqn. 43}$$

$$K_d = K_p T_v \qquad \text{Eqn. 44}$$

In all the PID controllers used in this research, values of K_d remained zero. Introduction of K_d aided little in increased performance and at times drastically increased simulation times. Thus, the K parameters derived from the Table 2's tuning parameters for a PI controller were used as starting points. Further iterations with slight adjustments to K_p and K_i often produced slightly better performance. Optimal performance was realized when a sub-critically damped, single overshoot transient response was witnessed in the T_{ao} response to a change in DAT setpoint (Siemens Building Technologies).

With the PI controller now optimally tuned, simulations were then performed with EnergyPlus data from the month of August. T_{wi}, mW and Q values were exported from the simulation into RStudio for the application of the Four-Parameter Curve Fit. An R script has been written to apply this non-linear regression as well as compute Flow and Flow/Delta T limits, all of which will be used during testing of the various control strategies. That script in available in Appendix L.4.

3.4.2. Advanced Control Logics

All required parameters are now established and subsequent simulations of the Simulink model with the advanced control strategies can now be performed. All control strategies will default to Classical PID control tracking on a DAT setpoint of 11°C when not operating in a saturation state. The step by step instructions for the effective testing of each coil can be found in Appendix L. Also found there is the Matlab scripts required to be run before and after each simulation.

The first advanced control logic modeled and investigated is Delta T Limiting. The essence of this strategy is that the Energy Valve™ will operate under Classical PID control when measured water-side Delta T is above the prescribed low limit. Error in the DAT when compared to its setpoint will induce either an increase or decrease in water flow through the Energy Valve™. At times when the measured water-side Delta T is below the limit, which is initially set to 5.55 K, the controller modulates water flow so the Delta T low limit is maintained. Control signals to the Energy Valve™ from the Classical PID logic and the Delta T Limiting logic will be compared to recognize when the control signal and subsequent water flow rate that comes from the Classical PID controller is below that of the Delta T limiting logic. At this point, Classical PID control will again take over as the system would not be experiencing Low Delta T Syndrome anymore. The

collective controller which implements this logic is coined the Delta T Manager ™ by Belimo and can be seen modeled below.

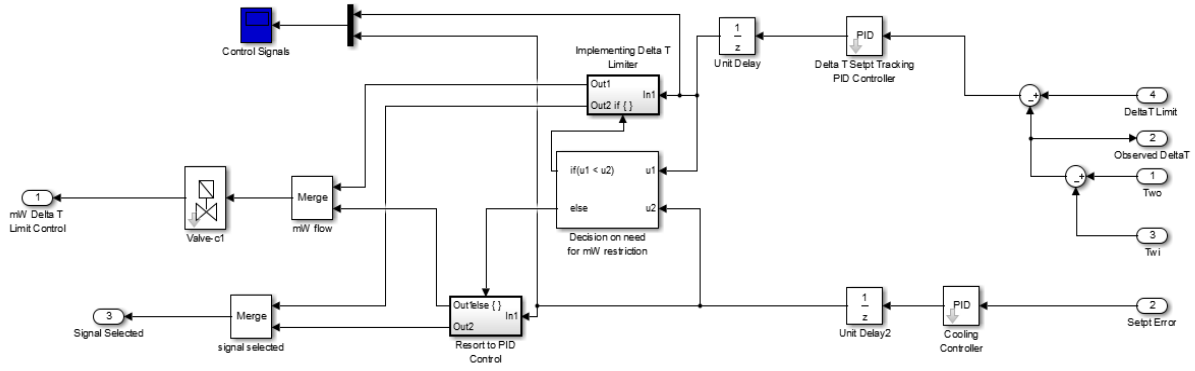

Figure 16: Delta T Limiting control logic modeled in Simulink.

Tuning of the PI controller that would track on a Delta T setpoint was accomplished via the same Ziegler Nichols closed loop tuning process as was done for the DAT tracking Classical PID controller. Maximum W_{ai}, T_{ai}, T_{wi} and mA values from the input parameters were used to calibrate the controller along with a step change in Delta T setpoint from 6 K to 5 K. The transition from Classical PID control to Delta T control includes a slight overshoot of the Delta T low limit before effective Delta T tracking can occur. This can be seen in Figure 17 where the Delta T limit is set to 5.55 K.

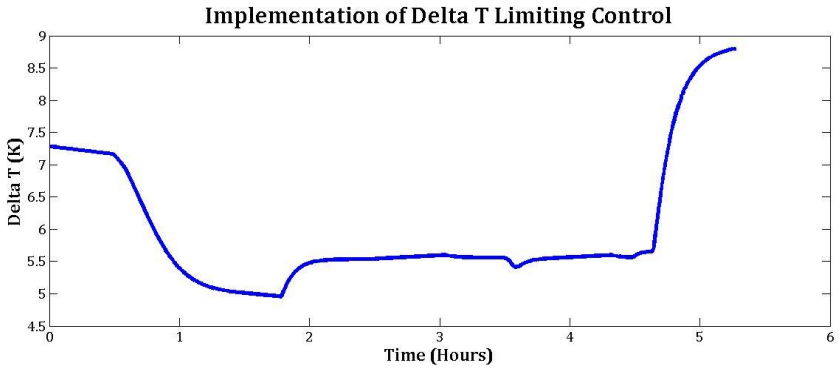

Figure 17: Delta T versus time plot at moment when Delta T Limiter is engaged.

The second advanced control strategy considered was Flow Limiting. The most simplistic of the advanced control logics, it merely sets a maximum flow rate which the valve will restrict flow to. The pressure independence and flow monitoring capabilities of the Energy Valve™ makes this possible as the valve is now no longer susceptible to hydronic pressure fluctuations in the system. Often times, control valves are too large and when coupled with Classical PID control, will increase flow to levels far beyond design rates in an effort to meet an unobtainable DAT setpoint. This is a primary cause of Low Delta T Syndrome which was discussed in the Literature Review.

Determination of the *mW* high limit was performed in the R script available in Appendix L.4. An iterative process was performed to determine when a Delta T of 5.55 K would be expected to be realized at design inlet water temperature. Such an estimate would be possible from the *b* coefficients obtained from the Four-Parameter Curve Fit. The *mW* at which this would occur was chosen to be the *mW* high limit, or *mWlimit*. This is merely calculated by setting Equations 1 and 3 equal and solving for *mWlimit*. Equation 45 below shows the relationship and Figure 18 graphically identifies where such a limit would occur. The Delta T Limit was again taken to be 5.55 K and the design T_{wi} was 6.7°C, as was used by EnergyPlus in sizing the geometric parameters of the coil. c_{pw} was taken to be 4,181 J/kg*K.

$$mW_{limit} C_{pw} DeltaT_{limit} = (b_o + b_1 T_{wi})(1 - e^{-(b_2 + b_3 T_{wi}) mW limit}) \qquad \text{Eqn. 45}$$

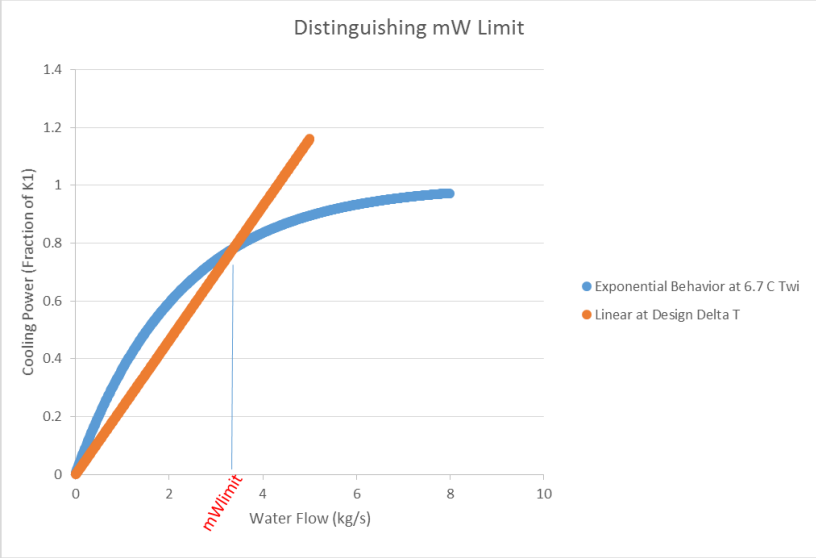

Figure 18: Determination of *mW* Limit.

The third advanced control logic investigated was that of Flow/Delta T Limiting. The quotient of measured water flow and Delta T was compared to a high limit. The high limit for such a controller was taken to be the quotient of the mWlimit divided by the DeltaT Limit of 5.5 K. The controller will operate in Classical PID DAT tracking control until its Flow/Delta T output exceeds the high limit. At that point, a second PI controller would modulate the valve to maintain the Flow/Delta T high limit. As before seen in the Delta T limiting strategy, constant comparison between the control signals from the Classical PID controller which is attempting to track the DAT setpoint and the secondary PI controller attempting to track *mW*/*Delta T* high limit will take place. The lower of the two control signals will be sent to the valve.

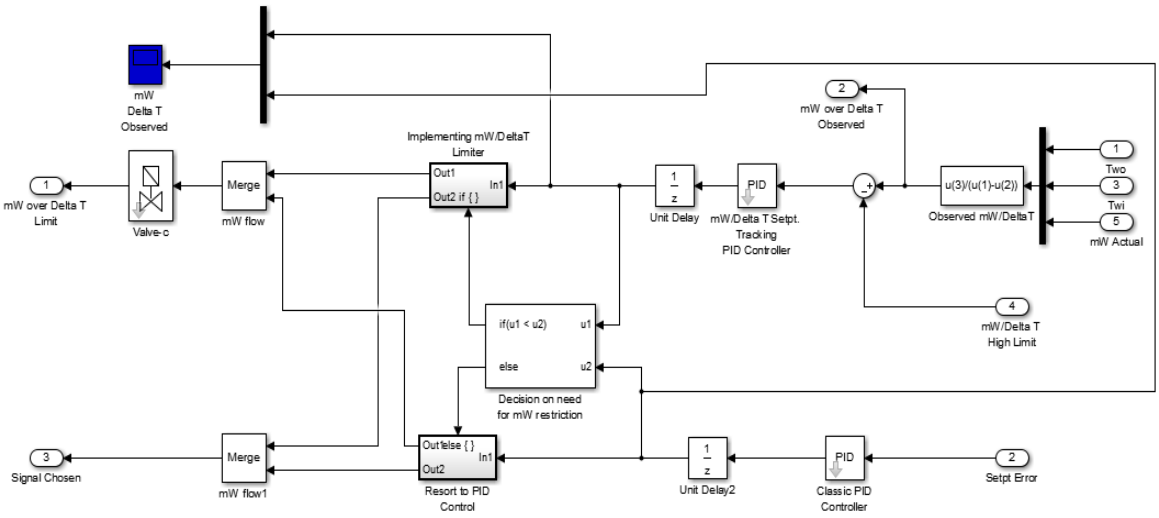

Figure 19: Flow/Delta T Limit control logic modeled in Simulink.

Tuning of the PI controller that would track on a Flow/Delta T setpoint was accomplished via the same Ziegler Nichols closed loop tuning process as was done for the DAT tracking Classical PID controller. Maximum W_{ai}, T_{ai}, T_{wi} and *mA* values from the input parameters were used to calibrate the controller along with a step change in *mW/Delta T* setpoint from 0.1 kg/s-K above high limit, down to the high limit. The transfer from Classical PID control to Flow/Delta T control includes a slight overshoot of the Flow/Delta T high limit before effective Flow/Delta T tracking can occur. This can be seen in Figure 20 where the Flow/Delta T high limit was set to 3 kg/s-K.

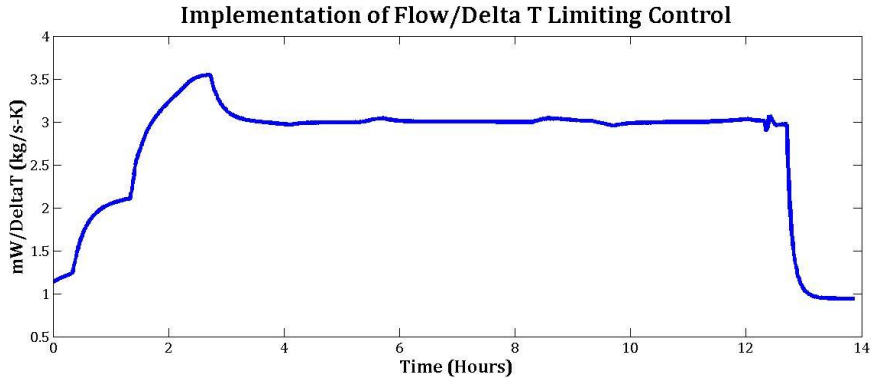

Figure 20: *mW*/Delta T vs time plot at moment when Flow/Delta T Limiter is engaged.

The last advanced control logic investigated is one not previously considered by Belimo's Research and Development (R&D) department and the University of Colorado Boulder. It is derived by the accurate saturation predictions that the Four-Parameter Curve Fit now provides us. Under normal operating conditions, the Energy Valve™ will again be controlled by Classical PID control which tracks DAT setpoint. Consistent monitoring of T_{wi} and the calculated Q will allow for comparison of observed cooling power (Q) to that of predicted maximum capacity k_1. k_1 is adjusted depending on T_{wi} as per Equation 19. At times when this ratio exceeds a prescribed saturation limit (e.g. 85%), it is deemed that the coil is operating in the saturation region. At that point, a secondary PI controller will track on that saturation limit. The lower of the two control signals will be sent to the valve.

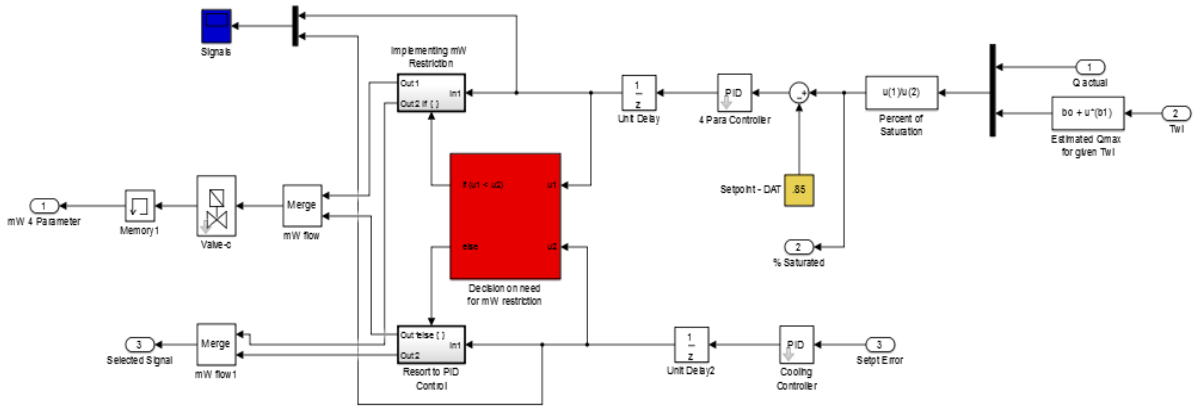

Figure 21: Four-Parameter control logic modeled in Simulink.

Tuning of the PI controller that would track on a saturation limit was accomplished via the same Ziegler Nichols closed loop tuning process as was done for the DAT tracking Classical PID controller. Maximum W_{ai}, T_{ai}, T_{wi} and mA values from the input parameters were used to calibrate the controller along with a step change in saturation setpoint from 0.9 to 0.85. The transfer from Classical PID control to Four-Parameter control includes a slight overshoot of the saturation limit

before effective saturation tracking can occur. This can be seen in Figure 22 where the saturation limit is set to 75%.

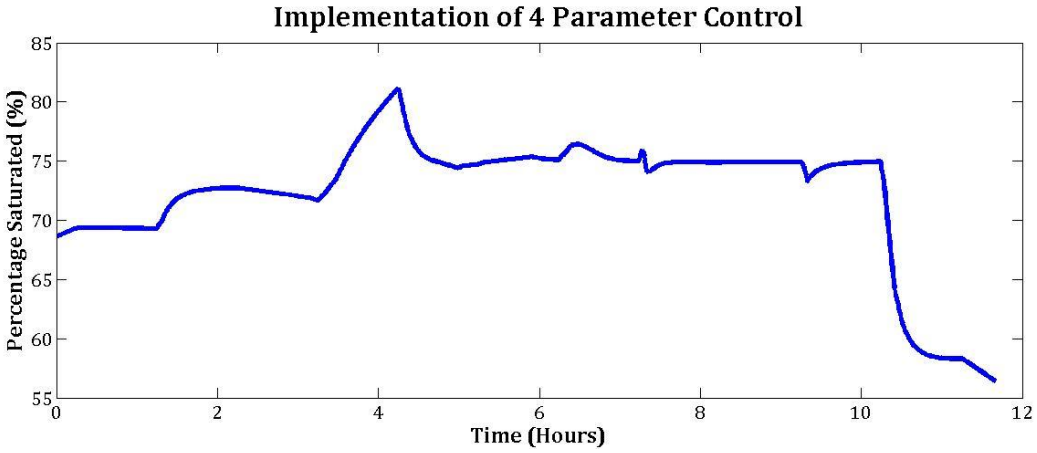

Figure 22: Percent saturation vs time plot at moment Four-Parameter control is engaged.

3.4.3. Strategy Testing and Comparison

After the all the control limits were established and appropriate tuning for each controller was performed, simulations with each control strategy were completed to investigate the hypothesis that the optimal control strategy will depend on application (CAV vs VAV), climate, and facility priorities.

A simplified model depicting how the controller, valve, coil and input air and water states are combined in Simulink in shown in Figure 23. This shows Classical PID control with DAT tracking. Models of other control strategies differ in their controller/valve assembly, as well as the established setpoints.

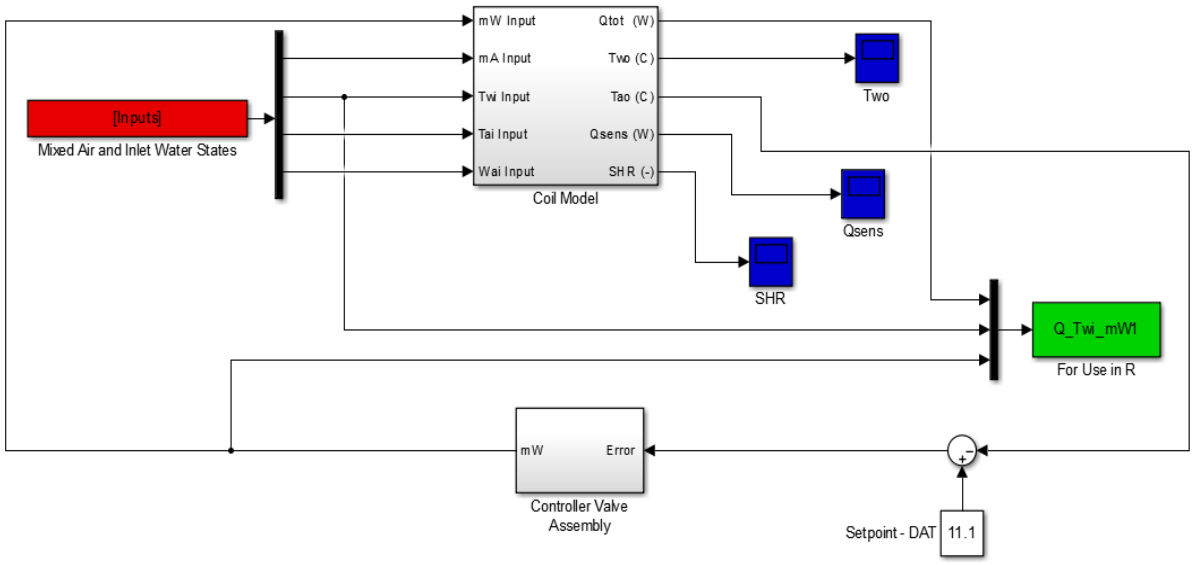

Figure 23: Complete Simulink model used in testing Classical PID control logic.

Though not completely shown in Figure 23 for brevity, outputs from each model include the mW, Q, T_{wi}, Integral Squared Error (*ISE*) over the course of the simulation, maximum DAT setpoint error, the total cooling power supplied, total pumping power used, control signal selection as well as Delta T. *ISE* is a measure of how well comfort is being met and is defined as:

$$ISE = \int_{t_o}^{t_{final}} (w(t) - y(t))^2 \; dt \qquad \text{Eqn. 46}$$

where $w(t)$ and $y(t)$ are the DAT setpoint and the measured DAT, respectively. Start time t_o was chosen to be one hour into the simulation to allow for the system to settle from disturbances due to initial conditions. The end time t_{final} was taken to be the end of the simulation.

Total cooling power supplied was taken to be the integral of Q over the course of the simulation. The pumping power (*PP*) was computed by use of an exponent equaling 2.2 in the following equation.

$$PP \propto mW^{2.2} \qquad \text{Eqn. 47}$$

Pump affinity laws estimate pumping power to be proportional to the cube of mW. However, that is when ideal scenario. In all reality, pump efficiency decreases with decreasing flow rate, and thus an exponent of 2.2 is more appropriate (Fact Sheet: Variable Frequency Drives). The above *PP* is not actually pumping power as we are leaving out the coefficient inherent to each individual pump. However, that coefficient would be assumed to remain constant between testing of the various control strategies and thus comparing *PP* for each simulation would provide insight in to the relative amounts of pumping power consumption each strategy required.

Testing of the various strategies were performed on 16 different coils. Those coils included the following from each of the four primary climates of Atlanta, L.A., Miami and Boulder:

- CAV 1 system from the Hospital model with a degrading T_{wi} schedule
- VAV 1 system from the Hospital model with a degrading T_{wi} schedule
- CAV 1 system from the Office model with a reset T_{wi} schedule
- VAV 1 system from the Office model with a reset T_{wi} schedule

The first round of testing included using all the established setpoints/limits derived from the methods already described. The complete step by step process with all appropriate Matlab and R scripts for this initial round of testing can be seen in Appendix L. From the data collected in each simulation, the following outputs for each simulation were put in a table for analysis of the results:

- Row configuration
- T_{wi} schedule
- *FPMC*
- *CV*
- Various controller limits
- *ISE* percentage increase from base case (DAT tracking control)
- Cooling power percentage decrease from base case

- Pumping power percentage decrease from base case
- Pumping power percentage decrease to *ISE* percentage increase ratio
- Pumping power percentage decrease to cooling power percentage decrease ratio
- Average Delta T

It is expected that some strategies will be more aggressive than others. An initial attempt to normalize the simulations was done through the metrics "Pumping power percentage decrease to *ISE* percentage increase ratio" and "Pumping power percentage decrease to cooling power percentage decrease ratio". This may be too simplistic as such ratios may change for a specific control strategy when varying its controller setpoint. A second round of testing was completed for the same coil set. It included taking the advanced strategy with the lowest *ISE* (least aggressive) as a baseline, and attempting to match the other advanced strategies' *ISE* by manipulation of their controller limits. This included numerous iterations for each advanced strategy on each coil. All *ISE* values for the four advanced control strategies were brought within 5% of each other and results published. This put all control strategies on an even playing field as they would induce an equal amount of discomfort on the occupants which the coil serves. Comparison of other values such as pumping power reduction from base case and average water-side Delta T could be more appropriately made.

4. Results

4.1. Cooling Coils Data

After substantial modifications to the template EnergyPlus models, saturation was achieved for all coil models, in all systems, at all locations of interest. Matlab was used to perform bin analysis in the Q vs mW plots for a variety of input parameters. Plots from select CAV 1 and VAV 2 coils in Atlanta's hospital model can be seen in Figures 24 through 35 below. Appendix F has more such plots for all locations investigated. It should be noted the vertical line of data points seen in each plot below are instances when the DAT setpoint could not be met and the maximum mW was being sent to the coil. Real world coils that are undersized at times exhibit similar behavior of the valve being fully opened, but pressure fluctuations in the CHWS would prevent such a distinct vertical line from developing in the Q vs mW profile. Such data was cropped out of the datasets prior to any analysis in R being performed.

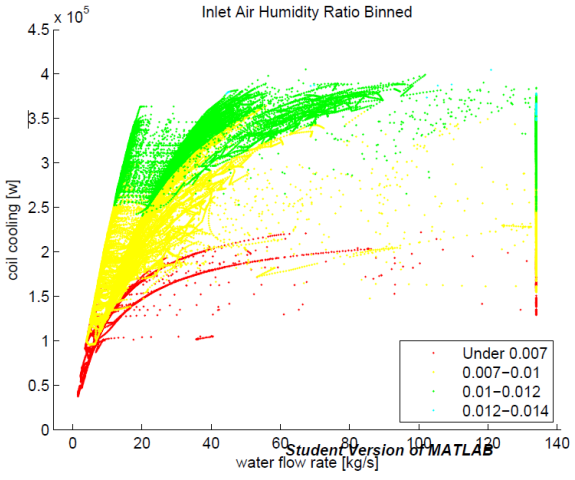

Figure 24: W_{ai} bin plot for Atlanta CAV 1.

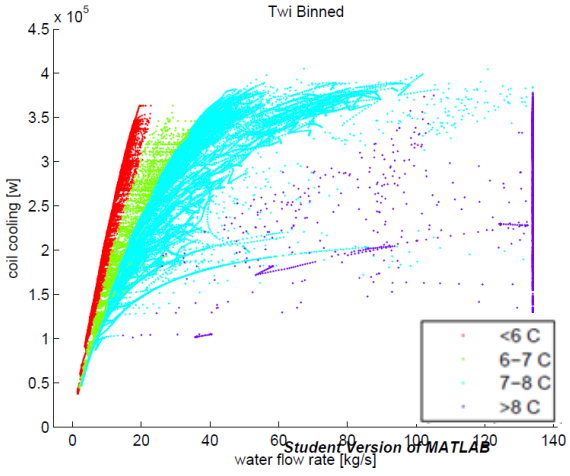

Figure 25: T_{wi} bin plot for Atlanta CAV 1.

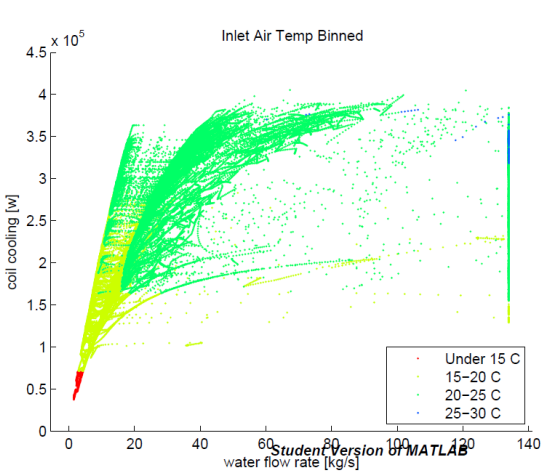

Figure 26: T_{ai} bin plot for Atlanta CAV 1.

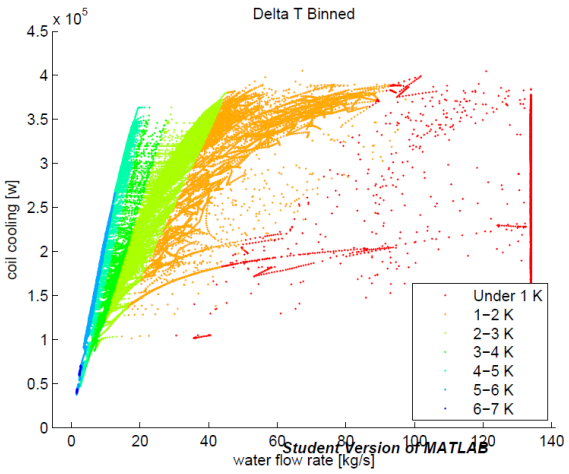

Figure 27: Delta T bin plot for Atlanta CAV 1.

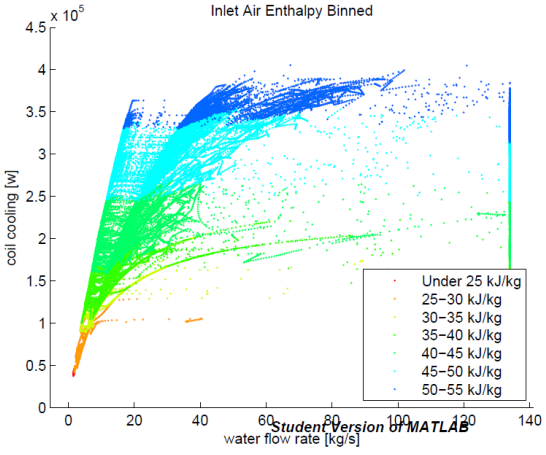

Figure 28: h_{ai} bin plot for Atlanta CAV 1.

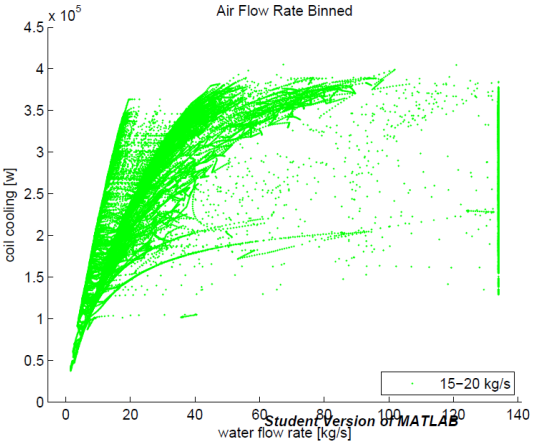

Figure 29: mA bin plot for Atlanta CAV 1.

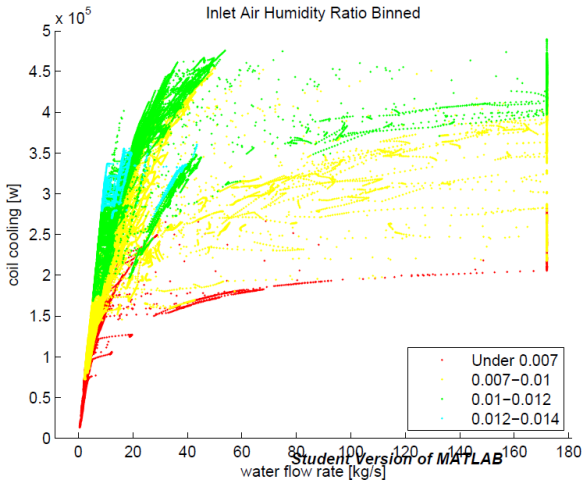

Figure 30: W_{ai} bin plot for Atlanta VAV 1.

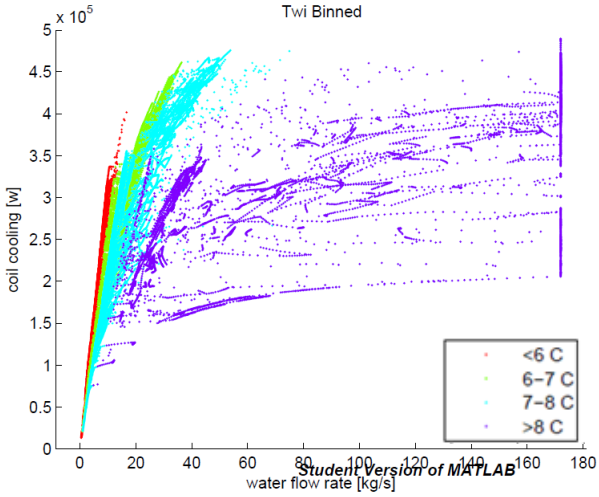

Figure 31: T_{wi} bin plot for Atlanta VAV 1.

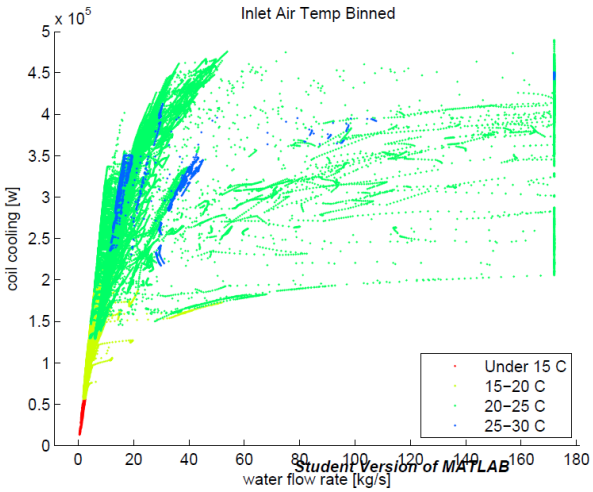

Figure 32: T_{ai} bin plot for Atlanta VAV 1.

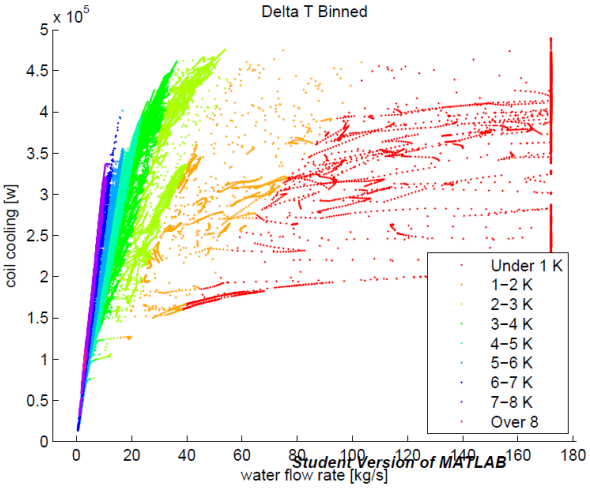

Figure 33: Delta T bin plot for Atlanta VAV 1.

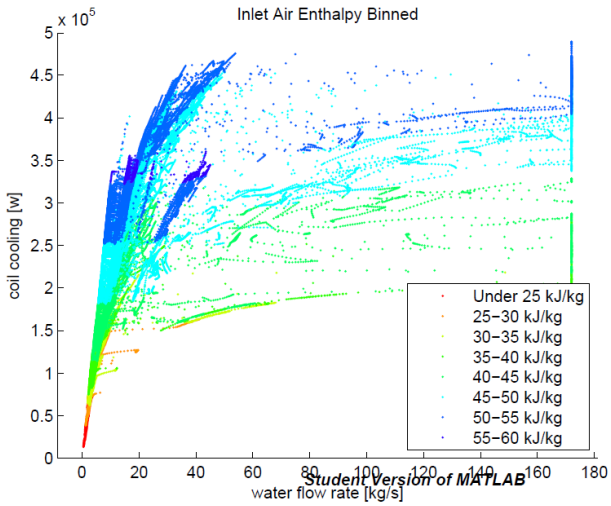

Figure 34: h_{ai} bin plot for Atlanta CAV 1.

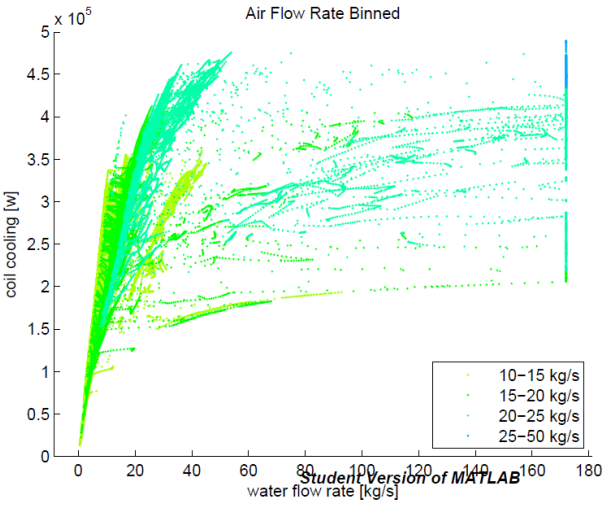

Figure 35: mA bin plot for Atlanta CAV 1.

Bin plots were produced for two reasons. First, they provided assurance as to the validity of the simulated data. Certain trends in the data were expected and were realized. For instance, cooling capacity generally increased with increasing W_{ai}, T_{ai} and mA for the same mW. Additionally, lower capacities and lower water-side Delta T's were observed for higher T_{wi} bins, as was expected (Taylor, 2002). Secondly, these plots provided an avenue to help identify differences between CAV and VAV coils for the same climate, as was discussed in detail in Spread of Inlet Water Temperature Bins subsection of Methodology.

4.1.1. Validation of Results

Five coils of varying UA values were produced and simulated for each system, thus a total of 80 different coils were initially generated to perform preliminary analysis on. To further validate the surrogate data, the geometric parameters of the coils were cross referenced with performance data of similar sized coils available in industry.

Prior to running any simulations, the fin thickness, fin spacing, tube diameters, tube spacing and row spacing were all verified to be representative of what is seen in industry. Various row configurations of the Atlanta's CAV 1 coils were compared to equivalent coils available in industry.

Specifically, the generated coils' cooling power densities (Q/m^2) were compared to manufacturer performance data of similarly sized coils.

EnergyPlus defaults to a 1.4 m tube length on when autosizing cooling coils' geometric parameters as can be seen the examining the autosizing process in EnergyPlus' Engineering Reference (Dept. of Energy, 2012). Coil dimensions and performance data were obtained for a KeepRite Series 80 chilled water coil. Technical specifications and performance data can be seen in Appendix G. Assuming 67°F (19.4°C) inlet air wet bulb temperature and a 45°F (7.2°C) inlet water temperature, the Atlanta CAV 1 coils were compared to the 60" (1.524 m) nominal tube length KeepRite coil. On the EP coils, when taking the design air flow rate divided by the coil area, a velocity just under 400 fpm (2.023 m/s) is found. The manufacturer's documented cooling power density (tons/ft2) was given the appropriate conversions and area adjustments to bring it on par with Atlanta's CAV 1 coil. Estimated coil capacities from the KeepRite coil of 409,503 W, 351,691 W, and 279,426 W were found for the eight-row, seven-row and six-row configurations, respectively. The design capacity output from EP was 374,157 W. Therefore, the EP coils were right on par with what is commercially available. The eight-row coil met the required capacity, the seven-row configuration did as well but with a lot more water flow, and the six-row coil was simply undersized for design conditions. See Figure 36 (a) through (c) for those three configurations.

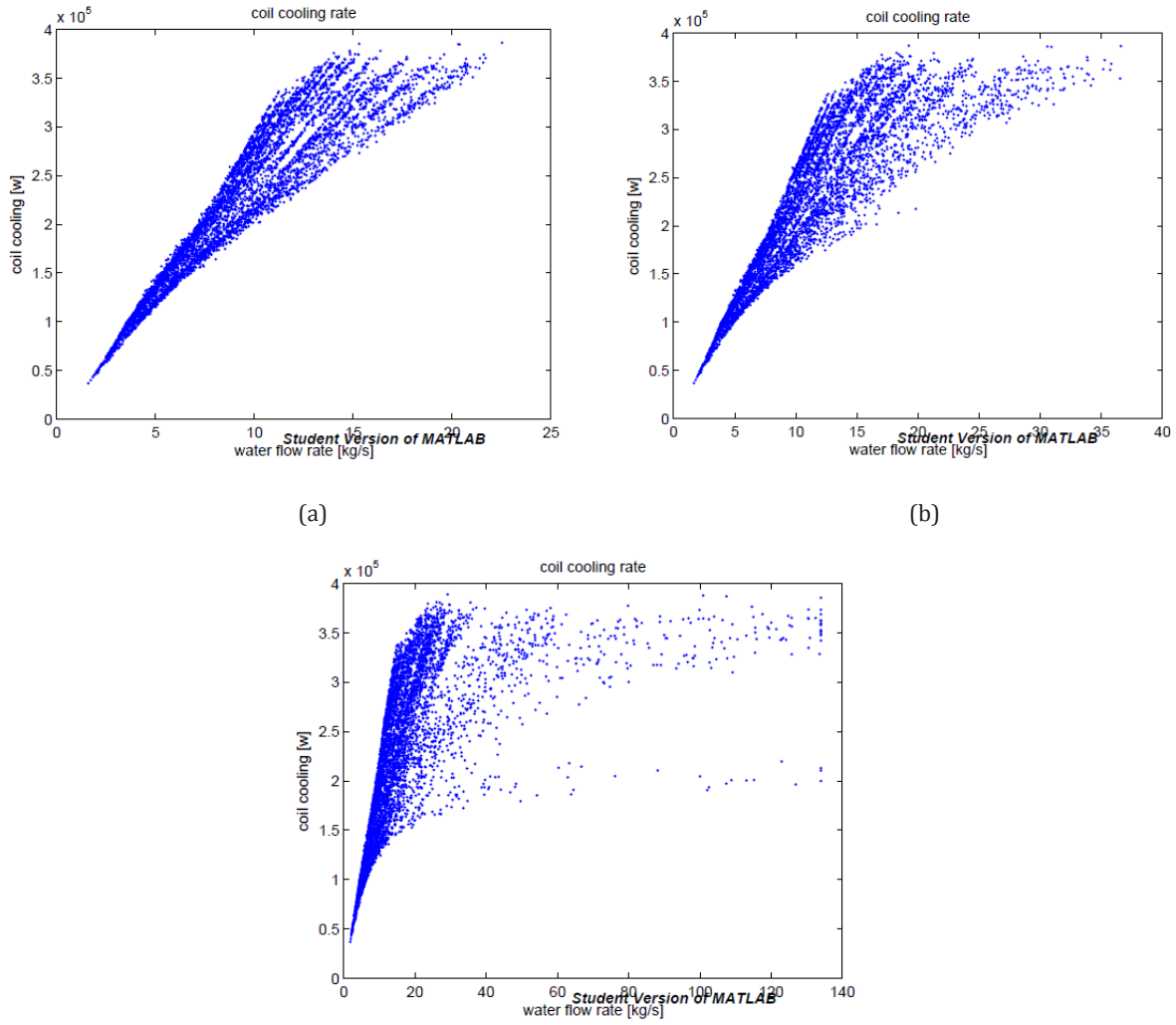

Figure 36: Q vs mW plots for (a) 8-row, (b) 7-row and (c) 6-row configurations.

It is concluded that the EP coils are realistic in their geometries and performance. The massive capacity requirements of this particular facility just call for them to be quite tall (on the order of 5 m).

4.1.2. Effects of Changing T_{wi} Schedule

All of the initial 80 coil simulations included a degrading T_{wi} schedule representative of the central chilled water plant unable to meet the higher loads seen in the hotter part of the days. To visually see the effects of implementing a T_{wi} reset schedule, which would have colder T_{wi}'s during

the hottest part of the day, T_{wi} bin plots were produced in Matlab for the same coil experiencing the two different T_{wi} schedules.

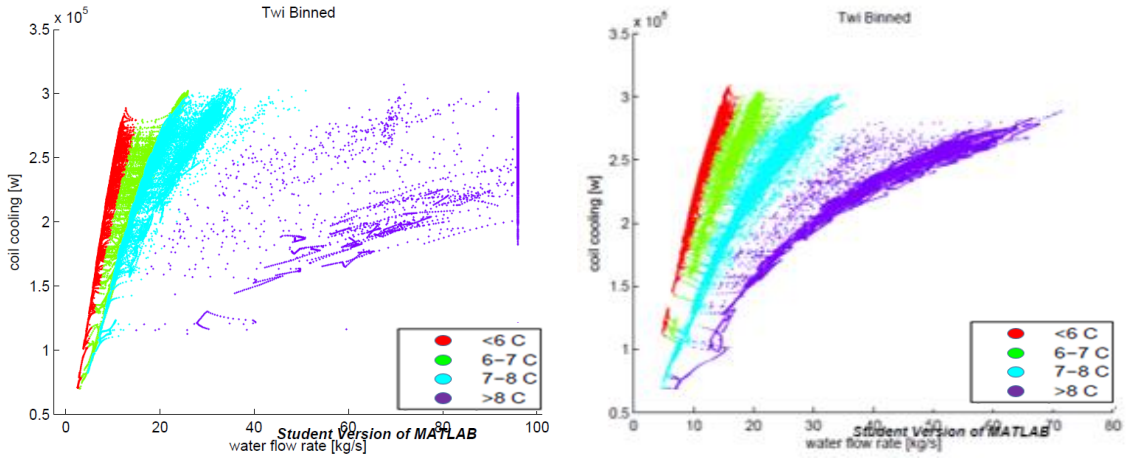

(a) (b)

Figure 37: (a) Degrading T_{wi} schedule. (b) T_{wi} reset scheduled used for the same system.

The coil shown in both Figure 37 (a) and 37 (b) was of a six-row configuration. Figure 38 below shows the results of the seven-row configuration for the same system simulated with a degrading T_{wi} scheduled. Figure 38 compares quite closely to the T_{wi} reset schedule imposed on the six-row configuration shown in Figure 37 (b). The other bin plots also compare nicely. It is apparent that implementation of a T_{wi} reset schedule could reduce the size of the required coil, saving on installation costs. Decreased chiller efficiencies and increased flow during low load periods as pointed out by Taylor (2002) may prove this approach to not be beneficial when looking at whole building energy consumption and life cycle cost analysis. Such decisions should be made on a case by case basis after performing appropriate energy modeling of the system in question.

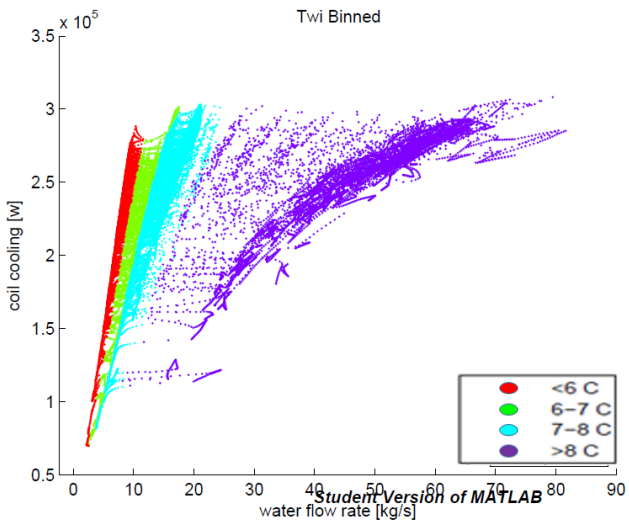

Figure 38: 7 row configuration coil with a degrading T_{wi} schedule.

4.2. Distinction between CAV and VAV AHU Applications

4.2.1. k_2 Deviation

The deviation in the exponential curvature (k_2) between the 5% and 95% quantiles of a dataset was expected to be substantially larger for VAV coils than for CAV in a specific climate based on the work of Thuillard *et al.* (2014). Regression on these quantiles was performed for all of the initial 80 coil datasets in RStudio. The R script which performed this analysis as well as instructions on how to properly apply the curve fits via this script can be seen in Appendix E. It was found that even with the large amount of data (six months' worth of five minute intervals), fitting of the exponential function through non-linear regression of the quantiles was difficult. Adjustments to the total number of *mW* bins and the portion of those bins used in the regression at times produced quite large deviations in the outputted coefficients k_1 and k_2. Figure 39 shows a scenario where subjectivity on the part of the analyst would largely affect the outputted coefficients. Selecting the first seven bins for the 95% quantile curve fit (yellow dots) would provide a much different set of *k* coefficients than if one chose the first 15 *mW* bins.

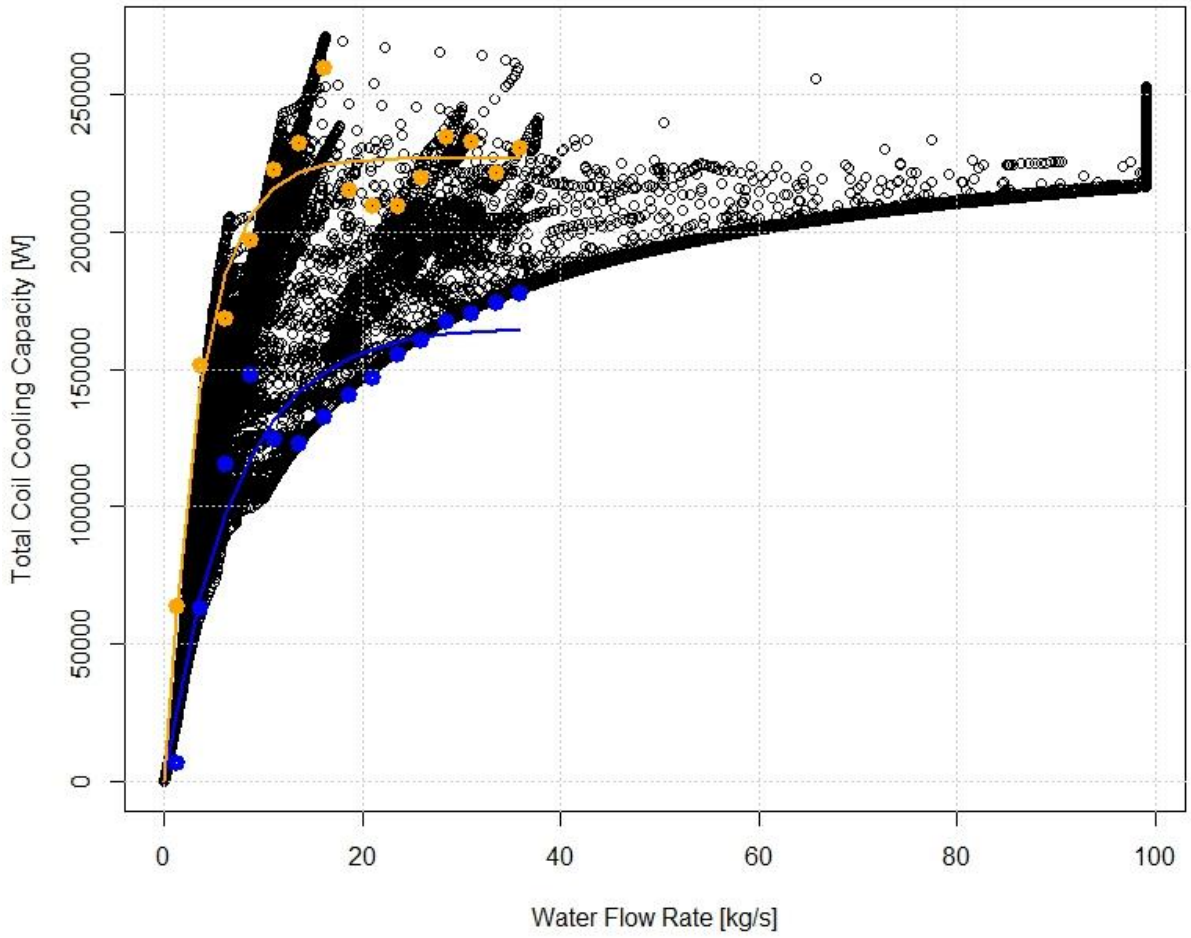

Figure 39: Regression on the 95% and 5% quantiles.

In an effort to fully document the repeatability of this fit, all 80 datasets were analyzed twice. The difference in the 5% quantile k_2 values between the analysis runs for the same dataset was on average 18%. The variability in the 95% quantile k_2 values was on average 11%. The repeatability of this method to obtain k_1 and k_2 coefficients for regression on the 5% and 95% quantiles was proven quite poor.

From the outputs of each analysis run, the hypothesis that CAV coils would maintain distinguishably lower variations in the k_2 coefficient between the 5% and 95% quantiles when

compared to VAV coils was tested. Table 3 (a) and (b) show the maximum and average deviations between those two quantiles for analysis runs #1 and #2.

Table 3: (a) Analysis run #1 results. (b) Analysis run #2 results.

(a)

ATLANTA SUMMARY	
Max k2 Deviation in CAVs (%)	33.31
Avg k2 Deviation in CAVs (%)	17.98
Max k2 Deviation in VAVs (%)	37.77
Avg k2 Deviation in CAVs (%)	18.36
BOULDER SUMMARY	
Max k2 Deviation in CAVs (%)	92.69
Avg k2 Deviation in CAVs (%)	32.86
Max k2 Deviation in VAVs (%)	62.66
Avg k2 Deviation in CAVs (%)	24.30
LOS ANGELES SUMMARY	
Max k2 Deviation in CAVs (%)	72.82
Avg k2 Deviation in CAVs (%)	38.05
Max k2 Deviation in VAVs (%)	39.38
Avg k2 Deviation in CAVs (%)	21.34
MIAMI SUMMARY	
Max k2 Deviation in CAVs (%)	166.06
Avg k2 Deviation in CAVs (%)	59.69
Max k2 Deviation in VAVs (%)	13.32
Avg k2 Deviation in CAVs (%)	8.07

(b)

ATLANTA SUMMARY	
Max k2 Deviation in CAVs (%)	113.97
Avg k2 Deviation in CAVs (%)	30.64
Max k2 Deviation in VAVs (%)	66.67
Avg k2 Deviation in CAVs (%)	26.90
BOULDER SUMMARY	
Max k2 Deviation in CAVs (%)	83.26
Avg k2 Deviation in CAVs (%)	28.70
Max k2 Deviation in VAVs (%)	62.66
Avg k2 Deviation in CAVs (%)	24.68
LOS ANGELES SUMMARY	
Max k2 Deviation in CAVs (%)	72.82
Avg k2 Deviation in CAVs (%)	40.22
Max k2 Deviation in VAVs (%)	54.00
Avg k2 Deviation in CAVs (%)	27.92
MIAMI SUMMARY	
Max k2 Deviation in CAVs (%)	59.70
Avg k2 Deviation in CAVs (%)	33.34
Max k2 Deviation in VAVs (%)	18.57
Avg k2 Deviation in CAVs (%)	9.33

In analysis run #1, only in the Atlanta climate did CAV coils have lower maximum and average deviations between the 5% and 95% quantiles' k_2 parameters. Even then, the slightly lower values are well within the amount of error these values have to begin with. In analysis run #2, the VAV coils in all climates maintained lower deviations in k_2 between the 5% and 95% quantiles, but again the differences are within the expected amount of error in the coefficients themselves due to the nature of this approach.

Attempting a different approach to distinguish between CAV and VAV datasets, barbell plots were performed with analysis run #2's data. Values of k_2 and k_1 for both the 5% and 95% quantiles

were plotted and connected together. Plots were performed showing all the coils of equal row configurations against each other. Figure 40 shows the plot of all eight-row coils and the remaining plots can be seen in Appendix E.3. The barbell handle for all VAV coils is red and for CAV coils, green.

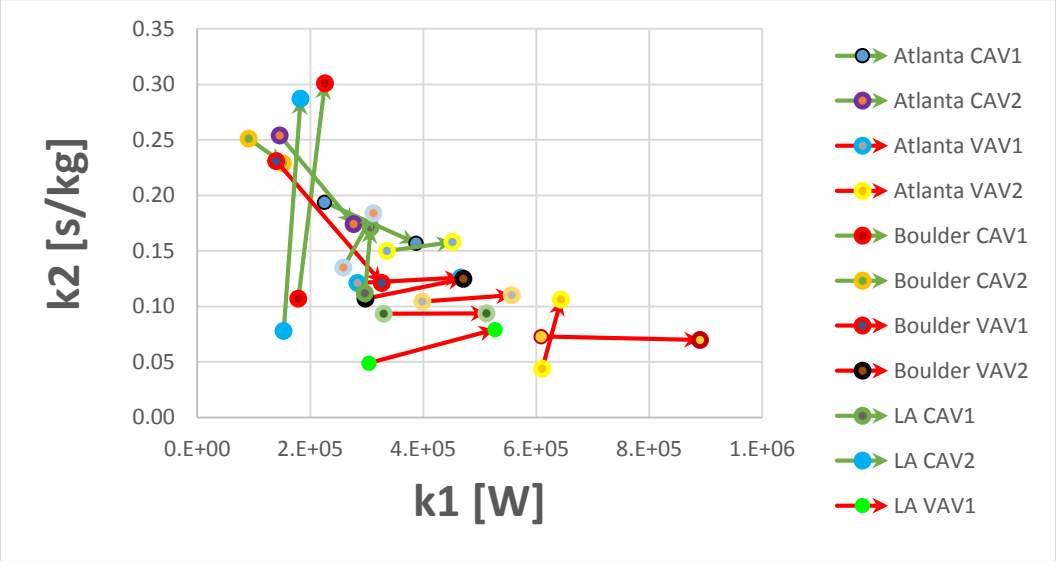

Figure 40: k_2 - k_1 barbell plot for all 8 row configuration coils.

Again, no distinguishable differences between the two applications can be seen. The fact that the k_1's for the VAVs are typically higher and the VAV k_2's are typically lower is solely attributed to the fact that the system loads for the VAV applications are larger in the template building models used from the Department of Energy.

If one was to trust these results, the hypothesis that comparison of the deviations in the k_2 coefficient between the 5% and 95% quantiles would distinguish whether a coil was CAV or VAV is rejected. Due to the inherent subjectivity of this approach and its lack of repeatability, no reliable conclusions could be drawn from the results of this approach. Prior to making any such conclusion, the Four-Parameter Curve Fit was used to investigate deviations in k_2 from the lower and upper portions of the Q vs mW plots.

Figure 41 shows the T_{wi} bin plot from Matlab on the left, and the R plot with constant T_{wi} lines on the right. It can be seen this is quite a good approximation. Figures 42 (a) and (b) show the same dataset with curve fits from the quantile bin analysis and with the Four-Parameter Curve Fit, respectively. The Four-Parameter Curve Fit approach took much of the subjectivity out of the equation. It also was much more repeatable.

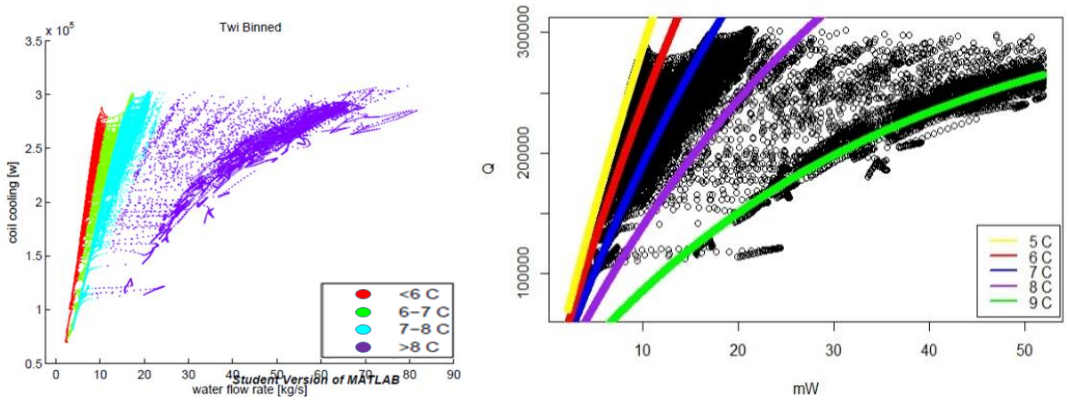

(a) (b)

Figure 41: (a) T_{wi} bin plot. (b) Cooresponding Four-Parameter Curve Fit predictions.

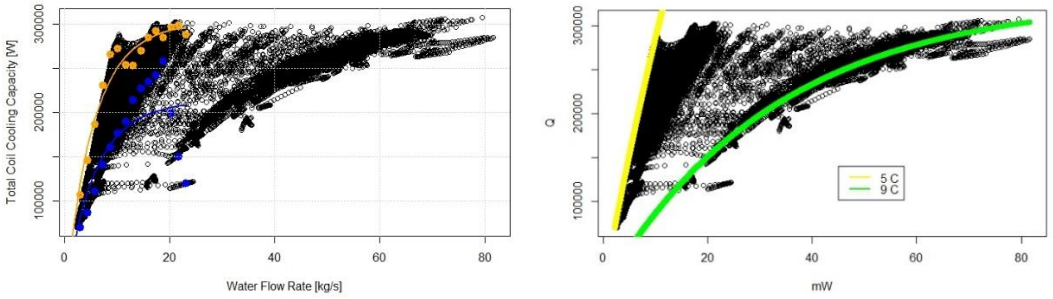

(a) (b)

Figure 42: (a) Regression on the mW bins' quantiles. (b) Constant T_{wi} lines from Four-Parameter Curve Fit.

When taking the constant T_{wi} lines at 5°C and 9°C as the upper and lower bounding curves, all coil datasets were again looked at. Results now show that CAV coils have higher k_2 deviation from

the low to high bounding curves of the data in all climates, completely negating the initial hypothesis. It is thus concluded that fluctuating inlet air humidity levels (W_{ai}) do play a dominate role in the exponential curvature of the Q vs mW plots.

4.2.2. Validation of k_2's Dependence on T_{wi}

In the Four-Parameter Curve Fit, the exponential curvature k_2 was made a function of inlet water temperature T_{wi} as seen in Equation 20. This contradicts findings in Thuillard *et al.* (2014). They found negligible dependence of k_2 on T_{wi} and T_{ai}, while finding appreciable dependence on W_{ai} and mA. The coefficient k_2 was derived from the effectiveness-NTU model in the Methodology, and it was suggested that though k_2 is effectively independent of T_{wi} for completely dry and completely wet coils, an indirect dependence on T_{wi} will occur for coils operating in a partially dry/partially wet scenario. To investigate the importance of including a dependence on T_{wi} in the k_2 estimate, parametric runs were performed with 32 coils sets (16 hospital and 16 office) over a variety of coil configurations and operating characteristics in which the Four-Parameter Curve Fit was compared to effectively a Three-Parameter Curve Fit. The Three-Parameter Curve Fit maintained a constant k_2 which replaced the ($b_2 + b_3T_{wi}$) term. The Three-Parameter Curve Fit can be seen in Equation 48:

$$Q = (b_o + b_1T_{wi})(1 - e^{-k_2mW}) \qquad \text{Eqn. 48}$$

For each coil set, the average W_{ai} for each T_{wi} bin was computed as well as the CV and Normalized Mean Biased Error ($NMBE$) for both the Three and Four-Parameter Curve Fits. $NMBE$ can be defined as follows

$$NMBE = \sum_{i=1}^{N}(y - x)/[mean(x)(N - DOF)] \qquad \text{Eqn. 49}$$

where x is an observed capacity point, y is the corresponding predicted capacity from the respective curve fit, N is the number of data points in which the non-linear regression is being performed on, and DOF is the number of degrees of freedom which is four for the Four-Parameter Curve Fit and

three for the Three-Parameter Curve Fit. Complete findings from such tests can be seen in Appendix J. As expected, the *CV* for each coils was slightly higher for the Three-Parameter Curve Fit than the Four-Parameter Curve Fit as it has one less degree of freedom to work with. The percentage increase in the *CV* values between the two curve fits averaged 3.85% for the office coils and 2.99% of the hospital coils. The *NMBE* were not consistently higher for the Three-Parameter Curve Fit due to the nature of the metric in which positive error cancels out negative error. Average inlet air humidity (W_{ai}) for the various T_{wi} bins did not vary as much as expected. Lower minimum outdoor air fractions coupled with large reductions in internally generated latent loads during the nighttime was expected to result in a lower average W_{ai} for T_{wi} bins that occur during such hours. Following this logic, the average W_{ai} was expected to be the highest for T_{wi} bins occurring during the occupied hours. For example, in a reset T_{wi} schedule scenario, the low temperature T_{wi} bins that occurs during the mid-afternoon hours would be expected to have a higher average W_{ai} than the warmest T_{wi} bin which occurs at night. However, this was not the case. The average W_{ai} across the T_{wi} bins remained relatively constant, both in simulations with T_{wi} reset schedules and degrading T_{wi} schedules. This may be attributed to the fact that dry bulb economizers were used in every simulation tested. Nighttime use of the economizers is expected to be more prevalent than daytime use, which may result in higher W_{ai} during the nighttime than expected. Dry bulb economizers compare return air temperature to outside air temperature. The outside air humidity ratio is not factored into a dry-bulb economizer's logic for when it should be utilized or not.

Variation in the predicted exponential curvature k_2 between the 5°C and 8°C for the Four-Parameter Curve Fit was also looked at. Average deviation between these two temperatures were 32.4% and 13.5% for the office and hospital coils, respectively. Again, all the detailed results of the 32 simulations can be seen in Appendix J. To graphically illustrate the significance of this variation,

normalized capacity curves for the CAV and VAV coils that most closely exhibited the average k_2 deviation can be seen below.

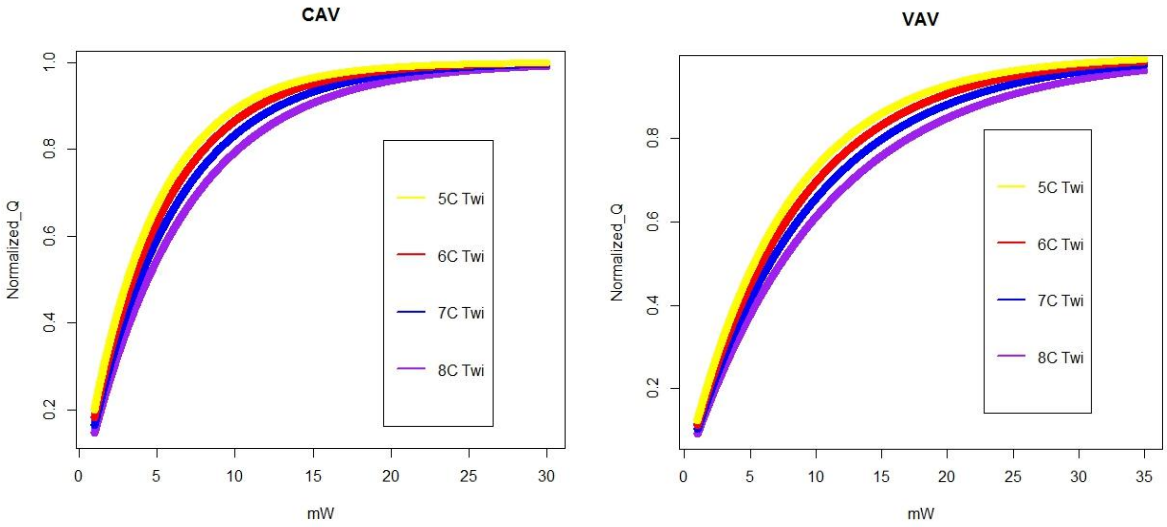

(a) (b)

Figure 43: Normalized capacity vs mW plots for (a) CAV and (b) VAV coils that have k_2 deviations between 5°C and 8°C T_{wi} lines most near the average deviations seen throughout the simulations.

The CAV and VAV coils that exhibit the maximum k_2 variation between the 5°C and 8°C T_{wi} lines can be seen below.

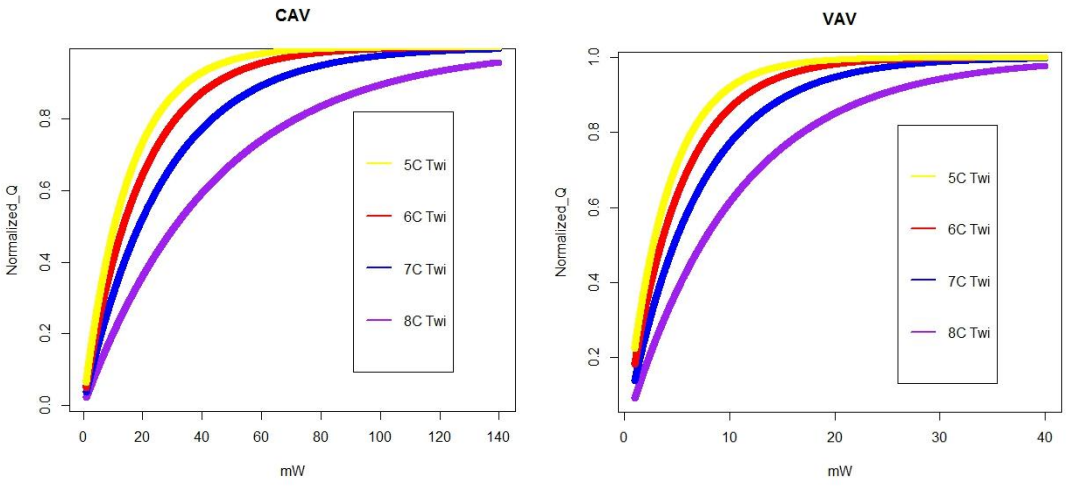

(a) (b)

Figure 44: Normalized capacity vs mW plots for (a) CAV and (b) VAV coils that have the most drastic k_2 deviations between 5°C and 8°C T_{wi} lines.

To some extent, every coil exhibited a dependence of k_2 on T_{wi} as can be seen in Appendix J. The original hypothesis that this may largely be due to increasing average W_{ai} for T_{wi} bins that are experienced during occupied hours was rejected. To further investigate, parametric runs on the Bellucci Simulink cooling coil model was accomplished to see if the findings of Thuillard *et al.* (2014) could be reproduced. Negligible k_2 dependence on T_{ai} was found, consistent with the paper's findings. Appreciable k_2 deviations when varying mA was found, also consistent with the paper's findings. This investigation found only a k_2 dependence on W_{ai} when the coils transitioned from sensible-only cooling to cooling with dehumidification. This is consistent with findings in the Methodology's investigation into k_2, particularly the comparison of Equations 35 and 38. Negligible dependence on W_{ai} occurred when all the W_{ai} values looked at were experiencing dehumidification or when all the W_{ai} values looked at were experiencing sensible-only cooling. Similarly, parametric runs with T_{wi} as the variable found a k_2 dependence on T_{wi} only when the dew point of inlet air falls within the range of T_{wi}'s being experienced by the coil. Lower T_{wi}'s have dehumidification occurring while a higher T_{wi}'s would have sensible-only cooling. Thus, the indirect k_2 dependence on T_{wi} previously stated was validated. Below is a normalized capacity versus water flow rate plot where three different T_{wi}*'s* were tested through a range of water flow rates. The constant dew point temperature in each run was 5.5°C. Both the 6°C and 7°C T_{wi} runs produced identical normalized curves as they had the same k_2 since the dew point is not reached and both scenarios maintain sensible-only cooling. The 5°C T_{wi} run produces a different exponential curvature due to the dehumidification occurring as the T_{wi} of 5°C falls below the dew point of 5.5°C.

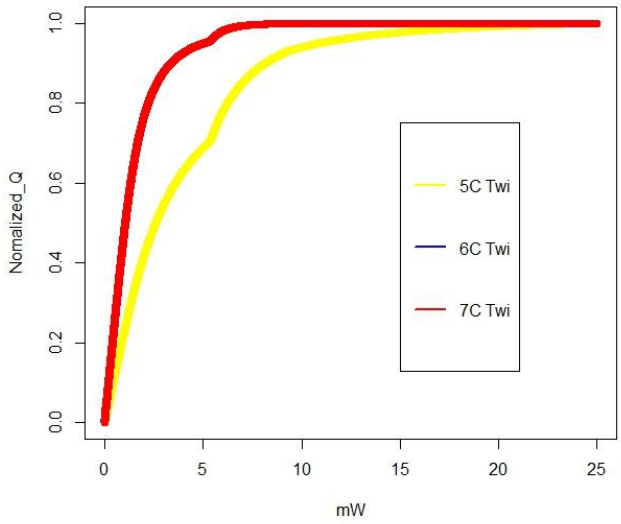

Figure 45: Normalized Q vs mW plot for range of T_{wi}*'s* that cross the inlet air's dew point.

Do to the limitation of the Bellucci Simulink model not being able to compute partially wet/partially dry cooling scenarios, one might expect the k_2 variation when crossing the latent cooling threshold to not be as severe. This may very well be the case, but the EnergyPlus coil does solve for partially wet/partially dry cooling scenarios and that coil still found a k_2 dependence on T_{wi} when the Four-Parameter Curve Fit was applied to its simulation data.

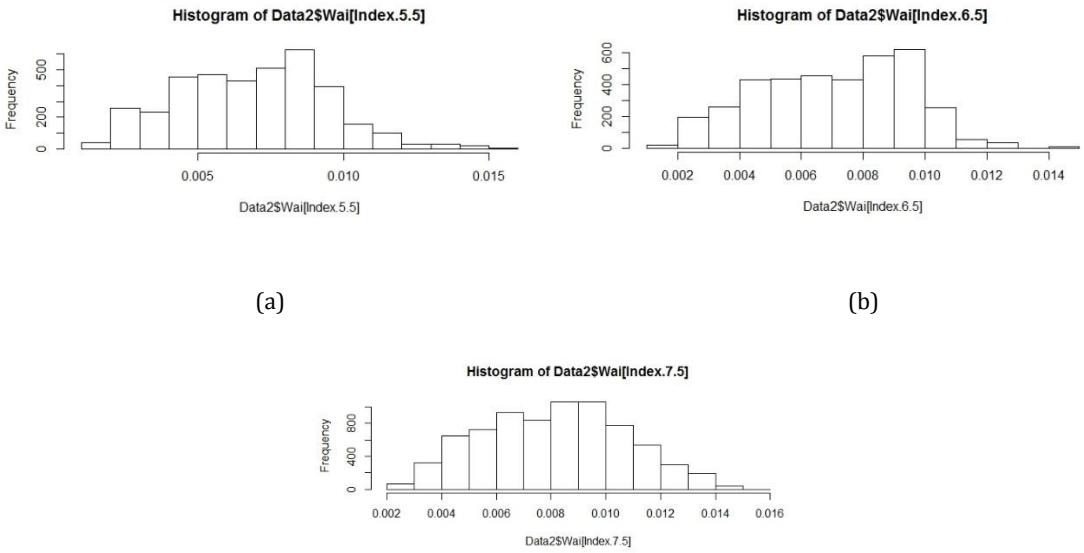

Figure 46: Inlet air humidity ratio distribution for (a) 5-6°C T_{wi} bin, (b) 6-7°C T_{wi} bin and (c) 7- 8°C T_{wi} bin.

Figure 46 above shows the various T_{wi} bins have roughly the same distribution of W_{ai}. Thus, colder T_{wi} bins would have a higher percentage of latent cooling instances than warmer T_{wi} bins. A regression on the lower T_{wi} data points would result in a normalized curve closer to that of a pure latent cooling scenario. A regression for the higher T_{wi} data points would result in a normalized curve closer to that of a sensible-only cooling scenario. This was further realized when the Three-Parameter Curve Fit was applied to various T_{wi} bins on two CAV coils from Boulder as seen in Table 4. As the T_{wi} is increased, the value of k_2 increases as the curvature is becoming more akin to the curvature of sensible-only cooling scenarios as seen by the red curve in Figure 45. As a dependence of k_2 on mA was found, VAV coils will not necessarily produce similar results due to an uneven distribution of air flow rates across the T_{wi} bins.

Table 4: Increases in k_2 realized with increases in T_{wi}.

Regression on Individual Temperature Bins with Three-Parameter Curve Fit				
Climate	**Coil**	**k_2 (5-6 C)**	**k_2 (6-7 C)**	**k_2 (7-8 C)**
Boulder	CAV 1 (6 Row)	0.063	0.091	0.095
Boulder	CAV 1 (7 Row)	0.040	0.044	0.073

4.2.3. Coefficient of Variation to Fraction of Predicted Maximum Capacity Relationships

It was hypothesized that defined relationships between *CV* and *FPMC* would exist for each climate and those relationships could then be used to predict coils of unknown applications (CAV or VAV). An R script for obtaining values of *CV* and *FPMC* for each coil can be seen in Appendix H. T_{wi} indicator temperatures of 6°C , 6.5°C , 7°C , 7.5°C , and 8°C were all evaluated to see if one provided a more defined relationship between *CV* and *FPMC*. The Four-Parameter Curve Fit and subsequent *CV* and *FPMC* calculations were performed on each of the initial 80 coil datasets. Miami's results are shown below.

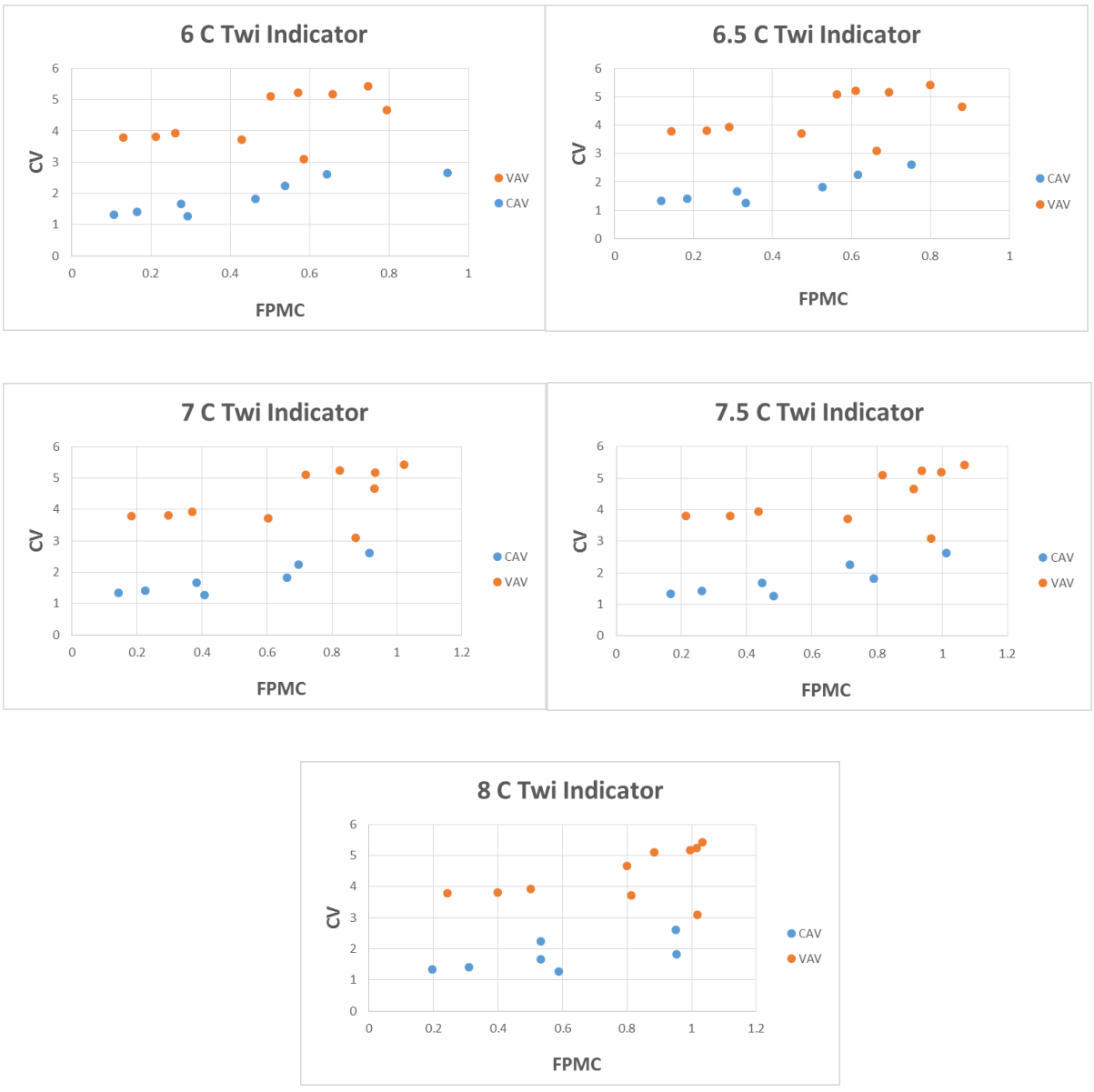

Figure 47: Miami's *CV* to *FPMC* relationships for a variety of indicator T_{wi}'s.

A definite distinction can be made between CAV and VAV coils. Similar results were found for the other three climates. Across the climates, the 6.5°C and 7°C T_{wi} indicator temperatures showed the strongest relationships. This may or may not be attributed to the fact the coils were sized in EnergyPlus based of a 6.7°C design inlet water temperature. Several outliers both seen and

foreseen needed further investigation for more thorough refinement of these relationships and are outlined in the following sub-sections of this report.

4.2.3.1. Data Indexing

When evaluating all the datasets throughout the climates, it was noticed that several coils had noticeably lower *CV* values than expected. This was attributed to the way the R script cropped the data prior to applying the Four-Parameter Curve Fit. The R script cuts out data points that are at the maximum allowable water mass flow rate as such behavior would not be experienced in a real world coils and may throw off the curve fit. For heavily undersized coils, large percentages of data points with higher T_{wi} values (those above 8°C) were located at the maximum allowable water mass flow rate. That is where the control valve was always wide open since the cooling requirements were not being met. That data was cropped out automatically in the initial R script, and subsequently the non-linear regression had an easier time fitting that data due to the smaller T_{wi} range the data now maintained. Consequently, some of the coils that were quite undersized had lower *CV* than expected.

To avoid this dilemma, the R script was modified to crop out all data points with T_{wi} above 8°C. The Four-Parameter Curve Fit was then applied to all remaining data. Figure 48 shows a slight improvement in the strength of the *CV* to *FPMC* relationships when implementing this methodology compared to the initial results for Atlanta. Similar results were seen for the other three climates.

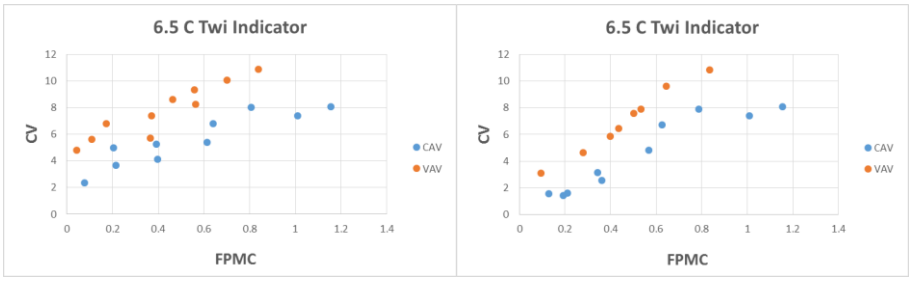

(a) (b)

Figure 48: *CV* to *FPMC* relationship improvements between the (a) initial run and (b) second run.

4.2.3.2. Times of No Cooling Load

Boulder's *CV* values were much higher than seen in other climates. This is partially attributed to Boulder being the only climate looked at that had heating loads during the period simulated in EnergyPlus. Initially, data points when mW was zero (Q was zero as well) were included in the dataset that the Four-Parameter Curve Fit was applied to. Including such points would increase the number of data points while keeping the Sum Squared Error (*SSE*) the same, as the points with zero cooling capacity would be perfectly predicted by the Four-Parameter Curve Fit. It may be expected that this would lead to a lower *CV*, but higher *CV* values persist because all these data points with Q at zero drastically bring down the mean capacity μ. This subsequently increases the *CV*. Thus, all data points with mW equal to zero needed to be cropped out of the dataset as well. This is a vital point that needs to be included in any future real world implementation of this strategy. Climates such as Boulder, where cooling is not required year-round would be most affected by such an oversight.

4.2.3.3. VAV Systems Performing Like CAV Systems

Evaluation on the initial *CV* to *FPMC* relationships shows several VAV data points that fall quite close to the CAV data points. All such data points came from coils serving the VAV 2 system of the hospital. Certain zones in the VAV 2 system were assigned minimum air flow fractions of one, while other zones were at 0.3. Thus, the VAV 2 fan had a minimum recorded air flow of between 75-80% of its maximum air flow rate, depending on climate and coil row configuration.

The VAV 2 system was in many ways performing more like a CAV than a VAV system. Therefore, an inaccurate CAV/VAV prediction in this instance may actually be beneficial in selecting the optimal control strategy. To further illustrate the effect of minimum air flow to maximum air flow fractions on the *CV* calculations, all zones in the Atlanta hospital's VAV 2 system were adjusted to minimum air flow fractions of 0.3. Due to the high internal load schedule, the minimum

experienced air flows for the system were between 39 and 48%. Still, such a reduction pushed their *CV* calculations even further from the CAV coils' data points, further strengthening the *CV* to *FPMC* relationship.

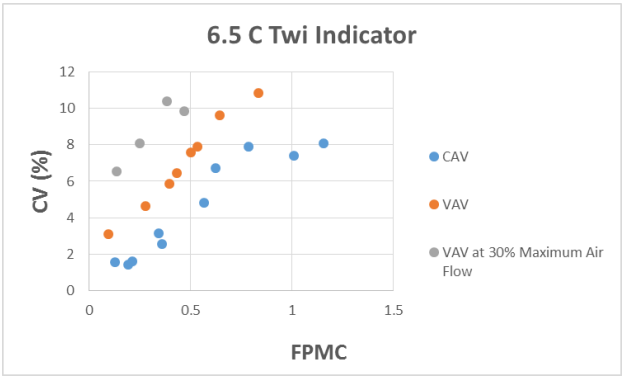

Figure 49: VAV coils with larger air flow fluctuations shown to have higher *CVs* for a given *FPMC*.

4.2.3.4. Outdoor Air Fraction Dependence

It was foreseen that the percentage of OA air entering a mixing box would adjust the *CV* to *FPMC* relationships. Further investigation into the dependence on *CV* to *FPMC* relationships on the fraction of outdoor air that exists in the entering air state needed to be performed. The default settings in the EP models did not utilize economizers for "free cooling" during times of appropriate outdoor air conditions. Zonal ventilation requirements were performed via a variety of methods which accounted both for occupancy and floor area. System ventilation rates were chosen to be computed by merely taking the sum of all the zonal requirements for the set of zones each system serves. Minimum outdoor air fractions of 25% and 30% were chosen for the VAV and CAV systems, respectively.

Outdoor air economizers utilize a controller which commands the return, exhaust and outdoor air intake dampers. During periods of favorable outdoor air conditions, cooling of the building can be performed by bringing higher fractions of outdoor air into the mixing box. This can

reduce the load on cooling coil, often times to zero. Economizers are low hanging fruit when it comes to increasing the energy efficiency of a building with minimal installation and maintenance costs. In fact, they are required for most locations in the United States (ASHRAE, 2010). The control logics implemented by such devices differ by climate and vary in complexity and performance. This is inherently due to variability in humidity ratios for both return and outside air. Bringing in more outdoor air when its dry bulb temperature is below that of return air may work well in coils providing only sensible cooling (dry coils), but this strategy alone can actually increase the cooling load on the system when the outdoor air humidity ratio is high. An economizer control schematic can be seen in Figure 50.

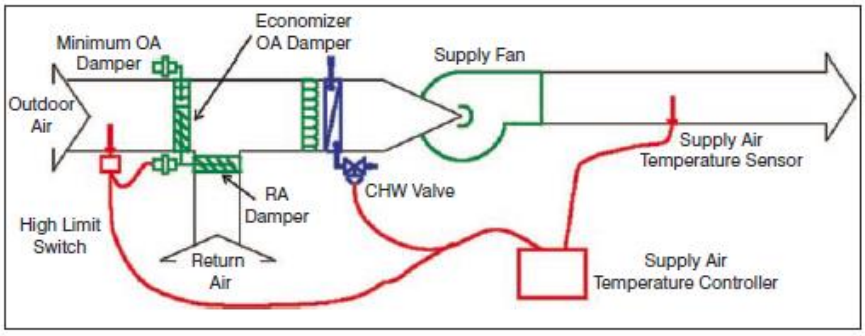

Figure 50: Outdoor air economizer controls (Taylor & Cheng, 2010).

It was predicted that implementation of an economizer cycle would affect the *CV* to *FPMC* relationships. It was expected that the Boulder location would be implementing such an economizer a larger percentage of the time and deviation from the initial *CV* to *FPMC* relationship would be highest there. Below are the results of simulating two CAV and two VAV systems with a fixed dry bulb economizer with a high limit of 23°C in the Boulder hospital. Slight increases in *CV* for both CAV and VAV coils can be seen in Figure 51.

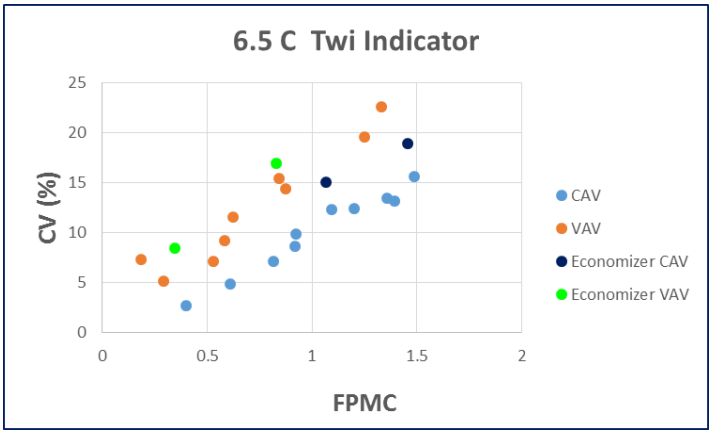

Figure 51: Boulder *CV* to *FPMC* relationships change when fixed dry-bulb economizers are implemented.

Seven of the most common control strategies for economizers which identify when an economizer should be utilized were recently evaluated (Taylor & Cheng, 2010). The procedure included modeling a typical office building for each of the ASHRAE climate zones. Expected annual energy savings when implementing an economizer with each of the control strategies was performed by comparing results to a base case without an economizer. The performance of each strategy varied widely depending on the climate, as was expected. When considering its low installation and maintenance costs, as well as inherent energy savings and minimal sensor error, the publication recommends a fixed dry-bulb control strategy for all climates, with differing high limit setpoints across the climate zones. Such recommendations can be seen in Table 5.

Table 5: Recommended fixed dry-bulb economizer settings (Taylor & Cheng, 2010).

Device Type	Acceptable in Climate Zone at Listed Setpoint	High Limit Logic (Economizer Off When):		Not Recommended In Climate Zone
		Equation	Description	
Fixed Dry Bulb	3C, 6B, 8	T_{OA} >75°F	Outdoor air temperature exceeds 75°F.	
	1B, 2B, 3B, 4B, 4C, 5B	T_{OA} >73°F	Outdoor air temperature exceeds 73°F.	
	5C, 6A, 7	T_{OA} >71°F	Outdoor air temperature exceeds 71°F.	
	1A, 2A, 3A, 4A, 5A	T_{OA} >69°F	Outdoor air temperature exceeds 69°F.	

Utilizing the recommended fixed dry bulb control strategy and the proposed high limit setpoints found in Table 5, all of the initial 80 coils were again simulated in EnergyPlus, now with use of an economizer. It is assumed that buildings that would be implementing an Energy Valve™ would also be adhering to energy codes which call for the use of an economizer. Thus, the finalized relationships for the *CV* to *FPMC* that will be extrapolated into a CAV/VAV climate dependent prediction tool will come from the outcomes of such simulations. Steps for manipulation of the EnergyPlus IDF files to incorporate such economizers can be seen in Appendix A.2.

4.2.4. CAV/VAV Prediction Tool

4.2.4.1. CV to FPMC Relationship Refinement

Refinement the *CV* to *FPMC* relationship was achieved by implementing appropriate economizer cycles on each of the buildings. All zones in the EnergyPlus building model that were served by VAV systems had their minimum air flow rate set to 30%. The revised R script, which applies the Four-Parameter Curve Fit and performs the *CV* and *FPMC* calculations from coil datasets, now crops out all times when no cooling load is imposed on the system. The revised R script also crops out data for inlet water temperatures above 8°C. The revised script is available with annotations in Appendix H.1.

For robustness of future implementation of this prediction method to real world applications, additional T_{wi} bins would need to be looked at and relationships established for the case in which a cooling coil operates with inlet temperatures far from those modeled in this body of research. For the purposes of this research, only a T_{wi} range of 5 – 8°C will be used in development of the *CV* to *FPMC* relationships.

The refined *CV* to *FPMC* relationships for the four climates can be seen in Figures 52 (a) through (d) below. These are the final relationships used in the development of a prediction tool

for coils whose application is unknown. For reasons discussed above, an inlet water temperature of 6.5°C was decided upon for use as the indicator temperature for the *FPMC* calculation.

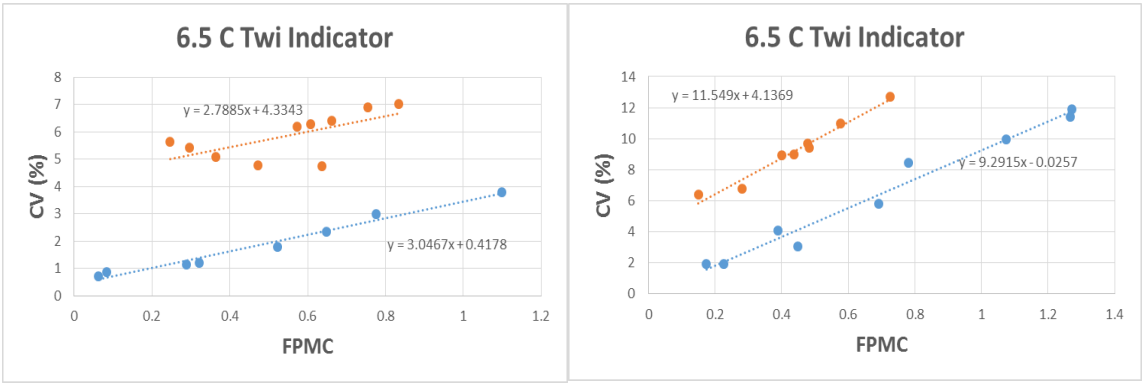

(a) (b)

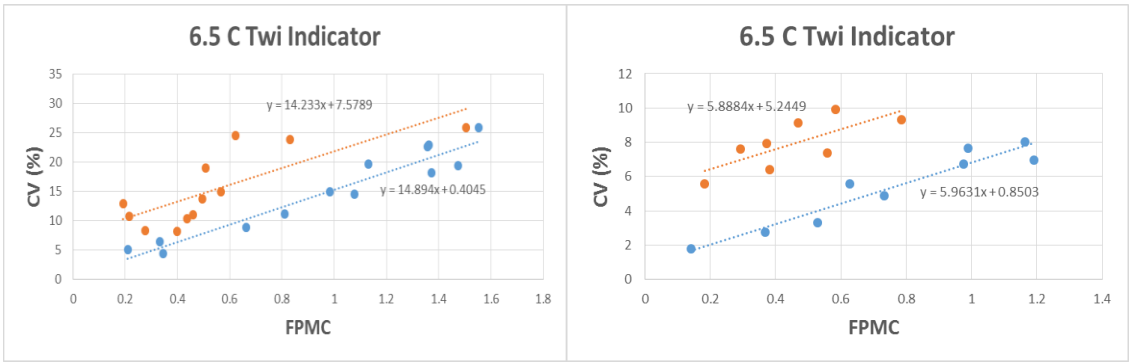

(c) (d)

Figure 52: Finalized *CV* to *FPMC* relationships for (a) Miami, (b) Atlanta, (c) Boulder and (d) L.A.

4.2.4.2. Liner Regression Relationship Plots

Linear regression was applied to the CAV and VAV coil data points on the *CV-FPMC* plots. This may not turn out to be the best approach. As can be seen in Figure 52 (a) above, the left most VAV data points actually exhibit a downward trend with increasing *FPMC*s. All these data points came from the same system, VAV 2. Further investigation into that particular system was performed and found the slope actually bottoms out and an upward trend can be seen as the coil

becomes more undersized. This parabolic behavior is evident in the left most region of the Boulder relationship, Figure 52 (c).

A parabolic curve fit to the VAV relationship may result in a better estimate of a particular climate's coil behavior, but the required time for such an investigation was not available. This and other recommendations for follow-on research is discussed in the Conclusion and Future Work section.

4.2.4.3. Climate Specific Prediction Tools

Two linear CV to FPMC relationships now exist for each climate, one for CAV and one for VAV. An additional R script was developed for each location with these linear relationships programmed in. A new coil of unknown application would be predicted to be CAV or VAV based on which of these two linear relationships it falls closer to. Issues with non-convergence of these Prediction Tools were primarily attributed to poor initial guess values of the four coefficients in the Four-Parameter Curve Fit. Numerous iterations and investigations into the best guess values that could be universally applied showed that making the b_o and b_1 coefficients' guess values as a fraction of the maximum observed capacity significantly reduced the non-convergence rate.

An additional adjustment of note is that there were instances where the T_{wi} bins in some VAV coils were so undefined, that RStudio converged on unexpected b_o and b_1 coefficients. As a result, calculated CV values were found to be much lower than expected. Shown again below is Equation 19 which defines k_1, or the maximum capacity expected to be reached for a given inlet water temperature.

$$k_1 = b_o + b_1 T_{wi} \qquad \text{Eqn. 19}$$

It would be expected that b_1 would always come out negative, but with heavily undersized VAV coils, that was not always the case. Thus, the R script Prediction Tools included an overriding

distinction: if the predicted cooling power at the maximum observed mW was higher for an inlet water temperature of 8°C than that of 5°C, a prediction of VAV would be given. An example of a VAV coil exhibiting such behavior is seen in Figure 53.

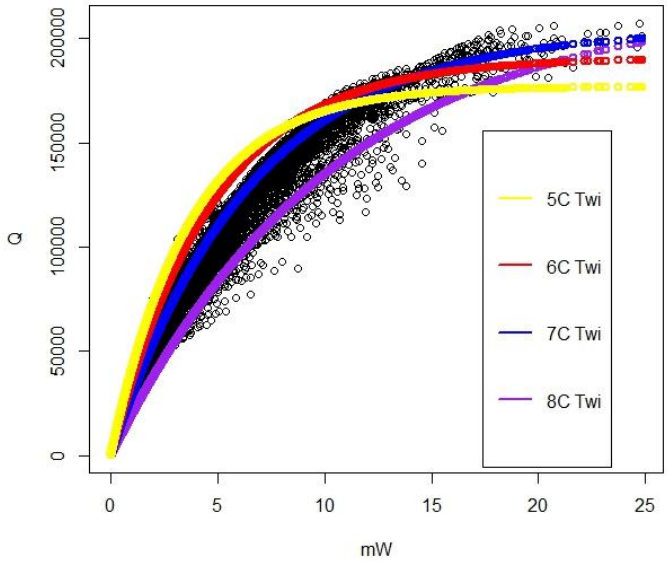

Figure 53: Instance when an unexpected b_1 coefficient leads to an incorrect prediction, thus the override prediction is used.

Purely setting b_1 constraints to not allow for negative values drastically increased the non-convergence rate of the Prediction Tool. Having an overriding distinction if b_1 was negative increased the inaccurate prediction rate as some CAV coils did converge on a negative b_1 coefficient, but the crossover of constant T_{wi} lines occurred far outside the mW range observed. Finalized Prediction Tools for each climate written in R can be seen in Appendix I.

4.2.4.4. Test Results

A variety of new, previously unseen, coils were produced to test the effectiveness of the CAV/VAV Prediction Tools in R. Economizers were used in every new coil, following the assumption that building owners investing in an Energy Valve™ are already meeting energy

standards and are reaping the benefits of economizers. For each of the four locations, the following adjustments were made to the hospital template models and resultant coils were simulated and tested:

- Minimum air flow fraction for all zones originally assigned to a CAV system were set to 30% on six-row configuration IDF models. This provided two new VAV coils for each location.
- Minimum air flow fraction for all zones originally assigned to a VAV system were set to 100% on six-row configuration IDF models. This provided two new CAV coils for each location.
- A T_{wi} resent schedule was implemented on six-row coil configuration IDF models. This provided two new CAV and two new VAV coils for each location.
- A different inputted .epw file for a location roughly 100 km away was used for the six-row coil configuration IDF models. Athens, GA weather was used for Atlanta. West Palm Beach, FL weather was used for Miami. San Diego-Miramar, CA weather was used for Los Angeles. Colorado Springs, CO weather was used for Boulder. This produced two new CAV and two new VAV coils for each location.
- Discharge air temperature setpoint was dropped from 11.1°C to 10.0°C on six-row configuration IDF models. This produced two new CAV coils and two new VAV coils for each location.

Up until this point, all *CV* to *FPMC* relationships were built on the same model building, the Department of Energy hospital template model. All test coils described above also were generated from that same source IDF model as well. To further investigate the robustness of the Prediction Tools, a completely separate building was modeled that utilized quite different construction and internal load schedules. The Department of Energy template for a large office building was used for this purpose. Acquisition of this template followed the same procedure as the hospital template.

The building consists of a twelve story, 46,320 m^2, rectangular shaped building with a basement and aspect ratio of 1.5. It has mass walls, a built-up flat roof with insulation above the decking, and a 38% window to wall ratio with even window distribution across the four exterior facades. Its envelope's thermal properties meet the ASHRAE 90.1-2004 minimums for its respective climate (ASHRAE, 2010).

The building maintains an HVAC operations schedule which shuts the HVAC system down at night. The original IDF model included four VAV systems. Adjustments were made to make two of those systems CAV. Other adjustments similar to those made for the hospital template to properly induce coil saturation and present realistic operating characteristics to the coils were also made. A step by step approach for all required IDF adjustments can be seen in Appendix A.4. Coil sizing for the large office building also mirrored the process used for the hospital. That step by step method is provided in Appendix B.

Test coil row configurations varied between five and seven-rows. Selected row configurations are highlighted in blue in Appendix C.2. Test coils generated from the large office building template model included the following scenarios:

- DAT setpoint of 12.8°C with a degrading T_{wi} schedule was initially simulated. This produced two new CAV and two new VAV test coils for each location.
- The DAT setpoint was dropped from 12.8°C to 11.1°C for all four systems. This produced two new CAV and two new VAV coils for each location.
- A T_{wi} reset schedule with a DAT setpoint of 12.8°C was simulated. This produced two new CAV and two new VAV coils for each location.
- The same alternate .epw weather files as described before were applied to the model operating under its initial DAT setpoint of 12.8°C and degrading T_{wi} schedule. This produced two new CAV and two new VAV coils for each location.

Collectively, a total of 128 new coils were tested, half of which came from the large office building model. The results can be seen in Tables 6-10.

Table 6: Miami CAV/VAV Prediction Tool Test Results.

MIAMI	**CAV 1**	**CAV 2**	**VAV 1**	**VAV 2**
Hospital				
DAT Setpoint Change to 10 C	PASS	PASS	PASS	PASS
Twi Reset Schedule Implemented	PASS	PASS	PASS	PASS
VAV systems converted to CAV	N/A	N/A	PASS	PASS
CAV systems converted to VAV	PASS	PASS	N/A	N/A
Alternative weather input	PASS	PASS	PASS	PASS
Large Office				
Normal settings	PASS	ERRORS	PASS	PASS
Twi Reset Schedule Implemented	PASS	ERRORS	PASS	PASS
DAT Setpoint Changed to 11.1 C	FAIL	ERRORS	PASS	PASS
Alternative weather input	FAIL	ERRORS	PASS	PASS

Table 7: Boulder CAV/VAV Prediction Tool Test Results.

BOULDER	**CAV 1**	**CAV 2**	**VAV 1**	**VAV 2**
Hospital				
DAT Setpoint Change to 10 C	PASS	PASS	PASS	PASS
Twi Reset Schedule Implemented	PASS	PASS	FAIL	FAIL
VAV systems converted to CAV	N/A	N/A	PASS	PASS
CAV systems converted to VAV	FAIL	FAIL	N/A	N/A
Alternative weather input	PASS	PASS	PASS	PASS
Large Office				
Normal settings	PASS	PASS	PASS	PASS
Twi Reset Schedule Implemented	PASS	PASS	FAIL	FAIL
DAT Setpoint Changed to 11.1 C	PASS	PASS	PASS	PASS
Alternative weather input	PASS	PASS	PASS	PASS

Table 8: L.A. CAV/VAV Prediction Tool Test Results.

LOS ANGELES	**CAV 1**	**CAV 2**	**VAV 1**	**VAV 2**
Hospital				
DAT Setpoint Change to 10 C	PASS	PASS	PASS	PASS
Twi Reset Schedule Implemented	PASS	PASS	PASS	PASS
VAV systems converted to CAV	N/A	N/A	PASS	PASS
CAV systems converted to VAV	ERRORS	PASS	N/A	N/A
Alternative weather input	PASS	PASS	PASS	PASS
Large Office				
Normal settings	FAIL	FAIL	PASS	PASS
Twi Reset Schedule Implemented	PASS	PASS	FAIL	FAIL
DAT Setpoint Changed to 11.1 C	PASS	PASS	PASS	PASS
Alternative weather input	FAIL	FAIL	PASS	PASS

Table 9: Atlanta CAV/VAV Prediction Tool Test Results.

ATLANTA	**CAV 1**	**CAV 2**	**VAV 1**	**VAV 2**
Hospital				
DAT Setpoint Change to 10 C	PASS	PASS	PASS	PASS
Twi Reset Schedule Implemented	PASS	PASS	FAIL	PASS
VAV systems converted to CAV	N/A	N/A	PASS	PASS
CAV systems converted to VAV	PASS	PASS	N/A	N/A
Alternative weather input	PASS	PASS	PASS	PASS
Large Office				
Normal settings	PASS	PASS	PASS	FAIL
Twi Reset Schedule Implemented	PASS	PASS	FAIL	FAIL
DAT Setpoint Changed to 11.1 C	FAIL	PASS	PASS	FAIL
Alternative weather input	PASS	PASS	PASS	FAIL

Table 10: Collective CAV/VAV Prediction Tool Test Results.

	Correct Prediction	Convergence Errors	Incorrect Prediction
Miami	26	4	2
Boulder	26	0	6
Atlanta	25	0	7
LA	25	1	6
Total	102	5	21
Percentage Rate	**79.69**	**3.91**	**16.41**

A correct prediction rate of nearly 80% was realized. Convergence errors with the R scripts occurred 3.91% of the time and incorrect predictions happed 16.4% of the time. Analyzing Tables 6 through 9 provides no clear distinction as to when accurate predictions or convergence errors are expected to persist. Many factors affect the performance of cooling coils and each of the coils tested saw a different set of factors to include, inlet water temperature schedules, DAT setpoints, internal loads, weather inputs, nighttime setbacks in rooms' thermostat settings, internal load schedules as well as host of others. The VAV 2 coil in Atlanta's large office building and the CAV 2 coil in Miami's large office building consistently produced errors in either inaccurate predictions or convergence. Such consistency is not unexpected however, it may just indicate the dominant factors which affect the coil's performance were those which were not changed between simulations, e.g. internal load schedules.

4.2.4.5. Predicting Coils in Unestablished Locations

The use of established *CV* to *FPMC* relationships has been shown, albeit through model data alone, to be effective in predicting whether a coil is operating in a CAV or VAV application. The question then persists, how could one utilize this knowledge to make such predictions in locations where *CV* to *FPMC* relationships have not been established? Utilizing the same approach for establishing said relationships for all conceivable locations in which the Energy Valve™ could be

used would require endless amounts of simulations. That approach is clearly unobtainable and ill-advised. Two other possible approaches exist.

The first option would be the use spatial inference on the coefficients of the linear *CV* to *FPMC* relationships for the locations that are established. These coefficients would be the slopes and intercepts for the linear regression lines describing the VAV and CAV data points on the *CV* to *FPMC* plots. Spatial inference utilizes geographic proximity of established locations to the new location in question, proportionally weights the coefficients of the established locations based off their relative proximities, and provides estimates of the coefficients for the location in question. With the four established locations being so largely separated geographically, this approach would also include a substantial amount of additional simulations before this method could be effectively tested. Due to time constraints, this body of research focused on a second option described next.

The second option consists of using the known *CV* to *FPMC* relationships of a particular location, and assuming those relationships to be constant throughout the ASHRAE climate zone that the location is sitting in. For example, the Prediction Tool established for Atlanta could be used for all locations in ASHRAE climate zone 3A.

Application of this second option was used in tests for three of the four established ASHRAE climate zones. Selection of unestablished locations for testing needed to meet two criteria. First, they needed to be in the same ASHRAE climate zone as one of the establish locations. Secondly, locations with large geographical separation from the established locations were chosen as to more thoroughly test the robustness of the CAV/VAV Prediction Tools. Miami falls within ASHRAE climate zone 1A, which is quite small geographically and thus Miami is the only location with available .epw weather files. Therefore, this particular climate zone was not tested. Atlanta's Prediction Tool was used to predict coils operating in Little Rock, AR. L.A.'s Prediction Tool was used to predict coils operating in Las Vegas, NV. Boulder's Prediction Tool was used to predict coils

operating in Reno, NV. The ASHRAE climate zone map with all such locations labeled on it can be seen in Figure 54.

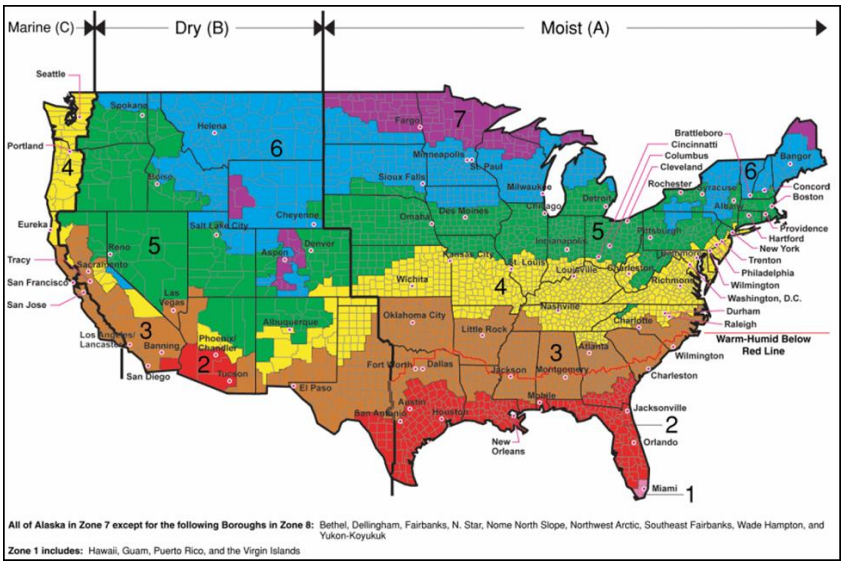

Figure 54: ASHRAE map of climate zones (Energy Modeling Maps).

Results of such tests were mixed. Atlanta's Prediction Tool performed very well for use in Little Rock. Eight tests were performed for each new location. All coils came from the hospital template. The only adjustment made was the initial simulation used a degrading T_{wi} schedule, while the second simulation used a T_{wi} Reset Schedule. Little Rock predictions came out to be 87.5% accurate.

Table 11: Application of Atlanta's Prediction Tool in Little Rock, AR test results.

Climate Zone 3A	**CAV 1**	**CAV 2**	**VAV 1**	**VAV 2**
Degrading Twi Schedule	PASS	PASS	PASS	PASS
Twi Reset Schedule Implemented	PASS	PASS	FAIL	PASS

The use of Boulder's Prediction Tool for coils operating in Reno had a 50% accurate prediction rate. A consistent downward offset of about 10% in computed *CV* values when

compared to predicted *CV* values was observed for all test coils. Thus, it makes sense that all coils would be predicted as CAV.

Table 12: Application of Boulder's Prediction Tool in Reno, NV test results.

Climate Zone 5B	**CAV 1**	**CAV 2**	**VAV 1**	**VAV 2**
Degrading Twi Schedule	PASS	PASS	FAIL	FAIL
Twi Reset Schedule Implemented	PASS	PASS	FAIL	FAIL

The use of the L.A. Prediction Tool for coils operating in Las Vegas had an accurate prediction rate of 62.5%, but the results were more sporadic than those seen in the previous case. No such consistent offset in computed *CV* values to predicted ones was observed. Some computed *CV* values were right on par with the predicted *CV* values, while other were quite a bit higher and some quite lower.

Table 13: Application of L.A.'s Prediction Tool in Las Vegas, NV test results.

Climate Zone 3B	**CAV 1**	**CAV 2**	**VAV 1**	**VAV 2**
Degrading Twi Schedule	PASS	FAIL	PASS	PASS
Twi Reset Schedule Implemented	FAIL	FAIL	PASS	PASS

The variability in the effectiveness of applying this method to differing ASHRAE climate zones was further investigated. Various data was looked at to distinguish why such variability exists, but focus was put on the use of economizers as well as the prevalence of sensible-only cooling. The use of economizers brings in higher percentages of outdoor air, which has more variability in its humidity and temperature than return air would.

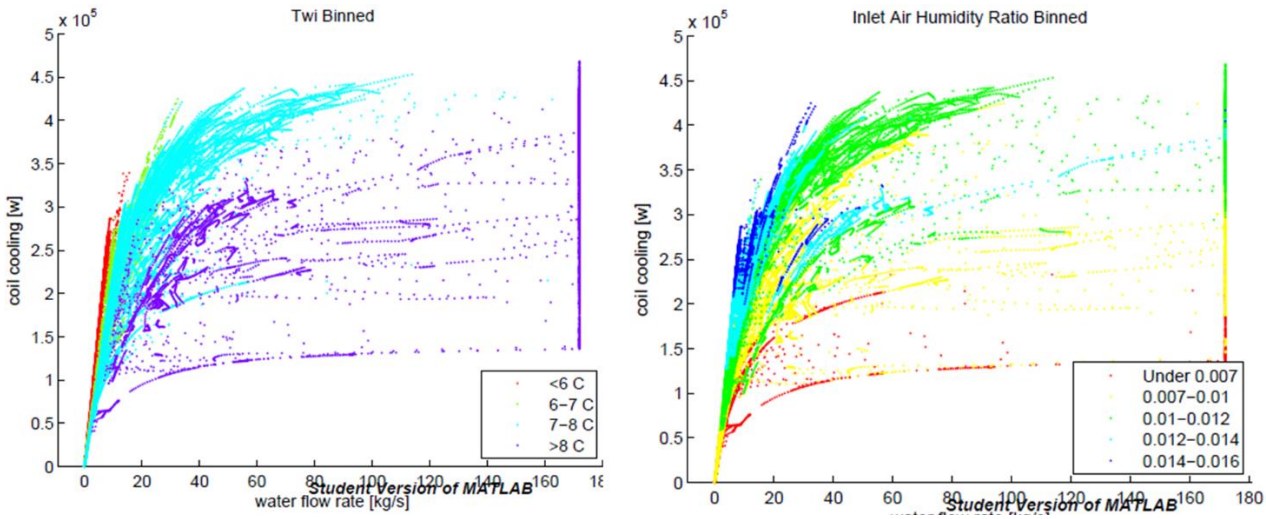

(a) (b)

Figure 55: (a) T_{wi} bin plot and (b) W_{ai} bin plot for an Atlanta hospital VAV 1 coil.

Focusing on the purple (>8°C) T_{wi} bin on the left hand plot of Figure 55, its spread is quite large. This is attributed to differing inlet humidity ratios as can be seen on the right hand plot's red, yellow and green points for those same data points. The amount of cooling for a given water flow rate goes up with higher inlet air humidity ratio, but that increase only becomes noticeable for W_{ai} values where dehumidification takes take place (i.e. $W_{ai} \geq \sim 0.007$) as can be seen in the right hand plot. Additionally, the increase in Q for a given increase in W_{ai} is highest when the coil first moves into cooling with dehumidification, and becomes less drastic as W_{ai} increases beyond that. This leads to a hierarchy in climates in regards to the performance of the Four-Parameter Curve Fit. If a coil experienced sensible only cooling 100% of the time, it is expected that the Four-Parameter Curve Fit would have the easiest time fitting the data for such a dry climate. Applying the Four-Parameter Curve Fit to a coil that experiences high amounts of latent cooling 100% of the time would not perform quite as well. The hardest climate to apply the Four-Parameter Curve Fit to would be one where roughly half the time the coil experienced sensible only cooling, and the other half experienced some dehumidification.

Simulations were again run for all four original locations, as well as the three new ones of Reno, Little Rock and Las Vegas. Numerous parameters were compared, but only the ones which showed the most insight are discussed. The average fraction of outdoor air by measuring both mass flow rate of outdoor air and mass flow rate of air across the coil was taken over the entire simulation period. The fraction of time that a coil experienced sensible-only cooling was also reported, as was the average sensible heat ratio (SHR) over the course of the entire simulation period. Updated versions of the Matlab scripts that generate these parameters can be seen in Appendix K.

Table 14: Outdoor air fraction and sensible-only prevalence investigation. Note: All four systems for each building were tested and had similar results. Only CAV 1 results are shown below.

CAV 1	Avg OA Fraction	Sensible Only Prevalence	Avg SHR	Design Dry Bulb (C)	Design Wet Bulb (C)
Atlanta	0.52	0.11	0.69	34.00	24.00
Little Rock	0.51	0.13	0.65	36.00	25.00
L.A.	0.97	0.06	0.63	27.20	17.80
Las Vegas	0.50	0.80	0.98	41.10	18.90
Boulder	0.76	0.65	0.91	32.20	15.00
Reno	0.76	0.91	0.99	33.30	15.50
Miami	0.34	0.00	0.63	32.20	25.00

The "Sensible Only Prevalence" seems to be the strongest indicator of how one location's prediction tool could be used elsewhere. Reno had a lot lower *CV* values for a given *FPMC* than was expected using Boulder's prediction tool. This is due to Boulder having roughly half its data points taken during sensible-only cooling, making density of data points high at the bounding regions of the T_{wi} bin. Since Reno is almost always experiencing sensible-only cooling, the vast majority of its data points fall together on the lower boundary of the T_{wi} bin. Thus, the Four-Parameter Curve Fit performs better and the *CV* values would be lower in Reno.

Parameters for Atlanta and Little Rock compare nicely. Despite the large geographical separation, their climates are closer in comparison than seen in the other two pairs of locations. Hence, 87.5% correct prediction rate was observed.

In the case of L.A. and Las Vegas, these cooling applications are at the two ends of the spectrum. L.A. has a latent component 94% of the time, while Las Vegas experiences purely sensible cooling 80% of the time. As mentioned before, having the overwhelming majority of data points at the either ends of the spectrum would result in lower *CV* calculations than if the Sensible Only Prevalence was measured in the middle at around 0.50. Therefore, using L.A.'s relationships to predict Las Vegas did not produce horrible results, but definitely more sporadic results as was discussed earlier. It would not be advised to use the L.A. Prediction Tool to predict Las Vegas. Follow-on research could further sub-divide established ASHRAE climate zones based on of expected inlet air conditions for buildings' cooling coils. Then, this approach of applying one location's established *CV* to *FPMC* relationship to other locations within the same sub-division of the same ASHRAE climate zone has serious promise. This potential continuation of research is discussed in the Conclusions and Future Work.

Looking at the four original climates in Table 14 sheds further insight as to why Boulder's *CV* to *FPMC* relationships were the least defined with relatively high *CV* values for both CAV and VAV coils. It seems this is attributed to the combination of its high outdoor air fractions and resultant large range of inlet humidity ratios.

4.2.4.6. Testing on Real World Datasets

Applying the *CV* to *FPMC* relationships derived from models to determining the application of a real world coil may present problems. If inlet and outlet water temperature sensors are calibrated incorrectly or drift over time, the CAV/VAV Prediction Tools may prove ineffective. Systems which experience outdoor air fractions far from the systems used in the relationship

derivation may be predicted incorrectly as well. Such systems would be a dedicated outdoor air system (DOAS) or a system serving only process loads with no outdoor air being brought in. As described earlier, the cooling coil model used in EnergyPlus is a steady state model. Real world transient behavior due to fluctuations in input parameters may provide higher *CV*s for the Four-Parameter Curve Fit for both CAV and VAV cases. If this is the case, established relationships may need to be derived from real world data alone, unless a consistent model bias could be clearly distinguished and factored in appropriately. This would be difficult however. As pointed out earlier, real world data has been difficult to obtain due the Energy Valve's recent introduction into industry, and the difficulty of getting logged data from building operators who maintain such valves.

Only two real world datasets were available for testing. They were from coils located on University of Colorado Boulder's campus. These were the coils used in the Bellucci (2012) research. A modified version of Boulder's Prediction Method was applied to these two coils, the script can be seen in Appendix N. It was unclear if the system served by the first coil (AHU-01) was a VAV system, as air flow rate measurements were not taken directly. Indirectly solving for *mA* through use of measure inlet and outlet air humidity ratios as well as water-side data showed a bell curve in air flow rates. Over 90% of the calculated air flow rates measured between 5 and 6 kg/s. The period of data looked at was from July 12th, 2013 through July 24th, 2013. The Boulder Prediction Tool predicted a CAV coil. This was expected as the system is operating very much like a CAV system, similar incorrect predictions were found for modeled VAV coils with minimal reductions in airflow as was discussed previously. Also discussed previously, such an incorrect prediction in this instance may be actually beneficial in the optimal control strategy selection since the system is behaving more like a CAV system. The system may in fact be a CAV, and the computed *mA* values had variability due to inconsistencies in measured data. If that is the case, the coil was predicted correctly.

The type of system served by the second coil tested (SF-6) was also unknown. Indirect calculation of *mA* proved a definite VAV application, with minimum airflow hovering around 50% of maximum airflow. The period looked at was from July 12th, 2013 to July 18th, 2013 as well as the 1st through the 30th of August, 2013. The gap was a result of obvious sensor errors being present. The Boulder Prediction Tool again predicted the coil's application as CAV. The two coils are plotted against the defined *CV* to *FPMC* relationships for Boulder to illustrate how they compare.

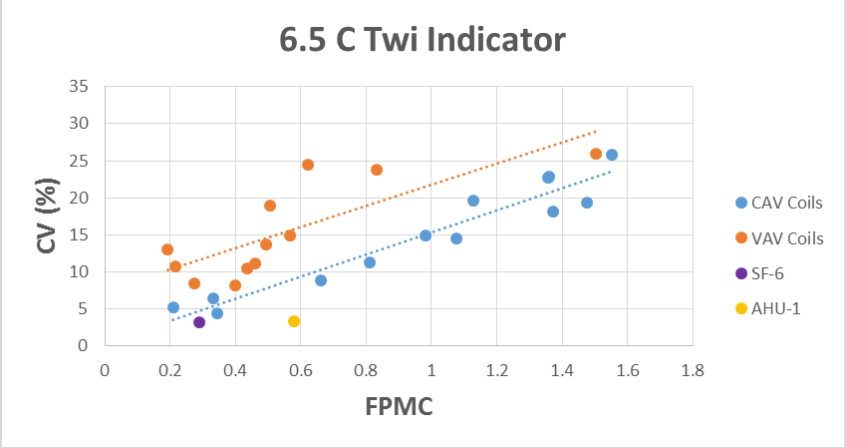

Figure 56: Real world coil results plotted against established *CV* to *FPMC* relationships for Boulder.

Error in the SF-6 prediction could very well be attributed to the region it fell in. The range of *FPMC*s from 0.2 – 0.6 is clearly defined very poorly. The abnormally low *CV* value for AHU-1 can be partially attributed to minimal fluctuations in airflow, if the coil is in fact serving a VAV system. An additional factor is the short time period for which the data was analyzed. Only a portion of the exponential curve could be seen with the limited data. Applying the Four-Parameter Curve Fit to a larger dataset which experiences larger variability in its loads would most likely increase the *CV*. Considering these explanations for the lower than expected *CV* values along with the fact that Boulder had the least defined *CV* to *FPMC* relationship of the four climates analyzed, applying the Four-Parameter Curve Fit in an effort to predict coil's application shows promise. Additionally, the

low *CV* values found in real world coils also further validates that the Four-Parameter Control strategy discussed in the next section of this report has potential for real world implementation.

4.3. Limitation Strategy Simulations

Five control strategies for the Energy Valve™ were tested through use of an NTU-effectiveness cooling coil model in Matlab-Simulink. Those strategies included Classical PID control with DAT tracking, Flow Limiting, Delta T Limiting, Flow/Delta T Limiting and the newly conceived Four-Parameter Control made available with the advent of the Four-Parameter Curve Fit's accurate predictions of when saturation is occurring. Before displaying the results, it is important to understand when the various advanced control logics would be implemented. Classical PID control with DAT tracking was used to produce the capacity vs water flow rate plots below for the Atlanta hospital's VAV 1 coil with a seven-row configuration. Red data points identify when a particular advanced strategy will be implemented.

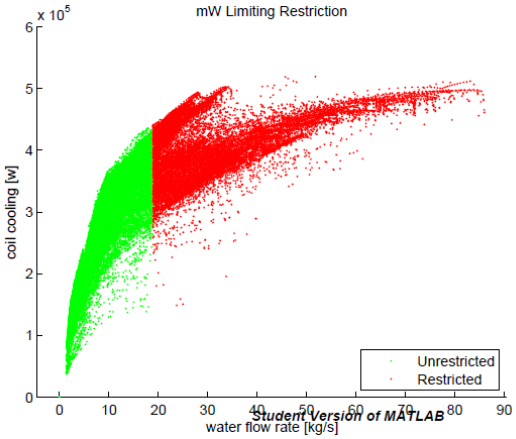

Figure 57: Flow Limiting times of restriction.

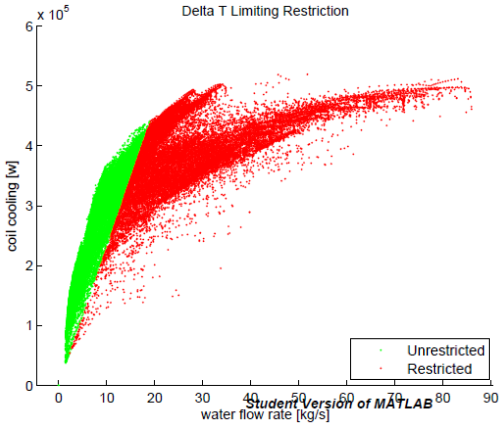

Figure 58: Delta T Limiting times of restriction.

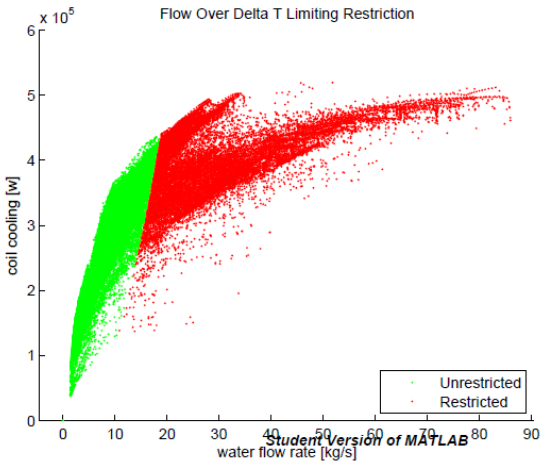

Figure 59: Flow/Delta T Limiting restriction.

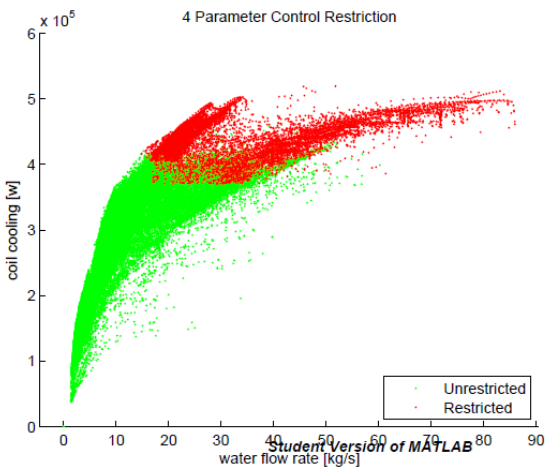

Figure 60: Four-Parameter Control restriction

The initial round of simulations was performed on 16 coils across the four characteristic climates of Boulder, Atlanta, Miami and L.A. The simulations included limits for the advanced controllers that were developed through the process outlined in the Methodology section of this report. These limit developments follow what would be reasonably expected to be used by the manufacturer Belimo. With no testing of the performance of the Four-Parameter Control strategy having been previously performed, that strategy was tested with four different limits to aid in the investigation of its effectiveness. Each of the 16 coils were tested with the five control strategies. Appendix M.1 has all the detailed results for each simulation run. An example of the results for one coil can be seen in Table 15 below.

Table 15: Initial test results for Boulder hospital CAV 1 system.

Climate	Building	System	Twi Schedule	Configuration	FPMC	CV	
Boulder	Hospital	CAV 1	Degrading	7 Row	1.33	22.6	
Control Strategy	Limit	ISE Increase (%)	Cooling Pwr Decrease (%)	Pumping Pwr Decrease (%)	Pumping/ISE	Pumping/Cooling	Avg Delta T
DAT Tracking	N/A	-	-	-			5.2
mW Limiting	7.78	1586	6.25	85	0.053	13.5	6.0
mW/DeltaT Limiting	1.4	2192	5.83	84	0.038	14.4	5.9
DeltaT Limiting	5.55	9323	12.20	85	0.009	7.0	6.0
4 Parameter Control	0.85	427	1.89	47	0.109	24.7	5.4
4 Parameter Control	0.8	860	3.03	66	0.077	21.9	5.6
4 Parameter Control	0.75	1584	4.76	78	0.050	16.5	5.9
4 Parameter Control	0.7	2662	7.05	83	0.031	11.7	6.1

Highlighted cells indicate which control logic performed best for the particular performance metric. The results above are quite representative of what was seen across the test coils. The *ISE* Increase metric is a percentage increased in *ISE* from the Classical PID control with DAT Tracking. The Cooling Power Decrease metric is a percentage decrease in cooling power when compared to the Classical PID control with DAT tracking. The Average Delta T is the average water-side temperature difference realized throughout the one month simulation. This metric might be of highest interest to district cooling applications where a low Delta T not only increases pumping power consumption, but it limits the system for further expansion (i.e. bringing more buildings onto the chilled water grid). It is apparent that the Four-Parameter Control at an 85% limit was far less aggressive compared to the other three advanced control logics when looking at the Pumping Power Decrease and Average Delta T metrics. An initial attempt to "normalize" the four advanced logics to more appropriately compare their performance was done with the Pumping/*ISE* and Pumping/Cooling metrics. The Pumping/*ISE* metric is a measure of percentage Pumping Power Reduction over the *ISE* percentage increase from the baseline case of Classical PID control. This metric would be of interest to someone looking for energy savings due to pumping reduction with thermal comfort remaining a concern. The Pumping/Cooling metric takes the percentage Pumping Power Reduction and divides it by the percentage Cooling Power Reduction. This metric would be of interest to someone looking for total energy savings. Such energy savings would be primarily due to pumping reduction but also savings may be realized by keeping the chillers more heavily loaded where their efficiencies are highest.

The collective results for all the simulations performed can be seen in Tables 16 through 19. The advanced control strategy that performed optimally for a given metric is identified. Where two or more strategies are identified, they had performed equally well.

Table 16: Initial simulation results for Largest Pumping Power Reduction metric.

	Largest Pumping Power Reduction			
	CAV COILS		VAV COILS	
	Degrading Twi	Reset Twi	Degrading Twi	Reset Twi
Boulder	Flow & Delta T	Delta T Limiting	Flow Limiting	Flow Limiting
Atlanta	Delta T Limiting	Delta T Limiting	Flow Limiting	Flow Limiting
Miami	Flow Limiting	Flow Limiting	Delta T Limiting	Delta T Limiting
L.A.	Flow Limiting	Flow Limiting	Delta T Limiting	Delta T Limiting

Table 17: Initial simulation results for the Largest Average Delta T metric.

	Largest Average Delta T			
	CAV COILS		VAV COILS	
	Degrading Twi	Reset Twi	Degrading Twi	Reset Twi
Boulder	Flow & Delta T	Flow/Delta T & Delta T	Flow Limiting	Delta T Limiting
Atlanta	Delta T Limiting	Delta T Limiting	Flow Limiting	Flow Limiting
Miami	Flow Limiting	Delta T Limiting	Flow Limiting	Flow Limiting
L.A.	Flow Limiting	Flow Limiting	Flow & Delta T	Flow & Delta T

Table 18: Initial simulation results for the *PP* Reduction to Cooling Reduction Ratio.

	Largest Pumping Reduction to Cooling Reduction Ratio			
	CAV COILS		VAV COILS	
	Degrading Twi	Reset Twi	Degrading Twi	Reset Twi
Boulder	4 Parameter Control	4 Parameter Control	Flow/Delta T Limiting	Flow/Delta T Limiting
Atlanta	4 Parameter Control	Flow/Delta T Limiting	4 Parameter Control	4 Parameter Control
Miami	4 Parameter Control	Flow/Delta T Limiting	Flow & Flow/Delta T	4 Parameter Control
L.A.	4 Parameter Control	Delta T Limiting	4 Parameter Control	Flow/Delta T Limiting

Table 19: Initial simulation results for *PP* Reduction to *ISE* Increase ratio.

	Largest Pumping Reduction to ISE Increase Ratio			
	CAV COILS		VAV COILS	
	Degrading Twi	Reset Twi	Degrading Twi	Reset Twi
Boulder	4 Parameter Control	4 Parameter Control	Flow/Delta T Limiting	Flow/Delta T Limiting
Atlanta	Flow Limiting	Flow Limiting	4 Parameter Control	4 Parameter Control
Miami	4 Parameter Control	Flow Limiting	Flow Limiting	4 Parameter Control
L.A.	4 Parameter Control	4 Parameter Control	Flow Limiting	Flow/Delta T Limiting

The Pumping Power Reduction and Average Delta T metrics show nearly identical results for the optimal strategies for the various coils. This is expected since a strategy that is substantially more restrictive will have less flow and a higher average Delta T. The "normalized" metrics of Pumping/*ISE* and Pumping/Cooling show the Four-Parameter Control was comparable to the other advanced strategies, in fact it had the highest prevalence of being labeled "optimal" for both metrics. Its prevalence as the optimal strategy was a little higher for CAV coils than VAV coils, which is expected since the 4 Parameter Curve Fit has been shown to have a more difficult time predicting the VAV datasets.

It was hypothesized that the optimal control strategy for each combination of climate, application (CAV/VAV) and facility priorities could be distinguished from performing such tests. In certain combinations of said variables, the results do show some promise. For example, if Pumping Power Reduction was the priority of the facility, Table 16 above quite clearly shows that for a given climate and application, the optimal strategy is consistent between the two coils that fall under that criteria. The same can be said if Average Delta T was the facility priority. Such distinction is not available when the Pumping/*ISE* or Pumping/Cooling would be facility priorities. In all cases however, it is obvious that the optimal strategy for a given coil could change with changes in its various strategies' limits. For example, a more aggressive Delta T limit for the Miami CAV coils could cause the Delta T Limiting strategy to beat out Flow Limiting strategy in the metrics of Pumping Power Reduction and Average Delta T. Additionally, the "normalized" metrics may not be constant for a particular coil when adjusting a strategy's setpoint. To put the strategies on a more even playing field for more appropriate comparison of their results, a second round of testing was conducted.

Table 15 above shows that the *ISE* increase from the baseline Classical PID control with DAT tracking was drastically different amongst the strategies. This metric can be thought of as the amount of the thermal discomfort for the occupants of the building. To more effectively

"normalize" the results, iterations were performed on the advanced strategies until the total *ISE's* for each were within 5% of each other. This allowed for more appropriate comparisons on the other four metrics of interest. The same 16 coils were tested in this manner. Table 20 shows an example of the test results for one such coil. Results for all the coils can be seen in Appendix M.2.

Table 20: Secondary test results for Atlanta office VAV 3 system.

Climate	Buildin	System	Twi Schedule	Configuration	FPMC	CV	
Atlanta	Office	VAV 3	Reset	5 Row	0.66	11.49	
Control Strategy	Limit	ISE Increase (%)	Cooling Pwr Decrease (%	Pumping Pwr Decrease (%)	Pumping/ISE	Pumping/Cooling	Avg Delta T
DAT Tracking	N/A	-	-	-			5.5
mW Limiting	6.5	2010	4.06	47	0.023	11.5	5.9
mW/DeltaT Limiting	1.05	2015	3.76	45	0.023	12.1	5.8
DeltaT Limiting	5.35	1991	2.37	31	0.015	12.9	5.7
4 Parameter Control	0.64	1935	2.45	26	0.014	10.8	5.7

The collective results for all the simulations performed can be seen in Tables 21 through 24. The advanced control strategy that performed optimally for a given metric is identified. Where two or more strategies are identified, they had performed equally well.

Table 21: Secondary simulation results for Largest Pumping Power Reduction metric.

	Largest Pumping Power Reduction			
	CAV COILS		VAV COILS	
	Degrading Twi	Reset Twi	Degrading Twi	Reset Twi
Boulder	Flow Limiting	Flow Limiting	Flow Limiting	Flow/Delta T Limiting
Atlanta	Flow Limiting	Flow Limiting	Flow Limiting	Flow Limiting
Miami	Flow Limiting	Flow Limiting	Flow Limiting	Flow Limiting
L.A.	Flow Limiting	Flow Limiting	Flow Limiting	Flow Limiting

Table 22: Secondary simulation results for the Largest Average Delta T metric.

	Largest Average Delta T			
	CAV COILS		VAV COILS	
	Degrading Twi	Reset Twi	Degrading Twi	Reset Twi
Boulder	Flow Limiting	Flow Limiting	Flow Limiting	Flow & Flow/Delta T
Atlanta	Flow Limiting	Flow Limiting	ALL	Flow Limiting
Miami	Flow Limiting	Flow Limiting	Flow Limiting	ALL
L.A.	Flow Limiting	Flow Limiting	Flow Limiting	Flow & Flow/Delta T

Table 23: Initial simulation results for the *PP* Reduction to Cooling Reduction Ratio.

	Largest Pumping Reduction to Cooling Reduction Ratio			
	CAV COILS		**VAV COILS**	
	Degrading Twi	**Reset Twi**	**Degrading Twi**	**Reset Twi**
Boulder	Delta T Limiting	Delta T Limiting	Delta T Limiting	Delta T Limiting
Atlanta	4 Parameter Control	4 Parameter Control	Delta T Limiting	Delta T Limiting
Miami	4 Parameter Control	Flow/Delta T Limiting	4 Parameter Control	Flow/Delta T Limiting
L.A.	Flow, Delta T & Flow/Delta T	4 Parameter Control	Flow/Delta T Limitin	Delta T Limiting

Table 24: Initial simulation results for *PP* Reduction to *ISE* Increase ratio.

	Largest Pumping Reduction to ISE Increase Ratio			
	CAV COILS		**VAV COILS**	
	Degrading Twi	**Reset Twi**	**Degrading Twi**	**Reset Twi**
Boulder	Flow & Flow/Delta T	Flow/Delta T Limiting	Flow & Flow/Delta T	Flow Limiting
Atlanta	Flow Limiting	Flow Limiting	Flow Limiting	Flow & Flow/Delta T
Miami	Flow Limiting	Flow Limiting	4 Parameter Control	Flow Limiting
L.A.	Flow, Delta T & Flow/Delta T	Flow Limiting	Flow Limiting	Flow & Flow/Delta T

In this second round of testing, Flow Limiting dominates in the Pumping Power Reduction, Pumping/*ISE* and Average Delta metrics, especially in CAV coils. The Four-Parameter Control continues to show promise the in Pumping/Cooling metric, more so in the CAV coils as its saturation prediction is inherently better for such coils. Based on this minimal set of coil simulations, it seems that Flow Limiting is the optimal choice for all climates for both CAV and VAV applications when Average Delta T, Pumping Power Reduction, or Pumping/*ISE* is the facility priority. In a scenario where Pumping/Cooling metric is of interest to the facility owner in an effort to reduce pumping power and more adequately load the chiller plant, the fault lines are slightly less defined. Delta T Limiting seems to perform well for both CAV and VAV coils in Boulder. Atlanta also seems to have a clearly defined optimal strategy for this scenario as well, but L.A. and Miami do not exhibit such distinction.

One final result from the 16 tested coils is the CAV/VAV accurate prediction rate. All datasets produced in the initial Classical PID control with DAT tracking simulation in Simulink were

exported into RStudio for development of the limits for the advanced strategies. While in that framework, those datasets were run though their respective climate's CAV/VAV Prediction Tool. An accurate prediction rate of 68.8% was found. This is below the 79.7% rate found in the previous 128 tests. This reduction in accuracy was not unexpected. The prediction tools were developed from *CV* to *FPMC* relationships found from coil simulations performed in EnergyPlus. The initial 128 tests were also from coils developed in EnergyPlus, although they had a variety of different operating characteristics. These last 16 coil datasets that were tested came from simulations with the less accurate Simulink model. It is less accurate in the fact that it cannot account for the partially wet/partially dry coil scenario, where the EnergyPlus coil can.

5. Conclusion and Future Work

5.1. Generation of Cooling Coil Data through Energy Modeling

The Energy Valve™ is the first of its kind and is relatively new to the marketplace. Consequently, the amount of data logged by Energy Valves and available for analysis is limited. As shown through numerous case studies, previous literature that has come out of the University of Colorado Boulder as well as in this research, there is substantial information to be gained through the Energy Valve's measurements of T_{wi}, T_{wo} and mW. Thorough analysis of datasets needs to be conducted to fully exploit the potential of the Energy Valve™. Development of such datasets through energy modeling is a quick way to attain data for this required analysis. There has been previous attempts to produce realistic coil data through use of the powerful software engine EnergyPlus, however saturation of the coils was not achieved (Buchanan, 2012). This research developed a methodology to produce coil data which indeed exhibited the saturation behavior observed in field tests.

This simulated data came from energy model simulations which account for realistic thermostat and occupancy schedules, the use of a dry-bulb economizer as well as fluctuating inlet water temperatures. The coil model selected for use in EnergyPlus was a LMTD/LMHD, steady state model capable of accurate capacity predictions for partially wet/partially dry coil scenarios. For future work in this area, several improvements can be made to further enhance the accuracy of the simulated data.

First, inlet water temperature profiles, whether they are degrading in nature or a reset schedule, should be modeled to correspond to the outdoor air temperature. This would more accurately resemble what would be seen in an actual chilled water system. This research implemented a daily schedule which remained consistent for every day of the simulation.

Secondly, transient coil models do exist however they are not currently available in EnergyPlus (Zhou & Braun, 2004). Manipulation of EnergyPlus, or finding an energy simulation tool as powerful as EnergyPlus that already incorporates such a transient model, could further enhance the validity of coil data produced through simulation.

Lastly, pressure fluctuations in the hydronic systems of the EnergyPlus model are not accounted for. Again, manipulation of EnergyPlus's basic framework or the use of some other software capable of modeling such pressure dependence will add to the validity of the simulated data.

5.2. Data Analysis – CAV/VAV Prediction

Analysis of the generated data was almost exclusively devoted to answering the question, "can it be determined if the coil is operating in a CAV system or VAV system through analysis of recorded Energy Valve™ data alone?" Previous research on coil saturation behavior suggests that the optimal control strategy that the Energy Valve™ should implement may be dependent on whether the coil operates in a CAV or VAV system (Thuillard *et al.,* 2014). Thus, if such a distinction can be made by the coil itself, Belimo could eliminate the potential for an input error from the installer of such a valve. Additionally, detection of when the operating state of the mechanical system changes could be achieved and the selected control strategy could be adjusted accordingly.

Several methods for making such a CAV or VAV prediction were investigated. The application of a Four-Parameter Curve Fit was found to show substantially more promise. The Four-Parameter Curve Fit is a non-linear regression on a coil's dataset. Both the maximum capacity at which the coil saturates at, as well as the exponential curvature the coil data follows proved to have dependencies on the inlet water temperature. This dependence on inlet water temperature is further complicated for VAV coils which have an added variable of changing air flow rates. Thus, the ability for the Four-Parameter Curve Fit to accurately predict the data is

substantially reduced for coils in a VAV application. The accuracy of the Four-Parameter Curve Fit in fitting the dataset was quantified through the Coefficient of Variation (*CV*). The relative size of the coil's rated capacity to the system it serves also plays a role in how well the Four-Parameter Curve Fit will perform. This relative size was quantified through the introduction of the term Fraction of Predicted Maximum Capacity (*FPMC*).

Numerous coils for four distinct climates had the Four-Parameter Curve Fit applied and the corresponding *CV* and *FPMC* recorded. For a given *FPMC*, CAV coils produced markedly lower *CV* values. Coils of unknown application were then predicted by applying the Four-Parameter Curve Fit to its dataset and comparing its *CV* and *FPMC* values to the already established *CV* to *FPMC* relationships for the same climate in which the coil was located. 128 coils that were subjected to a host of different operating characteristics were simulated and tested through this methodology. An accurate CAV/VAV prediction rate of 79.7% was achieved.

There will be times that the developed prediction tools will not work. With the strong push for low energy HVAC systems, dedicated outdoor air systems (DOAS) are becoming more common. Those same energy-minded building owners are more likely to incorporate intelligent pressure independent control valves in their systems. The CAV/VAV Prediction Tools were developed for systems which utilize a dry-bulb economizer. For climates such as Miami where the economizer is not utilized often, there would be expected differences in coil performance between an economizer coil and a coil serving a DOAS. Locations such as L.A. where the economizers are in use often may maintain a reasonable accurate prediction rate even for coils serving a DOAS. Similarly, coils serving purely process loads would be expected to predict incorrectly at a higher rate than that found in this research.

This research is the first to introduce the Four-Parameter Curve Fit and the methodology for a CAV/VAV Prediction Tool that is derived from it. There is plenty of more investigation to be

performed to improve the accuracy and robustness of such a tool. Suggested additional research in this area is as follows:

Further testing of real world datasets in the locations where established *CV* to *FPMC* relationships have been developed through modeling should be completed as such data becomes available. Results of such testing can lead to a better understanding of how to improve this prediction methodology.

Application of a Three-Parameter Curve Fit, which takes out the predicted exponential curvature's dependence on inlet water temperature, for development of *CV* to *FPMC* relationships may provide a higher CAV/VAV accurate prediction rate. The percentage increase in *CV* when reducing the Four-Parameter Curve Fit to a Three-Parameter Curve Fit may prove to be higher in VAV coils than CAV coils. This is attributed to the added variable of air flow rate in VAV applications which k_2 has been shown to have a strong dependence on (Thuillard *et al.,* 2014). This higher increase in VAV coils' *CV* would result in a larger gap between the linear *CV* to *FPMC* relationships developed for both CAV and VAV coils.

Ten CAV and ten VAV coils for each climate were used in developing the *CV* to *FPMC* relationships that were incorporated into the CAV/VAV Prediction Tools. Linear regression was performed on both the CAV and VAV data points on the *CV* vs *FPMC* plots. However, as seen in the case of Boulder, a linear fit may not be the best choice. Further investigation into other fits, such as a parabolic fit for the VAV data points should be conducted as it may increase the accuracy of the CAV/VAV Prediction Tools.

Preliminary analysis into the use of Prediction Tools for locations outside of where their *CV* to *FPMC* relationships were developed at, was performed. It was determined that even for two locations inside the same ASHRAE prescribed climate zone, the fraction of time sensible-only cooling prevailed changed drastically. It was shown than this fraction was a key indicator into

whether or not the utilization of Prediction Tool from a different location could be used in a new location. Future research could involve performing building simulations through the same methodology described in this report at a number of locations for each ASHRAE climate zone. The recorded fraction of time that sensible-only cooling prevailed could be used to further sub-divide the ASHRAE climate zones. Then, a Prediction Tool developed for one location could only be used for CAV/VAV predictions of coils in locations within the same climate zone sub-division.

The CAV/VAV Prediction Tools developed in this research are based on an indicator inlet water temperature of 6.5°C, as such a temperature was found to show the clearest distinction between CAV and VAV datasets. For coils that don't see such inlet water temperatures, the tools will not work. Thus, future work can be done to make more robust R scripts that can adapt for this scenario and have the *CV* to *FPMC* relationships developed from other indicator temperatures to still produce an accurate prediction.

Different coil models will produce differing results in terms cooling capacity for a given set of inlet parameters. Zhang (2012) highlights quite drastic differences in performance between coil models that differ only in their water-side convective coefficient predictions. For relationships to be built off models alone, the most accurate model needs to be used. Identifying which available cooling coil model that is would entail extensive comparison of simulated data to actual Energy Valve™ data, the latter of which has been proven to be scarce.

5.3. Optimal Strategy Testing

The capabilities of the Energy Valve™ to measure and record water temperatures and flow rate allow for this valve to implement control strategies far superior to the Classical PID control which tracks a DAT setpoint. Instances of saturation occurring in the coil can be predicted through a host of indicators. First, flow rates that exceed a certain flow limit (e.g. 1.5 times the design flow) can be assumed to pushing the coil into saturation. A resulting advanced control logic stemming

from this approach is called Flow Limiting. Saturation can also be predicted when the water-side Delta T falls below a certain threshold (e.g. 5.5 K). A second advanced control logic stemming from this saturation prediction is called Delta T Limiting. A hybrid of those two advanced strategies would be for saturation to be predicted when the ratio of flow to Delta T exceeds a prescribed high limit. The corresponding advanced control logic in this case is called Flow/Delta T Limiting.

All of these three advanced logics were analyzed in Thuillard *et al.* (2014). A fourth strategy is developed in this research, stemming from the new Four-Parameter Curve Fit. Since the Energy Valve™ indirectly measures cooling power, saturation can be predicted to be occurring when the measured cooling power is found to be over a certain percentage (e.g. 85%) of the predicted k_1 limit in the Four-Parameter Curve Fit for the T_{wi} the coil is experiencing at a given moment in time.

These four advanced control logics, as well as the Classical PID control logic were tested in Simulink. A simplified cooling coil model was utilized in a closed loop with a water valve and controller. Inlet air states, the air flow rate and the inlet water temperature were provided by the previous EnergyPlus simulations, and the water flow rate came from the water valve/controller assembly. All controllers were finely tuned through the Ziegler-Nichols closed loop tuning rules and simulations were performed for each of the five control logics.

It was predicted that an optimal control strategy could be identified for any combination of the following: climate, application (CAV/VAV) and facility priorities (energy consumption, thermal comfort, etc.). The determination of which strategy was "optimal" came from how the advanced control strategies performed on a given metric. Four metrics of interest which focused on the chilled water loop's energy consumption were investigated: pumping power reduction, average water-side Delta T, pumping reduction to cooling reduction ratio, and pumping reduction to *ISE* increase ratio. Due to the extensive and time consuming tuning process, coupled with simulation times exceeding 90 seconds on average, only 16 coils were tested. Though the EnergyPlus

generated data had six months of data on five minute timesteps, only the month of August was tested in this process.

A methodology for computing the limits for the various advanced control logics was developed and implemented. The newly developed Four-Parameter Control logic proved to perform comparably to the established strategies in the metrics of Pumping/*ISE* and Pumping/Cooling, especially in the CAV cases. This was expected due to the better predictions provided by the Four-Parameter Curve Fit for CAV coils when compared to VAV coils. In some instances, it seemed a single optimal strategy was evident for a given combination of climate, application and facility priority. However, only two coils for each such combination were tested and such a hypothesis was neither confirmed nor negated.

Continued research in this area is of high interest as it will push the Energy Valve™ closer to reaching its potential. Suggestions for future work in this area are as follows:

As discussed above, there may be benefits in the CAV/VAV prediction rate if the *CV* to *FPMC* relationships were derived from a Three-Parameter Curve Fit. Regardless if this is proven accurate, a Four-Parameter Curve Fit should be performed if such a non-linear regression is to be used in an advance control logic, as was done here in the Four-Parameter Control logic. This is due to the added accuracy of the curve fit that comes with the added degree of freedom, which in this case would be the linear dependence of k_2 on T_{wi}.

The Four-Parameter Control logic could further be improved by use of varying saturation limits. This research looked at fixed saturation limits (e.g. 75%). Thus, anytime the coil is providing more than 75% of its predicted maximum capacity for the T_{wi} it is operating at, saturation would be predicted and restriction on *mW* would ensue. However, depending on the exponential curvature of the coil data for a given T_{wi}, a saturation limit of 75% may restrict flow prematurely or restrict it too late. Compare the 5°C and 7°C T_{wi} lines in Figure 61 below. It may be sufficient to

implement a 75% saturation limit on the coil is if is operating at a T_{wi} of 5°C as the slope of the constant 5°C T_{wi} line is becoming more gradual at that point. However, implementing a 75% saturation limit on coil operating at a 7°C T_{wi} may be prematurely restricting the coil, as the slope at that location is still quite steep which means cooling power and flow rate are still tracking nicely and saturation is not occurring. The improvement to the Four-Parameter Curve Fit would then be to have saturation predicted based off the expected slope of the T_{wi} line as opposed to a set percentage of predicted k_1.

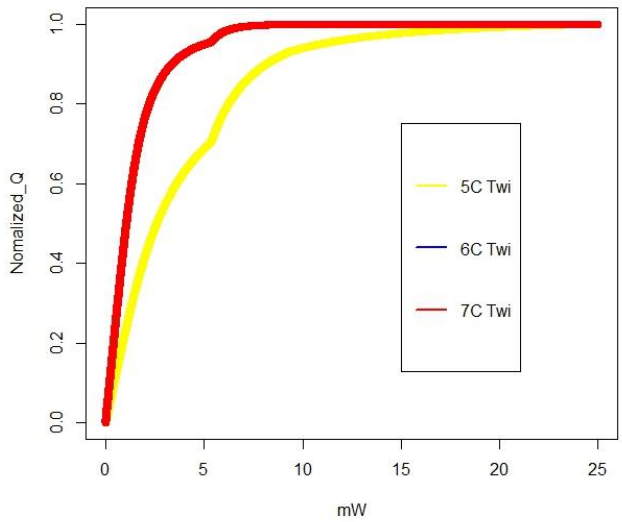

Figure 61: Variability in the slope of the constant T_{wi} lines exist at a chosen saturation limit of 75% of the Normalized Capacity.

A more extensive model could be developed to perform such optimal strategy testing. The determination of which strategy was "optimal" was made solely off of metrics that were indicators of energy performance of the chilled water system. However, in the case of VAV systems, the rise in discharge air temperature that results from restriction to chilled water flow may eventually result in increases in air flow rates. This would increase fan energy consumption. CAV systems, when operating under flow restriction from the Energy Valve™, may require less reheat for its zones

experiencing lower cooling loads. Thus, additional energy savings may be realized when the various advanced control logics are implemented. Therefore, future work in this area needs to investigate whole building energy consumption when developing metrics to test which strategy is "optimal".

In the model used in this research, deviation from DAT was used to represent thermal discomfort. A more extensive model, where zone loads with occupancy schedules are modeled and air flow rates for VAV systems are dependent on whether the room air temperature (RAT) setpoint is being met, would provide a more realistic simulation environment.

To most effectively account for the suggestions of the last two paragraphs, future optimal control strategy testing would best be performed outside of Simulink. Instead, incorporation of the various advanced control logics into EnergyPlus, or a similar energy simulation tool, would provide means for better capturing the effects of an advanced control strategy on whole building energy consumption.

References

ASHRAE. (2010). *Std 90.1 - Energy standard for buildings except low-rise residential buildings* (I-P ed.). Atlanta, GA: American Society of Heating, Refrigerating and Air-Conditioning Engineers.

Belimo Inc. (n.d.). MIT Tests New Energy Valve Technology at Charles Hayden Library and Reaps the Rewards of Higher Delta-T. Retrieved January 10, 2014, from http://energyvalve.com/case-studies.html

Belimo Inc. (n.d.). The Belimo Energy Valve Cures Medical University's Low Delta-T. Retrieved January 10, 2014, from http://energyvalve.com/case-studies.html

Bellucci, J. (2012). *Model Development and Experimental Validation of Pressure Independent Hydronic Circuits*. University of Colorado Boulder.

Brandemuehl, M.J., Gabel, S., and I. Andersen. (1993). A Toolkit for Secondary HVAC System Energy Calculations. *ASHRAE*.

Buchanan, B. (2012). *Chilled Water Plant Taxonomy and Energy Valve Modeling*. University of Colorado Boulder.

Commercial Prototype Building Models. (n.d.). Retrieved March 17, 2014, from http://www.energycodes.gov/commercial-prototype-building-models

Dept of Energy. (2012). *EnergyPlus Documentation* (Version 7.2 ed.). Ernest Orlando Lawrence Berkeley National Laboratory.

Elmahdy, A.H., Mitalas G.P. (1977). A Simple Model for Cooling and Dehumidifying Coils for Use in Calculating Energy Requirements for Buildings, *ASHRAE Transactions 83* (2), 103-117.

Energy Modeling Maps. (n.d.). Retrieved January 1, 2014, from http://energymodeling.pbworks.comW/page/18898438/Energy Modeling Maps

EnergyPlus. (n.d.). Retrieved January 1, 2014, from http://apps1.eere.energy.gov/buildings/energyplus/?utm_source=EnergyPlus&utm_medium=redirect&utm_campaign=EnergyPlus+redirect+1

Fact Sheet: Variable Frequency Drives. (n.d.). Retrieved April 1, 2014, from http://www.consumersenergy.com/uploadedFiles/EE_Programs_2011/Business/Resources/variable-frequency-drives.pdf?n=9944

Fiorino, D. (1999). Achieving High Chilled-Water Delta Ts. *ASHRAE Journal,* (November), 24-30.

Fiorino. D. (1996). Twenty-five Ways to Raise Your Chilled-Water Temperature Differential, *ASHRAE Transactions 102* (1), 567–572.

Henze, G., & Floss, A. (2011). Evaluation of Temperature Degradation in Hydraulic Flow Networks. *Energy and Buildings 43*, 1820-1828.

Henze, G.P., Henry, W., and M. Thuillard. (2013). Improving Campus Chilled Water Systems with

Intelligent Control Valves: A Field Study. Proceedings of the 2013 ASCE Architectural Engineering Conference. April 2-5, 2013. State College, PA. 103-112.

HPAC. (2007, January 1). Pressure-Independent Valves Simplify Air Base's Transition to Variable Flow. Retrieved September 24, 2014, from http://hpac.com/plumbing-piping-pumping/pressureindependent_valves_simplify

Kirsner, W. (1996). The Demise of the Primary-Secondary Pumping Paradigm for Chilled Water Plant Design. *Heating/Piping/AirConditioning* (November), 73-78.

MATLAB. (n.d.). Retrieved January 1, 2014, from http://www.mathworks.com/products/matlab/

Mitchell, J., & Braun, J. (2013). *Principles of Heating, Ventilation, and Air Conditioning in Buildings*. Hoboken, NJ: Wiley.

Moe, E. (2005). Building Performance with District Cooling. *ASHRAE Journal 47* (7), 46-53.

Reider, F. (2012). *Adaptive Real-Time Cooling Coil Curve Fitting Using a Computationally Simple Approach*. University of Colorado Boulder.

Siemens Building Technologies. (n.d.). *B0MC - Control Technology*.

Taylor Engineering. (2009). *CoolTools Chilled Water Plant Design Guide*. Taylor Engineering

Taylor, S. T. (2002). Degrading Chilled Water Plant Delta-T: Causes and Mitigation, *ASHRAE Transactions 108* (1). 641–653.

Taylor, S., & Cheng, C. (2010). Economizer High Limit Controls and Why Enthalpy Economizers Don't Work. *ASHRAE Journal*, (November 2010).

Taylor, S., & Stein, J. (2002). Balancing Variable Flow Hydronic Systems. *ASHRAE Journal,* (October 2002), 17-24.

Thuillard, M., Reider, F., & Henze, G. (2014). Energy Efficiency Strategies for Hydronic Systems through Intelligent Actuators. *ASHRAE Transactions,* NY-C073.

Wang, L., Watt, J., & Zhao, J. (2012). Model Based Building Chilled Water Loop Delta-T Diagnosis. Twelfth International Conference for Enhanced Building Operations.

Wirths, A. (2008). Einfluss der Netzrucklauftemperatur auf die Effizienz von Fernwarmesystemen 13, in: Dresdner Fernwarmekolloquium. September 23–24.

Zhang, Z., Li, H., Liu, J. (2012). Simulations of Chilled Water Cooling Coil Delta-T Characteristics, ASHRAE 2012 Annulus Conference, San Antonio, Texas.

Zhou, X., & Braun, J. (2004). Transient Modeling of Chilled Water Cooling Coils. International Refrigeration and Air Conditioning Conference. Paper 652.

Appendices

Appendix A: Manipulations to EnergyPlus Template IDF Files

A.1: Initial Coil Manipulations for Hospital Template Model

1. Open Text Editor in the file of interest

2. Ensure all Cooling Coils contain the following format for their description, only system references (e.g. CAV_1) need to be changed between coils:

```
Coil:Cooling:Water:DetailedGeometry,
  CAV_1_CoolC,          !- Name
  ALWAYS_ON,            !- Availability Schedule Name
  AUTOSIZE,             !- Maximum Water Flow Rate {m3/s}
  AUTOSIZE,             !- Tube Outside Surface Area {m2}
  AUTOSIZE,             !- Total Tube Inside Area {m2}
  AUTOSIZE,             !- Fin Surface Area {m2}
  AUTOSIZE,             !- Minimum Airflow Area {m2}
  AUTOSIZE,             !- Coil Depth {m}
  AUTOSIZE,             !- Fin Diameter {m}
  0.0015,               !- Fin Thickness {m}
  0.01445,              !- Tube Inside Diameter {m}
  0.0159,               !- Tube Outside Diameter {m}
  386.0,                !- Tube Thermal Conductivity {W/m-K}
  204.0,                !- Fin Thermal Conductivity {W/m-K}
  0.0018,               !- Fin Spacing {m}
  0.026,                !- Tube Depth Spacing {m}
  6,                    !- Number of Tube Rows
  AUTOSIZE,             !- Number of Tubes per Row
  CAV_1_CoolCDemand Inlet Node,  !- Water Inlet Node Name
  CAV_1_CoolCDemand Outlet Node,  !- Water Outlet Node Name
  CAV_1 Humidifier-CAV_1_CoolCNode,  !- Air Inlet Node Name
  CAV_1_CoolC-CAV_1_HeatCNode;  !- Air Outlet Node Name
```

3. Conduct a search in the Text Editor and ensure all references to Coil:Cooling:Water are changed to Coil:Cooling:Water:DetailedGeometry

4. Save and Close the Text Editor. Open the IDF Editor for the same IDF file.

5. Make the following changes in the Coil:Cooling:Water:DetailedGeometry model:

   Input "autosize" all coil parameters it allows you to

   Change fin thickness to 0.00015 [m]

   Change the number of tube rows to eight

6. Make the following changes in the Controller:WaterCoil model:

   Change the control variable to “temperature” for all controllers

7. Make the following changes in the Sizing:Parameters simulation parameter:

Change the Cooling Sizing Factor to 1.0

8. Make the following changes in the Sizing:Sizing simulation parameter:

Change Precool Design Temperature to 11.1

Change Central Cooling Design Supply Air Temperature to 11.1

Change Sizing Option to "Coincident"

Change Central Cooling Design Supply Air Humidity Ratio to 0.008

9. Make the following changes in the SetpointManager:MixedAir simulation parameter:

Set Fan Inlet Node Name, Fan Outlet Node Name and Setpoint Node or NodeList Name to

"CAV_1_CoolC-CAV_1_HeatCNode"

Note: Name of node will need to be adjusted between different systesms

9. Make the following changes in the Schedule:Compact simulation parameter:

Change various Occupancy Schedules as desired

Change thermostat setbacks to 26 C

Change CW-Loop-Temp-Schedule to reflect a Degrading T_{wi} Schedule. It should look as follows:

For: AllDays,
Until: 05:00,
5,
Until: 11:00,
7,
Until: 14:00,
7.5,
Until: 18:00,
9,
Until: 24:00,
7;

A.2: Introducing Economizers

1. Open IDF Editor for model of interest.

2. Make the following changes in the Controller:OutdoorAir simulation parameter:

Change Economizer Type to “FixedDryBulb”

Adjust Economizer Maximum Limit Dry Bulb Temperature to appropriate value from Table 5

A.3: Changing CAV Systems to VAV Systems

1. Open IDF Editor for model of interest.

2. Make the following changes in the AirTerminal:SingleDuct:VAV:Reheat simulation parameter:

Change all Constant Min Air Flow Fractions from 1.0 to 0.3

3. Other similar adjustments can be made to select systems. To view which zones are assigned to the various systems, to into AirLoopHVAC:ZoneSplitter simulation parameter.

A.4: Comprehensive Coil Manipulations for Office Template Model

1. Open Text Editor in the file of interest

2. Ensure all Cooling Coils contain the following format for their description, only system references (e.g. CAV_1) need to be changed between coils:

```
Coil:Cooling:Water:DetailedGeometry,
  CAV_1_CoolC,          !- Name
  ALWAYS_ON,            !- Availability Schedule Name
  AUTOSIZE,             !- Maximum Water Flow Rate {m3/s}
  AUTOSIZE,             !- Tube Outside Surface Area {m2}
  AUTOSIZE,             !- Total Tube Inside Area {m2}
  AUTOSIZE,             !- Fin Surface Area {m2}
  AUTOSIZE,             !- Minimum Airflow Area {m2}
  AUTOSIZE,             !- Coil Depth {m}
  AUTOSIZE,             !- Fin Diameter {m}
  0.0015,               !- Fin Thickness {m}
  0.01445,              !- Tube Inside Diameter {m}
  0.0159,               !- Tube Outside Diameter {m}
  386.0,                !- Tube Thermal Conductivity {W/m-K}
  204.0,                !- Fin Thermal Conductivity {W/m-K}
  0.0018,               !- Fin Spacing {m}
  0.026,                !- Tube Depth Spacing {m}
  6,                  !- Number of Tube Rows
  AUTOSIZE,             !- Number of Tubes per Row
  CAV_1_CoolCDemand Inlet Node,  !- Water Inlet Node Name
  CAV_1_CoolCDemand Outlet Node,  !- Water Outlet Node Name
  CAV_1 Humidifier-CAV_1_CoolCNode,  !- Air Inlet Node Name
  CAV_1_CoolC-CAV_1_HeatCNode;  !- Air Outlet Node Name
```

3. Conduct a search in the Text Editor and ensure all references to Coil:Cooling:Water are changed to Coil:Cooling:Water:DetailedGeometry

4. Save and Close the Text Editor. Open the IDF Editor for the same IDF file.

5. Make the following changes in the Coil:Cooling:Water:DetailedGeometry model:

Input "autosize" all coil parameters it allows you to

Change fin thickness to 0.00015 [m]

Change # of tube rows to 8

6. Make the following changes in the Controller:WaterCoil model:

Change the control variable to “temperature” for all controllers

7. Make the following changes in the Sizing:Parameters simulation parameter:

Change the Cooling Sizing Factor to 1.0

8. Make the following changes in the Sizing:Sizing simulation parameter:

Change Precool Design Temperature to 11.1

Change Central Cooling Design Supply Air Temperature to 11.1

Change Sizing Option to “Coincident”

Change Central Cooling Design Supply Air Humidity Ratio to 0.008

9. Make the following changes in the SetpointManager:MixedAir simulation parameter:

Set Fan Inlet Node Name, Fan Outlet Node Name and Setpoint Node or NodeList Name to

“CAV_1_CoolC-CAV_1_HeatCNode”

Note: Name of node will need to be adjusted between different systesms

10. Make the following changes in the Schedule:Compact simulation parameter:

Change various Occupancy Schedules as desired

Change thermostat setbacks to 26 C

Change CW-Loop-Temp-Schedule to reflect a Degrading T_{wi} Schedule. It should look as follows:

For: AllDays,

Until: 05:00,

5,

Until: 11:00,

7,

Until: 14:00,

7.5,

Until: 18:00,

9,

Until: 24:00,

7;

10. Make the following changes in the Controller:OutdoorAir simulation parameter:

Change Economizer Type to “FixedDryBulb”

Adjust Economizer Maximum Limit Dry Bulb Temperature to appropriate value from Table 5

Ensure Minimum Limit Type is set to “FixedMinimum”

Ensure Minimum Outdoor Air Schedule Name is set to MinOA_MotorizedDamper_Sched

Ensure Minimum Fraction Outdoor Air Schedule Name is blank

11. Make the following changes in the AirTerminal:SingleDuct:VAV:Reheat simulation parameter:

Change all Constant Min Air Flow Fractions from 3.0 to 1.0 for the following zones:

Core_bottom VAV Box

Perimeter_bot_ZN_3 VAV Box

Perimeter_bot_ZN_2 VAV Box

Perimeter_bot_ZN_1 VAV Box

Perimeter_bot_ZN_4 VAV Box

Core_mid VAV Box

Perimeter_mid_ZN_3 VAV Box

Perimeter_mid_ZN_2 VAV Box

Perimeter_mid_ZN_1 VAV Box

Perimeter_mid_ZN_4 VAV Box

Now, systems labeled VAV 1 and VAV 2 are actually behave as CAV systems. VAV 3 and VAV 5 remain VAV systems.

A.5: Adjusting Locations for Template Models

1. Open IDF Editor for a duplicate model of a location that falls within the same ASHRAE climate zone as the new location you are attempting to simulate.

2. Adjust all objects in Site:Location simulation parameter accordingly.

3. Adjust all objects in SizingPeriod:DesignDay simulation parameter accordingly.

Appendix B: Steps in Sizing Geometric Parameters of Coils

1. Run initial simulation through steps outlined in Appendix B.1 with the IDF that has all coil geometric parameters set to “autosize”.

2. Open the generated EIO file with any text editor tool.

3. Search for Coil:Cooling:Water. All autosized geometric parameters for all coils are shown.

4. Copy those over to an Excel file.

5. Incrementally reduce values for Fin Surface Area, Total Tube inside Surface Area, Total Tube Outside Surface Area, Number of Rows and Coil Depth by factor of $1/8^{th}$ is adjacent columns. Repeat this until values for a 4 row configuration are attained. End results should look similar to those Tables found in Appendix C.

6. Produce copies of the IDF files for each climate by inputting the developed geometric parameters in the Coil:Cooling:Water:DetailedGeometry simulation parameter. Specify a Maximum Water Flow Rate to 10 times the value autosized, as can be seen in the EIO file earlier. This will allow for the coil to enter into the saturation region for the smaller row configurations.

Appendix C: Produced Coil Geometries

C.1: Hospital Coils

	8 Row	7 Row	6 Row	5 Row	4 Row
ATLANTA - CAV 1					
Load [W]	374157				
Max Water Flow Rate [m3/s]	1.34E-02	1.34E-02	1.34E-02	1.34E-02	1.34E-02
# of Tubes per Row	184	184	184	184	184
Fin Diameter [m]	5.93761	5.9376	5.9376	5.9376	5.9376
Minimum Airflow Area [m2]	7.79865	7.7987	7.7987	7.7987	7.7987
Fin Surface Area [m2]	1391.351	1217.432	1043.513	869.5943	695.6755
Total Tube Inside Surface Area [m2]	93.58976	81.89104	70.19232	58.4936	46.79488
Tube Outside Surface Area [m2]	95.95968	83.96472	71.96976	59.9748	47.97984
Coil Depth [m]	0.208	0.182	0.156	0.13	0.104
# of Rows	8	7	6	5	4

	8 Row	7 Row	6 Row	5 Row	4 Row
ATLANTA - CAV 2					
Load [W]	236233.4				
Max Water Flow Rate [m3/s]	8.44E-03	8.43E-03	8.43E-03	8.43E-03	8.43E-03
# of Tubes per Row	117	117	117	117	117
Fin Diameter [m]	4.66517	4.665	4.665	4.665	4.665
Minimum Airflow Area [m2]	6.12738	6.13	6.13	6.13	6.13
Fin Surface Area [m2]	1093.181	956.5332	819.8856	683.238	546.5904
Total Tube Inside Surface Area [m2]	59.51088	52.07202	44.63316	37.1943	29.75544
Tube Outside Surface Area [m2]	61.01784	53.39061	45.76338	38.13615	30.50892
Coil Depth [m]	0.208	0.182	0.156	0.13	0.104
# of Rows	8	7	6	5	4

	8 Row	7 Row	6 Row	5 Row	4 Row
ATLANTA - VAV 1					
Load [W]	480326				
Max Water Flow Rate [m3/s]	1.72E-02	1.72E-02	1.72E-02	1.72E-02	1.72E-02
# of Tubes per Row	236	236	236	236	236
Fin Diameter [m]	8.54136	8.54	8.54	8.54	8.54
Minimum Airflow Area [m2]	11.2185	11.22	11.22	11.22	11.22
Fin Surface Area [m2]	2001.48	1751.3	1501.11	1250.93	1000.74
Total Tube Inside Surface Area [m2]	120.039	105.034	90.0293	75.0244	60.0195
Tube Outside Surface Area [m2]	123.079	107.694	92.309	76.9242	61.5394
Coil Depth [m]	0.208	0.182	0.156	0.13	0.104
# of Rows	8	7	6	5	4

	8 Row	7 Row	6 Row	5 Row	4 Row
ATLANTA - VAV 2					
Load [W]	875131				
Max Water Flow Rate [m3/s]	3.13E-02	3.13E-02	3.13E-02	3.13E-02	3.13E-02
# of Tubes per Row	430	430	430	430	430
Fin Diameter [m]	15.02194	15.02194	15.02194	15.02194	15.02194
Minimum Airflow Area [m2]	19.7303	19.7303	19.7303	19.7303	19.7303
Fin Surface Area [m2]	3520.065	3080.057	2640.049	2200.041	1760.033
Total Tube Inside Surface Area [m2]	218.7152	191.3758	164.0364	136.697	109.3576
Tube Outside Surface Area [m2]	224.2536	196.2219	168.1902	140.1585	112.1268
Coil Depth [m]	0.208	0.182	0.156	0.13	0.104
# of Rows	8	7	6	5	4

	8 Row	7 Row	6 Row	5 Row	4 Row
BOULDER - CAV 1					
Load [W]	2.78E+05				
Max Water Flow Rate [m3/s]	9.91E-03	9.91E-03	9.91E-03	9.91E-03	9.91E-03
# of Tubes per Row	137	137	137	137	137
Fin Diameter [m]	5.12E+00	5.12E+00	5.12E+00	5.12E+00	5.12E+00
Minimum Airflow Area [m2]	6.71938	6.71938	6.71938	6.71938	6.71938
Fin Surface Area [m2]	1198.798	1048.948	899.0985	749.2488	599.399
Total Tube Inside Surface Area [m2]	69.68368	60.97322	52.26276	43.5523	34.84184
Tube Outside Surface Area [m2]	71.44824	62.51721	53.58618	44.65515	35.72412
Coil Depth [m]	0.208	0.182	0.156	0.13	0.104
# of Rows	8	7	6	5	4

	8 Row	7 Row	6 Row	5 Row	4 Row
BOULDER - CAV 2					
Load [W]	144275.5				
Max Water Flow Rate [m3/s]	5.15E-03	5.15E-03	5.15E-03	5.15E-03	5.15E-03
# of Tubes per Row	71	71	71	71	71
Fin Diameter [m]	3.97E+00	3.97E+00	3.97E+00	3.97E+00	3.97E+00
Minimum Airflow Area [m2]	5.2092	5.2092	5.2092	5.2092	5.2092
Fin Surface Area [m2]	929.3692	813.1981	697.0269	580.8558	464.6846
Total Tube Inside Surface Area [m2]	36.11344	31.59926	27.08508	22.5709	18.05672
Tube Outside Surface Area [m2]	37.02792	32.39943	27.77094	23.14245	18.51396
Coil Depth [m]	0.208	0.182	0.156	0.13	0.104
# of Rows	8	7	6	5	4

	8 Row	7 Row	6 Row	5 Row	4 Row
BOULDER - VAV 1					
Load [W]	317166				
Max Water Flow Rate [m3/s]	1.13E-02	1.13E-02	1.13E-02	1.13E-02	1.13E-02
# of Tubes per Row	156	156	156	156	156
Fin Diameter [m]	7.62807	7.62807	7.62807	7.62807	7.62807
Minimum Airflow Area [m2]	10.019	10.019	10.019	10.019	10.019
Fin Surface Area [m2]	1787.47	1564.04	1340.61	1117.17	893.737
Total Tube Inside Surface Area [m2]	79.3478	69.4294	59.5109	49.5924	39.6739
Tube Outside Surface Area [m2]	81.3571	71.1875	61.0178	50.8482	40.6786
Coil Depth [m]	0.208	0.182	0.156	0.13	0.104
# of Rows	8	7	6	5	4

	8 Row	7 Row	6 Row	5 Row	4 Row
BOULDER - VAV 2					
Load [W]	574141.8				
Max Water Flow Rate [m3/s]	2.05E-02	2.05E-02	2.05E-02	2.05E-02	2.05E-02
# of Tubes per Row	282	282	282	282	282
Fin Diameter [m]	13.25456	13.25456	13.25456	13.25456	13.25456
Minimum Airflow Area [m2]	17.40898	17.40898	17.40898	17.40898	17.40898
Fin Surface Area [m2]	3105.92	2717.68	2329.44	1941.2	1552.96
Total Tube Inside Surface Area [m2]	143.4365	125.5069	107.5774	89.6478	71.71824
Tube Outside Surface Area [m2]	147.0686	128.6851	110.3015	91.9179	73.53432
Coil Depth [m]	0.208	0.182	0.156	0.13	0.104
# of Rows	8	7	6	5	4

	8 Row	7 Row	6 Row	5 Row	4 Row
MIAMI - CAV 1					
Load [W]	495004.5				
Max Water Flow Rate [m3/s]	1.77E-02	1.77E-02	1.77E-02	1.77E-02	1.77E-02
# of Tubes per Row	244	244	244	244	244
Fin Diameter [m]	6.19005	6.19005	6.19005	6.19005	6.19005
Minimum Airflow Area [m2]	8.13022	8.13022	8.13022	8.13022	8.13022
Fin Surface Area [m2]	1450.505	1269.192	1087.879	906.5657	725.2526
Total Tube Inside Surface Area [m2]	124.1082	108.5946	93.08112	77.5676	62.05408
Tube Outside Surface Area [m2]	127.2509	111.3445	95.43816	79.5318	63.62544
Coil Depth [m]	0.208	0.182	0.156	0.13	0.104
# of Rows	8	7	6	5	4

	8 Row	7 Row	6 Row	5 Row	4 Row
MIAMI - CAV 2					
Load [W]	268684.5				
Max Water Flow Rate [m3/s]	9.60E-03	9.60E-03	9.60E-03	9.60E-03	9.60E-03
# of Tubes per Row	132	132	132	132	132
Fin Diameter [m]	4.8427	4.8427	4.8427	4.8427	4.8427
Minimum Airflow Area [m2]	6.36056	6.36056	6.36056	6.36056	6.36056
Fin Surface Area [m2]	1134.782	992.934	851.0863	709.2386	567.3909
Total Tube Inside Surface Area [m2]	67.14048	58.74792	50.35536	41.9628	33.57024
Tube Outside Surface Area [m2]	68.84064	60.23556	51.63048	43.0254	34.42032
Coil Depth [m]	0.208	0.182	0.156	0.13	0.104
# of Rows	8	7	6	5	4

	8 Row	7 Row	6 Row	5 Row	4 Row
MIAMI - VAV 1					
Load [W]	549840				
Max Water Flow Rate [m3/s]	1.96E-02	1.96E-02	1.96E-02	1.96E-02	1.96E-02
# of Tubes per Row	271	271	271	271	271
Fin Diameter [m]	9.55128	9.55128	9.55128	9.55128	9.55128
Minimum Airflow Area [m2]	12.545	12.545	12.545	12.545	12.545
Fin Surface Area [m2]	2238.14	1958.37	1678.6	1398.83	1119.07
Total Tube Inside Surface Area [m2]	137.841	120.611	103.381	86.1509	68.9207
Tube Outside Surface Area [m2]	141.332	123.665	105.999	88.3325	70.666
Coil Depth [m]	0.208	0.182	0.156	0.13	0.104
# of Rows	8	7	6	5	4

	8 Row	7 Row	6 Row	5 Row	4 Row
MIAMI - VAV 2					
Load [W]	966270.7				
Max Water Flow Rate [m3/s]	3.45E-02	3.45E-02	3.45E-02	3.45E-02	3.45E-02
# of Tubes per Row	475	475	475	475	475
Fin Diameter [m]	15.82254	15.82254	15.82254	15.82254	15.82254
Minimum Airflow Area [m2]	20.78185	20.78185	20.78185	20.78185	20.78185
Fin Surface Area [m2]	3.71E+03	3.24E+03	2.78E+03	2.32E+03	1.85E+03
Total Tube Inside Surface Area [m2]	241.604	211.4035	181.203	151.0025	120.802
Tube Outside Surface Area [m2]	247.722	216.7568	185.7915	154.8263	123.861
Coil Depth [m]	0.208	0.182	0.156	0.13	0.104
# of Rows	8	7	6	5	4

	8 Row	7 Row	6 Row	5 Row	4 Row
LOS ANGELAS - CAV 1					
Load [W]	3.83E+05				
Max Water Flow Rate [m3/s]	1.37E-02	1.37E-02	1.37E-02	1.37E-02	1.37E-02
# of Tubes per Row	188	188	188	188	188
Fin Diameter [m]	6.14E+00	6.14E+00	6.14E+00	6.14E+00	6.14E+00
Minimum Airflow Area [m2]	8.061	8.061	8.061	8.061	8.061
Fin Surface Area [m2]	1438.155	1258.386	1078.617	898.8472	719.0777
Total Tube Inside Surface Area [m2]	95.62432	83.67128	71.71824	59.7652	47.81216
Tube Outside Surface Area [m2]	98.04576	85.79004	73.53432	61.2786	49.02288
Coil Depth [m]	0.208	0.182	0.156	0.13	0.104
# of Rows	8	7	6	5	4

	8 Row	7 Row	6 Row	5 Row	4 Row
LOS ANGELAS - CAV 2					
Load [W]	199147.4				
Max Water Flow Rate [m3/s]	7.11E-03	7.11E-03	7.11E-03	7.11E-03	7.11E-03
# of Tubes per Row	98	98	98	98	98
Fin Diameter [m]	4.82E+00	4.82E+00	4.82E+00	4.82E+00	4.82E+00
Minimum Airflow Area [m2]	6.33351	6.33351	6.33351	6.33351	6.33351
Fin Surface Area [m2]	1129.955	988.7106	847.4662	706.2219	564.9775
Total Tube Inside Surface Area [m2]	49.84672	43.61588	37.38504	31.1542	24.92336
Tube Outside Surface Area [m2]	51.10896	44.72034	38.33172	31.9431	25.55448
Coil Depth [m]	0.208	0.182	0.156	0.13	0.104
# of Rows	8	7	6	5	4

	8 Row	7 Row	6 Row	5 Row	4 Row
LOS ANGELAS - VAV 1					
Load [W]	378772				
Max Water Flow Rate [m3/s]	1.35E-02	1.35E-02	1.35E-02	1.35E-02	1.35E-02
# of Tubes per Row	187	187	187	187	187
Fin Diameter [m]	8.73111	8.73111	8.73111	8.73111	8.73111
Minimum Airflow Area [m2]	11.4677	11.4677	11.4677	11.4677	11.4677
Fin Surface Area [m2]	2045.95	1790.2	1534.46	1278.72	1022.97
Total Tube Inside Surface Area [m2]	95.1157	83.2262	71.3368	59.4473	47.5578
Tube Outside Surface Area [m2]	97.5242	85.3337	73.1432	60.9527	48.7621
Coil Depth [m]	0.208	0.182	0.156	0.13	0.104
# of Rows	8	7	6	5	4

	8 Row	7 Row	6 Row	5 Row	4 Row
LOS ANGELAS - VAV 2					
Load [W]	677388.2				
Max Water Flow Rate [m3/s]	2.42E-02	2.42E-02	2.42E-02	2.42E-02	2.42E-02
# of Tubes per Row	333	333	333	333	333
Fin Diameter [m]	15.09343	15.09343	15.09343	15.09343	15.09343
Minimum Airflow Area [m2]	19.82421	19.82421	19.82421	19.82421	19.82421
Fin Surface Area [m2]	3536.82	3094.717	2652.615	2210.512	1768.41
Total Tube Inside Surface Area [m2]	169.3771	148.205	127.0328	105.8607	84.68856
Tube Outside Surface Area [m2]	173.6662	151.9579	130.2496	108.5414	86.83308
Coil Depth [m]	0.208	0.182	0.156	0.13	0.104
# of Rows	8	7	6	5	4

C.2: Office Coils

Note: Row configurations highlighted is blue were used in testing of CAV/VAV Prediction Tools

	8 Row	7 Row	6 Row	5 Row	4 Row
ATLANTA - VAV 1 (CAV)					
Load [W]	270820.2				
Max Water Flow Rate [m3/s]	9.67E-02	9.67E-02	9.67E-02	9.67E-02	9.67E-02
# of Tubes per Row	1.34E+02	1.34E+02	1.34E+02	1.34E+02	1.34E+02
Fin Diameter [m]	3.75E+00	3.75E+00	3.75E+00	3.75E+00	3.75E+00
Minimum Airflow Area [m2]	4.92241	4.92241	4.92241	4.92241	4.92241
Fin Surface Area [m2]	8.78E+02	768.4272	658.6519	5.49E+02	439.1013
Total Tube Inside Surface Area [m2]	68.15776	59.63804	51.11832	42.5986	34.07888
Tube Outside Surface Area [m2]	69.88368	61.14822	52.41276	43.6773	34.94184
Coil Depth [m]	0.208	0.182	0.156	0.13	0.104
# of Rows	8	7	6	5	4

	8 Row	7 Row	6 Row	5 Row	4 Row
ATLANTA - VAV 2 (CAV)					
Load [W]	2710071.72				
Max Water Flow Rate [m3/s]	9.68E-01	9.68E-01	9.68E-01	9.68E-01	9.68E-01
# of Tubes per Row	1331	1331	1331	1331	1331
Fin Diameter [m]	39.47529	39.47529	39.47529	39.47529	39.47529
Minimum Airflow Area [m2]	5.18E+01	5.18E+01	5.18E+01	5.18E+01	5.18E+01
Fin Surface Area [m2]	9250.18014	8093.908	6937.635	5781.363	4625.09
Total Tube Inside Surface Area [m2]	676.99984	592.3749	507.7499	423.1249	338.4999
Tube Outside Surface Area [m2]	694.14312	607.3752	520.6073	433.8395	347.0716
Coil Depth [m]	0.208	0.182	0.156	0.13	0.104
# of Rows	8	7	6	5	4

	8 Row	7 Row	6 Row	5 Row	4 Row
ATLANTA - VAV 3					
Load [W]	265513.3				
Max Water Flow Rate [m3/s]	9.48E-02	9.48E-02	9.48E-02	9.48E-02	9.48E-02
# of Tubes per Row	131	131	131	131	131
Fin Diameter [m]	3.93289	3.93289	3.93289	3.93289	3.93289
Minimum Airflow Area [m2]	5.16559	5.16559	5.16559	5.16559	5.16559
Fin Surface Area [m2]	921.5882	806.39	691.191	575.993	460.794
Total Tube Inside Surface Area [m2]	66.63184	58.3029	49.9739	41.6449	33.3159
Tube Outside Surface Area [m2]	68.31912	59.7792	51.2393	42.6995	34.1596
Coil Depth [m]	0.208	0.182	0.156	0.13	0.104
# of Rows	8	7	6	5	4

	8 Row	7 Row	6 Row	5 Row	4 Row
ATLANTA - VAV 5					
Load [W]	143079.8				
Max Water Flow Rate [m3/s]	5.11E-02	5.11E-02	5.11E-02	5.11E-02	5.11E-02
# of Tubes per Row	71	71	71	71	71
Fin Diameter [m]	2.11E+00	2.11E+00	2.11E+00	2.11E+00	2.11E+00
Minimum Airflow Area [m2]	2.77585	2.77585	2.77585	2.77585	2.77585
Fin Surface Area [m2]	495.2372	433.3326	371.4279	309.5233	247.6186
Total Tube Inside Surface Area [m2]	36.11344	31.59926	27.08508	22.5709	18.05672
Tube Outside Surface Area [m2]	37.02792	32.39943	27.77094	23.14245	18.51396
Coil Depth [m]	2.08E-01	0.182	0.156	0.13	0.104
# of Rows	8	7	6	5	4

	8 Row	7 Row	6 Row	5 Row	4 Row
BOULDER - VAV 1 (CAV)					
Load [W]	165215				
Max Water Flow Rate [m3/s]	5.90E-02	5.90E-02	5.90E-02	5.90E-02	5.90E-02
# of Tubes per Row	82	82	82	82	82
Fin Diameter [m]	3.61E+00	3.61E+00	3.61E+00	3.61E+00	3.61E+00
Minimum Airflow Area [m2]	4.74E+00	4.74E+00	4.74E+00	4.74E+00	4.74E+00
Fin Surface Area [m2]	8.46E+02	740.5805	634.7833	528.9861	423.1889
Total Tube Inside Surface Area [m2]	4.17E+01	36.49492	31.28136	26.0678	20.85424
Tube Outside Surface Area [m2]	4.28E+01	37.41906	32.07348	26.7279	21.38232
Coil Depth [m]	0.208	0.182	0.156	0.13	0.104
# of Rows	8	7	6	5	4

	8 Row	7 Row	6 Row	5 Row	4 Row
BOULDER - VAV 2 (CAV)					
Load [W]	1728725.59				
Max Water Flow Rate [m3/s]	6.17E-01	6.17E-01	6.17E-01	6.17E-01	6.17E-01
# of Tubes per Row	849	849	849	849	849
Fin Diameter [m]	38.06983	38.06983	38.06983	38.06983	38.06983
Minimum Airflow Area [m2]	50.00216	50.00216	50.00216	50.00216	50.00216
Fin Surface Area [m2]	8920.83989	7805.735	6690.63	5575.525	4460.42
Total Tube Inside Surface Area [m2]	431.83536	377.8559	323.8765	269.8971	215.9177
Tube Outside Surface Area [m2]	442.77048	387.4242	332.0779	276.7316	221.3852
Coil Depth [m]	0.208	0.182	0.156	0.13	0.104
# of Rows	8	7	6	5	4

	8 Row	7 Row	6 Row	5 Row	4 Row
BOULDER - VAV 3					
Load [W]	161118.9				
Max Water Flow Rate [m3/s]	5.75E-02	5.75E-02	5.75E-02	5.75E-02	5.75E-02
# of Tubes per Row	80	80	80	80	80
Fin Diameter [m]	3.60322	3.60322	3.60322	3.60322	3.60322
Minimum Airflow Area [m2]	4.73259	4.73259	4.73259	4.73259	4.73259
Fin Surface Area [m2]	844.3367	738.795	633.252	527.71	422.168
Total Tube Inside Surface Area [m2]	4.07E+01	35.6048	30.5184	25.432	20.3456
Tube Outside Surface Area [m2]	4.17E+01	36.5064	31.2912	26.076	20.8608
Coil Depth [m]	0.208	0.182	0.156	0.13	0.104
# of Rows	8	7	6	5	4

	8 Row	7 Row	6 Row	5 Row	4 Row
BOULDER - VAV 5					
Load [W]	85925.46				
Max Water Flow Rate [m3/s]	3.07E-02	3.07E-02	3.07E-02	3.07E-02	3.07E-02
# of Tubes per Row	43	43	43	43	43
Fin Diameter [m]	1.83587	1.83587	1.83587	1.83587	1.83587
Minimum Airflow Area [m2]	2.41129	2.41129	2.41129	2.41129	2.41129
Fin Surface Area [m2]	430.1956	376.4211	322.6467	268.8722	215.0978
Total Tube Inside Surface Area [m2]	21.87152	19.13758	16.40364	13.6697	10.93576
Tube Outside Surface Area [m2]	22.42536	19.62219	16.81902	14.01585	11.21268
Coil Depth [m]	0.208	0.182	0.156	0.13	0.104
# of Rows	8	7	6	5	4

	8 Row	7 Row	6 Row	5 Row	4 Row
MIAMI - VAV 1 (CAV)					
Load [W]	2.83E+05				
Max Water Flow Rate [m3/s]	1.01E-01	1.01E-01	1.01E-01	1.01E-01	1.01E-01
# of Tubes per Row	140	140	140	140	140
Fin Diameter [m]	3.86813	3.86813	3.86813	3.86813	3.86813
Minimum Airflow Area [m2]	5.08053	5.08053	5.08053	5.08053	5.08053
Fin Surface Area [m2]	906.4121	793.1106	679.8091	566.5075	453.206
Total Tube Inside Surface Area [m2]	71.2096	62.3084	53.4072	44.506	35.6048
Tube Outside Surface Area [m2]	73.0128	63.8862	54.7596	45.633	36.5064
Coil Depth [m]	0.208	0.182	0.156	0.13	0.104
# of Rows	8	7	6	5	4

	8 Row	7 Row	6 Row	5 Row	4 Row
MIAMI - VAV 2 (CAV)					
Load [W]	2869185.68				
Max Water Flow Rate [m3/s]	1.0248	1.0248	1.0248	1.0248	1.0248
# of Tubes per Row	1.41E+03	1.41E+03	1.41E+03	1.41E+03	1.41E+03
Fin Diameter [m]	39.47105	39.47105	39.47105	39.47105	39.47105
Minimum Airflow Area [m2]	51.84258	51.84258	51.84258	51.84258	51.84258
Fin Surface Area [m2]	9249.18686	8093.039	6936.89	5780.742	4624.593
Total Tube Inside Surface Area [m2]	717.1824	627.5346	537.8868	448.239	358.5912
Tube Outside Surface Area [m2]	735.3432	643.4253	551.5074	459.5895	367.6716
Coil Depth [m]	0.208	0.182	0.156	0.13	0.104
# of Rows	8	7	6	5	4

	8 Row	7 Row	6 Row	5 Row	4 Row
MIAMI - VAV 3					
Load [W]	291960.7				
Max Water Flow Rate [m3/s]	1.04E-01	1.04E-01	1.04E-01	1.04E-01	1.04E-01
# of Tubes per Row	144	144	144	144	144
Fin Diameter [m]	3.99075	3.99075	3.99075	3.99075	3.99075
Minimum Airflow Area [m2]	5.24158	5.24158	5.24158	5.24158	5.24158
Fin Surface Area [m2]	935.146	818.253	701.36	584.466	467.573
Total Tube Inside Surface Area [m2]	73.24416	64.0886	54.9331	45.7776	36.6221
Tube Outside Surface Area [m2]	75.09888	65.7115	56.3242	46.9368	37.5494
Coil Depth [m]	0.208	0.182	0.156	0.13	0.104
# of Rows	8	7	6	5	4

	8 Row	7 Row	6 Row	5 Row	4 Row
MIAMI - VAV 5					
Load [W]	149993				
Max Water Flow Rate [m3/s]	5.36E-02	5.36E-02	5.36E-02	5.36E-02	5.36E-02
# of Tubes per Row	74	74	74	74	74
Fin Diameter [m]	2.14357	2.14357	2.14357	2.14357	2.14357
Minimum Airflow Area [m2]	2.81543	2.81543	2.81543	2.81543	2.81543
Fin Surface Area [m2]	502.2984	4.40E+02	3.77E+02	3.14E+02	2.51E+02
Total Tube Inside Surface Area [m2]	37.63936	32.93444	28.22952	23.5246	18.81968
Tube Outside Surface Area [m2]	38.59248	33.76842	28.94436	24.1203	19.29624
Coil Depth [m]	0.208	0.182	0.156	0.13	0.104
# of Rows	8	7	6	5	4

	8 Row	7 Row	6 Row	5 Row	4 Row
LOS ANGELAS - VAV 1 (CAV)					
Load [W]	1.82E+05				
Max Water Flow Rate [m3/s]	6.51E-02	6.51E-02	6.51E-02	6.51E-02	6.51E-02
# of Tubes per Row	9.00E+01	9.00E+01	9.00E+01	9.00E+01	9.00E+01
Fin Diameter [m]	3.66919	3.66919	3.66919	3.66919	3.66919
Minimum Airflow Area [m2]	4.81923	4.81923	4.81923	4.81923	4.81923
Fin Surface Area [m2]	859.7945	752.3202	644.8459	537.3716	429.8973
Total Tube Inside Surface Area [m2]	45.7776	40.0554	34.3332	28.611	22.8888
Tube Outside Surface Area [m2]	46.9368	41.0697	35.2026	29.3355	23.4684
Coil Depth [m]	0.208	0.182	0.156	0.13	0.104
# of Rows	8	7	6	5	4

	8 Row	7 Row	6 Row	5 Row	4 Row
LOS ANGELAS - VAV 2 (CAV)					
Load [W]	1711803.21				
Max Water Flow Rate [m3/s]	6.11E-01	6.11E-01	6.11E-01	6.11E-01	6.11E-01
# of Tubes per Row	841	841	841	841	841
Fin Diameter [m]	38.42314	38.42314	38.42314	38.42314	38.42314
Minimum Airflow Area [m2]	50.46622	50.46622	50.46622	50.46622	50.46622
Fin Surface Area [m2]	9003.63218	7878.178	6752.724	5627.27	4501.816
Total Tube Inside Surface Area [m2]	427.76624	374.2955	320.8247	267.3539	213.8831
Tube Outside Surface Area [m2]	438.59832	383.7735	328.9487	274.124	219.2992
Coil Depth [m]	0.208	0.182	0.156	0.13	0.104
# of Rows	8	7	6	5	4

	8 Row	7 Row	6 Row	5 Row	4 Row
LOS ANGELAS - VAV 3					
Load [W]	1.72E+05				
Max Water Flow Rate [m3/s]	6.16E-02	6.16E-02	6.16E-02	6.16E-02	6.16E-02
# of Tubes per Row	85	85	85	85	85
Fin Diameter [m]	3.55425	3.55425	3.55425	3.55425	3.55425
Minimum Airflow Area [m2]	4.66827	4.66827	4.66827	4.66827	4.66827
Fin Surface Area [m2]	832.8619	728.754	624.646	520.539	416.431
Total Tube Inside Surface Area [m2]	43.2344	37.8301	32.4258	27.0215	21.6172
Tube Outside Surface Area [m2]	44.3292	38.7881	33.2469	27.7058	22.1646
Coil Depth [m]	0.208	0.182	0.156	0.13	0.104
# of Rows	8	7	6	5	4

	8 Row	7 Row	6 Row	5 Row	4 Row
LOS ANGELAS - VAV 5					
Load [W]	91875.18				
Max Water Flow Rate [m3/s]	3.28E-02	3.28E-02	3.28E-02	3.28E-02	3.28E-02
# of Tubes per Row	46	46	46	46	46
Fin Diameter [m]	2.10542	2.10542	2.10542	2.10542	2.10542
Minimum Airflow Area [m2]	2.76533	2.76533	2.76533	2.76533	2.76533
Fin Surface Area [m2]	493.3607	431.6906	370.0205	308.3504	246.6804
Total Tube Inside Surface Area [m2]	23.39744	20.47276	17.54808	14.6234	11.69872
Tube Outside Surface Area [m2]	23.98992	20.99118	17.99244	14.9937	11.99496
Coil Depth [m]	0.208	0.182	0.156	0.13	0.104
# of Rows	8	7	6	5	4

C.3: Alternative Location Coils

Note: Only 6 Row configurations of the following were tested. The CAV 1, 6 Row configuration coil was that which was reported in Table 13 of the report for the investigation into the feasibility of testing alternative locations. Results from CAV 1 were representative of the results from only systems in the building for the particular outputs being investigated.

	8 Row	7 Row	6 Row	5 Row	4 Row
RENO - CAV 1					
Load [W]	263891				
Max Water Flow Rate [m3/s]	9.43E-02	9.43E-02	9.43E-02	9.43E-02	9.43E-02
# of Tubes per Row	130	130	130	130	130
Fin Diameter [m]	5.29716	5.29716	5.29716	5.29716	5.29716
Minimum Airflow Area [m2]	6.95746	6.95746	6.95746	6.95746	6.95746
Fin Surface Area [m2]	1241.27	1086.12	930.956	775.797	620.637
Total Tube Inside Surface Area [m2]	66.1232	57.8578	49.5924	41.327	33.0616
Tube Outside Surface Area [m2]	67.7976	59.3229	50.8482	42.3735	33.8988
Coil Depth [m]	0.208	0.182	0.156	0.13	0.104
# of Rows	8	7	6	5	4

	8 Row	7 Row	6 Row	5 Row	4 Row
RENO - CAV 2					
Load [W]	139526				
Max Water Flow Rate [m3/s]	4.98E-02	4.98E-02	4.98E-02	4.98E-02	4.98E-02
# of Tubes per Row	69	69	69	69	69
Fin Diameter [m]	4.11731	4.11731	4.11731	4.11731	4.11731
Minimum Airflow Area [m2]	5.40781	5.40781	5.40781	5.40781	5.40781
Fin Surface Area [m2]	964.803	844.203	723.602	603.002	482.402
Total Tube Inside Surface Area [m2]	35.0962	30.7091	26.3221	21.9351	17.5481
Tube Outside Surface Area [m2]	35.9849	31.4868	26.9887	22.4906	17.9924
Coil Depth [m]	0.208	0.182	0.156	0.13	0.104
# of Rows	8	7	6	5	4

	8 Row	7 Row	6 Row	5 Row	4 Row
RENO - VAV 1					
Load [W]	304428				
Max Water Flow Rate [m3/s]	1.09E-01	1.09E-01	1.09E-01	1.09E-01	1.09E-01
# of Tubes per Row	150	150	150	150	150
Fin Diameter [m]	7.69569	7.69569	7.69569	7.69569	7.69569
Minimum Airflow Area [m2]	10.1078	10.1078	10.1078	10.1078	10.1078
Fin Surface Area [m2]	1803.32	1577.9	1352.49	1127.07	901.659
Total Tube Inside Surface Area [m2]	76.296	66.759	57.222	47.685	38.148
Tube Outside Surface Area [m2]	78.228	68.4495	58.671	48.8925	39.114
Coil Depth [m]	0.208	0.182	0.156	0.13	0.104
# of Rows	8	7	6	5	4

	8 Row	7 Row	6 Row	5 Row	4 Row
RENO - VAV 2					
Load [W]	556310				
Max Water Flow Rate [m3/s]	1.99E-01	1.99E-01	1.99E-01	1.99E-01	1.99E-01
# of Tubes per Row	274	274	274	274	274
Fin Diameter [m]	13.5594	13.5594	13.5594	13.5594	13.5594
Minimum Airflow Area [m2]	17.8093	17.8093	17.8093	17.8093	17.8093
Fin Surface Area [m2]	3177.35	2780.18	2383.01	1985.84	1588.67
Total Tube Inside Surface Area [m2]	139.367	121.946	104.526	87.1046	69.6837
Tube Outside Surface Area [m2]	142.896	125.034	107.172	89.3103	71.4482
Coil Depth [m]	0.208	0.182	0.156	0.13	0.104
# of Rows	8	7	6	5	4

	8 Row	7 Row	6 Row	5 Row	4 Row
LAS VEGAS - CAV 1					
Load [W]	288567				
Max Water Flow Rate [m3/s]	1.03E-01	1.03E-01	1.03E-01	1.03E-01	1.03E-01
# of Tubes per Row	142	142	142	142	142
Fin Diameter [m]	4.85676	4.85676	4.85676	4.85676	4.85676
Minimum Airflow Area [m2]	6.37903	6.37903	6.37903	6.37903	6.37903
Fin Surface Area [m2]	1138.08	995.818	853.558	711.298	569.039
Total Tube Inside Surface Area [m2]	72.2269	63.1985	54.1702	45.1418	36.1134
Tube Outside Surface Area [m2]	74.0558	64.7989	55.5419	46.2849	37.0279
Coil Depth [m]	0.208	0.182	0.156	0.13	0.104
# of Rows	8	7	6	5	4

	8 Row	7 Row	6 Row	5 Row	4 Row
LAS VEGAS - CAV 2					
Load [W]	175412				
Max Water Flow Rate [m3/s]	6.27E-02	6.27E-02	6.27E-02	6.27E-02	6.27E-02
# of Tubes per Row	87	87	87	87	87
Fin Diameter [m]	3.77618	3.77618	3.77618	3.77618	3.77618
Minimum Airflow Area [m2]	4.95976	4.95976	4.95976	4.95976	4.95976
Fin Surface Area [m2]	884.866	774.257	663.649	553.041	442.433
Total Tube Inside Surface Area [m2]	44.2517	38.7202	33.1888	27.6573	22.1258
Tube Outside Surface Area [m2]	45.3722	39.7007	34.0292	28.3577	22.6861
Coil Depth [m]	0.208	0.182	0.156	0.13	0.104
# of Rows	8	7	6	5	4

	8 Row	7 Row	6 Row	5 Row	4 Row
LAS VEGAS - VAV 1					
Load [W]	381622				
Max Water Flow Rate [m3/s]	1.36E-01	1.36E-01	1.36E-01	1.36E-01	1.36E-01
# of Tubes per Row	188	188	188	188	188
Fin Diameter [m]	7.2713	7.2713	7.2713	7.2713	7.2713
Minimum Airflow Area [m2]	9.55036	9.55036	9.55036	9.55036	9.55036
Fin Surface Area [m2]	1703.87	1490.89	1277.9	1064.92	851.936
Total Tube Inside Surface Area [m2]	95.6243	83.6713	71.7182	59.7652	47.8122
Tube Outside Surface Area [m2]	98.0458	85.79	73.5343	61.2786	49.0229
Coil Depth [m]	0.208	0.182	0.156	0.13	0.104
# of Rows	8	7	6	5	4

	8 Row	7 Row	6 Row	5 Row	4 Row
LAS VEGAS - VAV 2					
Load [W]	712256				
Max Water Flow Rate [m3/s]	2.54E-01	2.54E-01	2.54E-01	2.54E-01	2.54E-01
# of Tubes per Row	350	350	350	350	350
Fin Diameter [m]	13.2245	13.2245	13.2245	13.2245	13.2245
Minimum Airflow Area [m2]	17.3695	17.3695	17.3695	17.3695	17.3695
Fin Surface Area [m2]	3098.87	2711.51	2324.15	1936.79	1549.43
Total Tube Inside Surface Area [m2]	178.024	155.771	133.518	111.265	89.012
Tube Outside Surface Area [m2]	182.532	159.716	136.899	114.083	91.266
Coil Depth [m]	0.208	0.182	0.156	0.13	0.104
# of Rows	8	7	6	5	4

	8 Row	7 Row	6 Row	5 Row	4 Row
LITTLE ROCK - CAV 1					
Load [W]	465194				
Max Water Flow Rate [m3/s]	1.66E-01	1.66E-01	1.66E-01	1.66E-01	1.66E-01
# of Tubes per Row	229	229	229	229	229
Fin Diameter [m]	6.17529	6.17529	6.17529	6.17529	6.17529
Minimum Airflow Area [m2]	8.11083	8.11083	8.11083	8.11083	8.11083
Fin Surface Area [m2]	1447.05	1266.16	1085.28	904.403	723.523
Total Tube Inside Surface Area [m2]	116.479	101.919	87.3589	72.7991	58.2393
Tube Outside Surface Area [m2]	119.428	104.5	89.5711	74.6426	59.714
Coil Depth [m]	0.208	0.182	0.156	0.13	0.104
# of Rows	8	7	6	5	4

	8 Row	7 Row	6 Row	5 Row	4 Row
LITTLE ROCK - CAV 2					
Load [W]	242983				
Max Water Flow Rate [m3/s]	8.68E-02	8.68E-02	8.68E-02	8.68E-02	8.68E-02
# of Tubes per Row	120	120	120	120	120
Fin Diameter [m]	4.79445	4.79445	4.79445	4.79445	4.79445
Minimum Airflow Area [m2]	6.29719	6.29719	6.29719	6.29719	6.29719
Fin Surface Area [m2]	1123.48	983.041	842.607	702.172	561.738
Total Tube Inside Surface Area [m2]	61.0368	53.4072	45.7776	38.148	30.5184
Tube Outside Surface Area [m2]	62.5824	54.7596	46.9368	39.114	31.2912
Coil Depth [m]	0.208	0.182	0.156	0.13	0.104
# of Rows	8	7	6	5	4

	8 Row	7 Row	6 Row	5 Row	4 Row
LITTLE ROCK - VAV 1					
Load [W]	496853				
Max Water Flow Rate [m3/s]	1.77E-01	1.77E-01	1.77E-01	1.77E-01	1.77E-01
# of Tubes per Row	245	245	245	245	245
Fin Diameter [m]	9.21102	9.21102	9.21102	9.21102	9.21102
Minimum Airflow Area [m2]	12.0981	12.0981	12.0981	12.0981	12.0981
Fin Surface Area [m2]	2158.4	1888.6	1618.8	1349	1079.2
Total Tube Inside Surface Area [m2]	124.617	109.04	93.4626	77.8855	62.3084
Tube Outside Surface Area [m2]	127.772	111.801	95.8293	79.8578	63.8862
Coil Depth [m]	0.208	0.182	0.156	0.13	0.104
# of Rows	8	7	6	5	4

	8 Row	7 Row	6 Row	5 Row	4 Row
LITTLE ROCK- VAV 2					
Load [W]	892021				
Max Water Flow Rate [m3/s]	3.19E-01	3.19E-01	3.19E-01	3.19E-01	3.19E-01
# of Tubes per Row	439	439	439	439	439
Fin Diameter [m]	15.9487	15.9487	15.9487	15.9487	15.9487
Minimum Airflow Area [m2]	20.9475	20.9475	20.9475	20.9475	20.9475
Fin Surface Area [m2]	3737.23	3270.08	2802.92	2335.77	1868.61
Total Tube Inside Surface Area [m2]	223.293	195.381	167.47	139.558	111.646
Tube Outside Surface Area [m2]	228.947	200.329	171.71	143.092	114.474
Coil Depth [m]	0.208	0.182	0.156	0.13	0.104
# of Rows	8	7	6	5	4

Appendix D: Steps in Performing EnergyPlus Simulations and Bin Plot Generation

D.1: Steps for Data Generation

1. Open Matlab and open "example_script_original.m". Make the following adjustments to ensure a 6 month simulation on 5 minute timesteps:

    Timestep = 12

    begin_month = 4;

    begin_day = 1;

    end_month = 9;

    end_day = 31;

2. Run “example_script_original”

3. Select "CAV_1" from pop- up window.

4. Save pdfs and RData.csv to its own folder.

5. Move the generated LOCATION#.csv file to working directory.

6. Make note of elevation in Matlab’s Workspace.

7. Open "testoriginal.m". Make the following changes to it:

    Change reference file in line 4.

    Input correct elevation in line 63.

8. Run "testoriginal.m".

9. Select "CAV_2" in pop-up window.

10. Save pdfs and RData.csv to its own folder.

11. Repeat steps 8 through 10 for VAV_1 and VAV_2.

12. Repeat steps 1 through 11 for all IDF files of interest

D.2: Matlab Script “example_script_original.m”

```
% Example Script
addpath(genpath(pwd))
clear;close all;clc
%% Energy Plus
% Define EP files to use
% current path
path_current = pwd;
% location of idf (either "hospital" or "large office" work with this
% script)
```

```
[FileName,FilePath] = uigetfile(fullfile(path_current,'EnergyPlus','buildings','*.idf'),'Select building
file');
file_idf = fullfile(FilePath,FileName);
% location of weather file
[FileName,FilePath] = uigetfile(fullfile(path_current,'EnergyPlus','weather','*.epw'),'Select weather
File');
file_epw = fullfile(FilePath,FileName);
% location of output
path_output = fullfile(path_current,'EnergyPlus','results');
% location of energy plus program
path_EP = uigetdir('c:','Locate EnergyPlus program directory');

% Simulation Parameters

% number of timesteps per hour in accordance with EP timestep requirements
timestep = 12;
func_EP_timestep(timestep,file_idf);

% simulation period
begin_month = 4;
begin_day = 1;
end_month = 9;
end_day = 30;
func_EP_run_period(begin_month,begin_day,end_month,end_day,file_idf)

% run EnergyPlus
func_EnergyPlus(file_idf,file_epw,path_output,path_EP)

%% Import results from EnergyPlus
% EP variable output file
[~,EP] = fileparts(file_idf);
file_EP = fullfile(path_output,[EP '.csv']);
% import results
[data,header] = xlsread(file_EP);
% head time from header (you can use datenum and datestr commands to
% further manipulate the time vector)
time = header(2:end,1);
% remove time from header
header = header(1,2:end)';
% separate out the Hour of the day
[Year Month Day Hour Min Sec]=datevec(time);
% create list of unique air handling units
list = cell(size(header));
for n = 1:numel(header);
   list{n} = header{n}(1:5);
end
list = unique(list);
% user select coil to use
selection = listdlg('ListString',list);
coil = list{selection};
```

```
% effectively remove unselected coils from header but preserve indexing
for n = 1:numel(header)
   check = strfind(header{n},coil);
   if isempty(check)
      header{n} = '';
   end
end
%function to find string in header and return index
f_ind = @(str,header)(find(~cellfun('isempty',(strfind(header,str)))));
% import relevent data series
% water mass flow rate
str = 'COOLCDEMAND INLET NODE:System Node Mass Flow Rate [kg/s](TimeStep)';
mW = data(:,f_ind(str,header));
% water inlet temperature
str = 'COOLCDEMAND INLET NODE:System Node Temperature [C](TimeStep)';
Twi = data(:,f_ind(str,header));
% water outlet temperature
str = 'COOLCDEMAND OUTLET NODE:System Node Temperature [C](TimeStep)';
Two = data(:,f_ind(str,header));
% air mass flow rate
str = 'COOLCNODE:System Node Mass Flow Rate [kg/s](TimeStep)';
mA = data(:,f_ind(str,header));
% air intlet temperature
str = 'COOLCNODE:System Node Temperature [C](TimeStep)';
Tai = data(:,f_ind(str,header));
% air outtlet temperature
str = 'HEATCNODE:System Node Temperature [C](TimeStep)';
Tao = data(:,f_ind(str,header));
% air inlet humidity
str = 'COOLCNODE:System Node Relative Humidity [%](TimeStep)';
RHai = data(:,f_ind(str,header));
% air outlet humidity
str = 'HEATCNODE:System Node Relative Humidity [%](TimeStep)';
RHao = data(:,f_ind(str,header));
% Total coil cooling rate
str = 'COOLC:Cooling Coil Total Cooling Rate [W](TimeStep)';
Q = data(:,f_ind(str,header));

% import elevation from EPW file.  Usefull calling the included
% Psychrometric functions.
Elevation = func_EP_elevation(file_epw);

%Produce enthalpy output
h = func_h_tdb_rh(Tai,RHai,Elevation);

%Produce absolute humidity output
Wai = func_w_tdb_rh(Tai,RHai,Elevation);

%% Plots
figure
```

```
plot(mW,Q,'.b')
xlabel('water flow rate [kg/s]')
ylabel('coil cooling [w]')
title('coil cooling rate')

figure
plot(Twi,'b','displayname','in')
hold on
plot(Two,'r','displayname','out')
xlabel('timestep')
ylabel('temperature [°C]')
title('coil water temperature')
legend('show')
legend('Location','Southeast')

figure
plot(Tai,'r','displayname','in')
hold on
plot(Tao,'b','displayname','out')
xlabel('timestep')
ylabel('temperature [°C]')
title('coil air temperature')
legend('show')
legend('Location','Southeast')

figure
plot(RHai,'r','displayname','in')
hold on
plot(RHao,'b','displayname','out')
xlabel('timestep')
ylabel('relative humidity [%]')
title('coil relative humidity')
legend('show')
legend('Location','Southeast')

figure
plot(mW,'b','displayname','water')
hold on
plot(mA,'r','displayname','air')
xlabel('timestep')
ylabel('mass flow rate [kg/s]')
title('coil flow rates')
legend('show')
legend('Location','Southeast')

%Inlet Air Temp Grouping
Taigroup=ordinal(Tai,{'Under 15 C','15-20 C','20-25 C','25-30 C','Over 30 C'},[],[0,15,20,25,30,100]);
figure
gscatter(mW,Q,Taigroup);
xlabel('water flow rate [kg/s]')
```

```
ylabel('coil cooling [w]')
title('Inlet Air Temp Binned')
legend('Location','Southeast')

%Inlet RH Grouping
RHaigroup=ordinal(RHai,{'Under 30%','30-45%','45-60%','60-75%','Over
70%'},[],[0,30,45,60,75,100]);
figure
gscatter(mW,Q,RHaigroup);
xlabel('water flow rate [kg/s]')
ylabel('coil cooling [w]')
title('Inlet Relative Humidity Binned')
legend('Location','Southeast')

%Inlet Enthalpy Grouping
hgroup=ordinal(h,{'Under 25 kJ/kg','25-30 kJ/kg','30-35 kJ/kg','35-40 kJ/kg','40-45 kJ/kg','45-50
kJ/kg','50-55 kJ/kg','55-60 kJ/kg','60-70 kJ/kg','Over 70
kJ/kg%'},[],[0,25,30,35,40,45,50,55,60,70,120]);
figure
gscatter(mW,Q,hgroup);
xlabel('water flow rate [kg/s]')
ylabel('coil cooling [w]')
title('Inlet Air Enthalpy Binned')
legend('Location','Southeast')

%Inlet Air Humidity Ratio Grouping
Waigroup=ordinal(Wai,{'Under 0.007','0.007-0.01','0.01-0.012','0.012-0.014','0.014-0.016','Over
0.016'},[],[0,0.007,0.01,0.012,0.014,0.016,0.2]);
figure
gscatter(mW,Q,Waigroup);
xlabel('water flow rate [kg/s]')
ylabel('coil cooling [w]')
title('Inlet Air Humidity Ratio Binned')
legend('Location','Southeast')
%Delta T Grouping
DeltaT = Two-Twi;
DeltaTgroup=ordinal(DeltaT,{'Under 1 K','1-2 K','2-3 K','3-4 K','4-5 K','5-6 K','6-7 K','7-8 K','Over
8'},[],[0,1,2,3,4,5,6,7,8,100]);
figure
gscatter(mW,Q,DeltaTgroup);
xlabel('water flow rate [kg/s]')
ylabel('coil cooling [w]')
title('Delta T Binned')
legend('Location','Southeast')

%Air Flow Rate Grouping
mAgroup=ordinal(mA,{'Under 5 kg/s','5-10 kg/s','10-15 kg/s','15-20 kg/s','20-25 kg/s','25-50
kg/s','50-75 kg/s','75-100 kg/s','Over 100 kg/s'},[],[0,5,10,15,20,25,50,75,100,200]);
figure
gscatter(mW,Q,mAgroup);
```

```
xlabel('water flow rate [kg/s]')
ylabel('coil cooling [w]')
title('Air Flow Rate Binned')
legend('Location','Southeast')


%Time of Day Grouping
Hourgroup=ordinal(Hour,{'Before 6','6-8am','8am-noon','noon-5pm','5pm-
midnight'},[],[0,6,8,12,17,24]);
figure
gscatter(mW,Q,Hourgroup);
xlabel('water flow rate [kg/s]')
ylabel('coil cooling [w]')
title('Time of Day Binned')
legend('Location','Southeast')

%Twi Grouping
Twigroup=ordinal(Twi,{'<6 C','6-7 C','7-8 C','>8 C'},[],[0,6,7,8,10]);
figure
gscatter(mW,Q,Twigroup);
xlabel('water flow rate [kg/s]')
ylabel('coil cooling [w]')
title('Twi Binned')
legend('Location','Southeast')

save2pdf('Twibin',13)
save2pdf('TODbin',12);
save2pdf('DeltaTbin',11);
save2pdf('mAbin',10);
save2pdf('Waibin',9);
save2pdf('haibin',8);
save2pdf('RHaibin',7);
save2pdf('Taibin',6);
save2pdf('QvsmW.pdf',1);

% cleanup
rmpath(genpath(pwd))
% save data for R analysis
 RData = [mW Q mA Tai Tao h RHai RHao Wai Twi Two DeltaT Month Day Hour Min];
 csvwrite('RData.csv',RData);

 % cleanup
 rmpath(genpath(pwd))
```

D.3: Matlab Script "testoriginal.m"

```
clear;close all;clc
%% Import results from EnergyPlus
% EP variable output file
file_EP = fullfile('BOULDERofficeReset.csv');
```

```
% import results
[data,header] = xlsread(file_EP);
% head time from header (you can use datenum and datestr commands to
% further manipulate the time vector)
time = header(2:end,1);
% remove time from header
header = header(1,2:end)';
% separate out the Hour of the day
[Year Month Day Hour Min Sec]=datevec(time);
% create list of unique air handling units
list = cell(size(header));
for n = 1:numel(header);
   list{n} = header{n}(1:5);
end
list = unique(list);
% user select coil to use
selection = listdlg('ListString',list);
coil = list{selection};
% effectively remove unselected coils from header but preserve indexing
for n = 1:numel(header)
   check = strfind(header{n},coil);
   if isempty(check)
      header{n} = '';
   end
end
%function to find string in header and return index
f_ind = @(str,header)(find(~cellfun('isempty',(strfind(header,str)))));
% import relevent data series
% water mass flow rate
str = 'COOLCDEMAND INLET NODE:System Node Mass Flow Rate [kg/s](TimeStep)';
mW = data(:,f_ind(str,header));
% water inlet temperature
str = 'COOLCDEMAND INLET NODE:System Node Temperature [C](TimeStep)';
Twi = data(:,f_ind(str,header));
% water outlet temperature
str = 'COOLCDEMAND OUTLET NODE:System Node Temperature [C](TimeStep)';
Two = data(:,f_ind(str,header));
% air mass flow rate
str = 'COOLCNODE:System Node Mass Flow Rate [kg/s](TimeStep)';
mA = data(:,f_ind(str,header));
% air intlet temperature
str = 'COOLCNODE:System Node Temperature [C](TimeStep)';
Tai = data(:,f_ind(str,header));
% air outtlet temperature
str = 'HEATCNODE:System Node Temperature [C](TimeStep)';
Tao = data(:,f_ind(str,header));
% air inlet humidity
str = 'COOLCNODE:System Node Relative Humidity [%](TimeStep)';
RHai = data(:,f_ind(str,header));
% air outlet humidity
```

```
str = 'HEATCNODE:System Node Relative Humidity [%](TimeStep)';
RHao = data(:,f_ind(str,header));
% Total coil cooling rate
str = 'COOLC:Cooling Coil Total Cooling Rate [W](TimeStep)';
Q = data(:,f_ind(str,header));

% import elevation from EPW file.  Usefull calling the included
% Psychrometric functions.
Elevation = 30;

%Produce enthalpy output
h = func_h_tdb_rh(Tai,RHai,Elevation);

%Produce absolute humidity output
Wai = func_w_tdb_rh(Tai,RHai,Elevation);

%% Plot
figure
plot(mW,Q,'.b')
xlabel('water flow rate [kg/s]')
ylabel('coil cooling [w]')
title('coil cooling rate')

figure
plot(Twi,'b','displayname','in')
hold on
plot(Two,'r','displayname','out')
xlabel('timestep')
ylabel('temperature [°C]')
title('coil water temperature')
legend('show')
legend('Location','Southeast')

figure
plot(Tai,'r','displayname','in')
hold on
plot(Tao,'b','displayname','out')
xlabel('timestep')
ylabel('temperature [°C]')
title('coil air temperature')
legend('show')
legend('Location','Southeast')

figure
plot(RHai,'r','displayname','in')
hold on
plot(RHao,'b','displayname','out')
xlabel('timestep')
ylabel('relative humidity [%]')
title('coil relative humidity')
```

```
legend('show')
legend('Location','Southeast')

figure
plot(mW,'b','displayname','water')
hold on
plot(mA,'r','displayname','air')
xlabel('timestep')
ylabel('mass flow rate [kg/s]')
title('coil flow rates')
legend('show')
legend('Location','Southeast')

%Inlet Air Temp Grouping
Taigroup=ordinal(Tai,{'Under 15 C','15-20 C','20-25 C','25-30 C','Over 30 C'},[],[0,15,20,25,30,100]);
figure
gscatter(mW,Q,Taigroup);
xlabel('water flow rate [kg/s]')
ylabel('coil cooling [w]')
title('Inlet Air Temp Binned')
legend('Location','Southeast')

%Inlet RH Grouping
RHaigroup=ordinal(RHai,{'Under 30%','30-45%','45-60%','60-75%','Over
70%'},[],[0,30,45,60,75,100]);
figure
gscatter(mW,Q,RHaigroup);
xlabel('water flow rate [kg/s]')
ylabel('coil cooling [w]')
title('Inlet Relative Humidity Binned')
legend('Location','Southeast')

%Inlet Enthalpy Grouping
hgroup=ordinal(h,{'Under 25 kJ/kg','25-30 kJ/kg','30-35 kJ/kg','35-40 kJ/kg','40-45 kJ/kg','45-50
kJ/kg','50-55 kJ/kg','55-60 kJ/kg','60-70 kJ/kg','Over 70
kJ/kg%'},[],[0,25,30,35,40,45,50,55,60,70,120]);
figure
gscatter(mW,Q,hgroup);
xlabel('water flow rate [kg/s]')
ylabel('coil cooling [w]')
title('Inlet Air Enthalpy Binned')
legend('Location','Southeast')

%Inlet Air Humidity Ratio Grouping
Waigroup=ordinal(Wai,{'Under 0.007','0.007-0.01','0.01-0.012','0.012-0.014','0.014-0.016','Over
0.016'},[],[0,0.007,0.01,0.012,0.014,0.016,0.2]);
figure
gscatter(mW,Q,Waigroup);
xlabel('water flow rate [kg/s]')
ylabel('coil cooling [w]')
```

```
title('Inlet Air Humidity Ratio Binned')
legend('Location','Southeast')
%Delta T Grouping
DeltaT = Two-Twi;
DeltaTgroup=ordinal(DeltaT,{'Under 1 K','1-2 K','2-3 K','3-4 K','4-5 K','5-6 K','6-7 K','7-8 K','Over
8'},[],[0,1,2,3,4,5,6,7,8,100]);
figure
gscatter(mW,Q,DeltaTgroup);
xlabel('water flow rate [kg/s]')
ylabel('coil cooling [w]')
title('Delta T Binned')
legend('Location','Southeast')

%Air Flow Rate Grouping
mAgroup=ordinal(mA,{'Under 5 kg/s','5-10 kg/s','10-15 kg/s','15-20 kg/s','20-25 kg/s','25-50
kg/s','50-75 kg/s','75-100 kg/s','Over 100 kg/s'},[],[0,5,10,15,20,25,50,75,100,200]);
figure
gscatter(mW,Q,mAgroup);
xlabel('water flow rate [kg/s]')
ylabel('coil cooling [w]')
title('Air Flow Rate Binned')
legend('Location','Southeast')


%Time of Day Grouping
Hourgroup=ordinal(Hour,{'Before 6','6-8am','8am-noon','noon-5pm','5pm-
midnight'},[],[0,6,8,12,17,24]);
figure
gscatter(mW,Q,Hourgroup);
xlabel('water flow rate [kg/s]')
ylabel('coil cooling [w]')
title('Time of Day Binned')
legend('Location','Southeast')

%Twi Grouping
Twigroup=ordinal(Twi,{'<6 C','6-6.5 C','6.5-7','7-7.5','7.5-8 C','>8 C'},[],[0,6,6.5,7,7.5,8,10]);
figure
gscatter(mW,Q,Twigroup);
xlabel('water flow rate [kg/s]')
ylabel('coil cooling [w]')
title('Twi Binned')
legend('Location','Southeast')

save2pdf('Twibin',13)
save2pdf('TODbin',12);
save2pdf('DeltaTbin',11);
save2pdf('mAbin',10);
save2pdf('Waibin',9);
save2pdf('haibin',8);
save2pdf('RHaibin',7);
```

```
save2pdf('Taibin',6);
save2pdf('QvsmW.pdf',1);

% cleanup
rmpath(genpath(pwd))
% save data for R analysis
 RData = [mW Q mA Tai Tao h RHai RHao Wai Twi Two DeltaT Month Day Hour Min];
 csvwrite('RData.csv',RData);

 % cleanup
 rmpath(genpath(pwd))
```

D.4: Additional Matlab Scripts Required in Working Directory

D.4.1: func_EP_timestep.m

```
function func_EP_timestep(TimeStep,file)
%% setup and input
if exist(file,'file') == 2
   data = fileread(file);
   %    datain = fopen(filename);
else
   disp('Input path or file not found.');
   return
end

% string to find
str = 'Timestep,';
data = f_string(TimeStep,str,data);

fout = fopen(file,'w');
fprintf(fout,'%s',data);
fclose(fout);

   function [data] = f_string(num,str,data)
      % index of string
      ind = strfind(data,str);

      % find end of line
      flag = 0;
      iter = 0;
      while flag == 0
         iter = iter+1;
         flag = strcmp(data(ind+iter),char(13));
      end
      ind_out = ind+iter-1;

      % find start of line
      flag = 0;
      iter = 0;
```

```
      while flag == 0
        iter = iter+1;
        flag = strcmp(data(ind-iter),char(10));
      end
      ind_in = ind-iter+1;


      % line string
      str_out = data(ind_in:ind_out);
      str_in(1:4) = char(32);
      str_in = [str_in str num2str(num) ';   !- Number of Timesteps per Hour'];

      % replace string
      data = strrep(data,str_out,str_in);
    end
end
```

D.4.2: func_EP_run_period.m

```
function func_EP_run_period(begin_month,begin_day,end_month,end_day,file)
%% setup and input
if exist(file,'file') == 2
   data = fileread(file);
   %    datain = fopen(filename);
else
   disp('Input path or file not found.');
   return
end

% string to find
str = '!- Begin Month';
data = f_string(begin_month,str,data);

% string to find
str = '!- End Month';
data = f_string(end_month,str,data);

% string to find
str = '!- Begin Day of Month';
data = f_string(begin_day,str,data);

% string to find
str = '!- End Day of Month';
data = f_string(end_day,str,data);


fout = fopen(file,'w');
fprintf(fout,'%s',data);
fclose(fout);
```

```
  function [data] = f_string(num,str,data)
    % index of string
    ind = strfind(data,str);

    % find end of line
    flag = 0;
    iter = 0;
    while flag == 0
      iter = iter+1;
      flag = strcmp(data(ind+iter),char(13));
    end
    ind_out = ind+iter-1;

    % find start of line
    flag = 0;
    iter = 0;
    while flag == 0
      iter = iter+1;
      flag = strcmp(data(ind-iter),char(10));
    end
    ind_in = ind-iter+1;


    % line string
    str_out = data(ind_in:ind_out);
    ind = strfind(str_out,'!');
    str_in(1:4) = char(32);
    str_in = [str_in num2str(num) ','];
    str_in(end+1:ind-1) = char(32);
    str_in = [str_in str];

    % replace string
    data = strrep(data,str_out,str_in);
  end
end
```

D.4.3: func_EnergyPlus.m

```
% function to exectute EnergyPlus given a valid filepath and filename for
% IDF an EPW files.  The output file and path is the same as the input.
% The path names must be followed by a backslash, \
% by Forest Reider 4/3/14
function func_EnergyPlus(file_idf,file_epw,path_output,path_EP)
%% make sure files and paths exist
check = exist(file_idf,'file');
if check==0
  error('IDF file does not exist')
end
check = exist(file_epw,'file');
```

```
if check==0
   error('EPW file does not exist')
end
check = exist(path_output,'dir');
if check==0
   error('output path does not exist')
end
check = exist(path_EP,'dir');
if check==0
   error('Energy Plus path does not exist')
end

%% Move to Output folder
% remember envoking folder
path = pwd;
% move to output folder
cd(path_output);

%% create file to manipulate
% name of building file
[path_idf,idf] = fileparts(file_idf);
% name of weather file
[path_epw,epw] = fileparts(file_epw);
% original EP bat file
EPbase = fullfile(path_EP,'RunEPlus.bat');
% process bat file
EPnew = fullfile(path_output,'RunEPlus.bat');
% generate process bat file in output dir
copyfile(EPbase,EPnew);
%% modify batch file

% read batch file
data = fileread(EPnew);

% find key line in batch file
strin = ':  This batch file will perform the following steps:';
k = strfind(data,strin);
% delete everything up to the key line
data(1:k-1) = [];

% create new lines before the key line in batch file
line1 = ['echo ===== %0 (Run EnergyPlus) %1 %2 ===== Start =====' char(13) char(10)];
line2 = ['set program_path=' path_EP '\' char(13) char(10)];
line3 = ['set program_name=EnergyPlus.exe' char(13) char(10)];
line4 = ['set input_path=' path_idf '\' char(13) char(10)];
line5 = ['set output_path=' path_output '\' char(13) char(10)];
line6 = ['set post_proc=' path_EP '\PostProcess\' char(13) char(10)];
line7 = ['set weather_path=' path_epw '\' char(13) char(10)];
line8 = ['set pausing=N' char(13) char(10)];
line9 = ['set maxcol=250' char(13) char(10)];
```

```
line10 = [char(13) char(10)];

% write new lines
data = [line1 line2 line3 line4 line5 line6 line7 line8 line9 line10 data];

% save new batch file
fout = fopen(EPnew,'w');
fprintf(fout,'%s',data);
fclose(fout);

%% run EP with modified file
%run EP in MatLab
system(['RunEPlus.bat' char(32) idf char(32) epw]);

%% Delete Temp Files
delete(EPnew);
% Return to envoking folder
cd(path);
```

D.4.4: func_EP_elevation.m

```
% function to get elevation in meters from EPW file assuming the elevation
% is the on the first line of the EWP file.
function elevation = func_EP_elevation(file_epw)
%% setup and input
if exist(file_epw,'file') == 2
   data = fileread(file_epw);
   %    datain = fopen(filename);
else
   disp('Input path or file not found.');
   return
end
% find end of first line of weather file
flag = 0;
iter = 0;
while flag == 0;
   % increment counter
   iter = iter+1;
   % check if character is a comma and record
   flag = strcmp(data(iter),',');
   if flag == 1;
      comma = iter;
   end
   % check if end of line to exit loop
   flag = strcmp(data(iter:iter+1),[char(13),char(10)]);
end
% output elevation
elevation = str2double(data(comma+1:iter-1));
```

D.4.5: func_w_tb_rh

```
function [HumidityRatio] = func_w_tdb_rh(Tai,RHai,Elevation)
z = Elevation; % [m]
t = Tai; % [°C]
rh = RHai/100; % [-] (input in percent)

%calculate pressure as a function of altitude
p = 101.325*(1-2.25577e-5*z)^5.2559*1000; % [Pa]

%coefficients from ASHRAE Fundamentals Psychrometrics
C8 = -5.8002206e03;
C9 = 1.3914993e00;
C10 = -4.8640239e-02;
C11 = 4.1764768e-05;
C12 = -1.4452093e-08;
C13 = 6.5459673e00;

%calc saturation pressure
K = t+273.15; % [K]
pws = exp(C8./K+C9+C10*K+C11.*K.^2+C12.*K.^3+C13*log(K)); % [Pa]

%calc  partial vapor pressure
pw = rh.*pws; % [Pa]

%calc humidity ratio
w = 0.621945.*pw./(p-pw); % [-]

%output
HumidityRatio = w; % [-]
```

D.4.6: save2pdf.m

```
%SAVE2PDF Saves a figure as a properly cropped pdf
%
%   save2pdf(pdfFileName,handle,dpi)
%
%   - pdfFileName: Destination to write the pdf to.
%   - handle:  (optional) Handle of the figure to write to a pdf.  If
%           omitted, the current figure is used.  Note that handles
%           are typically the figure number.
%   - dpi: (optional) Integer value of dots per inch (DPI).  Sets
%        resolution of output pdf.
%
%   Saves figure as a pdf with margins cropped to match the figure size.

%   (c) Gabe Hoffmann, gabe.hoffmann@gmail.com
%   Written 8/30/2007
%   Revised 9/22/2007,1,
%   Revised 1/14/2007
```

```
function save2pdf(pdfFileName,handle,dpi)

% Verify correct number of arguments
error(nargchk(0,3,nargin));

% If no handle is provided, use the current figure as default
if nargin<1
   [fileName,pathName] = uiputfile('*.pdf','Save to PDF file:');
   if fileName == 0; return; end
   pdfFileName = [pathName,fileName];
   dpi=600;
end
if nargin<2
   handle = gcf;
   dpi=600;
end
if nargin<3
   dpi = 600;
end

% Backup previous settings
prePaperType = get(handle,'PaperType');
prePaperUnits = get(handle,'PaperUnits');
preUnits = get(handle,'Units');
prePaperPosition = get(handle,'PaperPosition');
prePaperSize = get(handle,'PaperSize');

% Make changing paper type possible
set(handle,'PaperType','<custom>');

% Set units to all be the same
set(handle,'PaperUnits','inches');
set(handle,'Units','inches');

% Set the page size and position to match the figure's dimensions
paperPosition = get(handle,'PaperPosition');
position = get(handle,'Position');
set(handle,'PaperPosition',[0,0,position(3:4)]);
set(handle,'PaperSize',position(3:4));

% Save the pdf (this is the same method used by "saveas")
print(handle,'-dpdf',pdfFileName,sprintf('-r%d',dpi))

% Restore the previous settings
set(handle,'PaperType',prePaperType);
set(handle,'PaperUnits',prePaperUnits);
set(handle,'Units',preUnits);
set(handle,'PaperPosition',prePaperPosition);
set(handle,'PaperSize',prePaperSize);
```

D.4.7: func_h_tdb_rh.m

```
function [Enthalpy] = func_h_tdb_rh(Tai,RHai,Elevation)
z = Elevation; % [m]
t = Tai; % [°C]
rh = RHai/100; % [-] (input in percent)

%calculate pressure as a function of altitude
p = 101.325*(1-2.25577e-5*z)^5.2559*1000; %pressure, Pa

%coefficients from ASHRAE Fundamentals Psychrometrics
C8 = -5.8002206e03;
C9 = 1.3914993e00;
C10 = -4.8640239e-02;
C11 = 4.1764768e-05;
C12 = -1.4452093e-08;
C13 = 6.5459673e00;

%calc saturation pressure
K = t+273.15; %convert to kelvin, K
pws = exp(C8./K+C9+C10.*K+C11.*K.^2+C12.*K.^3+C13.*log(K)); %saturation pressure, Pa

%calc vapor pressure
pw = rh.*pws; %partial pressure, Pa

%calc humidity ratio
w = 0.621945.*pw./(p-pw);

%calc enthalpy
h = (1006.*t+w.*(2501000+1860.*t))/1000; %enthalpy, kJ/kg_da

%output
Enthalpy = h; %enthalpy, kJ/kg_da
```

Appendix E: Regression of Flow Bin Quantiles

E.1: Steps for Performing Regression of the Flow Bin Quantiles

1. Map to appropriate directory in RStudio
    - "Set as working directory"
2. Run "k2 Testing.R" script as seen in Appendix E.2
3. Adjust line 7 of script so the first 15 bins are covering the worthwhile data
    - Make this determination after running the initial simulation and evaluating the plot only, not by looking at K2 outputs, as this may induce subjective manipulation!
    - Can also adjust lines 40-43 as outlining data points may be throwing one of the two curve fits
4. Rerun script
5. Record k2lo and k2hi

E.2: R Script for Binning Data and Performing Regression

```
remove(list=objects())
graphics.off()
library(plyr)
library(ggplot2)
library(reshape2)
Data <- read.csv("RData.csv", sep=",", header=F)
factor <- cut(Data[,1], breaks=55)
DataDF <- data.frame(Data1,factor)
names(DataDF)<-
c("Flow","Capacity","mA","Tai","Tao","h","RHai","RHao","Wai","Twi","Two","DeltaT","Month","Day",
"Hour","Min","Bin")
ggplot(DataDF,aes(x=Flow,y=Capacity,group=Bin)) +
 geom_boxplot() +
 ylab("Total Coil Cooling Capacity [W]") +
 xlab("Water Flow Rate [kg/s]") + ggtitle("Coil Cooling Plot Capacity")
quants=c(0.05,0.25,0.5,0.75,0.95)
factQuantArray=tapply(Data[,2],factor,FUN=quantile,probs=quants)
```

```
factQuantDF=adply(factQuantArray,1)
meltedDat<-melt(factQuantDF,id.vars='X1')
names(meltedDat)<-c("Flow","Quantile","Capacity")
ggplot(meltedDat,aes(x=Flow,y=Capacity,group=Quantile)) +
 geom_line(aes(linetype=Quantile,color=Quantile)) + theme_bw() +
 ylab("Total Coil Cooling Capacity [W]") +
 xlab("Water Flow Rate [kg/s]") + ggtitle("Coil Cooling Plot Capacity") +
 theme(axis.text.x = element_text(angle = 90, hjust = 1, vjust = 0.5))
labs <- levels(factQuantDF$X1)
Lower <- as.numeric( sub("\\((.+),.*", "\\1", labs) )
Upper <- as.numeric( sub("[^,]*,([^]]*)\\]", "\\1", labs) )
Middle <- (Lower+Upper)/2
factorLocs <- cbind(Lower, Middle, Upper)
factQuantDF=cbind(factorLocs,factQuantDF)
names(factQuantDF)[4] <- c('Flow Bin')
write.table(factQuantDF,file = paste(paste(quants,collapse="_"),'.csv',sep=''),
        col.names=NA,sep=",", quote=T, row.names=T)
plot(Data[,2]~Data[,1],
   xlab="Water Flow Rate [kg/s]",
   ylab="Total Coil Cooling Capacity [W]")
points(factQuantDF[1:15,5]~factQuantDF[1:15,2], col='blue', lty=1, lwd=5)
points(factQuantDF[1:15,9]~factQuantDF[1:15,2], col='orange', lty=1, lwd=5)
grid()
mwlo <-  c(0, factQuantDF[1:15,2])
Qlo <- c(0, factQuantDF[1:15,5])
mwhi <-  c(0, factQuantDF[1:15,2])
Qhi <- c(0, factQuantDF[1:15,9])

flo <- Qlo ~ K1lo*(1-exp(-K2lo*mwlo))
fhi <- Qhi ~ K1hi*(1-exp(-K2hi*mwhi))
fitlo <- nls(flo, start = list(K1lo=max(Qlo),K2lo=1))
```

```
fithi <- nls(fhi, start = list(K1hi=max(Qhi),K2hi=1))
coef(fitlo)
coef(fithi)
lines(mwlo,predict(fitlo), col='blue', lty=1, lwd=2)
lines(mwhi,predict(fithi), col='orange', lty=1, lwd=2)
```

E.3: Bar Bell Plots

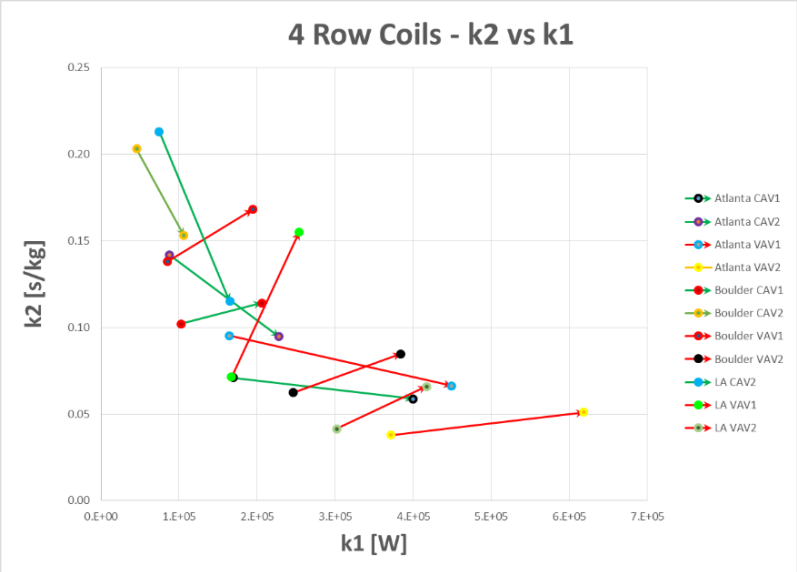

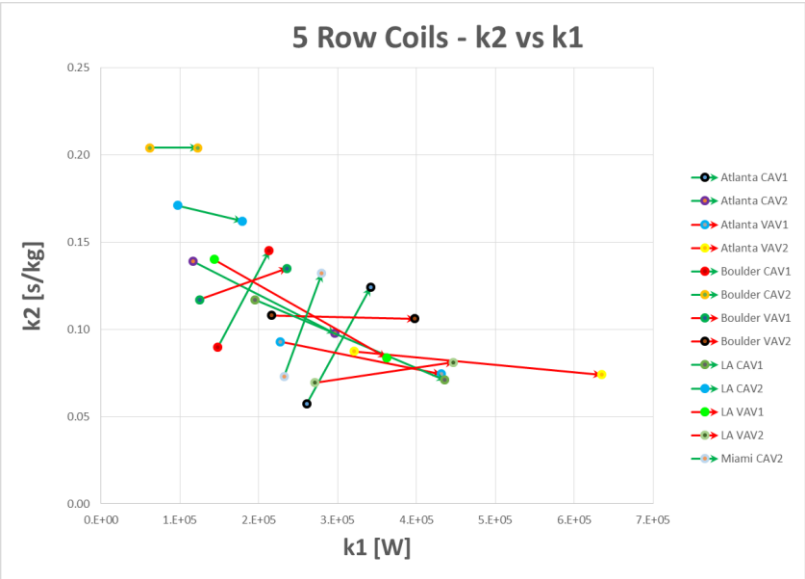

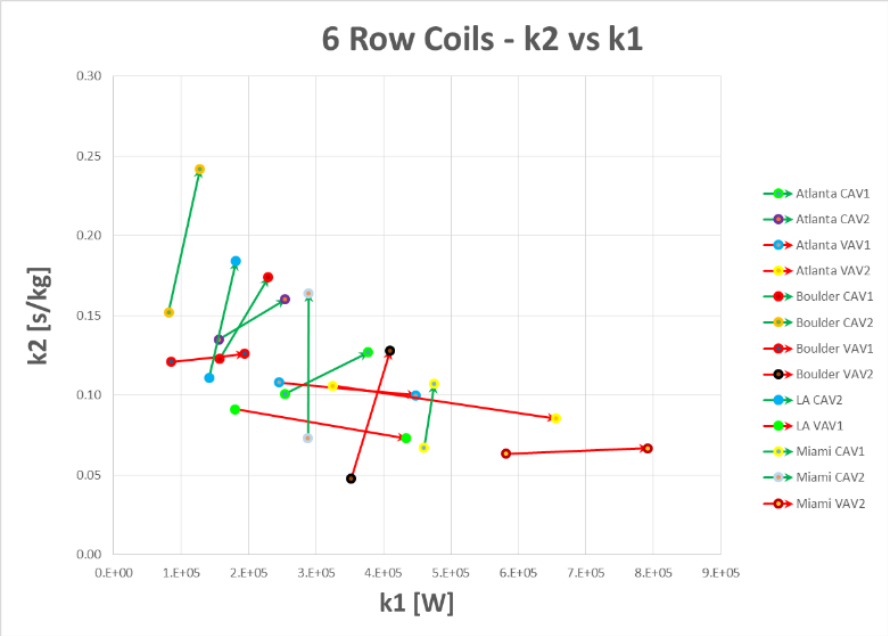
6 Row Coils - k2 vs k1
k2 [s/kg]
0.30
0.25
0.20
0.15
0.10
0.05
0.00
0.E+00
1.E+05
2.E+05
3.E+05
4.E+05
5.E+05
6.E+05
7.E+05
8.E+05
9.E+05
k1 [W]
Atlanta CAV1
Atlanta CAV2
Atlanta VAV1
Atlanta VAV2
Boulder CAV1
Boulder CAV2
Boulder VAV1
Boulder VAV2
LA CAV2
LA VAV1
Miami CAV1
Miami CAV2
Miami VAV2

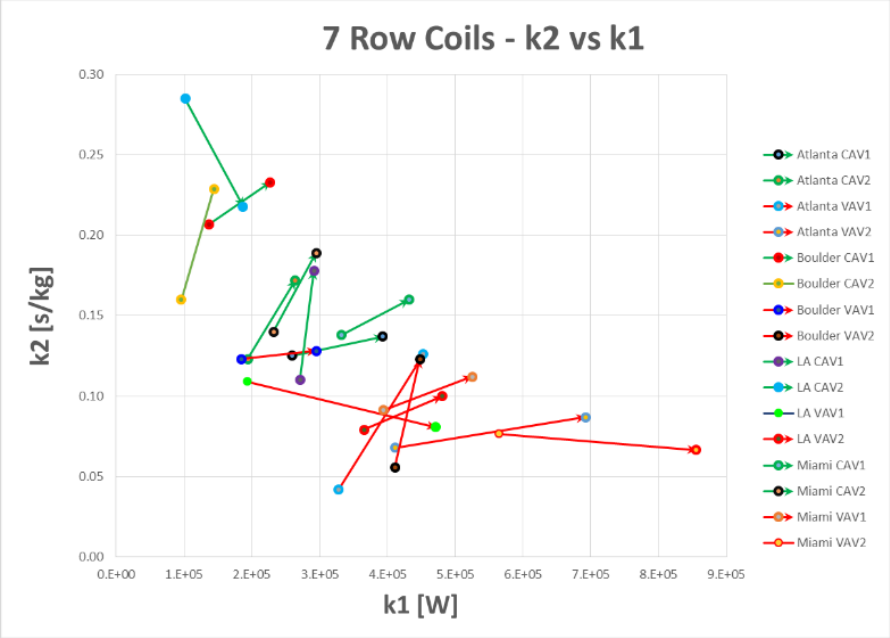
7 Row Coils - k2 vs k1
k2 [s/kg]
0.30
0.25
0.20
0.15
0.10
0.05
0.00
0.E+00
1.E+05
2.E+05
3.E+05
4.E+05
5.E+05
6.E+05
7.E+05
8.E+05
9.E+05
k1 [W]
Atlanta CAV1
Atlanta CAV2
Atlanta VAV1
Atlanta VAV2
Boulder CAV1
Boulder CAV2
Boulder VAV1
Boulder VAV2
LA CAV1
LA CAV2
LA VAV1
LA VAV2
Miami CAV1
Miami CAV2
Miami VAV1
Miami VAV2

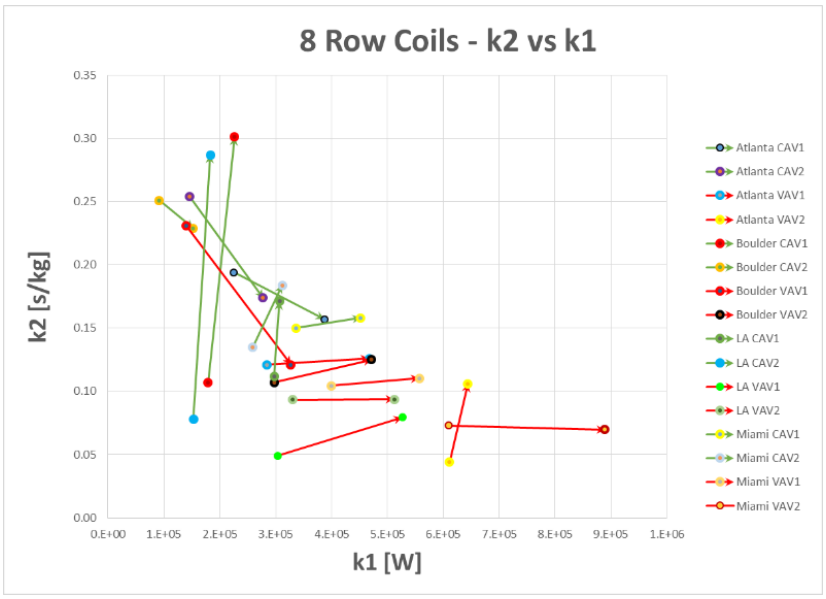
8 Row Coils - k2 vs k1
k2 [s/kg]
0.35
0.30
0.25
0.20
0.15
0.10
0.05
0.00
0.E+00
1.E+05
2.E+05
3.E+05
4.E+05
5.E+05
6.E+05
7.E+05
8.E+05
9.E+05
1.E+06
k1 [W]
Atlanta CAV1
Atlanta CAV2
Atlanta VAV1
Atlanta VAV2
Boulder CAV1
Boulder CAV2
Boulder VAV1
Boulder VAV2
LA CAV1
LA CAV2
LA VAV1
LA VAV2
Miami CAV1
Miami CAV2
Miami VAV1
Miami VAV2

Appendix F: Bin Plots for Select Systems

F.1: Atlanta CAV 1 5 Row Configuration

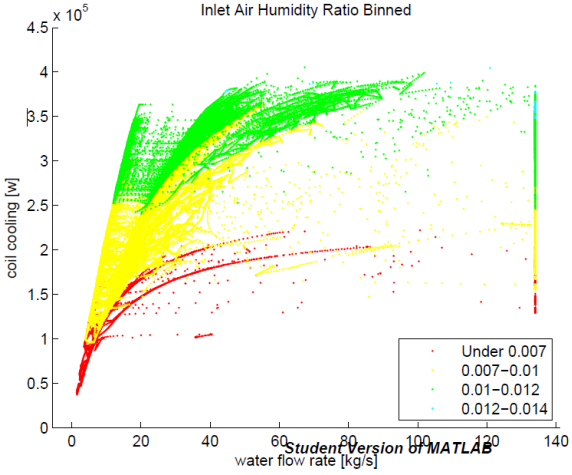

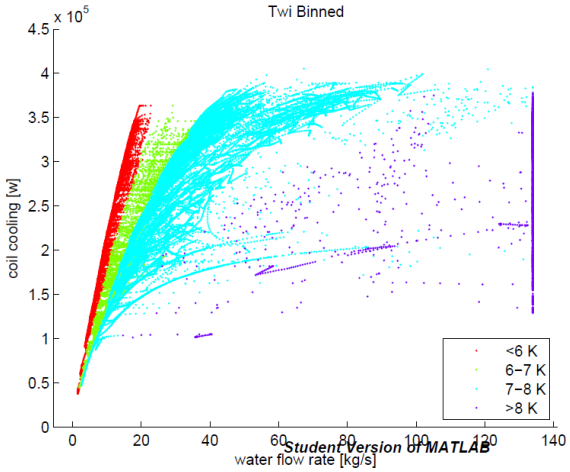

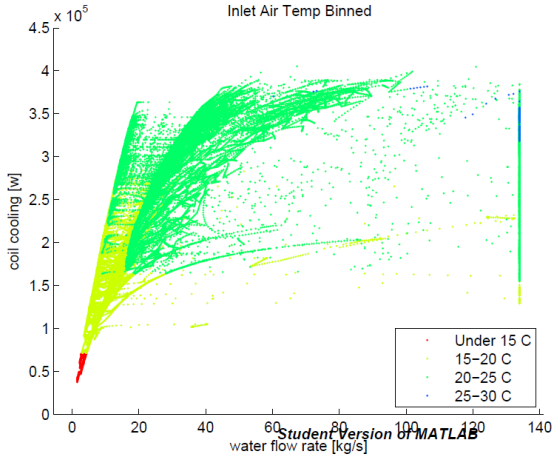

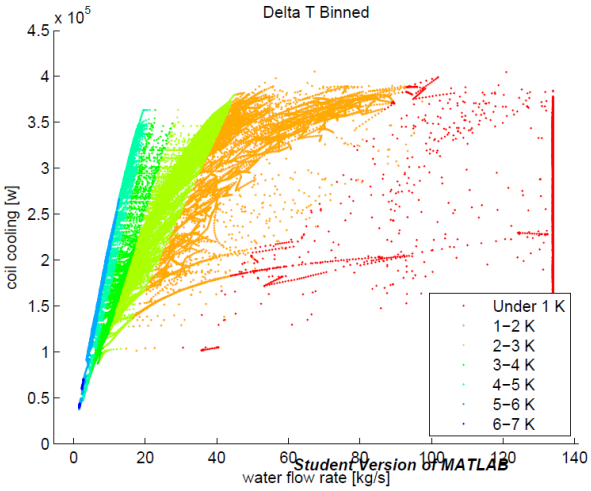

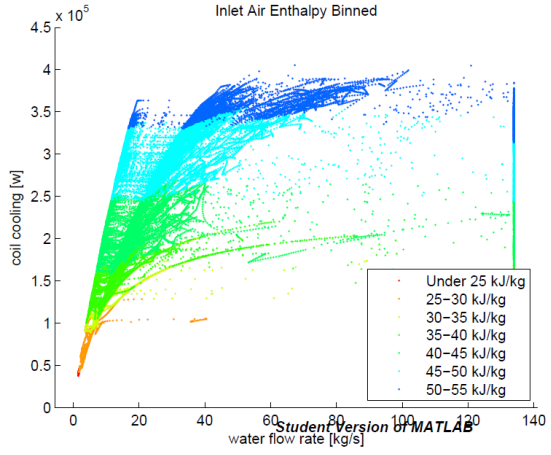

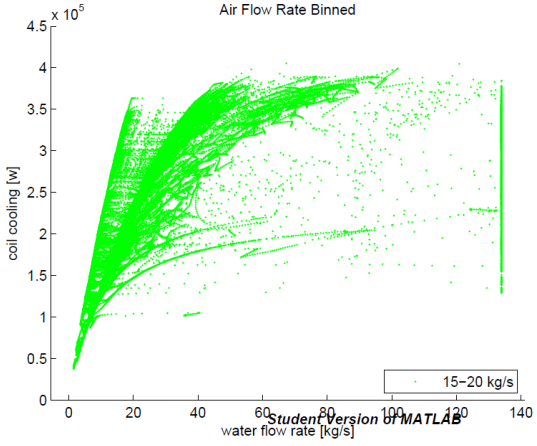

F.2: Atlanta VAV 1 6 Row Configuration

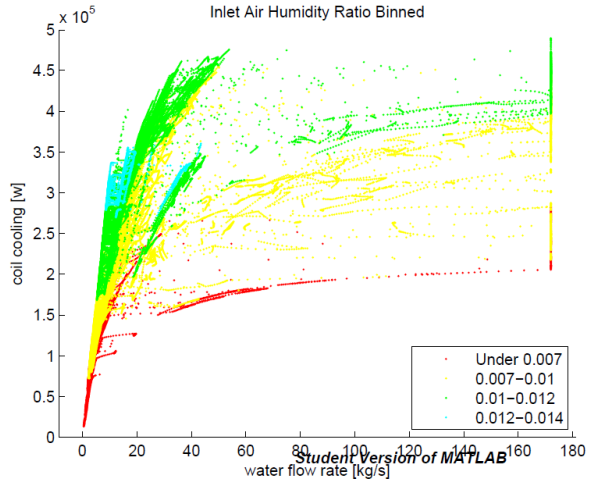

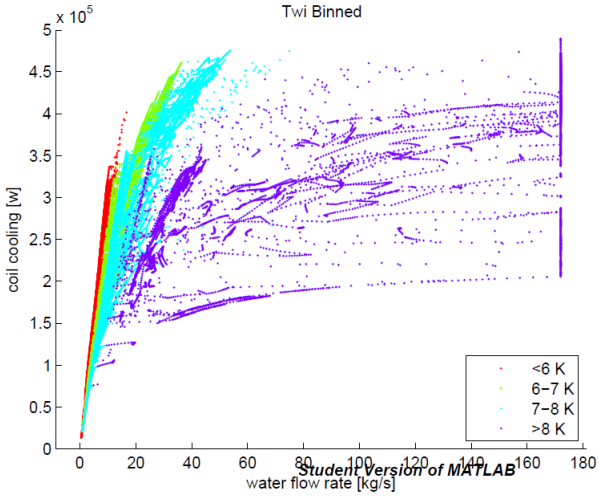

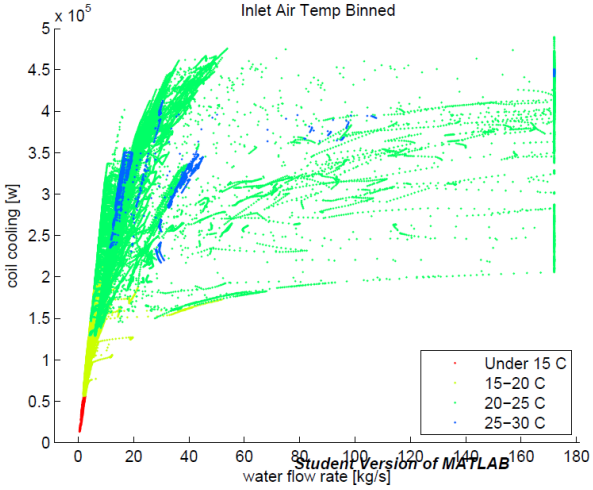

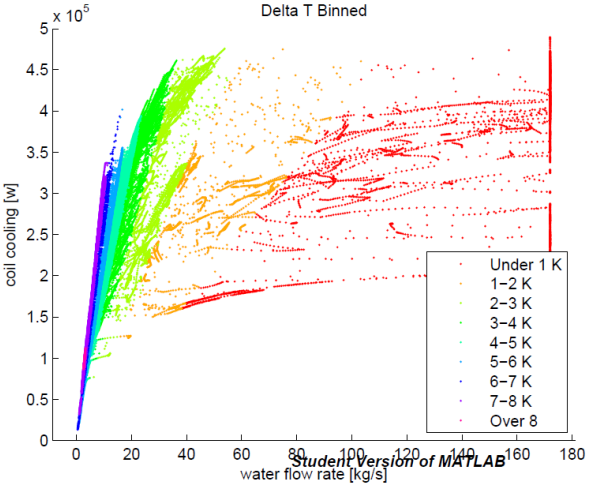

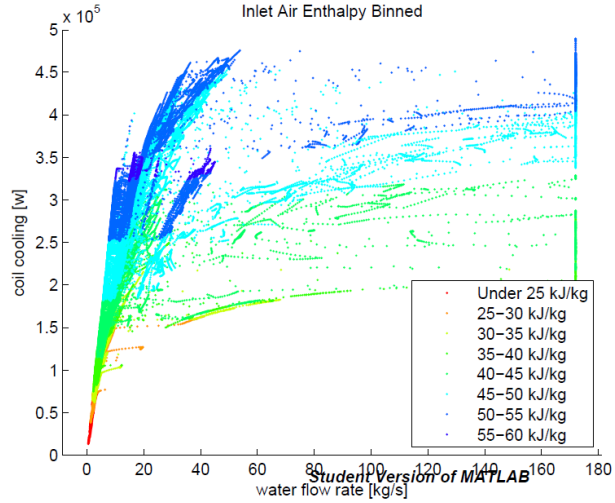

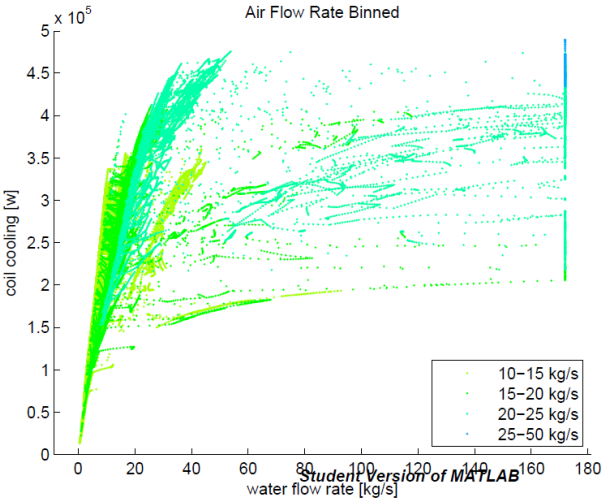

F.3: Boulder CAV 1 6 Row Configuration

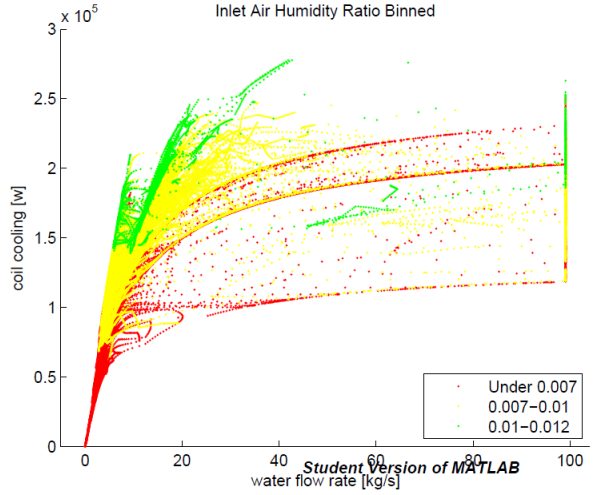

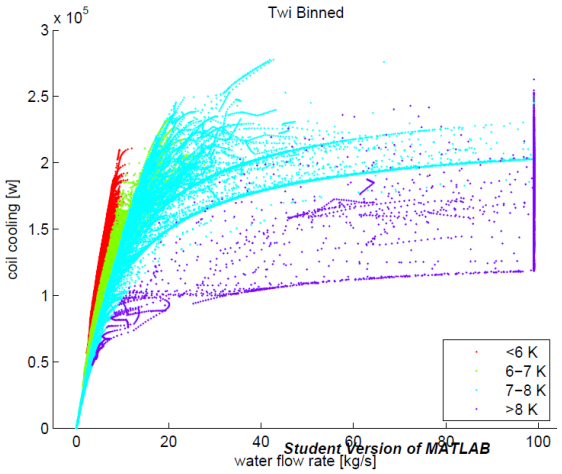

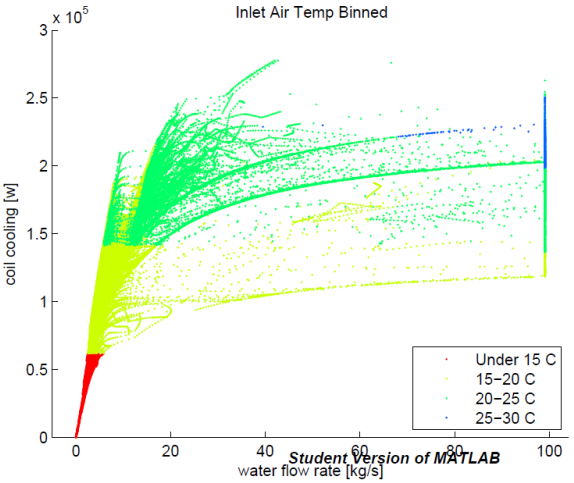

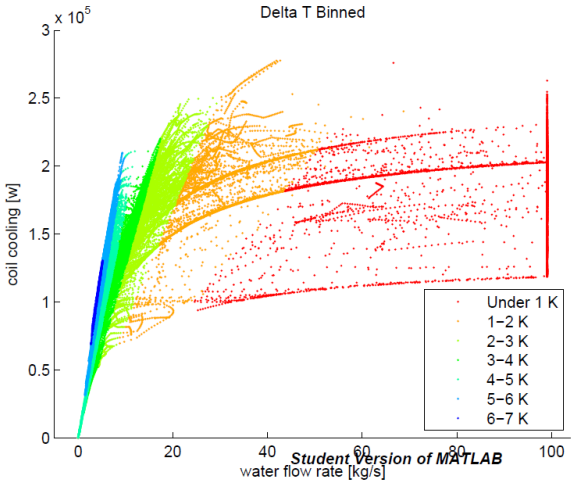

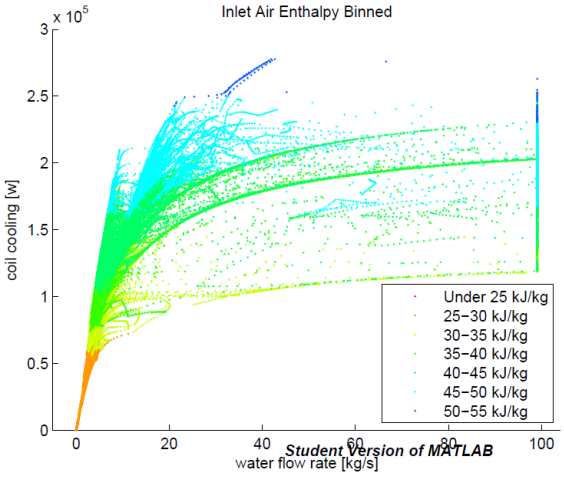

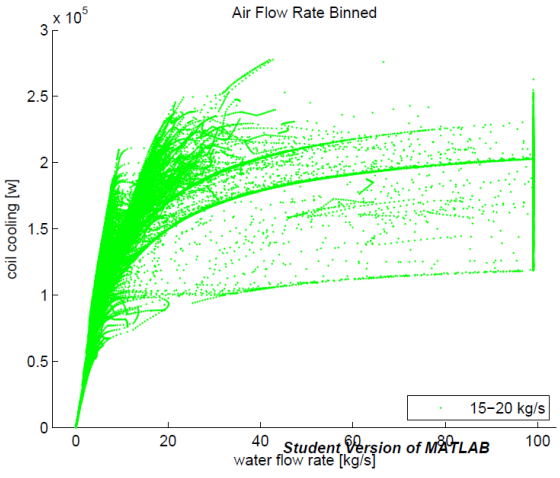

F.4: Boulder VAV 1 8 Row Configuration

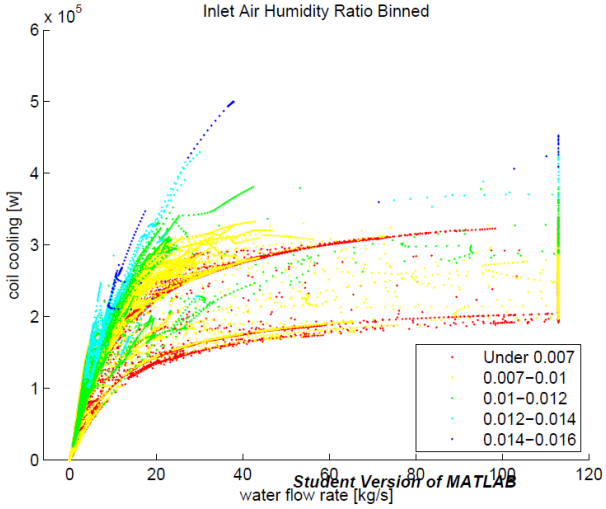

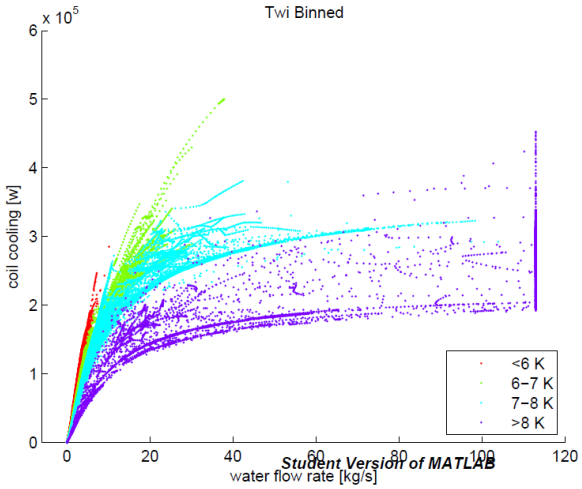

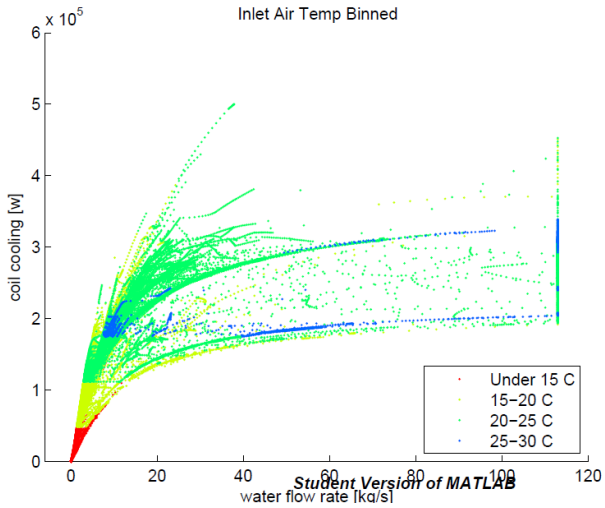

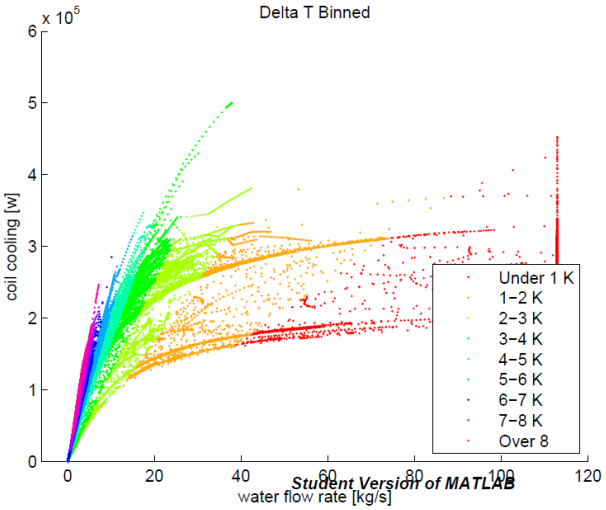

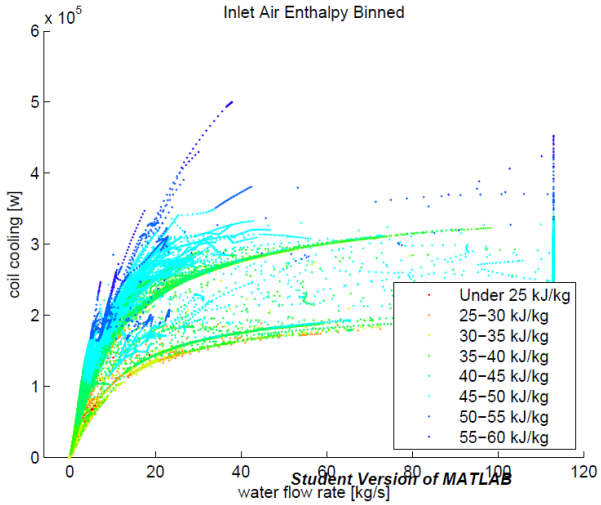

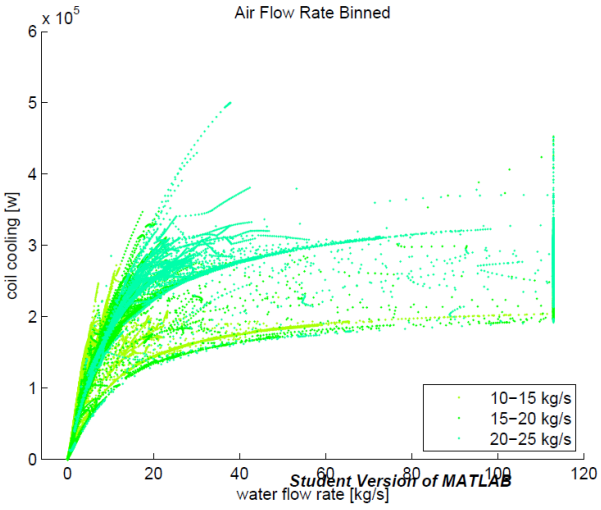

F.5: L.A. CAV 1 4 Row Configuration

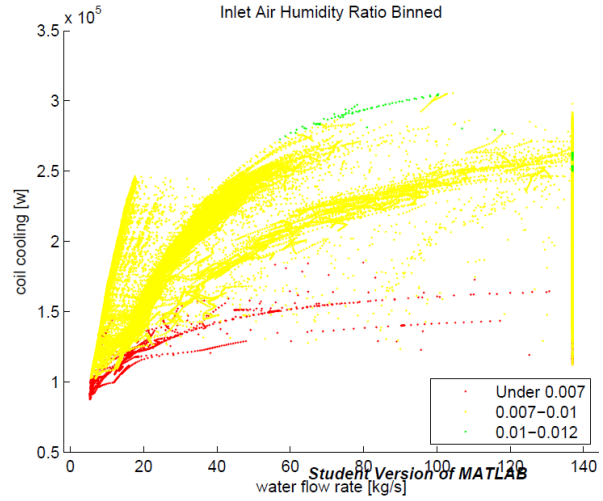

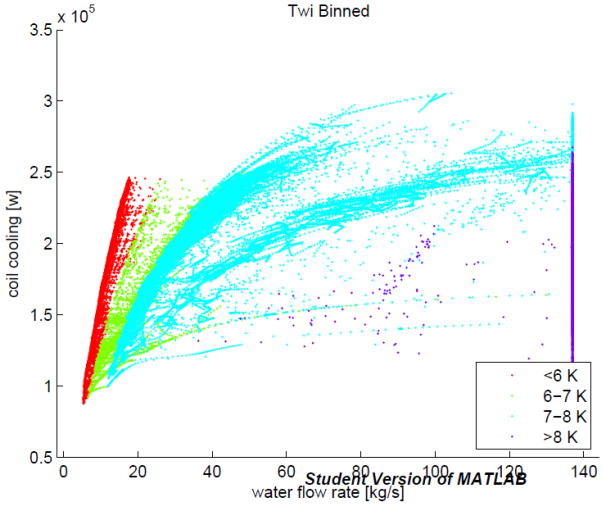

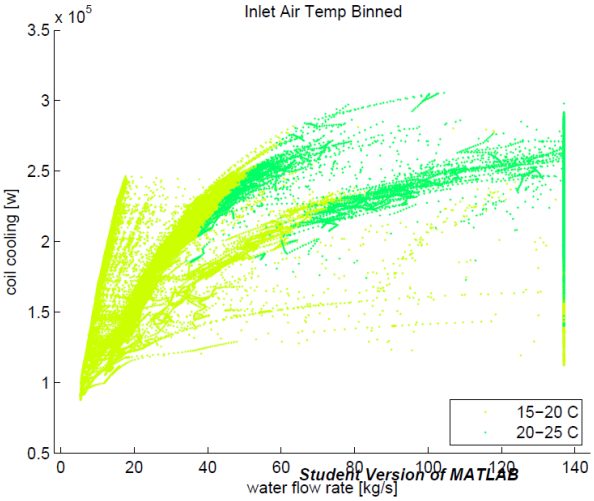

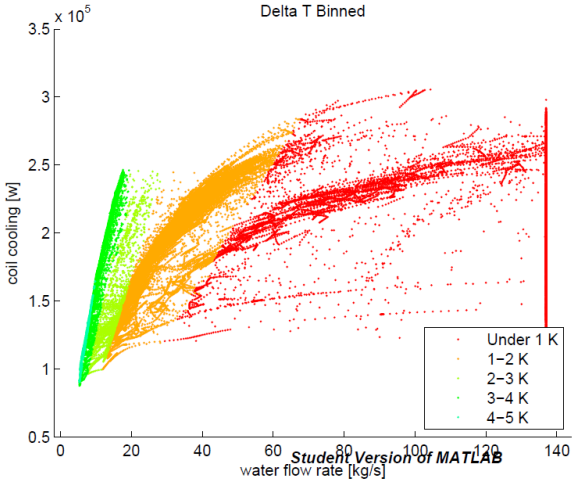

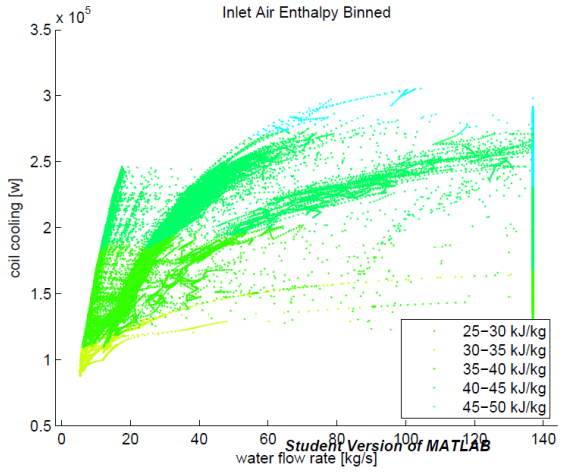

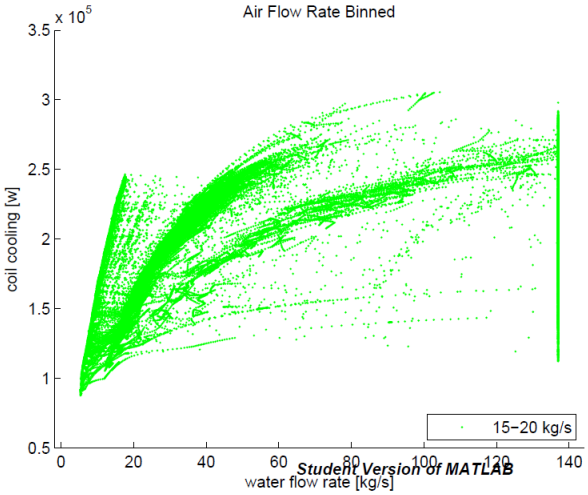

F.6: L.A. VAV 1 7 Row Configuration

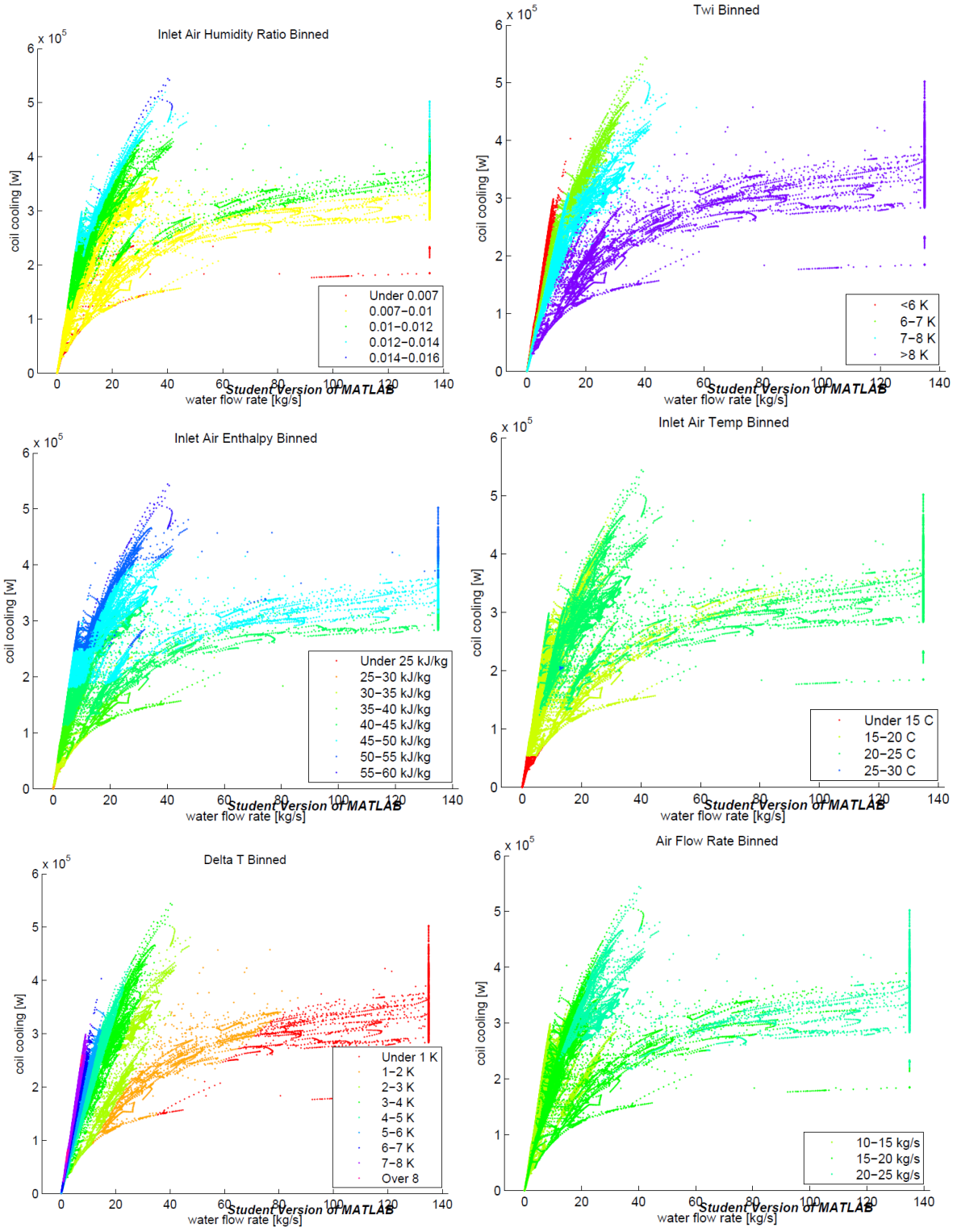

F.7: Miami CAV 1 4 Row Configuration

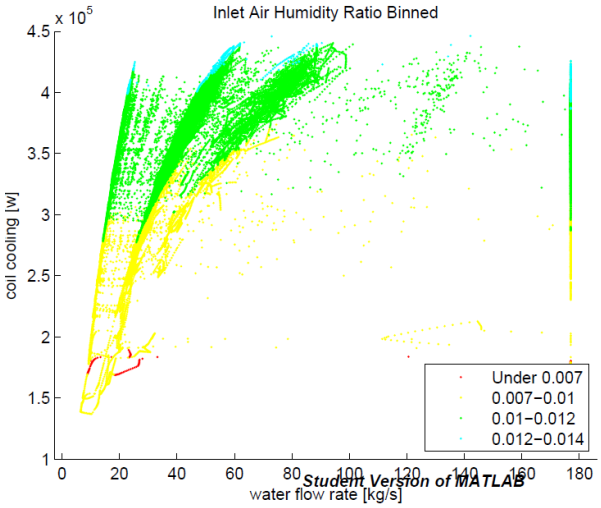

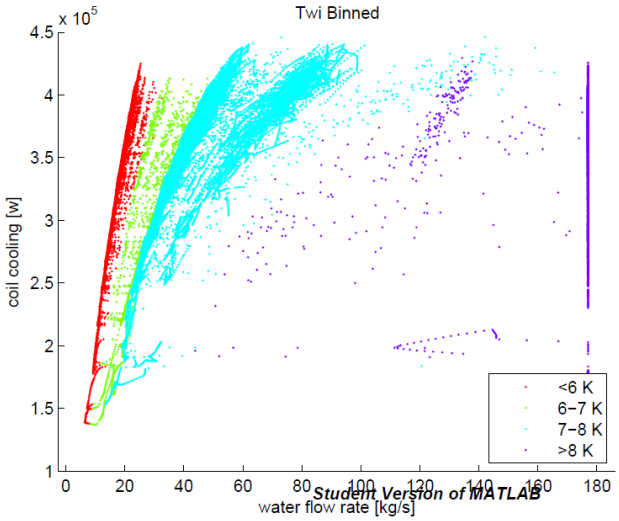

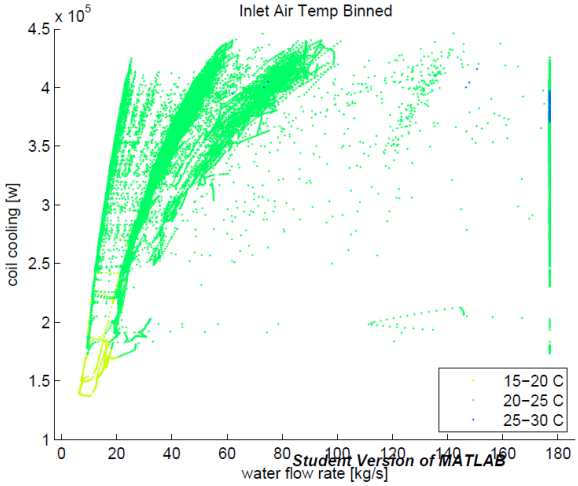

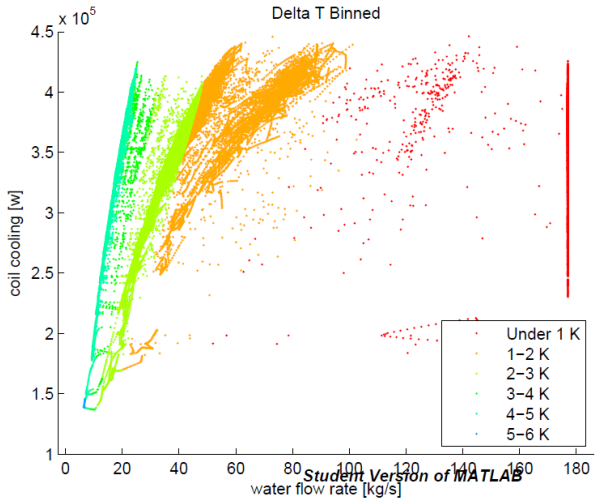

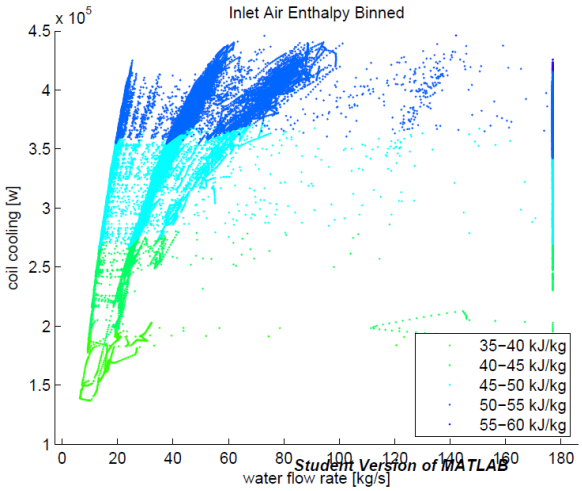

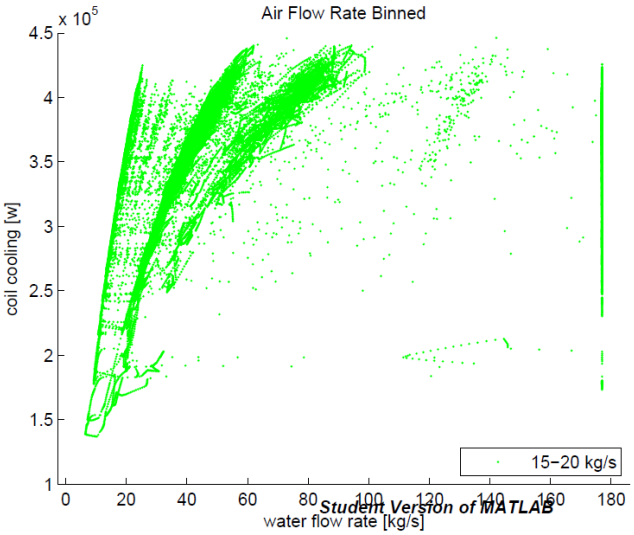

F.8: Miami VAV 1 7 Row Configuration

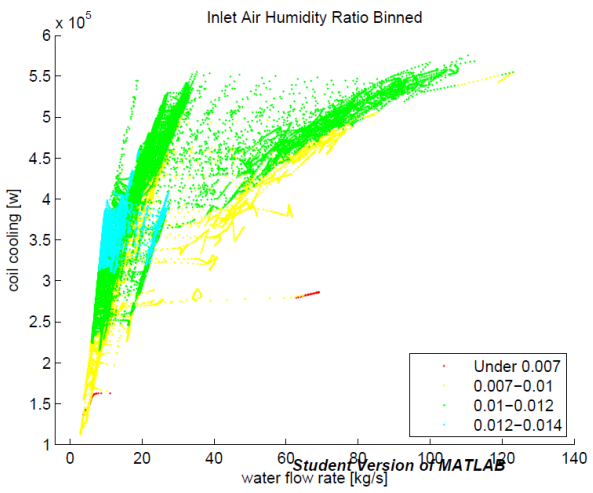

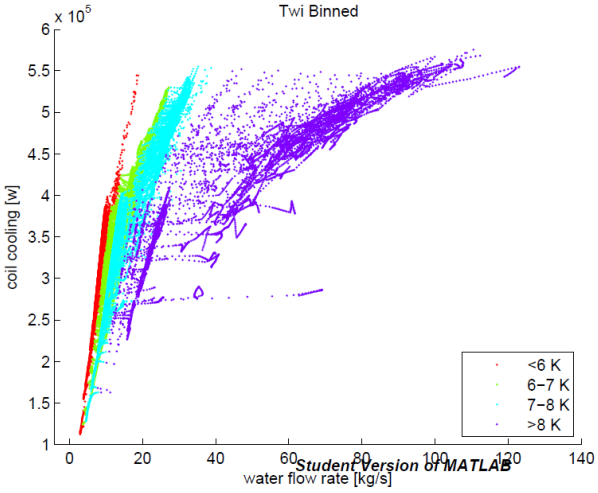

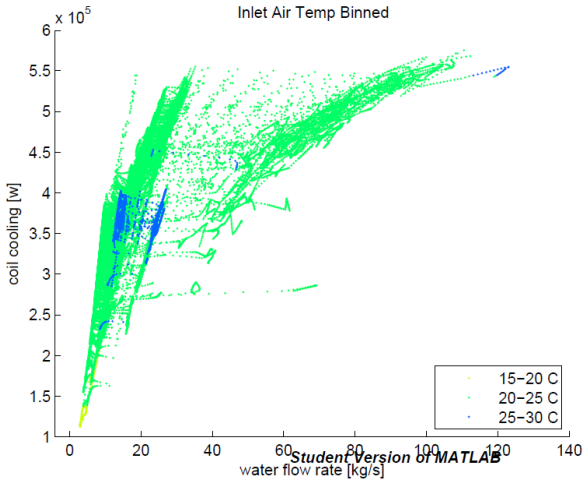

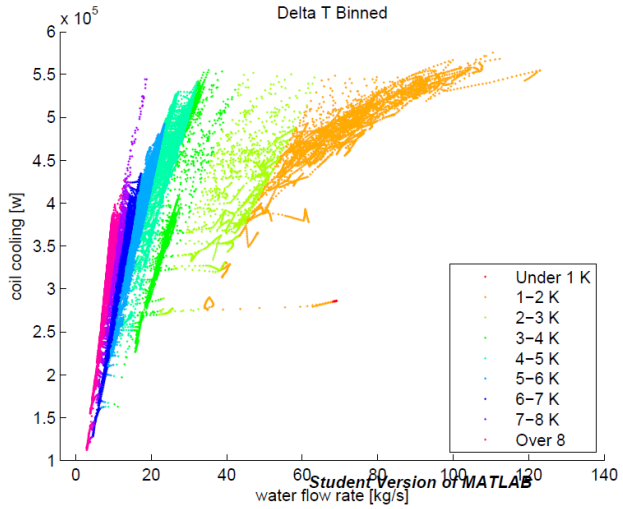

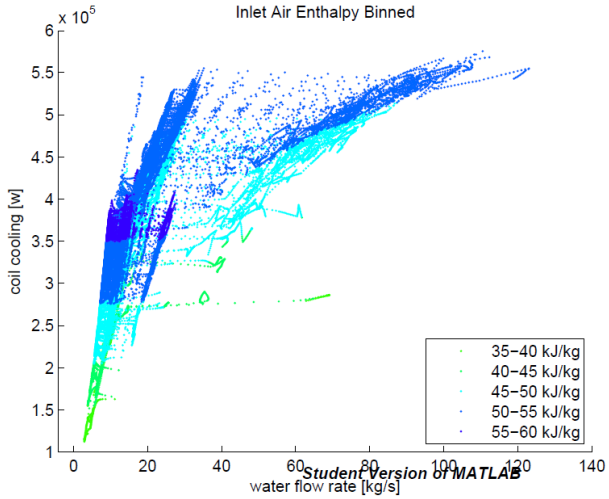

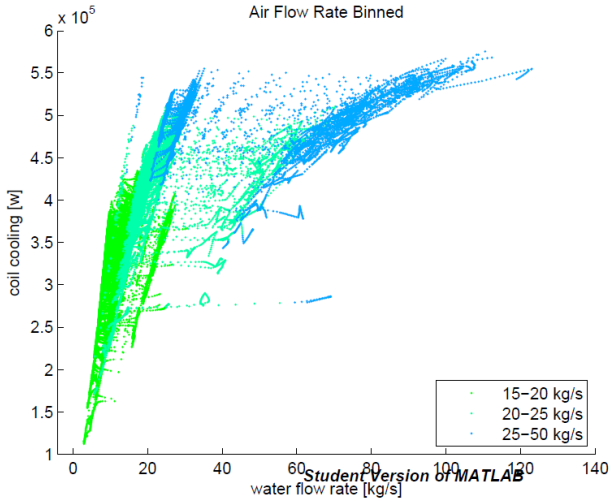

Appendix G: Technical Specification for Equivalent Coils on Market

KeepRite® REFRIGERATION

PRODUCT DATA & INSTALLATION

Bulletin K70-KWS-PDI-11
I064614

We are on the Internet
www.keepriterefrigeration.com

Water Cooling Coils

Type KWS Single Serpentine
Type KWH Half serpentine
Type KWD Double Serpentine

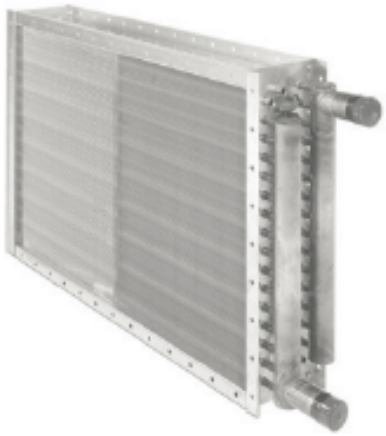

NOMENCLATURE

TYPE	MODEL	FACE DIMENSIONS
KW S D H	- 1 0 5 -	18 x 45

- Coil Type
- CIRCUITING:
  - S = Single Serpentine
  - D = Double Serpentine
  - H = Half Serpentine
- Fin Series (70, 80, 100 or 120) (100 shown)
- Rows Deep
- "W" Dimensions (inches)
- Nominal Tube Length (inches)

67°F, ENTERING AIR WET BULB, 45°F, ENTERING WATER, 53°F, LEAVING WATER

TABLE 4 - cont.

Face Velocity FPM		400		425		450		475		500		525		550		575		600	
NTL	Rows Deep	Tons per ft.²	Lvg. W.B. °F.	Tons per ft.²	Lvg. W.B. °F.	Tons per ft.²	Lvg. W.B. °F.	Tons per ft.²	Lvg. W.B. °F.	Tons per ft.²	Lvg. W.B. °F.	Tons per ft.²	Lvg. W.B. °F.	Tons per ft.²	Lvg. W.B. °F.	Tons per ft.²	Lvg. W.B. °F.	Tons per ft.²	Lvg. W.B. °F.
24"	4	1.14	56.3	.98	56.3	1.02	56.7	1.06	56.8	1.10	59.0	1.14	59.1	1.18	59.2	1.22	59.3	1.26	59.3
	6	1.32	54.3	1.38	54.6	1.43	54.9	1.49	55.0	1.55	55.2	1.60	55.4	1.66	55.6	1.71	55.7	1.77	55.9
	8	1.57	51.5	1.65	51.7	1.72	52.0	1.79	52.2	1.87	52.4	1.94	52.6	2.02	52.7	2.09	52.8	2.16	53.0
36"	4	1.05	57.2	1.10	57.4	1.14	57.6	1.18	57.8	1.22	58.0	1.27	58.1	1.31	58.2	1.35	58.4	1.40	58.4
	6	1.41	53.3	1.47	53.6	1.53	53.9	1.59	54.1	1.66	54.2	1.72	54.4	1.78	54.6	1.84	54.8	1.90	55.0
	8	1.64	50.7	1.72	50.9	1.80	51.1	1.88	51.3	1.96	51.5	2.04	51.7	2.13	51.8	2.21	51.9	2.29	52.0
48"	4	1.12	56.5	1.16	56.8	1.21	56.9	1.26	57.1	1.30	57.3	1.35	57.4	1.39	57.6	1.44	57.7	1.49	57.8
	6	1.46	52.8	1.53	53.0	1.59	53.3	1.65	53.6	1.72	53.7	1.78	53.9	1.85	54.1	1.91	54.2	1.98	54.3
	8	1.68	50.2	1.76	50.5	1.84	50.7	1.93	50.8	2.01	51.1	2.10	51.2	2.18	51.3	2.27	51.4	2.35	51.5
60"	4	1.16	56.1	1.20	56.4	1.25	56.6	1.30	56.7	1.34	57.0	1.39	57.1	1.44	57.3	1.49	57.4	1.54	57.5
	6	1.49	52.4	1.56	52.7	1.63	52.9	1.69	53.2	1.76	53.4	1.83	53.5	1.89	53.7	1.96	53.9	2.03	53.9
	8	1.71	49.8	1.79	50.2	1.88	50.3	1.97	50.4	2.05	50.7	2.13	50.9	2.22	51.0	2.30	51.1	2.38	51.3
72"	4	1.19	55.7	1.23	56.1	1.28	56.3	1.33	56.5	1.38	56.7	1.43	56.8	1.49	56.9	1.54	57.0	1.59	57.1
	6	1.52	52.1	1.59	52.3	1.66	52.6	1.72	52.9	1.79	53.1	1.86	53.3	1.92	53.5	1.99	53.6	2.06	53.7
	8	1.73	49.6	1.81	49.9	1.90	50.1	1.99	50.2	2.07	50.1	2.16	50.6	2.12*	51.6*	2.21*	51.9*	2.29*	52.0*
84"	4	1.21	55.5	1.26	55.8	1.31	56.0	1.36	56.2	1.41	56.4	1.46	56.6	1.52	56.6	1.57	56.8	1.62	56.9
	6	1.54	51.8	1.61	52.1	1.68	52.4	1.74	52.7	1.81	52.9	1.88	53.1	1.84*	54.1*	1.90*	54.3*	1.97*	54.4*
	8	1.74	49.5	1.82	49.8	1.83*	50.8*	1.91*	51.1*	1.99*	51.2*	2.07*	51.4*	2.15*	51.6*	2.23*	51.7*	2.31*	51.8*
96"	4	1.23	55.3	1.28	55.6	1.33	55.8	1.39	56.0	1.44	56.2	1.49	56.3	1.54	56.5	1.59	56.6	1.62	56.7
	6	1.55	51.7	1.62	52.0	1.60*	53.2*	1.66*	53.5*	1.73*	53.6*	1.79*	53.8*	1.86*	54.0*	1.92*	54.2*	1.99*	54.3*
	8	1.68*	50.2*	1.76*	50.5*	1.85*	50.6*	1.93*	50.8*	2.01*	51.1*	2.09*	51.3*	2.17*	51.4*	2.25*	51.6*	2.33*	51.7*
108"	4	1.24	55.2	1.29	55.5	1.34	55.8	1.40	55.9	1.45	56.1	1.40*	57.1*	1.45*	57.2*	1.50*	57.3*	1.55*	57.4*
	6	1.49*	52.4*	1.54*	52.9*	1.61*	53.1*	1.68*	53.3*	1.75*	53.4*	1.81*	53.7*	1.88*	53.8*	1.94*	54.0*	2.01*	54.1*
	8	1.70*	50.1*	1.78*	50.3*	1.86*	50.5*	1.94*	50.7*	2.03*	50.9*	2.11*	51.1*	2.19*	51.3*	2.27*	51.4*	2.35*	51.5*
120"	4	1.25	55.1	1.30	55.4	1.27*	56.4*	1.32*	56.6*	1.37*	56.7*	1.42*	56.9*	1.47*	51.0*	1.52*	57.1*	1.57*	57.2*
	6	1.50*	52.3*	1.56*	52.7*	1.63*	52.9*	1.69*	53.2*	1.76*	53.4*	1.82*	53.6*	1.89*	53.7*	1.95*	53.9*	2.02*	54.0*
	8	1.71*	49.8*	1.79*	50.2*	1.87*	50.4*	1.95*	50.6*	2.04*	50.8*	2.12*	51.0*	2.20*	51.1*	2.29*	51.2*	2.37*	51.4*

Appendix H: Application of the 4 Parameter Curve Fit

H.1: Finalized R Script for CV and FMPC Generation

```
#Cleaning up the workspace

remove(list=objects())

graphics.off()

library(plyr)

library(ggplot2)

library(reshape2)

#Bringing in the raw data

Data <- read.csv("RData.csv", sep=",", header=F)

names(Data)<-
c("Flow","Capacity","mA","Tai","Tao","h","RHai","RHao","Wai","Twi","Two","DeltaT","Month","Day",
"Hour","Min")

#Selection of applicable data to analyze. Line 15 Data$Flow maximum may need adjusting pending
the dataset

#in effort to crop out any data with valve wide open.  This limit would not need to be put in place
for

#real world application of this method

Index<-Data$Flow<=0.95*max(Data$Flow) & Data$Flow>0 & Data$Twi<=8

Data2<-Data[Index,]

Q<-Data2$Capacity

mW<-Data2$Flow

Twi<-Data2$Twi

#Applying the Curve Fit through non-linear regression

CurveFit<-nls(Q ~ (bo + b1*Twi)*(1 - exp(-(b2 + b3*Twi)*mW)),start = list(bo=max(Q),b1=-
10000,b2=.1,b3=.001))

#Assigning coefficients to outputs so to use in constant Twi curve generation below

bo<- coef(CurveFit)[1]

b1<- coef(CurveFit)[2]

b2<- coef(CurveFit)[3]

b3<- coef(CurveFit)[4]
```

```
#Drawing constant Twi prediction lines onto graph as sanity check. One can compare these to Matlab generated

#Twi bin plots

plot(mW,Q)

legend(0.8*max(mW),.6*max(Q),c("5C Twi","6C Twi","7C Twi","8C Twi"),lty=c(1,1,1,1),lwd=c(2,2,2,2),
    col=c("yellow","red","blue","purple"))

points(mW,(bo + b1*8)*(1 - exp(-(b2 + b3*8)*mW)),col='purple', lty=1, lwd=2)

points(mW,(bo + b1*7)*(1 - exp(-(b2 + b3*7)*mW)),col='blue', lty=1, lwd=2)

points(mW,(bo + b1*6)*(1 - exp(-(b2 + b3*6)*mW)),col='red', lty=1, lwd=2)

points(mW,(bo + b1*5)*(1 - exp(-(b2 + b3*5)*mW)),col='yellow', lty=1, lwd=2)

#Establishing the Range of values to look at for a particular sizing indicator temp maximum observed.

R<-0.2

#Identifying the number of degress of freedom for the curvefit that will be applied to each Twi bin

DOF<-4

#Setting up Twi of 6 as sizing indicator temp for Fraction of Predicted Maximum Capacity (FPMC)

k1.6<- (bo + b1*6)

Index.6<-Data2$Twi<=(6 + R) & Data2$Twi>=(6 - R)

ObservedMax.6<- max(Data2$Capacity[Index.6])

FPMC.6<-ObservedMax.6/k1.6

#Setting up Twi of 6.5 as sizing indicator temp for FPMC

k1.6.5<- (bo + b1*6.5)

Index.6.5<-Data2$Twi<=(6.5 + R) & Data2$Twi>=(6.5 - R)

ObservedMax.6.5<- max(Data2$Capacity[Index.6.5])

FPMC.6.5<-ObservedMax.6.5/k1.6.5

#Setting up Twi of 7 as sizing indicator temp for FPMC

k1.7<- (bo + b1*7)

Index.7<-Data2$Twi<=(7 + R) & Data2$Twi>=(7 - R)

ObservedMax.7<- max(Data2$Capacity[Index.7])
```

```
FPMC.7<-ObservedMax.7/k1.7
#Setting up Twi of 7.5 as sizing indicator temp for FPMC
k1.7.5<- (bo + b1*7.5)
Index.7.5<-Data2$Twi<=(7.5 + R) & Data2$Twi>=(7.5 - R)
ObservedMax.7.5<- max(Data2$Capacity[Index.7.5])
FPMC.7.5<-ObservedMax.7.5/k1.7.5
#Setting up Twi of 8 as sizing indicator temp for FPMC
k1.8<- (bo + b1*8)
Index.8<-Data2$Twi<=(8 + R) & Data2$Twi>=(8 - R)
ObservedMax.8<- max(Data2$Capacity[Index.8])
FPMC.8<-ObservedMax.8/k1.8
#The below measure is intended to be a "goodness of fit".
#Coefficient of Variation (CV) can be read as average deviation in data from
#predicted CurveFit as a percentage of maximum the mean capacity
CV<-sqrt(deviance(CurveFit)/(nrow(Data2)-DOF))*100/(mean(Q))
#Percentage of time data analyszed was at min mA
ind<-Data2$mA<=min(Data2$mA)
mAvariance<-nrow(Data2[ind,])/nrow(Data2)
#Outputs to document for each RData set
Outputs<-
c(FPMC.6,FPMC.6.5,FPMC.7,FPMC.7.5,FPMC.8,CV,mean(Q),max(mW),min(Data2$mA)/max(Data2$
mA),mAvariance)
OutputsDF<-matrix( Outputs, ncol=10, nrow=1)
FPMC.6
FPMC.6.5
FPMC.7
FPMC.7.5
FPMC.8
CV
```

Appendix I: Climate Specific CAV/VAV Prediction Tools

I.1: Boulder

```
#Cleaning up the workspace

remove(list=objects())

graphics.off()

library(plyr)

library(ggplot2)

library(reshape2)

#Bringing in the raw data

Data <- read.csv("RData.csv", sep=",", header=F)

names(Data)<-
c("Flow","Capacity","mA","Tai","Tao","h","RHai","RHao","Wai","Twi","Two","DeltaT","Month","Day",
"Hour","Min")

#Selection of applicable data to analyze. Line 15 Data$Flow maximum may need adjusting pending
the dataset

#in effort to crop out any data with valve wide open.  This limit would not need to be put in place
for

#real world application of this method

Index<-Data$Flow<=0.75*max(Data$Flow) & Data$Flow>0 & Data$Twi<=8

Data2<-Data[Index,]

Q<-Data2$Capacity

mW<-Data2$Flow

Twi<-Data2$Twi

#Applying the Curve Fit through non-linear regression

CurveFit<-nls(Q ~ (bo + b1*Twi)*(1 - exp(-(b2 + b3*Twi)*mW)),start = list(bo=2*max(Q),b1=-
0.1*max(Q),b2=.1,b3=.001))

#Assigning coefficients to outputs so to use in constant Twi curve generation below

bo<- coef(CurveFit)[1]

b1<- coef(CurveFit)[2]

b2<- coef(CurveFit)[3]

b3<- coef(CurveFit)[4]
```

```
#Drawing constant Twi prediction lines onto graph as sanity check. One can compare these to Matlab generated

#Twi bin plots

plot(mW,Q)

legend(0.8*max(mW),.6*max(Q),c("5C Twi","6C Twi","7C Twi","8C Twi"),lty=c(1,1,1,1),lwd=c(2,2,2,2),

    col=c("yellow","red","blue","purple"))

points(mW,(bo + b1*8)*(1 - exp(-(b2 + b3*8)*mW)),col='purple', lty=1, lwd=2)

points(mW,(bo + b1*7)*(1 - exp(-(b2 + b3*7)*mW)),col='blue', lty=1, lwd=2)

points(mW,(bo + b1*6)*(1 - exp(-(b2 + b3*6)*mW)),col='red', lty=1, lwd=2)

points(mW,(bo + b1*5)*(1 - exp(-(b2 + b3*5)*mW)),col='yellow', lty=1, lwd=2)

#Establishing the Range of values to look at for a particular sizing indicator temp maximum observed.

R<-0.2

#Identifying the number of degress of freedom for the curvefit that will be applied to each Twi bin

DOF<-4

#Setting up Twi of 6.5 as sizing indicator temp for FPMC

k1.6.5<- (bo + b1*6.5)

Index.6.5<-Data2$Twi<=(6.5 + R) & Data2$Twi>=(6.5 - R)

ObservedMax.6.5<- max(Data2$Capacity[Index.6.5])

FPMC.6.5<-ObservedMax.6.5/k1.6.5

#The below measure is intended to be a "goodness of fit".

#Coefficient of Variation (CV) can be read as average deviation in data from

#predicted CurveFit as a percentage of maximum the mean capacity

CV<-sqrt(deviance(CurveFit)/(nrow(Data2)-DOF))*100/(mean(Q))

#Outputs to document for each RData set

FPMC.6.5

CV

#Determination based of pre-established, climate dependent Cv to FPMC relationship

CV.CAV <- 14.89*FPMC.6.5 + 0.404

CV.VAV <- 14.23*FPMC.6.5 + 7.58
```

```
#VAV predictions will register as TRUE, CAV predictions will register as FALSE

abs(CV.VAV - CV)<abs(CV.CAV - CV)

#Accounting for b1 inaccurately being a positive value. It is allowed to be positive as long as

#crossover of constant Twi does not occur in the mW flow range plotted

#True mean to trust previous distinction, False means a VAV classification

((bo + b1*8)*(1 - exp(-(b2 + b3*8)*max(mW))))<=((bo + b1*5)*(1 - exp(-(b2 + b3*5)*max(mW))))
```

I.2: Atlanta

```
#Cleaning up the workspace

remove(list=objects())

graphics.off()

library(plyr)

library(ggplot2)

library(reshape2)

#Bringing in the raw data

Data <- read.csv("RData.csv", sep=",", header=F)

names(Data)<-
c("Flow","Capacity","mA","Tai","Tao","h","RHai","RHao","Wai","Twi","Two","DeltaT","Month","Day",
"Hour","Min")

#Selection of applicable data to analyze. Line 15 Data$Flow maximum may need adjusting pending
the dataset

#in effort to crop out any data with valve wide open.  This limit would not need to be put in place
for

#real world application of this method

Index<-Data$Flow<=0.75*max(Data$Flow) & Data$Flow>0 & Data$Twi<=8

Data2<-Data[Index,]

Q<-Data2$Capacity

mW<-Data2$Flow

Twi<-Data2$Twi

#Applying the Curve Fit through non-linear regression
```

```
CurveFit<-nls(Q ~ (bo + (b1)*Twi)*(1 - exp(-(b2 + b3*Twi)*mW)),
        start = list(bo=2*max(Q),b1=-0.1*max(Q),b2=.1,b3=.001))
#Assigning coefficients to outputs so to use in constant Twi curve generation below
bo<- coef(CurveFit)[1]
b1<- coef(CurveFit)[2]
b2<- coef(CurveFit)[3]
b3<- coef(CurveFit)[4]
#Drawing constant Twi prediction lines onto graph as sanity check. One can compare these to
Matlab generated
#Twi bin plots
plot(mW,Q)
legend(0.8*max(mW),.6*max(Q),c("5C Twi","6C Twi","7C Twi","8C
Twi"),lty=c(1,1,1,1),lwd=c(2,2,2,2),
     col=c("yellow","red","blue","purple"))
points(mW,(bo + b1*8)*(1 - exp(-(b2 + b3*8)*mW)),col='purple', lty=1, lwd=2)
points(mW,(bo + b1*7)*(1 - exp(-(b2 + b3*7)*mW)),col='blue', lty=1, lwd=2)
points(mW,(bo + b1*6)*(1 - exp(-(b2 + b3*6)*mW)),col='red', lty=1, lwd=2)
points(mW,(bo + b1*5)*(1 - exp(-(b2 + b3*5)*mW)),col='yellow', lty=1, lwd=2)
#Establishing the Range of values to look at for a particular sizing indicator temp maximum
observed.
R<-0.2
#Identifying the number of degress of freedom for the curvefit that will be applied to each Twi bin
DOF<-4
#Setting up Twi of 6.5 as sizing indicator temp for FPMC
k1.6.5<- (bo + b1*6.5)
Index.6.5<-Data2$Twi<=(6.5 + R) & Data2$Twi>=(6.5 - R)
ObservedMax.6.5<- max(Data2$Capacity[Index.6.5])
FPMC.6.5<-ObservedMax.6.5/k1.6.5
#The below measure is intended to be a "goodness of fit".
#Coefficient of Variation (CV) can be read as average deviation in data from
#predicted CurveFit as a percentage of maximum the mean capacity
```

```
CV<-sqrt(deviance(CurveFit)/(nrow(Data2)-DOF))*100/(mean(Q))

#Outputs to document for each RData set

FPMC.6.5

CV

#Determination based of pre-established, climate dependent Cv to FPMC relationship

CV.CAV <- 9.26*FPMC.6.5 - 0.026

CV.VAV <- 11.55*FPMC.6.5 + 4.14

#VAV predictions will register as TRUE, CAV predictions will register as FALSE

abs(CV.VAV - CV)<abs(CV.CAV - CV)

#Accounting for b1 inaccurately being a positive value. It is allowed to be positive as long as

#crossover of constant Twi does not occur in the mW flow range plotted

#True mean to trust previous distinction, False means a VAV classification

((bo + b1*8)*(1 - exp(-(b2 + b3*8)*max(mW))))<=((bo + b1*5)*(1 - exp(-(b2 + b3*5)*max(mW))))
```

I.3: Miami

```
#Cleaning up the workspace

remove(list=objects())

graphics.off()

library(plyr)

library(ggplot2)

library(reshape2)

#Bringing in the raw data

Data <- read.csv("RData.csv", sep=",", header=F)

names(Data)<-
c("Flow","Capacity","mA","Tai","Tao","h","RHai","RHao","Wai","Twi","Two","DeltaT","Month","Day",
"Hour","Min")

#Selection of applicable data to analyze. Line 15 Data$Flow maximum may need adjusting pending
the dataset

#in effort to crop out any data with valve wide open.  This limit would not need to be put in place
for

#real world application of this method
```

```
Index<-Data$Flow<=0.75*max(Data$Flow) & Data$Flow>0 & Data$Twi<=8

Data2<-Data[Index,]

Q<-Data2$Capacity

mW<-Data2$Flow

Twi<-Data2$Twi

#Applying the Curve Fit through non-linear regression

CurveFit<-nls(Q ~ (bo + b1*Twi)*(1 - exp(-(b2 + b3*Twi)*mW)),start = list(bo=2*max(Q),b1=-
.1*max(Q),b2=.1,b3=.001))

#Assigning coefficients to outputs so to use in constant Twi curve generation below

bo<- coef(CurveFit)[1]

b1<- coef(CurveFit)[2]

b2<- coef(CurveFit)[3]

b3<- coef(CurveFit)[4]

#Drawing constant Twi prediction lines onto graph as sanity check. One can compare these to
Matlab generated

#Twi bin plots

plot(mW,Q)

legend(0.8*max(mW),.6*max(Q),c("5C Twi","6C Twi","7C Twi","8C
Twi"),lty=c(1,1,1,1),lwd=c(2,2,2,2),

    col=c("yellow","red","blue","purple"))

points(mW,(bo + b1*8)*(1 - exp(-(b2 + b3*8)*mW)),col='purple', lty=1, lwd=2)

points(mW,(bo + b1*7)*(1 - exp(-(b2 + b3*7)*mW)),col='blue', lty=1, lwd=2)

points(mW,(bo + b1*6)*(1 - exp(-(b2 + b3*6)*mW)),col='red', lty=1, lwd=2)

points(mW,(bo + b1*5)*(1 - exp(-(b2 + b3*5)*mW)),col='yellow', lty=1, lwd=2)

#Establishing the Range of values to look at for a particular sizing indicator temp maximum
observed.

R<-0.2

#Identifying the number of degress of freedom for the curvefit that will be applied to each Twi bin

DOF<-4

#Setting up Twi of 6.5 as sizing indicator temp for FPMC

k1.6.5<- (bo + b1*6.5)
```

```
Index.6.5<-Data2$Twi<=(6.5 + R) & Data2$Twi>=(6.5 - R)
ObservedMax.6.5<- max(Data2$Capacity[Index.6.5])
FPMC.6.5<-ObservedMax.6.5/k1.6.5
#The below measure is intended to be a "goodness of fit".
#Coefficient of Variation (CV) can be read as average deviation in data from
#predicted CurveFit as a percentage of maximum the mean capacity
CV<-sqrt(deviance(CurveFit)/(nrow(Data2)-DOF))*100/(mean(Q))
#Outputs to document for each RData set
FPMC.6.5
CV
#Determination based of pre-established, climate dependent Cv to FPMC relationship
CV.CAV <- 3.05*FPMC.6.5 + 0.418
CV.VAV <- 2.79*FPMC.6.5 + 4.33
#VAV predictions will register as TRUE, CAV predictions will register as FALSE
abs(CV.VAV - CV)<abs(CV.CAV - CV)
#Accounting for b1 inaccurately being a positive value. It is allowed to be positive as long as
#crossover of constant Twi does not occur in the mW flow range plotted
#True mean to trust previous distinction, False means a VAV classification
((bo + b1*8)*(1 - exp(-(b2 + b3*8)*max(mW))))<=((bo + b1*5)*(1 - exp(-(b2 + b3*5)*max(mW))))
```

I.4: L.A.

```
#Cleaning up the workspace
remove(list=objects())
graphics.off()
library(plyr)
library(ggplot2)
library(reshape2)
#Bringing in the raw data
Data <- read.csv("RData.csv", sep=",", header=F)
```

```
names(Data)<-
c("Flow","Capacity","mA","Tai","Tao","h","RHai","RHao","Wai","Twi","Two","DeltaT","Month","Day",
"Hour","Min")

#Selection of applicable data to analyze. Line 15 Data$Flow maximum may need adjusting pending
the dataset

#in effort to crop out any data with valve wide open.  This limit would not need to be put in place
for

#real world application of this method

Index<-Data$Flow<=0.75*max(Data$Flow) & Data$Flow>0 & Data$Twi<=8

Data2<-Data[Index,]

Q<-Data2$Capacity

mW<-Data2$Flow

Twi<-Data2$Twi

#Applying the Curve Fit through non-linear regression

CurveFit<-nls(Q ~ (bo + b1*Twi)*(1 - exp(-(b2 + b3*Twi)*mW)),start = list(bo=2*max(Q),b1=-
0.1*max(Q),b2=.1,b3=.001))

#Assigning coefficients to outputs so to use in constant Twi curve generation below

bo<- coef(CurveFit)[1]

b1<- coef(CurveFit)[2]

b2<- coef(CurveFit)[3]

b3<- coef(CurveFit)[4]

#Drawing constant Twi prediction lines onto graph as sanity check. One can compare these to
Matlab generated

#Twi bin plots

plot(mW,Q)

legend(0.8*max(mW),.6*max(Q),c("5C Twi","6C Twi","7C Twi","8C
Twi"),lty=c(1,1,1,1),lwd=c(2,2,2,2),

    col=c("yellow","red","blue","purple"))

points(mW,(bo + b1*8)*(1 - exp(-(b2 + b3*8)*mW)),col='purple', lty=1, lwd=2)

points(mW,(bo + b1*7)*(1 - exp(-(b2 + b3*7)*mW)),col='blue', lty=1, lwd=2)

points(mW,(bo + b1*6)*(1 - exp(-(b2 + b3*6)*mW)),col='red', lty=1, lwd=2)

points(mW,(bo + b1*5)*(1 - exp(-(b2 + b3*5)*mW)),col='yellow', lty=1, lwd=2)
```

```
#Establishing the Range of values to look at for a particular sizing indicator temp maximum observed.
R<-0.2
#Identifying the number of degress of freedom for the curvefit that will be applied to each Twi bin
DOF<-4
#Setting up Twi of 6.5 as sizing indicator temp for FPMC
k1.6.5<- (bo + b1*6.5)
Index.6.5<-Data2$Twi<=(6.5 + R) & Data2$Twi>=(6.5 - R)
ObservedMax.6.5<- max(Data2$Capacity[Index.6.5])
FPMC.6.5<-ObservedMax.6.5/k1.6.5
#The below measure is intended to be a "goodness of fit".
#Coefficient of Variation (CV) can be read as average deviation in data from
#predicted CurveFit as a percentage of maximum the mean capacity
CV<-sqrt(deviance(CurveFit)/(nrow(Data2)-DOF))*100/(mean(Q))
#Outputs to document for each RData set
FPMC.6.5
CV
#Determination based of pre-established, climate dependent Cv to FPMC relationship
CV.CAV <- 5.96*FPMC.6.5 + 0.85
CV.VAV <- 5.89*FPMC.6.5 + 5.25
#VAV predictions will register as TRUE, CAV predictions will register as FALSE
abs(CV.VAV - CV)<abs(CV.CAV - CV)
#Accounting for b1 inaccurately being a positive value. It is allowed to be positive as long as
#crossover of constant Twi does not occur in the mW flow range plotted
#True mean to trust previous distinction, False means a VAV classification
((bo + b1*8)*(1 - exp(-(b2 + b3*8)*max(mW))))<=((bo + b1*5)*(1 - exp(-(b2 + b3*5)*max(mW))))
```

Appendix J: K2 Dependence on Twi Investigation Results

J.1: Large Office Coils

			Average Wai for Twi Bins			4 Parameter Curve Fit				3 Parameter Curve Fit					
Climate	Application	Twi Schedule	Wai (5.5 C)	Wai (6.5 C)	Wai (7.5 C)	b2 (s/kg)	b3 (s/kg-C)	NMBE	CV	CV	NMBE	K2 (s/kg)	CV Deviation (%)	NMBE Deviation (%)	k2 Deviation (%)
Boulder	CAV	Degrading	0.0083	0.0082	0.0075	0.436	-0.037	-0.002	14.534	14.721	-0.004	0.177	1.288	-56.631	43.626
Boulder	VAV	Degrading	0.0083	0.0082	0.0076	1.019	-0.111	-0.012	16.241	17.237	-0.021	0.216	6.133	-66.995	72.452
Boulder	CAV	Reset	0.0068	0.0070	0.0081	0.329	-0.021	-0.002	13.283	13.419	-0.002	0.181	1.028	16.455	28.914
Boulder	VAV	Reset	0.0072	0.0073	0.0082	0.181	0.008	-0.011	13.931	13.957	-0.012	0.231	0.190	-8.244	10.638
Miami	CAV	Degrading	0.0081	0.0093	0.0097	0.097	-0.009	0.000	4.898	5.842	-0.003	0.037	19.289	-843.538	47.592
Miami	VAV	Degrading	0.0115	0.0111	0.0110	0.192	-0.012	0.001	4.668	4.765	0.000	0.102	2.084	-56.175	27.848
Miami	CAV	Reset	0.0098	0.0098	0.0092	0.139	-0.015	-0.001	4.509	5.340	-0.002	0.033	18.436	-82.717	66.116
Miami	VAV	Reset	0.0108	0.0110	0.0110	0.184	-0.012	0.000	4.369	4.487	0.001	0.107	2.701	27.612	27.380
Atlanta	CAV	Degrading	0.0099	0.0105	0.0096	0.026	0.001	-0.001	2.461	2.469	-0.001	0.031	0.335	1.591	7.601
Atlanta	VAV	Degrading	0.0116	0.0113	0.0100	0.513	-0.052	-0.002	6.812	7.055	-0.004	0.131	3.555	-168.392	62.247
Atlanta	CAV	Reset	0.0099	0.0095	0.0102	0.069	-0.005	-0.001	2.272	2.321	-0.001	0.034	2.165	-9.246	33.429
Atlanta	VAV	Reset	0.0101	0.0098	0.0109	0.101	0.006	-0.004	6.583	6.608	-0.004	0.137	0.367	-11.131	12.946
LA	CAV	Degrading	0.0108	0.0106	0.0101	0.051	0.005	-0.005	7.088	7.142	-0.005	0.084	0.770	6.957	18.602
LA	VAV	Degrading	0.0108	0.0106	0.0101	0.086	0.013	0.005	6.912	6.993	0.006	0.179	1.168	10.671	25.366
LA	CAV	Reset	0.0100	0.0093	0.0104	0.106	-0.003	-0.004	6.291	6.310	-0.004	0.087	0.310	-0.906	9.119
LA	VAV	Reset	0.0101	0.0094	0.0105	0.300	-0.018	0.003	6.781	6.898	0.004	0.186	1.720	27.869	25.744

J.2: Hospital Coils

			Average Wai for Twi Bins			4 Parameter Curve Fit				3 Parameter Curve Fit					
Climate	Application	Twi Schedule	Wai (5.5 C)	Wai (6.5 C)	Wai (7.5 C)	b2 (s/kg)	b3 (s/kg-C	NMBE	CV	CV	NMBE	K2 (s/kg)	CV Deviation (%)	NMBE Deviation (%)	k2 Deviation (%)
Boulder	CAV	Degrading	0.008	0.009	0.009	0.077	-0.003	-0.004	19.035	19.053	-0.005	0.055	0.095	-14.927	16.405
Boulder	VAV	Degrading	0.008	0.008	0.008	0.093	0.000	-0.003	23.101	23.101	-0.003	0.094	0.000	0.574	0.226
Boulder	CAV	Reset	0.007	0.007	0.008	0.219	-0.017	0.002	14.195	14.361	0.002	0.099	1.173	-7.014	37.650
Boulder	VAV	Reset	0.007	0.007	0.008	0.159	-0.009	-0.009	16.276	16.444	-0.007	0.098	1.034	23.690	24.757
Miami	CAV	Degrading	0.011	0.011	0.011	0.006	0.001	0.000	1.293	1.757	0.000	0.012	35.969	72.436	19.589
Miami	VAV	Degrading	0.014	0.013	0.012	0.130	-0.009	0.000	7.584	7.731	0.000	0.067	1.939	8.659	29.722
Miami	CAV	Reset	0.011	0.011	0.011	0.004	0.000	0.000	0.660	0.668	0.000	0.004	1.281	-12.487	3.595
Miami	VAV	Reset	0.011	0.011	0.013	0.084	-0.001	-0.001	6.899	6.900	-0.001	0.080	0.008	-1.387	2.312
Atlanta	CAV	Degrading	0.010	0.010	0.010	0.017	0.001	-0.001	8.251	8.316	-0.001	0.023	0.787	44.739	11.726
Atlanta	VAV	Degrading	0.012	0.011	0.011	0.051	0.001	0.006	12.406	12.415	0.007	0.060	0.067	4.591	6.402
Atlanta	CAV	Reset	0.010	0.010	0.010	0.030	-0.001	-0.001	3.963	3.999	-0.001	0.021	0.896	1.958	16.379
Atlanta	VAV	Reset	0.010	0.010	0.011	0.065	0.001	0.003	9.791	9.794	0.003	0.074	0.024	-0.342	5.159
LA	CAV	Degrading	0.010	0.010	0.010	0.017	0.001	-0.001	4.693	4.868	0.000	0.025	3.722	71.816	15.132
LA	VAV	Degrading	0.010	0.010	0.010	0.046	0.002	0.002	10.445	10.471	0.002	0.057	0.247	14.956	8.593
LA	CAV	Reset	0.010	0.010	0.010	0.029	-0.001	0.000	2.725	2.738	0.000	0.024	0.489	116.036	7.291
LA	VAV	Reset	0.010	0.010	0.010	0.071	-0.002	-0.004	9.809	9.820	-0.004	0.061	0.113	1.994	7.077

Appendix K: Predicting Coils in Unestablished Location Investigation

The directions for the order of implementing the following Matlab scripts can be seen in Appendix D.1. Scripts in K.1 and K.2 contain adjustments to example_script_original.m and testoriginal.m for development of several new parameters. These scripts were utilized in the investigation of applying the climate specific CAV/VAV Prediction Tools to alternate location. K.3 contains additional scripts that need to be in Matlabs Working Directory in additional to all scripts available in Appendix D.4.

K.1: Updated Matlab "example_script.m"

```
% Example Script
addpath(genpath(pwd))
clear;close all;clc
%% Energy Plus
% Define EP files to use
% current path
path_current = pwd;
% location of idf (either "hospital" or "large office" work with this
% script)
[FileName,FilePath] = uigetfile(fullfile(path_current,'EnergyPlus','buildings','*.idf'),'Select building
file');
file_idf = fullfile(FilePath,FileName);
% location of weather file
[FileName,FilePath] = uigetfile(fullfile(path_current,'EnergyPlus','weather','*.epw'),'Select weather
File');
file_epw = fullfile(FilePath,FileName);
% location of output
path_output = fullfile(path_current,'EnergyPlus','results');
% location of energy plus program
path_EP = uigetdir('c:','Locate EnergyPlus program directory');

% Simulation Parameters

% number of timesteps per hour in accordance with EP timestep requirements
timestep = 6;
func_EP_timestep(timestep,file_idf);

% simulation period
begin_month = 4;
begin_day = 1;
end_month = 9;
end_day = 30;
func_EP_run_period(begin_month,begin_day,end_month,end_day,file_idf)

% run EnergyPlus
```

```
func_EnergyPlus(file_idf,file_epw,path_output,path_EP)

%% Import results from EnergyPlus
% EP variable output file
[~,EP] = fileparts(file_idf);
file_EP = fullfile(path_output,[EP '.csv']);
% import results
[data,header] = xlsread(file_EP);
% head time from header (you can use datenum and datestr commands to
% further manipulate the time vector)
time = header(2:end,1);
% remove time from header
header = header(1,2:end)';
% separate out the Hour of the day
[Year Month Day Hour Min Sec]=datevec(time);
% create list of unique air handling units
list = cell(size(header));
for n = 1:numel(header);
   list{n} = header{n}(1:5);
end
list = unique(list);
% user select coil to use
selection = listdlg('ListString',list);
coil = list{selection};
% effectively remove unselected coils from header but preserve indexing
for n = 1:numel(header)
   check = strfind(header{n},coil);
   if isempty(check)
      header{n} = '';
   end
end
%function to find string in header and return index
f_ind = @(str,header)(find(~cellfun('isempty',(strfind(header,str)))));
% import relevent data series
% water mass flow rate
str = 'COOLCDEMAND INLET NODE:System Node Mass Flow Rate [kg/s](TimeStep)';
mW = data(:,f_ind(str,header));
% water inlet temperature
str = 'COOLCDEMAND INLET NODE:System Node Temperature [C](TimeStep)';
Twi = data(:,f_ind(str,header));
% water outlet temperature
str = 'COOLCDEMAND OUTLET NODE:System Node Temperature [C](TimeStep)';
Two = data(:,f_ind(str,header));
% air mass flow rate
str = 'COOLCNODE:System Node Mass Flow Rate [kg/s](TimeStep)';
mA = data(:,f_ind(str,header));
% outdoor air mass flow rate
str = 'OAINLET NODE:System Node Mass Flow Rate [kg/s](TimeStep)';
mOA = data(:,f_ind(str,header));
% air intlet temperature
```

```
str = 'COOLCNODE:System Node Temperature [C](TimeStep)';
Tai = data(:,f_ind(str,header));
% air outtlet temperature
str = 'HEATCNODE:System Node Temperature [C](TimeStep)';
Tao = data(:,f_ind(str,header));
% air inlet humidity
str = 'COOLCNODE:System Node Relative Humidity [%](TimeStep)';
RHai = data(:,f_ind(str,header));
% air outlet humidity
str = 'HEATCNODE:System Node Relative Humidity [%](TimeStep)';
RHao = data(:,f_ind(str,header));
% Total coil cooling rate
str = 'COOLC:Cooling Coil Total Cooling Rate [W](TimeStep)';
Q = data(:,f_ind(str,header));
% Sensible coil cooling rate
str = 'COOLC:Cooling Coil Sensible Cooling Rate [W](TimeStep)';
Qs = data(:,f_ind(str,header));

% import elevation from EPW file.  Usefull calling the included
% Psychrometric functions.
Elevation = func_EP_elevation(file_epw);

%Produce enthalpy output
h = func_h_tdb_rh(Tai,RHai,Elevation);

%Produce enthalpy of saturated air at coil surface
%Relative humidity at coil surface is 100%
RHcs = 1.0;
hcs = func_hcs_tdb_rh(Twi,RHcs,Elevation);

%Producing outputs for use in the investigation into why CV/FPMC
%relationship change between locations
   %Average percentage of OA during simulation period
AvgPercentOA = mean(mOA./mA);
   %Range of inlet air enthalpy
Hmax = max(h);
Hmin = min(h);
Hrange = Hmax - Hmin;
Havg = mean(h);
   %Range of inlet air temperature
Tmax = max(Tai);
Tmin = min(Tai);
Trange = Tmax - Tmin;
Tavg = mean(Tai);
   %Enthalpy potential between air and coil surface
DeltaHmax = max(h - hcs);
DeltaHmin = min(h - hcs);
DeltaHrange = DeltaHmax - DeltaHmin;
DeltaHavg = mean(h - hcs);
   %Fining Sensible Heat Ratio and fraction of time where only sensible
```

```
   %cooling is occurings
SHR = nanmean(Qs./Q);
idx = Qs>=Q;
SensibleOnly = size(h(idx),1)/size(h,1);
   %Producing a matrix for easy export of these variables
Outputs =
[AvgPercentOA,SensibleOnly,SHR,Hmax,Hmin,Hrange,Havg,Tmax,Tmin,Trange,Tavg,DeltaHmax,Del
taHmin,DeltaHrange,DeltaHavg];

%Produce absolute humidity output
Wai = func_w_tdb_rh(Tai,RHai,Elevation);

%% Plots
figure
plot(mW,Q,'.b')
xlabel('water flow rate [kg/s]')
ylabel('coil cooling [w]')
title('coil cooling rate')

figure
plot(Twi,'b','displayname','in')
hold on
plot(Two,'r','displayname','out')
xlabel('timestep')
ylabel('temperature [°C]')
title('coil water temperature')
legend('show')
legend('Location','Southeast')

figure
plot(Tai,'r','displayname','in')
hold on
plot(Tao,'b','displayname','out')
xlabel('timestep')
ylabel('temperature [°C]')
title('coil air temperature')
legend('show')
legend('Location','Southeast')

figure
plot(RHai,'r','displayname','in')
hold on
plot(RHao,'b','displayname','out')
xlabel('timestep')
ylabel('relative humidity [%]')
title('coil relative humidity')
legend('show')
legend('Location','Southeast')

figure
```

```
plot(mW,'b','displayname','water')
hold on
plot(mA,'r','displayname','air')
xlabel('timestep')
ylabel('mass flow rate [kg/s]')
title('coil flow rates')
legend('show')
legend('Location','Southeast')

%Inlet Air Temp Grouping
Taigroup=ordinal(Tai,{'Under 15 C','15-20 C','20-25 C','25-30 C','Over 30 C'},[],[0,15,20,25,30,100]);
figure
gscatter(mW,Q,Taigroup);
xlabel('water flow rate [kg/s]')
ylabel('coil cooling [w]')
title('Inlet Air Temp Binned')
legend('Location','Southeast')

%Inlet RH Grouping
RHaigroup=ordinal(RHai,{'Under 30%','30-45%','45-60%','60-75%','Over
70%'},[],[0,30,45,60,75,100]);
figure
gscatter(mW,Q,RHaigroup);
xlabel('water flow rate [kg/s]')
ylabel('coil cooling [w]')
title('Inlet Relative Humidity Binned')
legend('Location','Southeast')

%Inlet Enthalpy Grouping
hgroup=ordinal(h,{'Under 25 kJ/kg','25-30 kJ/kg','30-35 kJ/kg','35-40 kJ/kg','40-45 kJ/kg','45-50
kJ/kg','50-55 kJ/kg','55-60 kJ/kg','60-70 kJ/kg','Over 70
kJ/kg%'},[],[0,25,30,35,40,45,50,55,60,70,120]);
figure
gscatter(mW,Q,hgroup);
xlabel('water flow rate [kg/s]')
ylabel('coil cooling [w]')
title('Inlet Air Enthalpy Binned')
legend('Location','Southeast')

%Inlet Air Humidity Ratio Grouping
Waigroup=ordinal(Wai,{'Under 0.007','0.007-0.01','0.01-0.012','0.012-0.014','0.014-0.016','Over
0.016'},[],[0,0.007,0.01,0.012,0.014,0.016,0.2]);
figure
gscatter(mW,Q,Waigroup);
xlabel('water flow rate [kg/s]')
ylabel('coil cooling [w]')
title('Inlet Air Humidity Ratio Binned')
legend('Location','Southeast')
%Delta T Grouping
DeltaT = Two-Twi;
```

```
DeltaTgroup=ordinal(DeltaT,{'Under 1 K','1-2 K','2-3 K','3-4 K','4-5 K','5-6 K','6-7 K','7-8 K','Over
8'},[],[0,1,2,3,4,5,6,7,8,100]);
figure
gscatter(mW,Q,DeltaTgroup);
xlabel('water flow rate [kg/s]')
ylabel('coil cooling [w]')
title('Delta T Binned')
legend('Location','Southeast')

%Air Flow Rate Grouping
mAgroup=ordinal(mA,{'Under 5 kg/s','5-10 kg/s','10-15 kg/s','15-20 kg/s','20-25 kg/s','25-50
kg/s','50-75 kg/s','75-100 kg/s','Over 100 kg/s'},[],[0,5,10,15,20,25,50,75,100,200]);
figure
gscatter(mW,Q,mAgroup);
xlabel('water flow rate [kg/s]')
ylabel('coil cooling [w]')
title('Air Flow Rate Binned')
legend('Location','Southeast')


%Time of Day Grouping
Hourgroup=ordinal(Hour,{'Before 6','6-8am','8am-noon','noon-5pm','5pm-
midnight'},[],[0,6,8,12,17,24]);
figure
gscatter(mW,Q,Hourgroup);
xlabel('water flow rate [kg/s]')
ylabel('coil cooling [w]')
title('Time of Day Binned')
legend('Location','Southeast')

%Twi Grouping
Twigroup=ordinal(Twi,{'<6 C','6-7 C','7-8 C','>8 C'},[],[0,6,7,8,10]);
figure
gscatter(mW,Q,Twigroup);
xlabel('water flow rate [kg/s]')
ylabel('coil cooling [w]')
title('Twi Binned')
legend('Location','Southeast')

save2pdf('Twibin',13)
save2pdf('TODbin',12);
save2pdf('DeltaTbin',11);
save2pdf('mAbin',10);
save2pdf('Waibin',9);
save2pdf('haibin',8);
save2pdf('RHaibin',7);
save2pdf('Taibin',6);
save2pdf('QvsmW.pdf',1);

% cleanup
```

```
rmpath(genpath(pwd))
% save data for R analysis
 RData = [mW Q mA Tai Tao h RHai RHao Wai Twi Two DeltaT Month Day Hour Min];
 csvwrite('RData.csv',RData);

 % cleanup
 rmpath(genpath(pwd))
```

K.2: Matlab "test.m"

```
clear;close all;clc
%% Import results from EnergyPlus
% EP variable output file
file_EP = fullfile('MIAMIOfficeReset.csv');
% import results
[data,header] = xlsread(file_EP);
% head time from header (you can use datenum and datestr commands to
% further manipulate the time vector)
time = header(2:end,1);
% remove time from header
header = header(1,2:end)';
% separate out the Hour of the day
[Year Month Day Hour Min Sec]=datevec(time);
% create list of unique air handling units
list = cell(size(header));
for n = 1:numel(header);
   list{n} = header{n}(1:5);
end
list = unique(list);
% user select coil to use
selection = listdlg('ListString',list);
coil = list{selection};
% effectively remove unselected coils from header but preserve indexing
for n = 1:numel(header)
   check = strfind(header{n},coil);
   if isempty(check)
      header{n} = '';
   end
end
%function to find string in header and return index
f_ind = @(str,header)(find(~cellfun('isempty',(strfind(header,str)))));
% import relevent data series
% water mass flow rate
str = 'COOLCDEMAND INLET NODE:System Node Mass Flow Rate [kg/s](TimeStep)';
mW = data(:,f_ind(str,header));
% water inlet temperature
str = 'COOLCDEMAND INLET NODE:System Node Temperature [C](TimeStep)';
Twi = data(:,f_ind(str,header));
% water outlet temperature
```

```
str = 'COOLCDEMAND OUTLET NODE:System Node Temperature [C](TimeStep)';
Two = data(:,f_ind(str,header));
% air mass flow rate
str = 'COOLCNODE:System Node Mass Flow Rate [kg/s](TimeStep)';
mA = data(:,f_ind(str,header));
% outdoor air mass flow rate
str = 'OAINLET NODE:System Node Mass Flow Rate [kg/s](TimeStep)';
mOA = data(:,f_ind(str,header));
% air intlet temperature
str = 'COOLCNODE:System Node Temperature [C](TimeStep)';
Tai = data(:,f_ind(str,header));
% air outtlet temperature
str = 'HEATCNODE:System Node Temperature [C](TimeStep)';
Tao = data(:,f_ind(str,header));
% air inlet humidity
str = 'COOLCNODE:System Node Relative Humidity [%](TimeStep)';
RHai = data(:,f_ind(str,header));
% air outlet humidity
str = 'HEATCNODE:System Node Relative Humidity [%](TimeStep)';
RHao = data(:,f_ind(str,header));
% Total coil cooling rate
str = 'COOLC:Cooling Coil Total Cooling Rate [W](TimeStep)';
Q = data(:,f_ind(str,header));
% Sensible coil cooling rate
str = 'COOLC:Cooling Coil Sensible Cooling Rate [W](TimeStep)';
Qs = data(:,f_ind(str,header));

% import elevation from EPW file.  Usefull calling the included
% Psychrometric functions.
Elevation = 10;

%Produce enthalpy output
h = func_h_tdb_rh(Tai,RHai,Elevation);

%Produce enthalpy output
h = func_h_tdb_rh(Tai,RHai,Elevation);

%Produce enthalpy of saturated air at coil surface
%Relative humidity at coil surface is 100%
RHcs = 1.0;
hcs = func_hcs_tdb_rh(Twi,RHcs,Elevation);

%Producing outputs for use in the investigation into why CV/FPMC
%relationship change between locations
  %Average percentage of OA during simulation period
AvgPercentOA = mean(mOA./mA);
  %Range of inlet air enthalpy
Hmax = max(h);
Hmin = min(h);
Hrange = Hmax - Hmin;
```

```
Havg = mean(h);
   %Range of inlet air temperature
Tmax = max(Tai);
Tmin = min(Tai);
Trange = Tmax - Tmin;
Tavg = mean(Tai);
   %Enthalpy potential between air and coil surface
DeltaHmax = max(h - hcs);
DeltaHmin = min(h - hcs);
DeltaHrange = DeltaHmax - DeltaHmin;
DeltaHavg = mean(h - hcs);
      %Fining Sensible Heat Ratio and fraction of time where only sensible
   %cooling is occurings
SHR = nanmean(Qs./Q);
idx = Qs>=Q;
SensibleOnly = size(h(idx),1)/size(h,1);
   %Producing a matrix for easy export of these variables
Outputs =
[AvgPercentOA,SensibleOnly,SHR,Hmax,Hmin,Hrange,Havg,Tmax,Tmin,Trange,Tavg,DeltaHmax,Del
taHmin,DeltaHrange,DeltaHavg];

%Produce absolute humidity output
Wai = func_w_tdb_rh(Tai,RHai,Elevation);

%% Plot
figure
plot(mW,Q,'.b')
xlabel('water flow rate [kg/s]')
ylabel('coil cooling [w]')
title('coil cooling rate')

figure
plot(Twi,'b','displayname','in')
hold on
plot(Two,'r','displayname','out')
xlabel('timestep')
ylabel('temperature [°C]')
title('coil water temperature')
legend('show')
legend('Location','Southeast')

figure
plot(Tai,'r','displayname','in')
hold on
plot(Tao,'b','displayname','out')
xlabel('timestep')
ylabel('temperature [°C]')
title('coil air temperature')
legend('show')
legend('Location','Southeast')
```

```
figure
plot(RHai,'r','displayname','in')
hold on
plot(RHao,'b','displayname','out')
xlabel('timestep')
ylabel('relative humidity [%]')
title('coil relative humidity')
legend('show')
legend('Location','Southeast')

figure
plot(mW,'b','displayname','water')
hold on
plot(mA,'r','displayname','air')
xlabel('timestep')
ylabel('mass flow rate [kg/s]')
title('coil flow rates')
legend('show')
legend('Location','Southeast')

%Inlet Air Temp Grouping
Taigroup=ordinal(Tai,{'Under 15 C','15-20 C','20-25 C','25-30 C','Over 30 C'},[],[0,15,20,25,30,100]);
figure
gscatter(mW,Q,Taigroup);
xlabel('water flow rate [kg/s]')
ylabel('coil cooling [w]')
title('Inlet Air Temp Binned')
legend('Location','Southeast')

%Inlet RH Grouping
RHaigroup=ordinal(RHai,{'Under 30%','30-45%','45-60%','60-75%','Over
70%'},[],[0,30,45,60,75,100]);
figure
gscatter(mW,Q,RHaigroup);
xlabel('water flow rate [kg/s]')
ylabel('coil cooling [w]')
title('Inlet Relative Humidity Binned')
legend('Location','Southeast')

%Inlet Enthalpy Grouping
hgroup=ordinal(h,{'Under 25 kJ/kg','25-30 kJ/kg','30-35 kJ/kg','35-40 kJ/kg','40-45 kJ/kg','45-50
kJ/kg','50-55 kJ/kg','55-60 kJ/kg','60-70 kJ/kg','Over 70
kJ/kg%'},[],[0,25,30,35,40,45,50,55,60,70,120]);
figure
gscatter(mW,Q,hgroup);
xlabel('water flow rate [kg/s]')
ylabel('coil cooling [w]')
title('Inlet Air Enthalpy Binned')
legend('Location','Southeast')
```

```
%Inlet Air Humidity Ratio Grouping
Waigroup=ordinal(Wai,{'Under 0.007','0.007-0.01','0.01-0.012','0.012-0.014','0.014-0.016','Over
0.016'},[],[0,0.007,0.01,0.012,0.014,0.016,0.2]);
figure
gscatter(mW,Q,Waigroup);
xlabel('water flow rate [kg/s]')
ylabel('coil cooling [w]')
title('Inlet Air Humidity Ratio Binned')
legend('Location','Southeast')
%Delta T Grouping
DeltaT = Two-Twi;
DeltaTgroup=ordinal(DeltaT,{'Under 1 K','1-2 K','2-3 K','3-4 K','4-5 K','5-6 K','6-7 K','7-8 K','Over
8'},[],[0,1,2,3,4,5,6,7,8,100]);
figure
gscatter(mW,Q,DeltaTgroup);
xlabel('water flow rate [kg/s]')
ylabel('coil cooling [w]')
title('Delta T Binned')
legend('Location','Southeast')

%Air Flow Rate Grouping
mAgroup=ordinal(mA,{'Under 5 kg/s','5-10 kg/s','10-15 kg/s','15-20 kg/s','20-25 kg/s','25-50
kg/s','50-75 kg/s','75-100 kg/s','Over 100 kg/s'},[],[0,5,10,15,20,25,50,75,100,200]);
figure
gscatter(mW,Q,mAgroup);
xlabel('water flow rate [kg/s]')
ylabel('coil cooling [w]')
title('Air Flow Rate Binned')
legend('Location','Southeast')


%Time of Day Grouping
Hourgroup=ordinal(Hour,{'Before 6','6-8am','8am-noon','noon-5pm','5pm-
midnight'},[],[0,6,8,12,17,24]);
figure
gscatter(mW,Q,Hourgroup);
xlabel('water flow rate [kg/s]')
ylabel('coil cooling [w]')
title('Time of Day Binned')
legend('Location','Southeast')

%Twi Grouping
Twigroup=ordinal(Twi,{'<6 C','6-6.5 C','6.5-7','7-7.5','7.5-8 C','>8 C'},[],[0,6,6.5,7,7.5,8,10]);
figure
gscatter(mW,Q,Twigroup);
xlabel('water flow rate [kg/s]')
ylabel('coil cooling [w]')
title('Twi Binned')
legend('Location','Southeast')
```

```
save2pdf('Twibin',13)
save2pdf('TODbin',12);
save2pdf('DeltaTbin',11);
save2pdf('mAbin',10);
save2pdf('Waibin',9);
save2pdf('haibin',8);
save2pdf('RHaibin',7);
save2pdf('Taibin',6);
save2pdf('QvsmW.pdf',1);

% cleanup
rmpath(genpath(pwd))
% save data for R analysis
 RData = [mW Q mA Tai Tao h RHai RHao Wai Twi Two DeltaT Month Day Hour Min];
 csvwrite('RData.csv',RData);

 % cleanup
 rmpath(genpath(pwd))
```

K.3: Additional Matlab Scripts Required in Matlab Directory

K.3.1: func_hcs_tdb_rh

```
function [Enthalpy] = func_h_tdb_rh(Twi,RHcs,Elevation)
z = Elevation; % [m]
t = Twi; % [°C]
rh = RHcs; % [-]

%calculate pressure as a function of altitude
p = 101.325*(1-2.25577e-5*z)^5.2559*1000; %pressure, Pa

%coefficients from ASHRAE Fundamentals Psychrometrics
C8 = -5.8002206e03;
C9 = 1.3914993e00;
C10 = -4.8640239e-02;
C11 = 4.1764768e-05;
C12 = -1.4452093e-08;
C13 = 6.5459673e00;

%calc saturation pressure
K = t+273.15; %convert to kelvin, K
pws = exp(C8./K+C9+C10.*K+C11.*K.^2+C12.*K.^3+C13.*log(K)); %saturation pressure, Pa

%calc vapor pressure
pw = rh.*pws; %partial pressure, Pa

%calc humidity ratio
w = 0.621945.*pw./(p-pw);
```

```
%calc enthalpy
h = (1006.*t+w.*(2501000+1860.*t))/1000; %enthalpy, kJ/kg_da

%output
Enthalpy = h; %enthalpy, kJ/kg_da
```

Appendix L: Optimal Control Strategy Testing Procedure and Scripts

L.1: Steps for Initial Testing Simulations

ESTABLISHING A NEW COIL MODEL TO BE SUBJECTED TO ENERGYPLUS INPUTS:

1. Copy in correct RData.csv file from EnergyPlus simulations into Matlab's working directory

2. Open NewPrerun.m script

    - Enter in correct elevation on line 5

    - Enter in proper coil parameters on lines 45 through 50

3. Run New_Prerun.m

4. Open and run TuningInputs.m script

5. Open PIDTuning.slx

    - Initially run with Inputs and PID control for mW

    - Ensure the following are met so we are working with a coil that can benefit from our advanced control logics

        -- Delta T goes below 5.55 quite a bit of the time

        -- Set point deviance on order of +3K

    - mWmax is brought down to just above max used in new model. This will help in controllability and better tuning of the PID's K paramters

    - Switch inputs to use mean Twi, Tai, and Wai values to tune PID controller on a step change

    - Use Z-N closed loop tuning rules for initial estimates, then play around to see if you can get even better performance

    - Run on 300 sec timesteps when tuning K parameters

    - Run one simulation on 30 sec timestep to generate coil data to apply the 4 Parameter Curve Fit to

6. Run PostRun.m script

7. Open RSTudio and run Strategies_CurveFit.R script. Make note of the following:

    - CV

    - FMPC for 6.5 C Twi

    - Coefficients bo, b1, b2, and b3

    - mWlimit

    -mW/DeltaTlimit

TUNING ADVANCED LOGICS' PID CONTROLLERS:

8. Open and run Matlab script TuningInputs4Para.m. This changes constant Tai, Wai and mA to tune the advanced controllers to.

9. Open DeltaTmgrTuning.slx model in Simulink

- Ensure max flow rate in valve is set to what was used in classical PID tuning
- Adjust Delta T step change from 6 K to 5 K
- Run Z-N closed loop tuning method to tune the PI controller for a starting point
- See if you can further improve performance of controller to a Delta T setpoint step change
- Transfer over chosen k parameter into DeltaTmgr.slx model for future testing
- Tuning can be performed on 300 sec timesteps to aid

in minimizing computation time

10. Open FlowoverDeltaTMgr.slx model in Simulink

- Ensure max flow rate in valve is set to what was used in classical PID tuning
- Adjust Setpoint mWoverDeltaT to what was determine when running Strategies_Limit.R
- Adjust the mWoverDeltaT step change to 0.1 below and 0.1 above that limit
- Run Z-N closed loop tuning method to tune the PI controller for a starting point
- See if you can further improve performance of controller to the setpoint step change
- Transfer over chosen k parameter into FlowoverDeltaTMgr.slx model for future testing
- Tuning can be performed on 300 sec timesteps to aid in minimizing computation time

11. Open FourParaTuning.slx model in Simulink

- Ensure max flow rate in valve is set to what was used in classical PID tuning
- Enter in b2 and b3 coefficients into controller mask
- Adjust the Percent Saturation setpoint step change from 0.9 to 0.85
- Run Z-N closed loop tuning method to tune the PI controller for a starting point
- See if you can further improve performance of controller to the setpoint step change
- Transfer over chosen k parameters and b coefficients into FourParmaterTesting.slx model for future testing
- Tuning can be performed on 300 sec timesteps to aid in minimizing computation time

TESTING STRATEGIES AGAINST ONE ANOTHER

12. Open PIDTuning.slx.

- Switch inputs from constant to EP generated data

- Run 30 day simulation on 30 sec timestep

- Look at some scope to ensure nothing abnormal occurred

- Open and run Second_PostRun.m script in Matlab

- Record outputs into Excel chart for given coil

- Repeat these steps for each control strategy. Ensure Classical PID k parameters are translated to each advance controller model prior to testing

13. Repeat steps 1-12 for the Hospital CAV 1 and VAV 1 coils on a degrading Twi schedule

14. Repeat steps 1-12 for the Office VAV 1 (CAV) and VAV 3 coils with a reset Twi schedule

L.2: Steps for Secondary Testing

1. Of the Flow Limiting, Flow/DeltaT Limiting and Delta T Limiting Strategies, take the one with the lowest ISE value during initial simulations and use that value as a baseline.

2. Open other 3 advanced controller models in Simulink (including 4ParaTesting.slx).

3. Perform iterations on each one by adjusting their respective setpoints until all ISE's for the four advanced controllers fall within 5% of each other.

4. With each newly calibrated model, perform a final simulation, run Second_PostRun.m and record the results.

L.3: Matlab Scripts Required to be in Working Directory

L.3.1: NewPrerun.m

```
addpath(genpath(pwd))
clear;close all;clc
%I changed the input for Coil Height (line 32) and R_tube (line 40) to
%match those of EP and took out the fouling factor
%Establish elevation of location in which coil is being simulated
Elevation = 1650;

%Inport RData.csv as .mat file for use in Simulink simulation
load('RData.csv');
%Cropped RData for only August timestamps
RData2 = RData(35137:43776,:);
%Creating a timestamp to be used in Simulink input data
startValue = 0;
endValue = 24*3600*30; %the amount of seconds in the simulation period
nElements = 8640; %amount of data intervals when using 5 min timesteps
time = linspace(startValue,endValue,nElements);
```

```
timestamp = transpose(time);
%Creating a matrix with only the requried data for Simulink simulations
Inputs = [timestamp RData2(:,3) RData2(:,10) RData2(:,4) RData2(:,9)];
%Establishing mWmax as will be applied to several PID controllers in
%Simulink
mWmax = max(RData2(:,1));

%% Typical Coil Input Properties
%Coil Geometric Properties
N_FinsPerMeter = 1/0.0018; %[]
TubeInDiam = 0.01445; %[m]
TubeOutDiam = 0.0159; %[m]
FinWidth = .00015; %[m]

N_Rows = 6; %[]
N_TubesPerRow = 80; %[]
CoilHeight = N_TubesPerRow*0.026; %[m] coil fin diameter is used instead, see EnergyPlus
reference guide for explanation
TISA = 30.5; %[m2] total inside surface area, this is an output from EnergyPlus which is used to
estimate width of coil
CoilWidth = TISA/(pi()*TubeInDiam*N_TubesPerRow*N_Rows); % [m] coil width
CoilDepth = 0.156; %[m]
FinDiameterEP = 3.6; %[m]
FinHeight = (FinDiameterEP + CoilHeight)/2; %[m] this is more of a correction factor to allow A_Fin
to be more closely aligned with EP outputs


%Coil Material Properties
K_Tube = 386; %[W/m-C]
K_Fin = 204; %[W/m-C]

%% Advanced Coil Input Properties
%Coil Fluid Properties
CpLiq = 4186; %[J/kg*C]
DynViscLiq = 0.001519; %[kg/m-s]
K_Liq = 0.5576; %[W/m-C]
LatHeatVap = 2501000; %[J/kg]
CpVap = 1860; %[J/kg-C]
CpAir = 1006; %[J/kg-C]
DynViscAir = 0.0000182; %[kg/m-s]
K_Air = 0.026; %[W/m-C]
%Other
FoulingFactor = 0.0000030; %[m^2-C/W]
TimeConstant = 0; %[s]

%Circuiting
%number of circuits usually equal to number of tubes per row. If edited it
%will most likely be set to half of the number of tubes per row.
%C = 1, full circuit; C = 2, half circuit
Circuiting = 2; %specify circuiting
```

```
%NTU-effectiveness relationship
% 0 = cross-flow and 1 = counter-flow
NTU_eff_relation = 1;

%% Coil Static Parameter Calculations
% Row Spacing
RowSpacing = CoilDepth/N_Rows; %[m]

% Fin Density related Parameters
%number of fins
N_Fins = round(N_FinsPerMeter*CoilWidth); %[]
%number of spaces between fins
N_Spaces = N_Fins+1; %[]
%width of space between fins
FinSpace = (CoilWidth-N_Fins*FinWidth)/(N_Spaces); %[]

% Transform Coil Height to Effective Fin Height
%area of a single side of fin as viewed from water flow direction
A_FinProfile = FinHeight*CoilDepth; %[m^2]
%area of fin profile per intersecting tube
A_FinPerTubeIntersection = A_FinProfile/(N_TubesPerRow*N_Rows);
%effective tube diameter by using effective fin diameter that correlates to
%same area
FinDiameter = sqrt(4*A_FinPerTubeIntersection/pi); %[m]
%effective fin height
%Error in geometric input often indicated by a negative fin height
if FinDiameter >= TubeOutDiam
   FinHeight = (FinDiameter-TubeOutDiam)/2; %[m]
else
   disp('Geometric input not physically possible')
   return
end

% Minimum Airflow Area
%minimum area for airflow when viewing the coil face area from direction of
%air flow
%coil face area
A_Face = CoilHeight*CoilWidth; %[m^2]
%area of fin edges
A_FinEdge = N_Fins*CoilHeight*FinWidth; %[m^2]
%area of tube sections in space between fins at maximum tube diameter
A_TubeMax = N_TubesPerRow*N_Spaces*FinSpace*TubeOutDiam; %[m*2]
%minimum airflow area
A_MinAirflow = A_Face-A_FinEdge-A_TubeMax; %[m*2]

%Error in geometric input often indicated by a negative minimum airflow area
if A_MinAirflow <= 0;
   disp('Geometric input not physically possible')
   return
```

```
end

% Air-side Contact Area
%section area of tube as it passes through plate fin
A_TubeIntersectionAnnulus = pi*(TubeOutDiam/2)^2; %[m^2]
%air contact area of combined fins less the tube annuli
A_Fin = 2*N_Fins*(A_FinProfile-N_TubesPerRow*N_Rows*A_TubeIntersectionAnnulus); %[m^2]
%air contact area of tube sections in fin spaces
A_TubeOut = N_Spaces*N_Rows*N_TubesPerRow*pi*TubeOutDiam*FinSpace; %[m^2]
%air-side contact area
A_AirSide = A_Fin+A_TubeOut; %[m^2]

% Water-side Contact Area
%area of tube contact with water
A_WaterSide = N_Rows*N_TubesPerRow*CoilWidth*pi*TubeInDiam; %[m^2]

% Number of Circuits
N_Circuits = N_TubesPerRow/Circuiting; %[]

% Tube Spacing
TubeSpacing = CoilHeight/N_TubesPerRow; %[m]

% Hydrolic Diameter
HydrolicDiamLiq = TubeInDiam; %[m]
HydrolicDiamAir = 4*A_MinAirflow*CoilDepth/A_AirSide; %[m]

% Tube Length
TubeLength = CoilWidth; %[m]

% Conduction Resistance
R_TubeCond = 0.5*TubeInDiam*log(TubeOutDiam/TubeInDiam)/K_Tube+FoulingFactor;
%[m^2*C/W]

% Pressure as a function of alititude
%from ASHRAE Fundementals - Psychrometrics
Pressure = 101325*(1-2.25577*10^(-5)*Elevation)^5.2559; %[Pa]

% Dynamic Liquid Viscocity at the Wall
DynViscLiqWall = 0.93*DynViscLiq; %[kg/m-s]

% Coefficients phi Dry Fin Efficiency Calculation
RTube = TubeOutDiam/2;
mFin = TubeSpacing/2;
lFin = sqrt(RowSpacing^2+mFin^2)/2;
RRat = 1.27*mFin/RTube*sqrt(lFin/mFin-0.3);
phi = (RRat-1)*(1+0.35*log(RRat));

% C1 and C2 for j-factor correlation
c1 = 0.159*(FinWidth/FinHeight)^0.141*(HydrolicDiamAir/FinWidth)^0.065;
c2 =  -0.323*(FinWidth/FinHeight)^0.049*((FinSpace+FinWidth)/FinWidth)^0.077;
```

```
%% Create Table Lookup for Condensate Temp from hsat
%given an atmoshperic pressure create lookup table for Tdb for 100 relative humidity
%given an enthalpy
RH = 100;
Tdb = 0:.01:40;
p = Pressure;

%coefficients from ASHRAE Fundamentals Psychrometrics
C8 = -5.8002206e03;
C9 = 1.3914993e00;
C10 = -4.8640239e-02;
C11 = 4.1764768e-05;
C12 = -1.4452093e-08;
C13 = 6.5459673e00;

hsat = zeros(1,numel(Tdb));
for i = 1:numel(Tdb);
   t = Tdb(i);

   %calc saturation pressure - ASHRAE Fundaments-Psychrometrics eqn. 6
   K = t+273.15; %convert to kelvin, K
   pws = exp(C8/K+C9+C10*K+C11*K^2+C12*K^3+C13*log(K)); %saturation pressure, Pa

   %calculate saturation humidity ratio
   %ASHRAE Fundamentsl-Psychrometrics eqn. 23
   ws = 0.621945*pws/(p-pws); %stauration humidity ratio at dry-bulb, ratio

   %ASHRAE Fundamentals-Psychrometrics eqn. 32
   h = CpAir*t+ws*(LatHeatVap+CpVap*t); %enthalpy at first air-state, kJ/kg

   hsat(i) = h;
end

%lookup table for T based on hsat
Table_hsat_Tdb = [hsat' Tdb'];

%% List needed Variables
TimeConstant;
TubeInDiam;
TubeOutDiam;
N_TubesPerRow;
N_Rows;
N_Spaces;
N_Circuits;
FinWidth;
FinDiameter;
FinSpace;
TubeSpacing;
HydrolicDiamAir;
```

```
HydrolicDiamLiq;
A_AirSide;
A_WaterSide;
A_Fin;
A_MinAirflow;
TubeLength;
R_TubeCond;
phi;
c1;
c2;
```

L.3.2: TuningInputs.m

```
mA = mean(RData2(:,3));
Tai = mean(RData2(:,4));
Wai = mean(RData2(:,9));
Twi = mean(RData2(:,10));
```

L.3.3: PostRun.m

```
%Export data into usable file for R to perform 4 Parameter Curve
csvwrite('newRData.csv',Q_Twi_mW);

%Twi Grouping
Flow = Q_Twi_mW(:,3);
InletWater = Q_Twi_mW(:,2);
Capacity = Q_Twi_mW(:,1);
Twigroup=ordinal(InletWater,{'<6 C','6-7 C','7-8 C','>8 C'},[],[0,6,7,8,10]);
figure
gscatter(Flow,Capacity,Twigroup);
xlabel('water flow rate [kg/s]')
ylabel('coil cooling [w]')
title('Twi Binned')
legend('Location','Southeast')

save2pdf('TwibinAug',1)


%Inlet Air Humidity Ratio Grouping
Wai = Q_Twi_mW(:,4);
Waigroup=ordinal(Wai,{'Under 0.007','0.007-0.01','0.01-0.012','0.012-0.014','0.014-0.016','Over
0.016'},[],[0,0.007,0.01,0.012,0.014,0.016,0.2]);
figure
gscatter(Flow,Capacity,Waigroup);
xlabel('water flow rate [kg/s]')
ylabel('coil cooling [w]')
title('Inlet Air Humidity Ratio Binned')
legend('Location','Southeast')
%Delta T Grouping
DeltaT = Q_Twi_mW(:,5);
```

```
DeltaTgroup=ordinal(DeltaT,{'Under 1 K','1-2 K','2-3 K','3-4 K','4-5 K','5-6 K','6-7 K','7-8 K','Over
8'},[],[0,1,2,3,4,5,6,7,8,100]);
figure
gscatter(Flow,Capacity,DeltaTgroup);
xlabel('water flow rate [kg/s]')
ylabel('coil cooling [w]')
title('Delta T Binned')
legend('Location','Southeast')


 % cleanup
 rmpath(genpath(pwd))
```

L.3.4: TuningInputs4Para.m

```
mA = mean(RData2(:,3));
Tai = max(RData2(:,4));
Wai = max(RData2(:,9));
Twi = max(RData2(:,10));
```

L.3.5: SecondPostRun.m

```
%Producing outputs that need to be recorded in order to accurately compare
%the various advanced control strategies

%Cropping out initial dynamic behavior before settling occurs in simulation
%Remove the first hour's data (on 30 sec fixed timesteps)

%maximum setpoint error
SPError = -min(SetpointDeviance(120:86401,1));

%Integral Squarred Error
TotalISE = max(ISE(120:86401,1))-ISE(120,1);

%Cooling power provided to system
Cooling_pwr = max(CoolingPwrSupplied(:,1));

%Max flow used
MaxFlow = max(MaxmW(120:86401,1));

%Pumping power
Pump_pwr = max(SummerFlowPower(:,1));

%Average Delta T
DeltaTAvg = mean(DeltaT(120:86401,1));

%Min Delta T
DeltaTmin = min(DeltaT(120:86401,1));

%Max Delta T
```

```
DeltaTmax = max(DeltaT(120:86401,1));

%Fraction of time advanced control strategy is used
IndexFraction = SignalSelection <= 1;
Fraction = numel(SignalSelection(IndexFraction))/numel(SignalSelection);

%Outputs
OUTPUTS = [Fraction SPError TotalISE Cooling_pwr MaxFlow Pump_pwr DeltaTAvg DeltaTmin
DeltaTmax];
```

L.3.6: RestrictionPlots.m

```
%mW Limiting Restriction
Flow = Q_Twi_mW1(:,3);
InletWater = Q_Twi_mW1(:,2);
Capacity = Q_Twi_mW1(:,1);
mWgroup=ordinal(Flow,{'Unrestricted','Restricted'},[],[0,18.91,1000]);
figure
gscatter(Flow,Capacity,mWgroup,['green','red']);
xlabel('water flow rate [kg/s]')
ylabel('coil cooling [w]')
title('mW Limiting Restriction')
legend('Location','Southeast')

save2pdf('mWRestriction',1)

%Delta T Limiting
DeltaT = -Q_Twi_mW1(:,5);
DeltaTgroup=ordinal(DeltaT,{'Unrestricted','Restricted'},[],[-100,-5.5,0]);
figure
gscatter(Flow,Capacity,DeltaTgroup,['green','red']);
xlabel('water flow rate [kg/s]')
ylabel('coil cooling [w]')
title('Delta T Limiting Restriction')
legend('Location','Southeast')

save2pdf('DeltaTRestriction',2)

%Flow/Delta T Limiting
mW_DT=-Flow./DeltaT;
DeltaTgroup=ordinal(mW_DT,{'Unrestricted','Restricted'},[],[0,3.41,100]);
figure
gscatter(Flow,Capacity,DeltaTgroup,['green','red']);
xlabel('water flow rate [kg/s]')
ylabel('coil cooling [w]')
title('Flow Over Delta T Limiting Restriction')
legend('Location','Southeast')

save2pdf('mWDeltaTRestriction',3)
```

```
%4 Para Control
FourPara=Q_Twi_mW1(:,4);
FourParagroup=ordinal(FourPara,{'Unrestricted','Restricted'},[],[0,0.85,100]);
figure
gscatter(Flow,Capacity,FourParagroup,['green','red']);
xlabel('water flow rate [kg/s]')
ylabel('coil cooling [w]')
title('4 Parameter Control Restriction')
legend('Location','Southeast')

save2pdf('4ParaRestriction',4)

%Twi Grouping
Twigroup=ordinal(InletWater,{'<6 C','6-7 C','7-8 C','>8 C'},[],[0,6,7,8,10]);
figure
gscatter(Flow,Capacity,Twigroup);
xlabel('water flow rate [kg/s]')
ylabel('coil cooling [w]')
title('Twi Binned')
legend('Location','Southeast')

save2pdf('TwiBinPlot',5)

 % cleanup
 rmpath(genpath(pwd))
```

L.4: R Script for Optimal Strategy Testing

L.4.1: Strategies_CruveFit.R

```
#Updated Miami Script for troubleshooting R errors

#Cleaning up the workspace

remove(list=objects())

graphics.off()

library(plyr)

library(ggplot2)

library(reshape2)

#Bringing in the raw data

Data <- read.csv("newRData.csv", sep=",", header=F)

names(Data)<-c("Capacity","Twi","Flow")

#Selection of applicable data to analyze. Line 15 Data$Flow maximum may need adjusting pending
the dataset
```

```
#in effort to crop out any data with valve wide open.  This limit would not need to be put in place for

#real world application of this method

Index<- Data$Flow<=0.95*max(Data$Flow) & Data$Flow>0 & Data$Twi<=8

Data2<-Data[Index,]

Q<-Data2$Capacity

mW<-Data2$Flow

Twi<-Data2$Twi

#Applying the Curve Fit through non-linear regression

CurveFit<-nls(Q ~ (bo + b1*Twi)*(1 - exp(-(b2 + b3*Twi)*mW)),start = list(bo=2*max(Q),b1=-0.1*max(Q),b2=.1,b3=.001))

#Assigning coefficients to outputs so to use in constant Twi curve generation below

bo<- coef(CurveFit)[1]

b1<- coef(CurveFit)[2]

b2<- coef(CurveFit)[3]

b3<- coef(CurveFit)[4]

#Drawing constant Twi prediction lines onto graph as sanity check. One can compare these to Matlab generated

#Twi bin plots

plot(mW,Q)

legend(0.8*max(mW),.6*max(Q),c("5C Twi","6C Twi","7C Twi","8C Twi"),lty=c(1,1,1,1),lwd=c(2,2,2,2),

    col=c("yellow","red","blue","purple"))

points(mW,(bo + b1*8)*(1 - exp(-(b2 + b3*8)*mW)),col='purple', lty=1, lwd=2)

points(mW,(bo + b1*7)*(1 - exp(-(b2 + b3*7)*mW)),col='blue', lty=1, lwd=2)

points(mW,(bo + b1*6)*(1 - exp(-(b2 + b3*6)*mW)),col='red', lty=1, lwd=2)

points(mW,(bo + b1*5)*(1 - exp(-(b2 + b3*5)*mW)),col='yellow', lty=1, lwd=2)

#Setting key parameters

k1.6.7<- (bo + b1*6.7)

#Establishing the Range of values to look at for a particular sizing indicator temp maximum observed.
```

```
R<-0.2
#Identifying the number of degress of freedom for the curvefit that will be applied to each Twi bin
DOF<-4
#Setting up Twi of 6.5 as sizing indicator temp for FPMC
k1.6.5<- (bo + b1*6.5)
Index.6.5<-Data2$Twi<=(6.5 + R) & Data2$Twi>=(6.5 - R)
ObservedMax.6.5<- max(Data2$Capacity[Index.6.5])
FPMC.6.5<-ObservedMax.6.5/k1.6.5
#The below measure is intended to be a "goodness of fit".
#Coefficient of Variation (CV) can be read as average deviation in data from
#predicted CurveFit as a percentage of maximum the mean capacity
CV<-sqrt(deviance(CurveFit)/(nrow(Data2)-DOF))*100/(mean(Q))
##Determining limits for several advanced control strategies
#Finding mW when design Twi of 6.7 C theoretically experiences a delta T low limit of 5.55
f <- function (mWlimt) mWlimt*4181.4*5.55-(bo+b1*6.7)*(1-exp(-(b2 + b3*6.7)*mWlimt));
convergence <- uniroot(f, lower = 0.1, upper = 400, tol = 0.0001);
mWlimit <- convergence$root
#Finding the flow over delta T limit
flowoverDTlimit <- mWlimit/5.55
#Outputs for second Simulink Run
Outputs<- c(bo,b1,b2,b3,mWlimit,flowoverDTlimit)
OutputsDF<-matrix(Outputs, ncol=6, nrow=1)
#Outputs to document for each RData set
FPMC.6.5
CV
```

Appendix M: Optimal Control Strategy Testing Results

M.1: Initial Round of Simulations

Climate	Building	System	Twi Schedule	Configuration	FPMC	CV	
Miami	Hospital	CAV 1	Degrading	7 Row	0.704	1.73	
Control Strategy	Limit	ISE Increase (%	Cooling Pwr Decrease (%	Pumping Pwr Decrease (%	Pumping/ISE	Pumping/Cooling	Avg Delta T
DAT Tracking	N/A	-	-	-			5.0
mW Limiting	15.69	3750	4.65	53	0.014	11.3	5.8
mW/DeltaT Limiting	2.82	4110	4.26	51	0.012	12.0	5.7
DeltaT Limiting	5.55	4970	4.54	52	0.010	11.4	5.7
4 Parameter Control	0.85	387	0.49	17	0.044	34.7	5.1
4 Parameter Control	0.8	1309	1.22	29	0.022	23.5	5.2
4 Parameter Control	0.75	3119	2.31	38	0.012	16.5	5.4
4 Parameter Control	0.7	6325	4.19	48	0.008	11.4	5.7

Climate	Building	System	Twi Schedule	Configuration	FPMC	CV	
Miami	Hospital	VAV 1	Degrading	7 Row	0.72	3.92	
Control Strategy	Limit	ISE Increase (%)	Cooling Pwr Decrease (%)	Pumping Pwr Decrease (%)	Pumping/ISE	Pumping/Cooling	Avg Delta T
DAT Tracking	N/A	-	-	-			7.4
mW Limiting	18.91	625	3.30	70	0.112	21.2	7.8
mW/DeltaT Limiting	3.41	976	3.30	70	0.072	21.2	7.5
DeltaT Limiting	5.55	1181	3.75	71	0.060	19.1	7.5
4 Parameter Control	0.85	1255	3.90	71	0.056	18.1	7.6
4 Parameter Control	0.8	2126	5.85	77	0.036	13.1	7.8
4 Parameter Control	0.75	3387	8.11	82	0.024	10.1	8.0
4 Parameter Control	0.7	5180	10.77	85	0.016	7.9	8.4

Climate	Building	System	Twi Schedule	Configuration	FPMC	CV	
Miami	Office	VAV 1 (CAV)	Reset	7 Row	0.35	6.52	
Control Strategy	Limit	ISE Increase (%)	Cooling Pwr Decrease (%	Pumping Pwr Decrease (%	Pumping/ISE	Pumping/Cooling	Avg Delta T
DAT Tracking	N/A	-	-	-			4.5
mW Limiting	7.16	5065	9.90	52	0.010	5.2	5.4
mW/DeltaT Limiting	1.72	7781	9.20	50	0.006	5.4	5.4
DeltaT Limiting	5.55	122932	20.55	49	0.000	2.4	5.6
4 Parameter Control	0.85	7	0.00	0	-0.006	40.3	4.5

Climate	Building	System	Twi Schedule	Configuration	FPMC	CV	
Miami	Office	VAV 3	Reset	4 Row	0.73	4.97	
Control Strategy	Limit	ISE Increase (%)	Cooling Pwr Decrease (%)	Pumping Pwr Decrease (%)	Pumping/ISE	Pumping/Cooling	Avg Delta T
DAT Tracking	N/A	-	-	-			5.7
mW Limiting	6.96	710	1.09	17	0.024	15.7	5.8
mW/DeltaT Limiting	1.25	525	0.74	13	0.026	18.2	5.7
DeltaT Limiting	5.55	15664	5.08	19	0.001	3.7	5.8
4 Parameter Control	0.8	157	0.18	4	0.028	24.8	5.7
4 Parameter Control	0.75	598	0.56	10	0.016	16.9	5.7
4 Parameter Control	0.7	1628	1.24	15	0.009	12.1	5.8
4 Parameter Control	0.65	3527	2.15	19	0.006	9.1	5.9

Climate	Building	System	Twi Schedule	Configuration	FPMC	CV	
LA	Hospital	CAV 1	Degrading	7 Row	0.59	8.15	
Control Strategy	Limit	ISE Increase (%)	Cooling Pwr Decrease (%)	Pumping Pwr Decrease (%)	Pumping/ISE	Pumping/Cooling	Avg Delta T
DAT Tracking	N/A	-	-	-			5.0
mW Limiting	10.01	11741	12.45	76	0.006	6.1	6.3
mW/DeltaT Limiting	1.82	8693	9.38	71	0.008	7.5	6.0
DeltaT Limiting	5.55	6499	6.80	64	0.010	9.4	5.7
4 Parameter Control	0.8	164	0.16	9	0.054	55.1	5.0
4 Parameter Control	0.75	466	0.44	17	0.036	38.6	5.0
4 Parameter Control	0.7	1102	0.90	25	0.023	28.0	5.1
4 Parameter Control	0.65	2234	1.67	35	0.015	20.7	5.2

Climate	Building	System	Twi Schedule	Configuration	FPMC	CV	
LA	Hospital	VAV 1	Degrading	6 Row	0.283	6.32	
Control Strategy	Limit	ISE Increase (%)	Cooling Pwr Decrease (%)	Pumping Pwr Decrease (%)	Pumping/ISE	Pumping/Cooling	Avg Delta T
DAT Tracking	N/A	-	-	-			6.6
mW Limiting	10.01	327	1.82	42	0.128	23.0	6.7
mW/DeltaT Limiting	1.82	842	2.39	47	0.056	19.8	6.6
DeltaT Limiting	5.55	1828	4.17	56	0.031	13.5	6.7
4 Parameter Control	0.85	186	0.46	16	0.085	34.2	6.4
4 Parameter Control	0.8	392	0.92	25	0.065	27.6	6.5
4 Parameter Control	0.75	707	1.55	34	0.048	21.8	6.5
4 Parameter Control	0.7	1200	2.36	42	0.035	17.6	6.6

Climate	Building	System	Twi Schedule	Configuration	FPMC	CV	
LA	Office	VAV 1 (CAV)	Reset	5 Row	0.78	2.1	
Control Strategy	Limit	ISE Increase (%)	Cooling Pwr Decrease (%)	Pumping Pwr Decrease (%)	Pumping/ISE	Pumping/Cooling	Avg Delta T
DAT Tracking	N/A	-	-	-			4.1
mW Limiting	5.76	39503	22.73	82	0.002	3.6	6.3
mW/DeltaT Limiting	1.04	29280	19.26	78	0.003	4.1	6.0
DeltaT Limiting	5.55	21316	15.10	69	0.003	4.6	5.6
4 Parameter Control	0.75	34	0.02	0	-0.001	-1.9	4.1
4 Parameter Control	0.7	289	0.21	0	0.001	1.9	4.1
4 Parameter Control	0.65	1153	0.89	3	0.003	3.7	4.2
4 Parameter Control	0.6	3500	2.28	9	0.003	4.0	4.3

Climate	Building	System	Twi Schedule	Configuration	FPMC	CV	
LA	Office	VAV 3	Reset	4 Row	1.04	19.4	
Control Strategy	Limit	ISE Increase (%)	Cooling Pwr Decrease (%)	Pumping Pwr Decrease (%)	Pumping/ISE	Pumping/Cooling	Avg Delta T
DAT Tracking	N/A	-	-	-			6.1
mW Limiting	3.8	5431	0.84	6	0.001	7.5	6.2
mW/DeltaT Limiting	0.68	384	0.08	1	0.002	8.8	6.1
DeltaT Limiting	5.55	249850	7.13	12	0.000	1.7	6.2
4 Parameter Control	0.75	0	0.00	0	#DIV/0!	#DIV/0!	6.1

Climate	Building	System	Twi Schedule	Configuration	FPMC	CV	
Atlanta	Hospital	CAV 1	Degrading	8 Row	0.58	2.04	
Control Strategy	Limit	ISE Increase (%)	Cooling Pwr Decrease (%)	Pumping Pwr Decrease (%)	Pumping/ISE	Pumping/Cooling	Avg Delta T
DAT Tracking	N/A	-	-	-			5.8
mW Limiting	16.67	484	1.28	24	0.050	18.9	6.0
mW/DeltaT Limiting	3	947	1.51	27	0.028	17.7	6.0
DeltaT Limiting	5.55	2231	2.47	33	0.015	13.2	6.2
4 Parameter Control	0.75	84	0.09	4	0.042	40.1	5.9
4 Parameter Control	0.7	453	0.68	16	0.034	22.8	5.9
4 Parameter Control	0.65	1357	1.57	25	0.018	15.9	6.0
4 Parameter Control	0.6	3067	3.00	34	0.011	11.3	6.2

Climate	Building	System	Twi Schedule	Configuration	FPMC	CV	
Atlanta	Hospital	VAV 1	Degrading	6 Row	0.69	6.06	
Control Strategy	Limit	ISE Increase (%)	Cooling Pwr Decrease (%)	Pumping Pwr Decrease (%)	Pumping/ISE	Pumping/Cooling	Avg Delta T
DAT Tracking	N/A	-	-	-			6.8
mW Limiting	14.97	626	5.24	80	0.128	15.2	7.1
mW/DeltaT Limiting	2.7	751	4.55	78	0.104	17.2	6.8
DeltaT Limiting	5.55	1147	5.98	81	0.071	13.6	7.0
4 Parameter Control	0.85	46	0.18	21	0.460	117.5	6.3
4 Parameter Control	0.8	104	0.71	45	0.432	63.7	6.4
4 Parameter Control	0.75	229	1.40	57	0.250	40.8	6.5
4 Parameter Control	0.7	430	2.33	66	0.153	28.2	6.6

Climate	Building	System	Twi Schedule	Configuration	FPMC	CV	
Atlanta	Office	VAV 1 (CAV)	Reset	6 Row	0.52	9.58	
Control Strategy	Limit	ISE Increase (%)	Cooling Pwr Decrease (%)	Pumping Pwr Decrease (%)	Pumping/ISE	Pumping/Cooling	Avg Delta T
DAT Tracking	N/A	-	-	-			5.6
mW Limiting	9.01	48	0.05	1	0.022	23.0	5.6
mW/DeltaT Limiting	1.62	46	0.02	1	0.015	40.3	5.6
DeltaT Limiting	5.55	102342	9.56	19	0.000	2.0	5.9
4 Parameter Control	0.75	0	0.00	0	#DIV/0!	#DIV/0!	5.6

Climate	Building	System	Twi Schedule	Configuration	FPMC	CV	
Atlanta	Office	VAV 3	Reset	5 Row	0.66	11.49	
Control Strategy	Limit	ISE Increase (%)	Cooling Pwr Decrease (%)	Pumping Pwr Decrease (%)	Pumping/ISE	Pumping/Cooling	Avg Delta T
DAT Tracking	N/A	-	-	-			5.5
mW Limiting	9.01	3145	5.42	53	0.017	9.8	6.0
mW/DeltaT Limiting	1.62	2015	3.76	45	0.023	12.1	5.8
DeltaT Limiting	5.55	4578	4.08	37	0.008	9.0	5.7
4 Parameter Control	0.8	64	0.10	4	0.058	35.8	5.5
4 Parameter Control	0.75	260	0.45	10	0.039	22.9	5.5
4 Parameter Control	0.7	749	1.17	18	0.024	15.6	5.6
4 Parameter Control	0.65	1686	2.19	25	0.015	11.4	5.7

Climate	Building	System	Twi Schedule	Configuration	FPMC	CV	
Boulder	Hospital	CAV 1	Degrading	7 Row	1.33	22.6	
Control Strategy	Limit	ISE Increase (%)	Cooling Pwr Decrease (%)	Pumping Pwr Decrease (%)	Pumping/ISE	Pumping/Cooling	Avg Delta T
DAT Tracking	N/A	-	-	-			5.2
mW Limiting	7.78	1586	6.25	85	0.053	13.5	6.0
mW/DeltaT Limiting	1.4	2192	5.83	84	0.038	14.4	5.9
DeltaT Limiting	5.55	9323	12.20	85	0.009	7.0	6.0
4 Parameter Control	0.85	427	1.89	47	0.109	24.7	5.4
4 Parameter Control	0.8	860	3.03	66	0.077	21.9	5.6
4 Parameter Control	0.75	1584	4.76	78	0.050	16.5	5.9
4 Parameter Control	0.7	2662	7.05	83	0.031	11.7	6.1

Climate	Building	System	Twi Schedule	Configuration	FPMC	CV	
Boulder	Hospital	VAV 1	Degrading	8 Row	0.89	29.76	
Control Strategy	Limit	ISE Increase (%)	Cooling Pwr Decrease (%)	Pumping Pwr Decrease (%)	Pumping/ISE	Pumping/Cooling	Avg Delta T
DAT Tracking	N/A	-	-	-			5.9
mW Limiting	7.19	1402	8.99	93	0.066	10.4	6.7
mW/DeltaT Limiting	1.29	1357	6.66	92	0.068	13.8	6.5
DeltaT Limiting	5.55	2578	8.18	91	0.035	11.1	6.5
4 Parameter Control	0.85	985	6.96	45	0.046	6.5	6.3
4 Parameter Control	0.8	1493	9.13	49	0.033	5.4	6.4
4 Parameter Control	0.75	2160	11.53	53	0.025	4.6	6.5
4 Parameter Control	0.7	3005	14.17	58	0.019	4.1	6.6

Climate	Building	System	Twi Schedule	Configuration	FPMC	CV	
Boulder	Office	VAV 1 (CAV)	Reset	5 Row	1.33	13.8	
Control Strategy	Limit	ISE Increase (%)	Cooling Pwr Decrease (%)	Pumping Pwr Decrease (%)	Pumping/ISE	Pumping/Cooling	Avg Delta T
DAT Tracking	N/A	-	-	-			4.1
mW Limiting	5.24	11959	13.18	70	0.006	5.3	5.1
mW/DeltaT Limiting	0.93	15175	13.94	71	0.005	5.1	5.1
DeltaT Limiting	5.55	70475	26.89	76	0.001	2.8	5.4
4 Parameter Control	0.85	458	0.88	5	0.011	5.6	4.1
4 Parameter Control	0.8	727	1.42	6	0.008	4.2	4.1
4 Parameter Control	0.75	1496	2.53	7	0.005	2.8	4.2
4 Parameter Control	0.7	3507	4.55	14	0.004	3.0	4.4

Climate	Building	System	Twi Schedule	Configuration	FPMC	CV	
Boulder	Office	VAV 3	Reset	6 Row	1.07	24.1	
Control Strategy	Limit	ISE Increase (%)	Cooling Pwr Decrease (%)	Pumping Pwr Decrease (%)	Pumping/ISE	Pumping/Cooling	Avg Delta T
DAT Tracking	N/A	-	-	-			5.2
mW Limiting	3.62	2349	2.88	94	0.040	32.6	5.5
mW/DeltaT Limiting	0.652	850	1.11	93	0.109	83.9	5.3
DeltaT Limiting	5.55	13605	6.61	93	0.007	14.1	5.8
4 Parameter Control	0.85	4308	1.75	58	0.013	33.0	5.3
4 Parameter Control	0.8	5821	2.35	61	0.010	26.0	5.4
4 Parameter Control	0.75	7955	3.29	65	0.008	19.8	5.5
4 Parameter Control	0.7	10906	4.82	69	0.006	14.3	5.6

M.2: Final Round of Simulations

Climate	Building	System	Twi Schedule	Configuration	FPMC	CV	
Miami	Hospital	CAV 1	Degrading	7 Row	0.704	1.73	
Control Strategy	Limit	ISE Increase (%)	Cooling Pwr Decrease (%	Pumping Pwr Decrease (%	Pumping/ISE	Pumping/Cooling	Avg Delta T
DAT Tracking	N/A	-	-	-			5.0
mW Limiting	15.69	3750	4.65	53	0.014	11.3	5.8
mW/DeltaT Limiting	3	3554	3.18	48	0.013	15.0	5.6
DeltaT Limiting	5.27	3656	2.73	45	0.012	16.4	5.5
4 Parameter Control	0.745	3564	2.02	39	0.011	19.0	5.4

Climate	Building	System	Twi Schedule	Configuration	FPMC	CV	
Miami	Hospital	VAV 1	Degrading	7 Row	0.72	3.92	
Control Strategy	Limit	ISE Increase (%)	Cooling Pwr Decrease (%)	Pumping Pwr Decrease (%)	Pumping/ISE	Pumping/Cooling	Avg Delta T
DAT Tracking	N/A	-	-	-			7.4
mW Limiting	18.91	625	3.30	70	0.112	21.2	7.8
mW/DeltaT Limiting	4.8	608	1.96	62	0.101	31.5	7.3
DeltaT Limiting	4.8	642	2.20	63	0.099	28.8	7.4
4 Parameter Control	0.91	609	2.09	60	0.098	28.4	7.3

Climate	Building	System	Twi Schedule	Configuration	FPMC	CV	
Miami	Office	VAV 1 (CAV)	Reset	7 Row	0.35	6.52	
Control Strategy	Limit	ISE Increase (%)	Cooling Pwr Decrease (%)	Pumping Pwr Decrease (%)	Pumping/ISE	Pumping/Cooling	Avg Delta T
DAT Tracking	N/A	-	-	-			4.5
mW Limiting	7.16	5065	9.90	52	0.010	5.2	5.4
mW/DeltaT Limiting	1.72	5111	6.81	42	0.008	6.1	5.2
DeltaT Limiting	4.05	5252	2.37	11	0.002	4.5	4.7
4 Parameter Control	0.85	7	0.00	0	-0.006	40.3	4.5

Climate	Building	System	Twi Schedule	Configuration	FPMC	CV	
Miami	Office	VAV 3	Reset	4 Row	0.73	4.97	
Control Strategy	Limit	ISE Increase (%)	Cooling Pwr Decrease (%)	Pumping Pwr Decrease (%)	Pumping/ISE	Pumping/Cooling	Avg Delta T
DAT Tracking	N/A	-	-	-			5.7
mW Limiting	7.3	512	0.85	15	0.028	17.1	5.7
mW/DeltaT Limiting	1.25	525	0.74	13	0.026	18.2	5.7
DeltaT Limiting	5.55	525	0.25	4	0.007	14.0	5.7
4 Parameter Control	0.7552	530	0.51	9	0.017	17.5	5.7

Climate	Building	System	Twi Schedule	Configuration	FPMC	CV	
LA	Hospital	CAV 1	Degrading	7 Row	0.73	4.61	
Control Strategy	Limit	ISE Increase (%)	Cooling Pwr Decrease (%)	Pumping Pwr Decrease (%)	Pumping/ISE	Pumping/Cooling	Avg Delta T
DAT Tracking	N/A	-	-	-			5.0
mW Limiting	7	455	61.75	95	0.209	1.5	5.8
mW/DeltaT Limiting	1.2	462	61.61	95	0.205	1.5	5.7
DeltaT Limiting	5	450	61.42	94	0.209	1.5	5.7
4 Parameter Control	0.74	477	61.50	94	0.197	1.5	5.7

Climate	Building	System	Twi Schedule	Configuration	FPMC	CV	
LA	Hospital	VAV 1	Degrading	6 Row	0.283	6.32	
Control Strategy	Limit	ISE Increase (%)	Cooling Pwr Decrease (%)	Pumping Pwr Decrease (%)	Pumping/ISE	Pumping/Cooling	Avg Delta T
DAT Tracking	N/A	-	-	-			6.1
mW Limiting	16.25	461	1.63	42	0.091	25.8	6.7
mW/DeltaT Limiting	4.6	419	0.80	33	0.078	41.0	6.5
DeltaT Limiting	4	434	0.67	30	0.070	44.9	6.5
4 Parameter Control	0.845	423	0.31	17	0.039	53.2	6.5

Climate	Building	System	Twi Schedule	Configuration	FPMC	CV	
LA	Office	VAV 1 (CAV)	Reset	5 Row	0.78	2.1	
Control Strategy	Limit	ISE Increase (%)	Cooling Pwr Decrease (%)	Pumping Pwr Decrease (%)	Pumping/ISE	Pumping/Cooling	Avg Delta T
DAT Tracking	N/A	-	-	-			4.1
mW Limiting	9.7	4853	6.09	48	0.010	7.9	4.8
mW/DeltaT Limiting	2.08	4932	5.71	47	0.009	8.2	4.7
DeltaT Limiting	5	5004	5.59	43	0.009	7.8	4.7
4 Parameter Control	0.58	5116	3.20	14	0.003	4.3	4.4

Climate	Building	System	Twi Schedule	Configuration	FPMC	CV	
LA	Office	VAV 3	Reset	4 Row	1.04	19.4	
Control Strategy	Limit	ISE Increase (%)	Cooling Pwr Decrease (%)	Pumping Pwr Decrease (%)	Pumping/ISE	Pumping/Cooling	Avg Delta T
DAT Tracking	N/A	-	-	-			6.1
mW Limiting	3.8	5431	0.84	6	0.001	7.5	6.2
mW/DeltaT Limiting	0.5	5535	0.64	5	0.001	7.6	6.2
DeltaT Limiting	4.758	5201	0.21	0	0.000	1.5	6.1

Climate	Building	System	Twi Schedule	Configuration	FPMC	CV	
Atlanta	Hospital	CAV 1	Degrading	8 Row	0.58	2.04	
Control Strategy	Limit	ISE Increase (%)	Cooling Pwr Decrease (%)	Pumping Pwr Decrease (%)	Pumping/ISE	Pumping/Cooling	Avg Delta T
DAT Tracking	N/A	-	-	-			5.8
mW Limiting	16.67	507	0.55	23	0.045	41.8	6.0
mW/DeltaT Limiting	3.8	484	0.09	18	0.038	196.6	5.9
DeltaT Limiting	4.5	498	0.10	18	0.036	177.8	5.9
4 Parameter Control	0.72	512	-0.02	14	0.028	-832.1	5.9

Climate	Building	System	Twi Schedule	Configuration	FPMC	CV	
Atlanta	Hospital	VAV 1	Degrading	6 Row	0.69	6.06	
Control Strategy	Limit	ISE Increase (%)	Cooling Pwr Decrease (%)	Pumping Pwr Decrease (%)	Pumping/ISE	Pumping/Cooling	Avg Delta T
DAT Tracking	N/A	-	-	-			6.8
mW Limiting	14.97	626	5.24	80	0.128	15.2	7.1
mW/DeltaT Limiting	3.3	638	4.02	76	0.120	19.0	6.8
DeltaT Limiting	4.8	612	3.75	75	0.123	20.1	6.7
4 Parameter Control	0.666	636	3.20	71	0.111	22.1	6.7

Climate	Building	System	Twi Schedule	Configuration	FPMC	CV	
Atlanta	Office	VAV 1 (CAV)	Reset	6 Row	0.52	9.58	
Control Strategy	Limit	ISE Increase (%)	Cooling Pwr Decrease (%)	Pumping Pwr Decrease (%)	Pumping/ISE	Pumping/Cooling	Avg Delta T
DAT Tracking	N/A	-	-	-			5.6
mW Limiting	10.01	48	0.05	1	0.022	23.0	5.6
mW/DeltaT Limiting	1.62	46	0.02	1	0.015	40.3	5.6
DeltaT Limiting	4.36	50	0.01	0	0.002	15.8	5.6

Climate	Building	System	Twi Schedule	Configuration	FPMC	CV	
Atlanta	Office	VAV 3	Reset	5 Row	0.66	11.49	
Control Strategy	Limit	ISE Increase (%)	Cooling Pwr Decrease (%	Pumping Pwr Decrease (%)	Pumping/ISE	Pumping/Cooling	Avg Delta T
DAT Tracking	N/A	-	-	-			5.5
mW Limiting	6.5	2010	4.06	47	0.023	11.5	5.9
mW/DeltaT Limiting	1.05	2015	3.76	45	0.023	12.1	5.8
DeltaT Limiting	5.35	1991	2.37	31	0.015	12.9	5.7
4 Parameter Control	0.64	1935	2.45	26	0.014	10.8	5.7

Climate	Building	System	Twi Schedule	Configuration	FPMC	CV	
Boulder	Hospital	CAV 1	Degrading	7 Row	0.848	17.59	
Control Strategy	Limit	ISE Increase (%)	Cooling Pwr Decrease (%)	Pumping Pwr Decrease (%)	Pumping/ISE	Pumping/Cooling	Avg Delta T
DAT Tracking	N/A	-	-	-			5.2
mW Limiting	7.78	1586	6.25	85	0.053	13.5	6.0
mW/DeltaT Limiting	1.6	1539	4.44	82	0.053	18.5	5.8
DeltaT Limiting	4.5	1592	3.44	78	0.049	22.7	5.6
4 Parameter Control	0.75	1584	4.76	78	0.050	16.5	5.9

Climate	Building	System	Twi Schedule	Configuration	FPMC	CV	
Boulder	Hospital	VAV 1	Degrading	8 Row	0.89	31.6	
Control Strategy	Limit	ISE Increase (%)	Cooling Pwr Decrease (%)	Pumping Pwr Decrease (%)	Pumping/ISE	Pumping/Cooling	Avg Delta T
DAT Tracking	N/A	-	-	-			5.9
mW Limiting	7.19	1402	8.99	93	0.066	10.4	6.7
mW/DeltaT Limiting	1.29	1357	6.66	92	0.068	13.8	6.5
DeltaT Limiting	5.15	1346	5.31	89	0.066	16.8	6.4
4 Parameter Control	0.815	1325	8.45	48	0.036	5.6	6.4

Climate	Building	System	Twi Schedule	Configuration	FPMC	CV	
Boulder	Office	VAV 1 (CAV)	Reset	5 Row	1.33	13.8	
Control Strategy	Limit	ISE Increase (%)	Cooling Pwr Decrease (%)	Pumping Pwr Decrease (%)	Pumping/ISE	Pumping/Cooling	Avg Delta T
DAT Tracking	N/A	-	-	-			4.1
mW Limiting	5.24	11959	13.18	70	0.006	5.3	5.1
mW/DeltaT Limiting	1.03	11979	11.87	68	0.006	5.7	5.0
DeltaT Limiting	4.18	12058	6.87	44	0.004	6.4	4.5
4 Parameter Control	0.63	11579	9.92	24	0.002	2.4	4.8

Climate	Building	System	Twi Schedule	Configuration	FPMC	CV	
Boulder	Office	VAV 3	Reset	6 Row	1.07	24.1	
Control Strategy	Limit	ISE Increase (%)	Cooling Pwr Decrease (%)	Pumping Pwr Decrease (%)	Pumping/ISE	Pumping/Cooling	Avg Delta T
DAT Tracking	N/A	-	-	-			5.2
mW Limiting	4.5	808	1.28	92	0.114	72.3	5.3
mW/DeltaT Limiting	0.652	850	1.11	93	0.109	83.9	5.3
DeltaT Limiting	3.62	834	0.43	90	0.108	210.3	5.2
4 Parameter Control	1.15	857	0.28	48	0.056	172.4	5.1

Appendix N: Modified Boulder CAV/VAV Prediction Tool

```
#Cleaning up the workspace

remove(list=objects())

graphics.off()

library(plyr)

library(ggplot2)

library(reshape2)

#Bringing in the raw data

Data <- read.csv("Realworlddata2.csv", sep=",", header=F)

names(Data)<-c("FlowGPM","TwiF","TwoF","AirflowLpers")

#Selection of applicable data to analyze. Line 15 Data$Flow maximum may need adjusting pending the dataset

#in effort to crop out any data with valve wide open.  This limit would not need to be put in place for

#real world application of this method

Index<-Data$FlowGPM>0 & Data$TwiF<=46.4

Data2<-Data[Index,]

mW<-Data2$Flow*0.063

Twi<-(Data2$TwiF-32)*5/9

Two<-(Data2$TwoF-32)*5/9

cp<-4180

Q<-mW*cp*(Two-Twi)

mA<-(Data2$AirflowLpers)

Data3<-cbind(mW,Twi,Two,Q)

DeltaT<-Two-Twi

#Applying the Curve Fit through non-linear regression

CurveFit<-nls(Q ~ (bo + b1*Twi)*(1 - exp(-(b2 + b3*Twi)*mW)),start = list(bo=100000,b1=-.1*max(Q),b2=.1,b3=.001))

#Assigning coefficients to outputs so to use in constant Twi curve generation below

bo<- coef(CurveFit)[1]
```

```
b1<- coef(CurveFit)[2]

b2<- coef(CurveFit)[3]

b3<- coef(CurveFit)[4]


#Drawing constant Twi prediction lines onto graph as sanity check. One can compare these to Matlab generated

#Twi bin plots

plot(mW,Q)

legend(0.8*max(mW),.6*max(Q),c("5C Twi","6C Twi","7C Twi","8C Twi"),lty=c(1,1,1,1),lwd=c(2,2,2,2),

    col=c("yellow","red","blue","purple"))

points(mW,(bo + b1*8)*(1 - exp(-(b2 + b3*8)*mW)),col='purple', lty=1, lwd=2)

points(mW,(bo + b1*7)*(1 - exp(-(b2 + b3*7)*mW)),col='blue', lty=1, lwd=2)

points(mW,(bo + b1*6)*(1 - exp(-(b2 + b3*6)*mW)),col='red', lty=1, lwd=2)

points(mW,(bo + b1*5)*(1 - exp(-(b2 + b3*5)*mW)),col='yellow', lty=1, lwd=2)

#Establishing the Range of values to look at for a particular sizing indicator temp maximum observed.

R<-0.2

#Identifying the number of degress of freedom for the curvefit that will be applied to each Twi bin

DOF<-4

#Setting up Twi of 6.5 as sizing indicator temp for FPMC

k1.6.5<- (bo + b1*6.5)

Index.6.5<-Data3[,2]<=(6.5 + R) & Data3[,3]>=(6.5 - R)

ObservedMax.6.5<- max(Data3[,4][Index.6.5])

FPMC.6.5<-ObservedMax.6.5/k1.6.5

#The below measure is intended to be a "goodness of fit".

#Coefficient of Variation (CV) can be read as average deviation in data from

#predicted CurveFit as a percentage of maximum the mean capacity

CV<-sqrt(deviance(CurveFit)/(nrow(Data3)-DOF))*100/(mean(Q))

#Outputs to document for each RData set

FPMC.6.5
```

```
CV
#Determination based of pre-established, climate dependent Cv to FPMC relationship
CV.CAV <- 14.89*FPMC.6.5 + 0.404
CV.VAV <- 14.23*FPMC.6.5 + 7.58
#VAV predictions will register as TRUE, CAV predictions will register as FALSE
abs(CV.VAV - CV)<abs(CV.CAV - CV)
#Accounting for b1 inaccurately being a positive value. It is allowed to be positive as long as
#crossover of constant Twi does not occur in the mW flow range plotted
#True mean to trust previous distinction, False means a VAV classification
((bo + b1*8)*(1 - exp(-(b2 + b3*8)*max(mW))))<=((bo + b1*5)*(1 - exp(-(b2 + b3*5)*max(mW))))
```

Appendix O: Maxima Proof for k1 and k2 Derivations

Coil Analysis

1 Dry coil analysis

Property Assumptions

```
(%i1) assume( cpa > 0, cpw > 0, cs > 0, mA > 0, UA > 0, UAw > 0) $
```

Determining k1 from analysis of classical theory on Effectiveness/NTU model. As the coil approaches k1, water flow would be extreremly high, thus the waterside capacitance rate would be Cmax
Capacitance ratio and NTU would then be as follows

```
(%i2) C : mA*cpa/(mW*cpw) $
      NTU : UA/(mA*cpa) $
      Qdry : (1-exp(-NTU*(1-C)))/(1-C*exp(-NTU*(1-C)))*mA*cpa*(Tai-Twi) $
```

k1 would be the limit of Q as mW goes to infinity

```
(%i5) k1dry : limit(Qdry,mW,inf);
```

(%o5) $-\%e^{-\frac{UA}{cpa\,mA}}\left(\left(cpa\,Twi-cpa\,Tai\right)mA\,\%e^{\frac{UA}{cpa\,mA}}+\left(cpa\,Tai-cpa\,Twi\right)mA\right)$

Determining k2 by dividing the limit of the derivative of Q as mW goes to 0 by k1. At low water flow rates, the capacitance ratio becomes flipped, and the NTU equation changes as well

```
(%i6) C : mW*cpw/(mA*cpa) $
      NTU : UA/(mW*cpw) $
      Qdry : (1-exp(-NTU*(1-C)))/(1-C*exp(-NTU*(1-C)))*mW*cpw*(Tai-Twi) $
      dQdmW : diff(Qdry,mW) $
      limdQdmW : limit(dQdmW,mW,0, plus);
```

(%o10) $cpw\,Tai-cpw\,Twi$

As shown from the output of the equation below, k2 has no dependence on Twi

```
(%i11) k2dry : ratsimp (limdQdmW/k1dry);
       diff (k2dry, Twi);
```

(%o11) $\frac{cpw\,\%e^{\frac{UA}{cpa\,mA}}}{cpa\,mA\,\%e^{\frac{UA}{cpa\,mA}}-cpa\,mA}$

(%o12) 0

2 Wet coil analysis

```
(%i13) C : mA*cs/(mW*cpw) $
       NTU : UAw/mA $
       Qwet : (1-exp(-NTU*(1-C)))/(1-C*exp(-NTU*(1-C)))*mA*(hai-hwsati) $
       k1wet : limit(Qwet,mW,inf) $
       dQwdmW : diff(Qwet,mW) $
       limdQwdmW:limit(dQwdmW,mW,0,plus);
```

(%o18) $-\frac{cpw\,hwsati-cpw\,hai}{cs}$

As shown from the output of the equation below, k2 has no dependence on hwsati, and thus no depedence on Twi

```
(%i19) k2wet : ratsimp (limdQwdmW/k1wet);
       diff(k2wet, hwsati);
```

(%o19) $\frac{cpw\,\%e^{UAw/mA}}{cs\,mA\,\%e^{UAw/mA}-cs\,mA}$

(%o20) 0